

1976

Study of the president costa e silva bridge during construction and service (steel structure), Final Report, March 1976

A. Ostapenko

D. H. DePaoli

J. H. Daniels

J. E. O'Brien

Follow this and additional works at: <http://preserve.lehigh.edu/engr-civil-environmental-fritz-lab-reports>

Recommended Citation

Ostapenko, A.; DePaoli, D. H.; Daniels, J. H.; and O'Brien, J. E., "Study of the president costa e silva bridge during construction and service (steel structure), Final Report, March 1976" (1976). *Fritz Laboratory Reports*. Paper 2100.
<http://preserve.lehigh.edu/engr-civil-environmental-fritz-lab-reports/2100>

This Technical Report is brought to you for free and open access by the Civil and Environmental Engineering at Lehigh Preserve. It has been accepted for inclusion in Fritz Laboratory Reports by an authorized administrator of Lehigh Preserve. For more information, please contact preserve@lehigh.edu.

A STUDY OF THE PRESIDENT COSTA E SILVA BRIDGE
DURING CONSTRUCTION AND SERVICE
(STEEL STRUCTURE)

F I N A L R E P O R T

by

A. Ostapenko, D. H. DePaoli, J. H. Daniels,
J. E. O'Brien, B. T. Yen, M. E. Bhatti, J. W. Fisher

Submitted to

ECEX - Empresa de Engenharia e
Construção de Obras Especiais, Rio de Janeiro

Lehigh University

Fritz Engineering Laboratory Report No. 397.6

March 1976

TABLE OF CONTENTS

	<u>Page</u>
1. <u>INTRODUCTION</u>	
1.1 Objectives and Scope of Study	1.1
1.2 The Bridge, Need for Field Study	1.4
1.3 Construction Procedure	1.8
1.4 Instrumentation and Equipment Used in Field Study	1.10
1.5 Work Schedule, Organization of Report	1.12
1.6 Tables and Figures	1.15
2. <u>INSTRUMENTATION SYSTEMS</u>	
2.1 Types and Location of Instrumentation	2.1
2.2 Strain and Temperature Gages for Static Studies	2.4
2.3 Mechanical and Scratch Gages	2.7
2.3.1 Scratch Gages	2.7
2.3.2 Mechanical Gage System	2.13
2.4 Strain Gages for Stress History (Traffic) Studies	2.17
2.4.1 Strain Gage	2.17
2.4.2 Strain Recording System	2.18
2.4.3 Traffic Identification and Location	2.19
2.4.4 Strain Recording Periods	2.19
2.4.5 Traffic Count Record	2.21
2.5 Tables and Figures	2.22
3. <u>STATIC STRESSES AND FORCE HISTORY</u> (A. Ostapenko and D. H. DePaoli)	
3.1 General	3.1
3.2 Observations During Construction	3.2

TABLE OF CONTENTS (Cont.)

	<u>Page</u>
3.3 Analysis of Strain, Scratch and Mechanical Gage Readings for Construction Stages	3.5
3.3.1 Maximum Stresses for Construction Stages	3.5
3.3.2 Scratch Gage Records for Construction Stages	3.7
3.3.3 Adjustment of Section Properties	3.10
3.3.4 Conclusions	3.12
3.4 Test Load Stresses and Distribution of Loads Between Boxes	3.14
3.4.1 Test Load Program	3.14
3.4.2 Stresses due to Test Loads	3.16
3.4.3 Scratch Gage Record for Test Loads	3.22
3.4.4 Distribution of Loads Between Boxes	3.24
3.5 Force History	3.26
3.5.1 Erection	3.26
3.5.2 Placement of Pavement and Parapets	3.28
3.5.3 Service	3.29
3.5.4 Mechanical Gage Readings	3.33
3.5.5 Conclusions	3.36
3.6 Tables and Figures	3.38
4. <u>TEMPERATURE STUDIES</u> (M. E. Bhatti, D. H. DePaoli and A. Ostapenko)	
4.1 Instrumentation and Schedule	4.1
4.1.1 Need for Temperature Studies	4.1
4.1.2 Instrumentation for Measurement of Temperature	4.3
4.1.3 Schedule of Readings	4.4

TABLE OF CONTENTS (Cont.)

	<u>Page</u>
4.2 Thermal Stress Analysis	4.5
4.2.1 General	4.5
4.2.2 Thermo-Elastic Analysis of Beams	4.5
1) Thermal Stresses Due to Non-Linear Temperature Distribution	4.5
2) Thermal Stresses in Indeterminate Structures	4.8
4.3 Method of Thermo-Elastic Analysis of the President Costa e Silva Bridge	4.12
4.3.1 Structural System	4.12
1) Structure and Assumptions	4.12
2) Suddivision of Bridge Girder into Segments and Elements	4.14
4.3.2 Generation of Thermal Distribution in the Bridge from Field Measurements	4.15
1) Temperature Distribution in Sections at FB27 and FB57	4.16
2) Temperature Distribution Along the Bridge	4.16
4.4 Field Measurements of Temperature	4.18
4.4.1 Temperature Data of February 1974	4.18
4.4.2 Temperature Data of June 1974	4.20
4.4.3 Temperature Data of January 1975	4.22
4.5 Analysis of Thermal Stresses	4.24
4.5.1 Thermal Stresses for Sample Data of February 1974	4.24
4.5.2 Thermal Stresses for January 1975 Data	4.26

TABLE OF CONTENTS (Cont.)

	<u>Page</u>
4.6 Scratch Gage Record of Thermal Effects	4.27
4.7 Summary and Recommendations	4.30
4.7.1 Summary	4.30
4.7.2 Recommendations	4.31
1) Temperature Change for Design of Steel Bridges Under Rio de Janeiro Conditions	4.31
2) Thermo-Elastic Analysis of Steel Bridges	4.32
3) Scratch Gages	4.32
4) Future Use of Instrumentation in the President Costa e Silva Bridge	4.33
4.8 Tables and Figures	4.34
5. <u>EFFECTIVE PLATE WIDTH AND TRANSVERSE STRESSES DUE TO POISSON'S RATIO EFFECT</u> (J. E. O'Brien and A. Ostapenko)	
5.1 Observed Transverse Strain Patterns and Possible Causes	5.1
5.2 Analysis	5.2
5.2.1 Assumptions and Procedure	5.2
5.2.2 Method of Analysis and Computation of Stresses	5.4
5.3 Effective Width and Resultant Stresses	5.11
5.4 Conclusions	5.14
5.5 Tables and Figures	5.16
6. <u>STRESS HISTORY - ORTHOTROPIC DECK STRESSES UNDER TRAFFIC</u> (J. H. Daniels, B. T. Yen and J. W. Fisher)	
6.1 Introduction	6.1
6.2 Field Testing	6.3
6.2.1 Controlled Load Tests - Feb. 26, 1974	6.3
6.2.2 Controlled Load Tests - June 3 and 5, 1974	6.3
6.2.3 Random Traffic: May 30 - June 5, 1974	6.6

TABLE OF CONTENTS (Cont.)

	<u>Page</u>
6.3 Results of Controlled Load Test	6.6
6.3.1 Controlled Load Tests - Feb. 26, 1974	6.6
6.3.2 Significance of Results - Feb. 26, 1974	6.7
6.3.3 Controlled Load Tests - June 3 and 5, 1974	6.8
6.4 Results of Random Traffic Studies - May - June 1974	6.9
6.4.1 Stress Range Histograms	6.9
6.4.2 Vehicle Position Histograms	6.9
6.5 Traffic Analysis	6.10
6.5.1 Traffic During Strain Recording Periods (May - June 1974)	6.10
6.5.2 Traffic During 1974-75	6.10
6.5.3 Estimated Axle and Vehicle Weights	6.11
6.6 Analysis of Orthotropic Deck Welded Details for Fatigue Susceptibility	6.14
6.6.1 Splices of the Trapezoidal Stiffening Ribs	6.15
6.6.2 Connection of Trapezoidal Stiffening Ribs to the Floor Beam	6.18
6.6.3 Connection of Stiffening Rib to Orthotropic Plate	6.19
6.7 Conclusions and Recommendations	6.22
6.8 Tables and Figures	6.26
<u>7. SUMMARY AND RECOMMENDATIONS</u>	
7.1 Summary	7.1
7.1.1 Bridge Behavior During Construction	7.2
7.1.2 Bridge Behavior Under Test Loads	7.3
7.1.3 Temperature Studies	7.3

TABLE OF CONTENTS (Cont.)

	<u>Page</u>
7.1.4 Force History -- Variation of Bridge Forces with Time	7.4
7.1.5 Orthotropic Deck Stresses Under Traffic	7.5
7.2 Recommendations Pertinent to the President Costa e Silva Bridge	7.6
7.2.1 Inspection of Orthotropic Deck Components for Fatigue Cracks	7.6
7.2.2 Monitoring of Bridge Stresses with Scratch and Mechanical Gages	7.6
7.3 Recommendations for the Use of Instrumentation Installed in the Bridge	7.7
7.3.1 Mechanical Gage System	7.7
7.3.2 Scratch Gages	7.8
7.3.3 Orthotropic Deck Gages	7.8
7.3.4 Additional Temperature Studies	7.8
7.4 Recommendations for Design of Other Steel Bridges	7.9
7.4.1 Method of Analysis	7.9
7.4.2 Temperature Distribution	7.9
7.4.3 Thermo-Elastic Analysis of Steel Bridges	7.9
7.4.4 Scratch Gages	7.10
7.4.5 Stresses due to Poisson's Ratio Effect	7.10
8. <u>ACKNOWLEDGEMENTS</u>	8.1
9. <u>REFERENCES</u>	9.1

TABLE OF CONTENTS (Contd.)

	<u>Page</u>
<u>APPENDIX A -- SYSTEM OF ELECTRIC STRAIN AND</u>	
<u>TEMPERATURE GAGES</u>	
(A. Ostapenko and J. E. O'Brien)	
A.1 Location of Electric Gages in Cross Sections	A.1
A.2 Wiring and Switching System, Correlation Table	
A.2.1 Wiring System in Bridge	A.3
A.2.2 Switching Stations -- Connection Panels	A.4
A.2.3 Correlation Table of B&F, Cable Gage Nos.	A.5
A.3 Junction Box in Curb at FB51	A.6
A.4 Tables and Figures	A.8
<u>APPENDIX B -- COMPUTER PROGRAM FOR THERMO-ELASTIC ANALYSIS</u>	
<u>OF THE PRESIDENT COSTA E SILVA BRIDGE</u>	
(M. E. Bhatti and A. Ostapenko)	
B.1 Introduction	B.1
B.2 The Structure of Program and Identification	B.1
B.3 Purpose and Method	B.2
B.4 Restrictions and Limitations	B.3
B.5 Non-Standard Machine Operations Instructions	B.4
B.6 Data Preparation and Input	B.4
B.6.1 Card Input Form: Temperature	B.5
B.6.2 Card Input Form: Geometry	B.6
B.7 Instructions for Job Execution	B.7
B.8 Output Form Description	B.9
B.9 Symbol List and Definition	B.9
B.10 Listing of Computer Program	B.16
B.11 Sample Input -- Temperature Data for January 1975	B.30
B.12 Selected Sample Output for Temperature Data of January 1975	B.30

TABLE OF CONTENTS (Cont.)

	<u>Page</u>
<u>APPENDIX C -- COMPUTER PROGRAM FOR ANALYSIS OF POISSON'S</u> <u>RATIO EFFECT</u> (A. Ostapenko and J. E. O'Brien	
C.1 Introduction	C.1
C.2 Fundamental Matrices for Force Method of Analysis	C.2
C.3 Computer Program	C.7
C.3.1 General Procedure and Subroutines	C.7
C.3.2 Symbol List and Definitions	C.9
C.3.3 Listing of Computer Program	C.12
C.3.4 Input Format and Sample	C.21
C.3.5 Description and Sample of Output	C.22

1. INTRODUCTION

1.1 Objectives and Scope of Study

Design, fabrication and construction of the President Costa e Silva Bridge between Rio de Janeiro and Niteroi in Brazil presented many unique problems. The three spans over the main shipping channel of this monumental structure are of steel twin-box girder type, and the center span is of an unprecedented length (300m) for this type of cross section.

Only a very few field studies are available on box girder structures and even those are on short span bridges. Also, the emphasis has been on the service stress conditions rather than on the construction stages.

The objectives of the field study on the President Costa e Silva Bridge were the following:

- 1) Monitoring of stresses at some selected points during construction for deviations from the computed values. Occurrence of any large deviation would have indicated a need for some corrective measures.

- 2) Collection of extensive data on the stress and temperature conditions during construction and after completion, and the use of this data in an evaluation of the accuracy of the assumptions and methods used in the design of the bridge and in the preparation of recommendations useful for design of future bridges of similar type.

3) Acquisition of information on the stress history for the orthotropic deck under regular traffic conditions. This was used to gain some insight into the possibility of fatigue damage.

The research program designed to achieve these objectives had several aspects which were unique and appeared for the first time in the world. These were:

1) taking readings on a bridge during construction for the purpose of comparing the measured and computed stresses,

2) the test load program on the completed bridge,

3) the extent and complexity of the total strain gage instrumentation, and

4) the extent of the instrumentation for a comprehensive temperature study during and after construction.

Of direct service to the safety of the bridge were the strain readings during construction and the results of the orthotropic deck studies.

The project lasted two years, from August 1973 until August 1975, and involved six trips by the researchers to the bridge site in Rio. All reduction of the field data, analysis and evaluation, the preparation of the progress reports and of the final report were performed at Lehigh University.

The principal findings of this study are that the method of analysis used in design was quite accurate since the design stresses deviated only insignificantly from the values measured during construction; the actual temperature distribution is non-linear and produces thermal stresses smaller than assumed in design; gross

cross-sectional stresses in the bridge due to diurnal temperature variation are greater than due to traffic loads; transverse bending stresses due to Poisson's ratio effect, although not critical in this bridge were measured to be of significant magnitude to be considered in design of other bridges; the orthotropic deck stresses due to traffic are typical for this type of structure and indicate that there should be no concern for fatigue cracks for at least fifteen (15) years and that periodic inspections should be made thereafter.

1.2 The Bridge, Need for Field Study

Opening of the President Costa e Silva Bridge took place in March 1974, after nearly five years of work. As shown in the insert of Fig. 1.1, the bridge spans the Guanabara Bay between the cities of Rio de Janeiro and Niteroi and serves the combined population of over five million in the two cities in addition to providing a short-cut for the interstate highway BR101 along the coast. The bridge has an overall length of over 13 kilometers with 8.5 kilometers over water and carries six lanes of traffic. (1.1)* An overall view of the bridge is given in Fig. 1.1.

Previously, the only ways to commute from one city to the other was to drive 110 km around the bay or to take a ferry. The idea of creating a permanent crossing between the two cities existed for a long time. One notable enterprise which nearly came to fruition except for the failure in securing funds was the railroad tunnel proposed by Eng. H. L. Bucknell a century ago in 1876. Many other proposals have been made since then, including tunnels, a suspension bridge, and even an airship propelled by an engine of 3000 hp and guided on a cable suspended from a series of balloons (1929). (1.2) In 1968, after a thorough feasibility study, the Brazilian Department of Highways** decided to build a bridge, directly connecting the two population centers.

Even though the 2.5-kilometer stretch of water near the mouth of the bay seemed to be a logical choice of the bridge site, an 8.5-kilometer stretch further inland was chosen for several reasons. If the

*Numbers in parentheses indicate publications listed by Chapters in References (Chapter 10).

**DNER - Departamento Nacional de Estradas de Rodagem.

2.5-kilometer site had been used, the bridge would have had exits into heavily populated congested areas, not into the existing highway system, as it does now. Also, at the chosen site, the foundation piles of the piers did not have to be driven as deeply. Less interference with the local and oceanic maritime traffic in the Rio harbor, as well as the presence of two nearby airports, were further factors in determining the selected site.

A series of five-span prestressed concrete box girders of segmental construction was found to be the most suitable system for spanning most of this stretch of water. However, the three long spans over the shipping channel had to be built as a steel box girder, and the central span of 300 m is the longest one in the world for a box girder. (In the overall view of the bridge in Fig. 1.1, the three steel spans over the shipping channel are seen as the center of the humped portion in the distance. In the right bottom insert they are labeled A, B and C.)

Because of the magnitude of this project, the Department of Highways created a special bridge authority, ECEX*. The function of ECEX under energetic guidance by its President, Col. João Carlos Guedes, was to coordinate and supervise the combined efforts of the many design and contracting firms that participated in building this structure. The two parts of the bridge, concrete and steel, were designed and built by two different groups of firms.

*ECEX - Empresa de Construcao e Exploracao da Ponte Presidente Costa e Silva, later renamed Empresa de Engenharia e Construcao de Obras Especiais.

Structural design and construction supervision of the steel part of the bridge were carried out by Howard Needles Tammen and Bergendoff, International, Inc. of Kansas City (HNTB). The steel girders were fabricated in large panels in Great Britain and then shipped to Rio de Janeiro. There, the segments were assembled and erected by the joint venture of three companies: Redpath Dorman and Long, Ltd., The Cleveland Bridge and Engineering Co., Ltd., both of Great Britain, and a Brazilian subcontractor Montreal Engenharia S.A.

The steel girder over the shipping channel presented some new challenges. Besides unique construction techniques employed for the first time, the sheer unprecedented size of the bridge girder led to concern about the accuracy and reliability of design assumptions and methods. Some new high strength steels were used for the first time in such a large structure, and many problems had to be resolved, for example, the welding of plates up to 60 mm thickness in this material. (1.3) It is thus only natural that the design had to be somewhat conservative for this unusual structure.

However, it was still deemed advisable to conduct an on-site measurement of stresses during construction and, after completion, under traffic loads. A Lehigh University research team was invited by ECEX to perform this study.* It was also evident that with the instrumentation installed, this study presented a fortuitous opportunity to expand the scope beyond the immediate needs of this

*A separate study has been conducted on the concrete portion of the bridge by the Laboratorio Nacional de Engenharia Civil - L.N.E.C., Portugal.

particular bridge to the aspects applicable to the design of box girder bridges in general and thus to benefit Bridge Engineering Science. A need for a broader general study was also underscored by some recent failures of large box girder bridges: The Danube Bridge in Vienna in November 1969, the Milford Haven Bridge in Wales in June 1970, the Westgate Bridge in Melbourne in October 1970, and the Koblenz Bridge in November 1971. (1.4)

1.3 Construction Procedure

The steel portion of the bridge had an overall length of 848 meters and consisted of a symmetrical three-span continuous girder with 30-meter cantilevers and two suspended 44-meter segments, one at each end, which served as transitions to the concrete spans. For the purpose of erection, the three-span girder was treated in three portions: a 176-meter center portion with full cross section (shown dark in the middle of span B of the right insert in Fig. 1.1) and two 292-meter side spans. This configuration can be seen in Figs. 1.2 f, e and d. Each side consisted of two long segments of half cross section.

Several very unique construction techniques were used in the building of the steel portion of the bridge. As mentioned above, large plate panels of the box girders were fabricated in Great Britain, then shipped to Rio de Janeiro where they were assembled on land into the large box segments.

The first segment assembled was the 4000-ton, 176-meter center portion which was made water-tight so that it could be used as a giant pontoon to aid in the erection of other segments. In Fig. 1.3 which shows the four segments of the side span still on land on the jetties, the pontoon is seen already in the water in the right foreground. The whole construction sequence is shown in Fig. 1.2.

The first step was the erection of the 292-meter Niteroi side span. Fabricated as two separate box girders, it was transported one box at a time on the pontoon to the piers where the boxes were

set on the pier rings (Fig. 1.2a). The pier rings were platforms of steel box construction that surrounded each set of dual pier shafts and provided support for the box girders. Then as shown in Fig. 1.4, the rings were jacked to the top of the pier shafts where the separate girders were slid together and welded to form one unit. The Rio side span (the second step) was erected in a similar manner (Fig. 1.2b). The third step was the erection of the 44-meter end span on the Niteroi side (Fig. 1.2c). This span was fabricated as two separate girders, floated out, and hoisted individually into position. The erection of the center span (the pontoon) was the fourth step (Fig. 1.2d). This span was jacked up out of the water on four jacking columns suspended from both side spans. In position at the top, it was bolted to the side spans to form a continuous three-span structure. The fifth step was the erection of the other 44-meter end span on the Rio side (Fig. 1.2e). Painting, placement of pavement, guardrails and median barrier, etc. completed the construction.

For the convenience of reference in later chapters of this report, the following specific construction stages are listed here:

- a. Side span segment (south or north half) on jetties before transfer to pontoon.
- b. Side span segment on pontoon after transfer from jetties.
- c. Side span on pontoon before transfer to pier rings.
- d. Side span on pier rings after transfer from pontoon.
- e. Center span segment in the water before it is lifted.
- f. Center span segment lifted out of the water.

1.4 Instrumentation and Equipment Used in Field Study

Of immediate interest in this field study was the performance of the bridge under construction loads. Other topics to be investigated were the behavior under test loads, the assumptions of the linearity of stress and temperature distribution and of the load distribution between the individual boxes, the secondary stresses due to Poisson's ratio effect, and the stress histories due to temperature fluctuations and moving traffic loads. An extensive instrumentation program was needed and this was designed by the Lehigh University team in the United States and then implemented on the bridge with help of the personnel of ECEX and HNTB.

Although the longest (300-meter) span is subjected to the highest dead and live load stresses, of greater concern during construction were the side spans. Thus, the instrumentation was installed in the Rio side span indicated by C in Fig. 1.1 (only after completion, a scratch gage was placed in the center span). Furthermore, the construction sequence made it impossible to place any instrumentation inside the middle portion of the center span because it was used as a pontoon for transporting the side spans and had to be periodically flooded in the process. Also, for safety reasons, no access inside the center box portion was permitted.

One of the unique aspects of this investigation was the extent of instrumentation. Five cross sections were instrumented in the Rio side span: two at the piers, one at the beginning of the haunch

at the central pier and two within the span. In addition, instrumentation was placed on the orthotropic plate components of the top flange for studying stresses due to traffic loads near the left pier (FB17) and near one of the in-span sections (FB42).

Five types of instrumentation were used on the bridge. Static stresses due to construction and test loads were measured by 305 electric-resistance strain gages, a mechanical gage and 8 scratch gages. For the dynamic stresses due to traffic, there was another set of 67 electric-resistance strain gages, and for the temperature, 52 electric-resistance temperature gages.

The equipment for taking readings of the electrical gages was of three types. During the movement of the north box of the Rio side span from the jetties to the pontoon and then to the pier rings, static readings were taken with a Budd Digital Strain Indicator.* All subsequent static readings were taken with a B&F Multi-Channel Digital Strain Indicator** in conjunction with a teletype. The transient strain variation in the orthotropic plate due to dynamic traffic load was recorded by means of a multi-channel oscillograph.

The use of different instrumentation systems for what may appear to be the same purpose was justified by the complementary nature of their capabilities as well as a need to have a back-up system if one of the systems malfunctioned at a critical stage.

*Budd, Model A-110

**B&F Instruments, Model SY 161-100-U

1.5 Work Schedule, Organization of Report

Work of this project extended over two years from August 1973 till the end of August 1975. The general project progress schedule of Fig. 1.5 shows the research phases with respect to the planned and actual time schedule, as well as the approximate percentage of completion at the end of each month. A description of the activities on the project is given in detail in three Progress Reports issued in the course of work (1.6, 1.7, 1.8) and there is no need to repeat all of it here. However for convenience, a brief listing, punctuated by the trips of the Lehigh University researchers to Rio de Janeiro*, is presented below.

Trip No.*	Date(s)	Activity in Rio and Between Trips
1	13 to 20 July 1973	J. W. Fisher prepared the research proposal in Rio in accordance with the needs of ECEX and taking into consideration the actual field conditions. (1.5)
	Between trips 1 and 2	Design of instrumentation systems and making arrangements for the needed supplies and equipment.
2	2 to 12 Sept. 1973	A. Ostapenko and H. T. Sutherland with assistance from ECEX and HNTB staff started installing instrumentation; H. T. Sutherland remained in Rio to complete.
	Between trips 2 and 3	Staff at Lehigh developed details of the reading sequences and gage switching operations for trip 3.
3	1 to 14 Oct. 1973	A. Ostapenko and H. T. Sutherland in Rio. Readings made on the north and some on the south box during the construction stages a, b, c, d (listed in Art. 1.3).

*Referencing to the same trip numbers is used throughout this report for identifying readings.

Trip No.	Date(s)	Activity in Rio and Between Trips
	Between trips 3 and 4	Redesign of wiring and switching system for construction stages e and f (listed in Art. 1.3). Reduction* and analysis** of some data from trip 3.
4	14 Nov. to 15 Dec. 1973	A. Ostapenko and H. T. Sutherland in Rio. Instrumentation modified and readings made for construction stages e and f.
	Between trips 4 and 5	Reduction of data from trip 4 and some analysis. Detailed design of instrumentation for orthotropic plate and test load studies.
5	15 Feb. to 6 March 1974	A. Ostapenko, H. T. Sutherland, J. H. Daniels in Rio. Instrumentation modified or installed and readings made for four test load positions, controlled traffic load, temperature conditions during the day (all previous readings were at night).
	Between trips 5 and 6	Reduction and analysis of data. Preparation of Progress Report No. 1 (19 July 1973 - 31 March 1974, F.E.L. Report No. 397.2). (1.6) Design of modified instrumentation system for trip 6. HNTB staff took mechanical gage readings on the bridge in Rio.

*The term Date Reduction signifies conversion of the numerical readings obtained in the field to strains and temperature and then to stresses and cross-sectional forces. The original readings were in the form of hand filled tables, perforated tape, light-sensitive tape, and traces on the scratch gage targets. Their conversion involved the development of suitable computer programs for the numerical and analytical operations involved, error studies, manual and/or automatic plotting of the principal or other stresses, photographing the scratch gage targets in the electron microscope and subsequent interpretation of the traces, statistical analysis of the deck gage readings, etc. In summary, the term Data Reduction covers all the operations needed to prepare the data accumulated in the field for the subsequent analysis.

**The term Analysis signifies the work which followed after the data was reduced. This means: determination of the reasons for a specific stress variation in a cross section and for the deviations from the theoretically established stress distributions, and an explanation of any inconsistencies found in the field. This phase also involved preparation of recommendations for the modification of design procedures in the light of the actual behavior of the structure.

Trip No.	Date(s)	Activity in Rio and Between Trips
6	26 May to 13 June 1974	J. H. Daniels, B. T. Yen and H. T. Sutherland in Rio. Readings taken on orthotropic plate under controlled trucks and regular traffic. Some temperature gages were also read to establish the time dependent temperature variation in the bridge.
	Between trips 6 and 7	All field data reduced and most of it analyzed. Preparation of Progress Report No. 2 (1 April to 30 Sept. 1974, F.E.L. Report No. 397.4). (1.7) Drafting of some parts of Final Report (this report). Preparations for trip 7.
7	5 to 19 Jan. 1975	A. Ostapenko, H. T. Sutherland, D. H. DePaoli J. E. O'Brien in Rio. Modification of instrumentation and readings for a comprehensive temperature study. Modification of scratch gages. Transferral of instrumentation and equipment to ECEX for further use.
	Between trip 7 and end of project	Reduction of new data. Analysis of all data. Preparation of Progress Report No. 3 (1 Oct. 1974 to 31 March 1975, F.E.L. Report 397.5). (1.8) Writing of the final report.

1.6 Chapter 1 - Figures

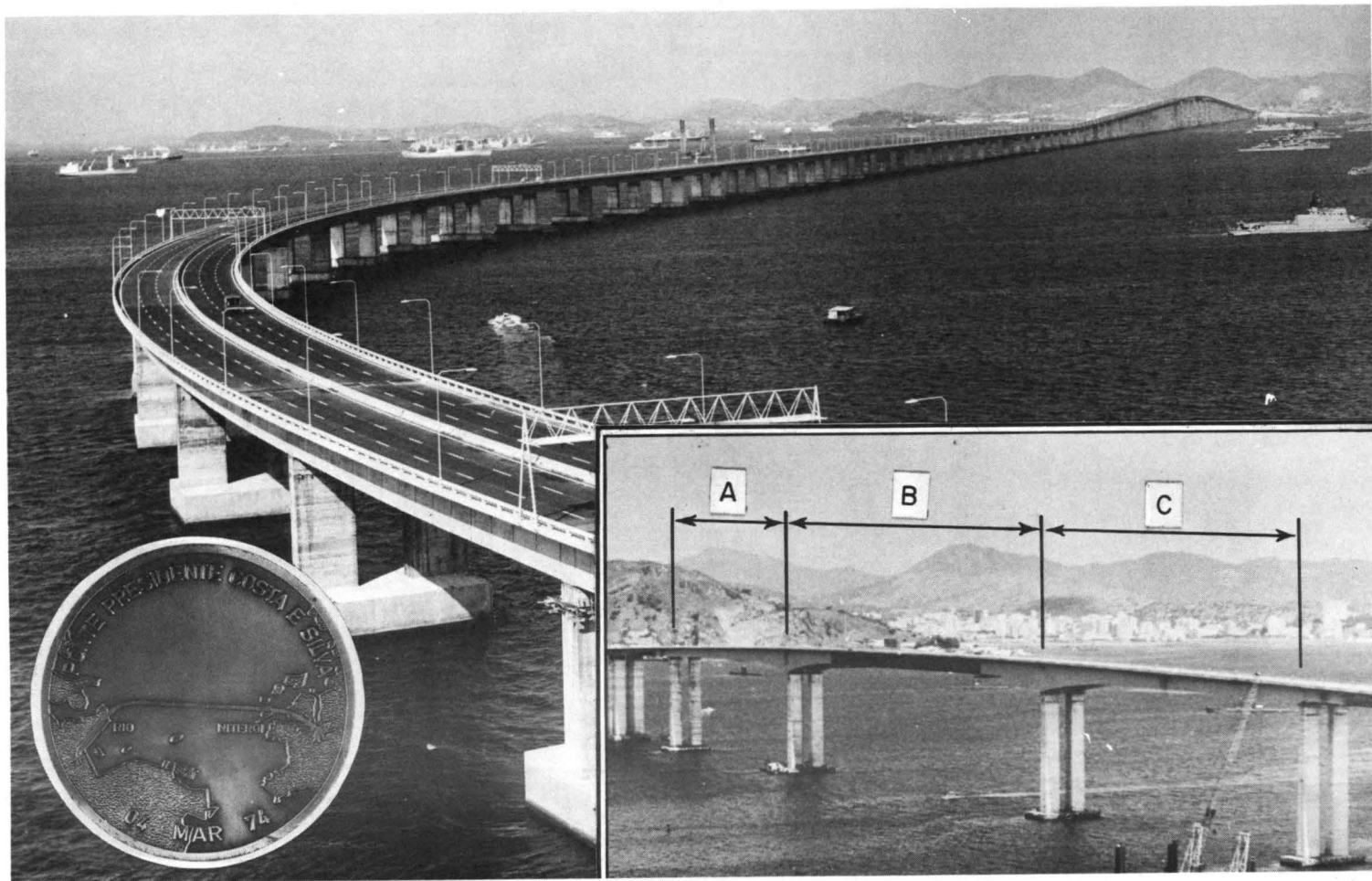


Fig. 1.1 The President Costa e Silva Bridge
Left Insert: Geographic Location
Right Insert: Steel Spans of Shipping Channel

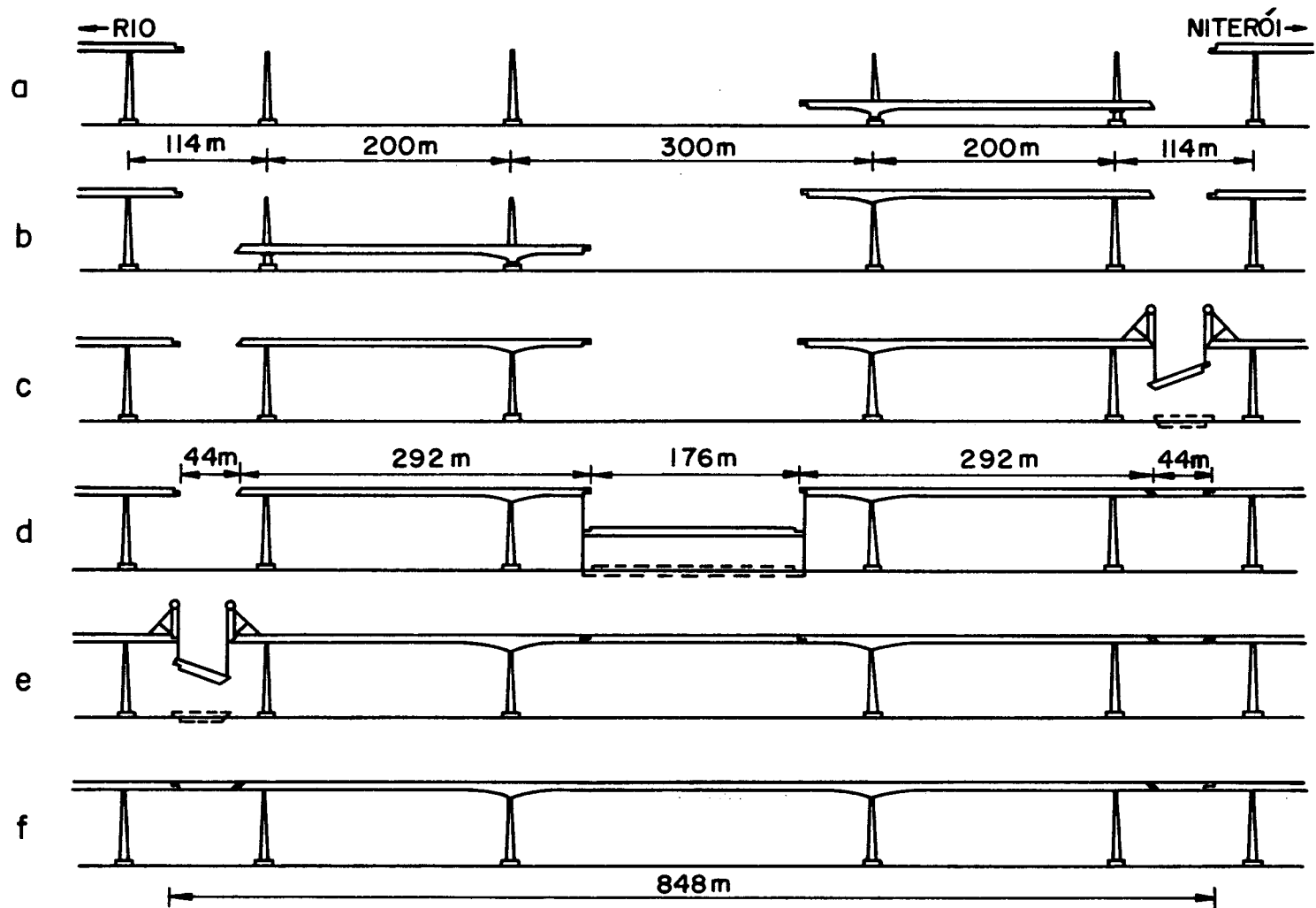


Fig. 1.2 Construction Sequence of Steel Portion

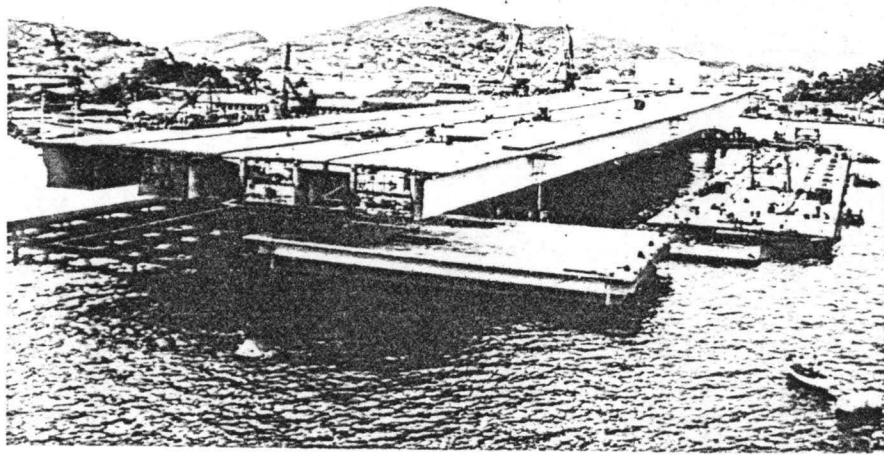


Fig. 1.3 Segments of Side and Central Spans Before Erection

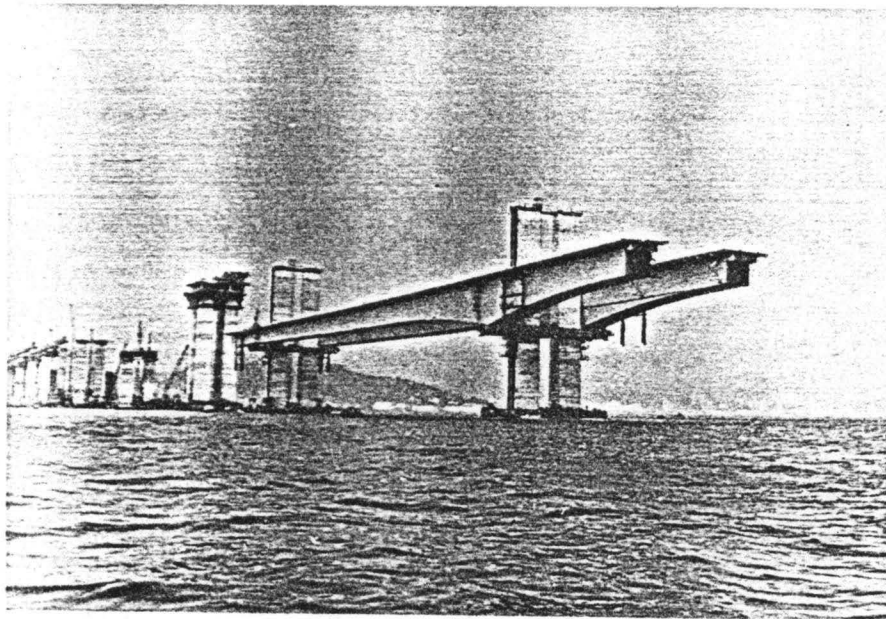




Fig. 1.4 Side Spans Being Jacked to Top of Piers

FIG. 1.5 PROJECT PROGRESS SCHEDULE

RESEARCH PHASE	ITEM *	1973					1974												1975					Est. % Compl.						
		A	S	O	N	D	J	F	M	A	M	J	J	A	S	O	N	D	J	F	M	A	M		J	J	A			
I ERECTION STRESSES	A. PLANNING & PREP.	1	100																											100
	B. INSTRUMENTATION & MEASUREMENTS	2, 3 & 4		100																										100
II COMPLETED BRIDGE	A. PLANNING & PREP.	1	80					90		100																				100
	B. INSTRUMENTATION	2, 3 & 4, 5		80																100										100
	C. STRESS MEAS.																													
	1. Controlled Load, Temp.	5																											100	
2. Normal Traffic & Temp.	6																											100		
III A. DATA REDUCTION		7				4		10	20	35	55	80	90	100															100	
	B. ANALYSIS	7, 8						5	10	25	40	60	80	90	100														100	
	C. REPORT PREPARATION	8							P																				100**	
OVERALL COMPLETION		3	8	11	16	19	22	28	32	36	40	45	50	55	60	65	70	75	80	84	88	92	94	96	98	100			100	

397.6

* Items in Exhibit A of Reference 1.5  Actual Effort P = Progress Report

** Actual completion of the Final Report was delayed till March 1976 due to errors found in computer program.  Planned F = Final Report

2. INSTRUMENTATION SYSTEMS

2.1 Types and Location of Instrumentation

The purpose of the instrumentation was to measure strain changes and temperature distribution in the bridge. Electric-resistance gages (strain and temperature), a mechanical gage and scratch gages were used to accomplish this. This instrumentation was installed in five cross sections in the Rio side span of the bridge near floor beams FB17, 27, 42, 51 and 57, as shown in Fig. 2.1.

With St. Venant's principle in mind, it was decided not to place the gages directly at the floor beams and transverse stiffeners. Instead the gages were placed 40 or 50 cm (approximately twice the spacing of longitudinal stiffeners) from the floor beams to avoid local disturbances. The decision to locate the gages at a particular cross section and on a specific side of a floor beam was based on the following reasons (Fig. 2.1):

FB17: This cross section, located at an end support, is subjected to a statically determinate moment which can be easily calculated. The gages were placed on the Rio side to take advantage of the static determinacy of the cantilever for both moment and shear.

FB27: This cross section was chosen because it has typical cross bracing. Also, it provided an opportunity to study temperature distribution on an average-depth cross section within the span and thus subjected

to the cooling effect of wind. The Niteroi side was chosen because of a cross-sectional splice on the other side that might have caused local disturbances. Also, a special internal bracket was temporarily installed on the Rio side to avoid load overstressing when the girders were transported on the pontoons.

FB42: Located near mid-span, this cross section experiences the greatest moment change while having small shear. This section, being without cross bracing, was selected because of its sensitivity to cross-sectional deformation and because of its usefulness in studying load distribution between the two box girders. Since a scaffold had to be built to monitor dynamic stresses at a splice in the orthotropic deck on the Rio side, it was decided to take advantage of the scaffold and place the gages there.

FB51: This cross section is located at the beginning of the haunch where non-linear normal stress distribution was expected. Not only temporary erection brackets but also a reinforcement truss caused local disturbance on the Rio side, thus the Niteroi side was chosen.

FB57: This cross section is the deepest (13.04 m) and is also located at an interior support. The haunch is the steepest and its effect on the stresses should be most pronounced. The large mass of the section and the reduced wind effect due to the piers under it

provide counterpart conditions to FB27 for temperature studies. The Rio side was selected so that the data could be correlated with the analysis of other sections under study in the span.

In addition to the instrumentation over the full cross section, electric resistance strain gages were placed at the splices of the orthotropic deck (orthotropic plate of the top flange) near FB17 and FB42 as indicated in Fig. 2.1 (labeled "Deck Gages"). These locations were selected because of the difference in the plate thickness -- 10 mm at FB17 and 16 mm at FB42.

A few electric resistance strain gages were placed on the reinforcement truss of the bottom flange in the north box, west of FB51 (towards Rio) as shown in Fig. 2.1.

A general view inside the north box is shown in Fig. 2.2. The instrumented section is the first one with the cross bracing and a transverse bottom girder containing oval pass-through openings (FB51). The cables hanging around the cross braces and those strung along the left wall are part of the instrumentation. A cat walk at the top was used in the installation and inspection of the electric gages and for taking readings with the mechanical gage.

2.2 Strain and Temperature Gages for Static Studies

An electric-resistance gage (strain or temperature) might be described as a short piece of thin wire which functions by changing its resistance. In the case of a strain gage, this happens when it is subjected to a stretching or a contraction of the material to which it is cemented; a temperature gage, on the other hand, is very little affected by straining but is sensitive to temperature variations. The resistance change is measured and converted to strain changes or temperature changes as applicable. Being the same in appearance and requiring the same method of installation and wiring, these two types of gages are described here together.

There were three configurations of strain gages: longitudinal - parallel to the girder axis - for measuring longitudinal strains (and thus stresses); transverse - perpendicular to the girder axis - mostly on the transverse framing members; and rosette - a combination of three linear gages oriented at 45° to each other - for measuring shearing and principal stresses.

Electric-resistance strain and temperature gages were installed in the five sections near FB17, 27, 42, 51 and 57, as shown in Fig. 2.1 by dashed lines. A sample of the positions of individual gages in a cross section is given in Fig. 2.3 (FB27). There are temperature gages (symbolized by triangles), longitudinal gages (circles) and three-gage rosettes (crosses). A number in an oval designates a cable, each cable serving two gages. A combined total for all five sections was 52 temperature and 305 strain gages (357 altogether) and their positions in the five sections are described in Appendix A.1.

The sequence of the static readings made with electrical gages is listed in Table 2.1. Each set of readings is identified by the trip number (see Art. 1.5) and the order of the set during that trip. The date, the starting time and an indicative description are also given in the table.

Three different methods were used in the making and recording of the electrical gage readings. During the transfer of the north box girder from the jetties to the piers in October 1975 (Readings Nos. 3.0 to 3.4 and construction stages "a" to "d" of Art. 1.3) the Datran unit was used and the readings were taken by hand. The Datran unit was housed temporarily in a wooden shack on the top flange of the girder at FB51, as indicated schematically in Fig. 2.4a. Since only $9\frac{1}{2}$ cables (19 gages) could lead from FB17 and 27 into one of the switching boxes connected to Datran -- the other box served the gages from FB42, 51 and 57 -- two switching soldering stations were established (indicated by boxes and brushes in Fig. 2.4a), one in a shack at FB27 and the other in the shack at FB51. The gages then were read in seven groups (a total of 226 gages in the north box).

In December 1973, during the lifting of the center span, reading Nos. 4.0 to 4.2 (construction stages "e" and "f" of Art. 1.3), the more sophisticated B&F unit was used as the data acquisition device. As shown in Fig. 2.4b, the B&F was stored in a shack on the deck and it recorded readings from both boxes automatically by means of a teletype. Since readings from the 357 gages were being taken and the B&F could only handle 100, switching soldering stations were again needed; this time they were placed inside the box at FB27 and FB51 as shown symbolically in Fig. 2.4b by panels and brushes.

Since the readings taken after December 1973 were on the completed structure (Readings during trips 5, 6 and 7) a truck was used to house the B&F unit (Fig. 2.4c). A set of plugs was installed in the concrete curb at FB51, and the truck could drive up for the B&F unit to be connected into the gaging system at any time. Switching at FB51 and FB27 inside the north box was necessary for these readings in the same manner as in December 1973. The wiring and switching system used during trip 7 remains on the bridge and the detailed description of it is given in Appendices A.2 and A.3.

2.3 Mechanical and Scratch Gages

2.3.1 Scratch Gages

Scratch gages provide a permanent and continuous record of the stress changes from the time the gage targets are installed until they are removed. Scratch gages are very convenient for use on bridges, since requiring no external data recording equipment, they do not interfere with construction operations or the normal flow of bridge traffic. Also, during the flotation stages of construction of the Rio-Niteroi bridge, when the boxes were completely sealed, other methods of continuous stress measurement were impractical, but the scratch gages, once installed, could be merely left in place for recording stresses during the whole construction sequence. Subsequent to construction, the scratch gages would have recorded any unusual occurrences such as pier settlement, ship impact, large equipment passing over the bridge, etc.

Eight (8) scratch gages were installed in the Rio-Niteroi bridge. Depending on the needs, the location of some gages was changed from one construction stage to another. For example, during the transfer of the north box from the jetties to the pontoon and then to the piers, scratch gages were installed on the outside surface of the top flange at FB27 and FB42, and later removed and installed inside the box for the stage of the center span lift. Other scratch gages were installed inside the box near the top and bottom flanges and left there.

In the completed structure, the scratch gages are located at FB17, FB27, FB42, FB57 and FB87 (middle of the center span), all inside the box. The position on the web, close to but not on the flanges, was dictated by convenience of installation, and a need to keep the gages from condensation water (or during construction, rain) which might accumulate at the bottom and from excessive vibration of the top flange due to traffic. The final position of each gage is listed in Fig. 2.5.

In subsequent text, scratch gages are identified by their location in the structure. For example FB27T means at floor beam 27 at the top of the web and FB27B at the bottom.

Since the initial installation in October 1973, the gages have recorded construction stress changes, test load stress changes, and thermal stress changes. A full summary of all scratch gage records (traces) is contained in Table 2.2. This table lists the period covered by each scratch gage target, its location in the bridge, and the type of trace obtained.

A scratch gage can be described as a steel strap having one end fixed to the structure surface under it, and the other free end bearing a brass ring. A scratch is made on the brass ring by a sharp point attached to the structure surface when the structure deforms due to stress or temperature changes. Since the strap is made of steel similar to the bridge members, the scratch gages are temperature compensating and record only the strains caused by the stresses produced by temperature or loads.

As shown in Fig. 2.6a (here only the portion to the right of the "riveted connection" is discussed), two base plates, one large A and one small B support other components of the scratch gage mechanism. (2.1) There are two bundles of thin steel wires, one long C, and one short D, and a scribe point E at the end of the scribe arm F. The right end of the long wire bundle C and the right end of the scribe arm F are mounted on the small base plate. The right end of the short wire bundle D is attached to the large base plate. Two small rollers G on the large base plate hold the left edge of the target H while allowing it to rotate. The target is a circular polished brass ring, 23.6 mm (0.93 in.) in diameter. The ends of the two wire bundles rest obliquely (pointing counterclockwise) in the peripheral groove of the target on the right side and press it against the rollers. The scribe point bears down on the face of the target ring.

The small base plate and the extension strap (to which the large base plate is riveted) are attached to the structure to be investigated by "attachment screws". As the structure deforms (undergoes a change in strain) in the direction of the gage, the two base plates move relative to one another. When they move away from each other as a result of tensile deformation, the scribe point scratches an approximately radial trace on the target surface. At the same time the long wire bundle C is retracted and its tip slides back (clockwise) in the target groove while the tendency of the target to rotate along with the bundle tip is prevented by the short wire bundle D.

When the base plates move toward each other due to a compressive deformation, the scribe point moves radially on the target surface, but the target in this case does not remain stationary -- it rotates counterclockwise -- being pushed by the tip of the long wire bundle. The short bundle in this case does not resist rotation. The result is that the scratched trace on the target surface is at an angle of 45° with respect to the target radius.

When another tensile deformation is imposed, and the gage bases move apart, another radial scratch is recorded resulting in a continuous zig-zag trace.

The distance between the attachment screws is the gage length. It is divided into the length of the scratch in computing the strains. However, to improve the sensitivity, the gage length is usually increased by attaching the left end of the large base plate A to a steel strap whose far end is then connected to the structure as shown in Fig. 2.6a.

The scratch gages installed in the bridge originally (October and December 1973), had a gage length of 30.5 cm (Fig. 2.6a). This was an optimum gage length for the expected construction stress changes of the order of 2500 kg/cm^2 (35 ksi). Stress changes in the completed bridge were much smaller (0 to 525 kg/cm^2), and it was desirable to increase the gage sensitivity. This was accomplished in January 1975 by bolting additional extension straps to the original ones. In this manner, all gage lengths were increased to 100 cm (Fig. 2.6b), with the exception of FB57T, where the length could only be increased

to 90 cm due to an obstruction (See Fig. 2.5). A supporting screw placed under the edge at midpoint prevented flapping of the long extension straps.

The scratch zig-zag traces made by the gage on the targets vary from approximately 0.025 mm to 0.25 mm in amplitude. Obviously, they can only be measured using some form of magnification. Also, some method of permanently recording the traces is necessary. An optical microscope system was tried, but it proved unsatisfactory. However a scanning electron microscope (SEM) gave excellent results. The advantages of the SEM are as follows: (1) a large observation area for scanning the target to aid in finding the scribe marks, (2) good depth of high resolution field which made it easier to determine where on the target the scribe may have made several passes caused by several stress changes occurring without advancement of the target, (3) a magnification variable to any power, and (4) a permanently affixed polaroid camera.

Analysis of the scratch gage traces was made from the photographs. A trace, like a typical one shown in Fig. 2.7, goes from left to right and each vertical "zig" (radial on the target) indicates a tensile stress change while a slanted "zag" going up to the right indicates a compressive stress change. The stress change for a particular "zig" or "zag" is computed from

$$\Delta\sigma = \frac{AE}{GM} \quad (2.1)$$

where $\Delta\sigma$ = stress change

A = vertical (radial) amplitude of the "zig" or "zag"

E = modulus of elasticity of steel ($E = 2.1 \times 10^6$ kg/cm²)

G = gage length

M = magnification factor of the photograph

Two considerations must be kept in mind when analyzing the record on a scratch gage target. Although the target contains a complete stress history for the period from target installation to removal, the initial stress condition of the member at the time of target installation, although not known, serves as the "zero" stress condition of the scribe point on the target. Secondly, stress changes below a certain level will not result in target advancement (rotation) due to a slight slack in the long wire bundle (driver bundle). As a result, the radial back and forth motion of the scribe point will produce a small polished area until a compressive stress change, greater than this critical level, forces the target to rotate. According to literature (2.1), the critical stress level should be 300 kg/cm² (4.3 ksi) for the 30.5 cm (12 in.) gage length and 100 kg/cm² (1.4 ksi) for the 100 cm gage length. Some gages, however, have proven to be substantially more sensitive.

A sample stress change computation is shown in Fig. 2.7. The trace is a record of the construction stress changes in the north box at FB42B. During the transfer of the girder from the jetties to the pontoon, FB42B underwent a compressive stress change causing the scratch gage scribe to move from a position at the bottom left hand

side of the photograph to the top center position. The radial (perpendicular to the circumferential groove lines on the target) distance between the two points is 7.1 cm. With the magnification factor of 215 and the gage length of 30.5 cm, Eq. 2.1 yields a stress change of 2250 kg/cm^2 . A similar procedure was followed in computing all stress changes recorded on the scratch gage targets.

2.3.2 Mechanical Gage System

The mechanical gage system is a system of data acquisition in which the distance between two target holes predrilled at a series of locations in the bridge girder is measured by means of a special gage (mechanical gage). The difference between two readings taken at a particular location divided by the original distance between the two target holes gives the strain change produced by the change in loading between these readings.

The mechanical gage system does not provide a continuous recording of strain changes as do the scratch gages. However, the readings are more accurate and the target holes require less maintenance. Also, only one gage is used for readings at many locations whereas a separate scratch gage is needed for each location. The advantage of the mechanical gage system over the electric gage system is that no external data recording equipment is required and that the readings from different time periods can be directly compared for establishing a stress history.

Mechanical gage readings were taken at all instrumented sections (except FB87) on both the north and south boxes at the locations indicated in Figs. 2.8 and 2.9. The sequence of the readings and the locations measured each time are listed in Table 2.3. A total of ten sets were made covering the three stages of construction and several times after completion.

The mechanical gage consists of two conical points connected to a leverage mechanism which transmits the relative motion between the points to a dial gage for measurement.* As shown schematically in Fig. 2.10a, the points are inserted into the holes predrilled in the structure. The holes were drilled using special drill bits which made a beveled shoulder on each hole perimeter so that the line of contact would not be susceptible to damage. (See the detail of Fig. 2.10a.) The holes were also filled with grease and covered with adhesive tape to inhibit rusting during the intervals between readings.

At fifteen of the locations, temperature compensating bars (Fig. 10b) were attached with Epoxy cement in close vicinity of the gage holes. Asterisks in Table 2.3 indicate the locations where compensating bars were read. The difference of strains in the structure and in the compensating bars gives the strain which produces stresses.

To take measurements, the conical points of the gage were fitted into the holes. The points are angled more sharply than the

*The mechanical gage used was manufactured by Jean Marion Construitor, DILATO, 67 Rue de Peuilley, Paris. The gage had a length of 20 cm.

beveled shoulders, thus they contact the shoulders only on a circular plane (Detail of Fig. 10a). After the dial gage was read, the gage was taken out, turned around and the procedure repeated. This was repeated so that three or four readings were taken at each location and then averaged.

An Invar bar is provided with the mechanical gage. The bar does not change its length with temperature changes, and it was measured several times during each period of readings, providing a correction factor for any change in the zero adjustment of the dial gage from one period to another.

The data reduction procedure for mechanical gage readings at a particular location is summarized by the following formulas; the first equation giving the change in strain where temperature compensating bars were read:

$$\Delta\epsilon_{i,i+1} = \frac{1}{G} \{ (R_{i+1} - CB_{i+1}) - (R_i - CB_i) \} \quad (2.2)$$

At locations where temperature compensating bars were not read, the following equation was used:

$$\Delta\epsilon_{i,i+1} = \frac{1}{G} \{ (R_{i+1} - IR_{i+1}) - (R_i - IR_i) \} \quad (2.3)$$

where:

R_i = The reading between gage holes on the structure for the i -th reading period.

CB_i = The reading between gage holes on the compensating bar for the i -th reading period.

IR_i = The reading between gage holes on the Invar bar for the i -th reading period.

R_{i+1} , CB_{i+1} , IR_{i+1} are the respective readings for the $(i+1)$ th reading period.

G = gage length (20 cm)

An alternative equation can be used to compute the strain change produced only by stress change:

$$\Delta\epsilon_{i,i+1} = \frac{1}{G} \{ (R_{i+1} - IR_{i+1}) - (R_i - IR_i) \} - \alpha_T (T_{i+1} - T_i) \quad (2.4)$$

where T_{i+1} = temperature at the $(i+1)$ th reading period and T_i = temperature at the i -th reading period.

2.4 Strain Gages For Stress History (Traffic) Studies

2.4.1 Strain Gages

Electrical resistance strain gages were mounted on the underside of the orthotropic deck near floorbeams 17 and 42 as shown in Figs. 2.11 to 2.14.

Figure 2.11 shows a layout of the gages as viewed from the underside of the deck with web A to the left and floorbeam 17 near the bottom. Traffic from Niteroi to Rio therefore travels from bottom to top of the figure. The gages were placed in groups along three cross-sections A, B and C as shown in the figure. The cross-sections, gages and gage numbering system are shown in Fig. 2.12 for floorbeam 17. The cross-sections in Fig. 2.12 are oriented so that Niteroi to Rio traffic is travelling towards the viewer and web A is to the left. Figures 2.13 and 2.14 are similar to Figs. 2.11 and 2.12 but show the layout of the gages near floorbeam 42.

The two floorbeam locations (17 and 42) were selected primarily to provide strain readings for two different deck plate thicknesses. The plate thickness at floorbeam 17 was less than that at floorbeam 42.

Each of the gage locations shown in Figs. 2.11 to 2.14 was selected on the basis of one of the following criteria: (1) to provide representative strain data on the cross section of the orthotropic deck, (2) to obtain strain data in the vicinity of the splice plates located on the sides and bottom of some of the trapezoidal stiffeners and (3) to show strains adjacent to a floorbeam and web location.

The type and direction of all strain gages are also shown in Figs. 2.11 to 2.14 and Table 2.4. Most are single strain gages mounted either on the deck plate or on the trapezoidal stiffeners and oriented transverse to the direction of traffic. At each floorbeam location three single gages were mounted on the bottom of the trapezoidal stiffeners and oriented parallel to the direction of traffic. In addition, several rosette strain gages were placed at locations shown in the figures.

All gages are $\frac{1}{4}$ in. long electrical resistance foil gages. Weather-proof coatings were applied to provide long term protection of the gages from moisture and the interior environment of the box girders. A quarter-bridge, three-wire hookup was used, which automatically provided lead-in wire and temperature compensation to all gages.

2.4.2 Strain Recording System

Strain variations due to test truck and vehicular loading on the deck were recorded by an ultraviolet oscillograph trace recorder which provided up to ten analog traces on light sensitive paper. A typical analog trace is shown in Fig. 2.15 in which the strain variations for 10 gages are recorded during the passage of a vehicle over the deck near floorbeam 17. Only truck traffic and other large vehicles were recorded. Passenger automobiles and small vehicles such as panel trucks were excluded from the recorded traffic because the strains generated by these vehicles were observed to be very low.

2.4.3 Traffic Identification and Location

In order to correlate truck traffic over the deck near floorbeam 17 with the recorded strains the type of truck producing each particular strain record was visually observed and recorded. The truck type was recorded using both the DNER classifications shown in Table 2.5 and the USA system shown in Table 2.6. This was done for all strain records during May and June 1974. In addition, the 120 trucks recorded on May 30, 1974 (See Table 2.7) were photographed as they were about to pass over the orthotropic deck near floorbeam 17. A typical photograph is shown in Fig. 2.16. The deck markings appearing in the figure were used to determine the location of each of the 120 trucks in relation to the gages near floorbeam 17.

A layout of the deck markings is shown in Fig. 2.17. The graduated strip transverse to the direction of traffic is directly over floorbeam 17. The long narrow strip parallel to the traffic is over Web A. The long wide strip parallel to the traffic is one of the middle lane markers. The 5 small crosses shown in the figure are located directly above the approximate midpoint of each of the 5 groups of gages shown in Fig. 2.11

2.4.4 Strain Recording Periods

The chronological records of strain data acquisition are shown in Table 2.7 for the two intervals of time that tests were made on the bridge deck.

During the February 1974 field study strain magnitudes from 6 gages at floorbeam 17 and 6 gages at floorbeam 42 were recorded for each test truck run over and off the plank runways. No traffic was recorded since the bridge was not open to traffic until March 4, 1974. Strains were first recorded at these two locations under the static test loads described in Art. 3.3. Strains from 33 gages at floorbeam 17 and 36 gages at floorbeam 42 were recorded during the static tests. Following the static test loading of the bridge one of the test trucks was used to obtain strain magnitudes at the two locations under crawl and speed run conditions on and off the runways. On the basis of the strain records, floorbeam 17 was selected for the major stress history study in May and June 1974. During the second test period a total of 18 hours of strain data were acquired at the floorbeam 17 location over a 5 day period for use in the stress analysis reported in Chapter 6. This included data from vehicular truck traffic plus crawl and speed runs of the test truck. No data was recorded at the floorbeam 42 location at this time.

Strain magnitudes from all 33 gages at floorbeam 17 were initially recorded during the passage of 120 truck type vehicles. The bridge was open to traffic during this study. The 120 trucks were therefore selected from normal vehicular traffic. Due to the limitation of the oscillograph recorder, three groups of data were needed in order to sample the 33 gages. Strain magnitudes at all gages were also recorded during crawl runs of the test truck which are described in Art. 6.1.2.

The strains at all gages resulting from the 120 trucks described above were examined for magnitude. Seventeen gage locations at floorbeam 17 having the largest strain magnitudes were selected for the remaining stress history studies described in Chapter 6. The strains from these 17 gages were recorded in two groups using the oscillograph recorded.

2.4.5 Traffic Count Record

A continuous count of all bridge traffic on an hourly basis, 24 hours per day and 7 days per week, is recorded by DNER from toll booth information. This record was made available by DNER for the period March 4, 1974 to May 31, 1975 for the statistical evaluation reported in Chapter 6.

2.5 Chapter 2 - Tables and Figures

Table 2.1: Sequence of Electrical Gage Static Readings

TRIP	READING NUMBER	DATE	START TIME	DESCRIPTION
1	1	17Jul73		No readings during this trip
2	2	03Sep73		No readings (Installation of Instrumentation)
3	3.0	08Oct73	16:10	Side span on jetties
	3.1	09Oct73	13:00	Side span on jetties
	3.2	10Oct73	00:20	Side span on pontoon
	3.3	11Oct73	22:25	Side span on pontoon
	3.4	12Oct73	05:50	Side span on pier rings
4	4.0	12Dec73	00:36	Pontoon in water
	4.1	13Dec73	09:30	Pontoon suspended (day)
	4.2	13Dec73	20:40	Pontoon suspended (night)
5	5.0	25Feb74	06:45	Zero readings - test loads
	5.1	24Feb74	22:52	Load position 1
	5.2	25Feb74	03:25	Load position 2
	5.3	25Feb74	20:36	Zero reading - test loads
	5.4	25Feb74	23:58	Load position 3
	5.5	26Feb74	02:35	Load position 4
	5.6	26Feb74	14:15	Temperature study
5.7	27Feb74	11:05	Temperature study	
6	6.1	10Jun74	08:56	Temperature study
	6.2	11Jun74	07:50	Temperature study
7	7.1	16Jan75	23:00	Temperature study

North Box

Table 2.2 Listing of Scratch Gage Records









SCRATCH GAGE TARGETS					
No.	STATION (Longitud. Location)	PERIOD From - To	PATTERN		COMMENTS
1	2	3	4	5	6
1	FB27 -Bot.	OCT73 -14DEC73		**	Good record: Jetties-pontoon-piers- pontoon lift
2	FB27 -Top	OCT73 -02DEC73		**	Good record: Jetties-pontoon-piers
3	FB42 -Top (outside)	OCT73 -02DEC73		**	Good record: Jetties-pontoon-piers (Gage may have been jarred causing scratch irregularity)
4	FB17 -Top	14DEC73 -28FEB74			No scratch on target, only some dots
5	FB17 -Bot.	14DEC73 -28FEB74			No scratch on target
6	FB27 -Bot.	14DEC73 -28FEB74		*	Faint blob
7	FB42 -Top	OCT73 -28FEB74		**	Good record: Jetties-pontoon-pier- pontoon lift
8	FB42 -Bot.	OCT73 -28FEB74		**	Good record: Jetties-pontoon-pier- pontoon lift-parapet placement-test loads (also recorded daily thermal stress changes)
9	FB57 -Top	14DEC73 -28FEB74		*	Line of small scratch marks recorded on tar- get-apparently the result of daily ther- mal stress changes
* - Approximate magnification = 50 ** - Approximate magnification = 300					

Table 2.2 (Cont. 1) Listing of Scratch Gage Records







SCRATCH GAGE TARGETS (Page 2)					
No.	STATION (Longitud. Location)	PERIOD From - To	PATTERN		COMMENTS
1	2	3	4	5	6
10	FB57 -Bot.	14DEC73 -28FEB74		*	Target advancement and compressive scratch recorded, but angle appears too flat and scratch may have resulted from a jarring of the gage
11	FB87-Top (Center span)	22FEB74 -28FEB74			No scratch on target
12	FB17 -Top	28FEB74 -06JUN74			No scratch on target
13	FB27 -Bot.	28FEB74 -06JUN74		**	No scratch, only some blobs
14	FB42 -Top	28FEB74 -06JUN74		**	Scratch probably a result of other than bridge stress changes (possibly a jarring of the target)
15	FB42 -Bot.	28FEB74 -06JUN74		**	Good results: thermal stress changes subsequent to test loadings
16	FB57 -Top	28FEB74 -06JUN74			No scratch on target
17	FB57 -Bot.	28FEB74 -06JUN74		**	Small blob - no target advancement
18	FB87 -Top	28FEB74 -06JUN74		**	Small blob - no target advancement
<p>* - Approximate magnification = 50 ** - Approximate magnification - 300</p>					

Table 2.2 (Cont. 2) Listing of Scratch Gage Records


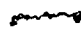





SCRATCH GAGE TARGETS (PAGE 3)					
1	STATION (Longitud. Location)	PERIOD From - To	PATTERN	5	COMMENTS
1	2	3	4	5	6
19	FB17 -Top	6JUN74 -10JAN75			No scratch on target
20	FB27 -Bot	6JUN74 -10JAN75		*	Good record: Daily thermal stress changes. Approximately 80 separate zigs
21	FB42 -Top	6JUN74 -10JAN75		*	Weak trace.
22	FB42 -Bot	6JUN74 -9JAN75		*	Good record: Daily thermal stress changes. Approximately 130 separate zigs.
23	FB42 -Bot	11JAN75 -15JAN75		**	Good record: 5 thermal stress changes recorded. (Gage extension in place)
24	FB57 -Top	6JUN74 -9JAN75		**	16 separate zigs. Gage appears to have operated properly for only 2 weeks
25	FB57 -Bot	6JUN74 -8JAN75			No scratch on target
26	FB57 -Bot	10JAN75 -14JAN75		**	Jumble of scratches. (Gage extension in place)
27	FB87 -Top	6JUN74 -11JAN75		**	Small scratch. No target advancement
* - Approximate magnification = 50 ** - Approximate magnification = 200					

Table 2.2 (Cont. 3) Listing of Scratch Gage Records


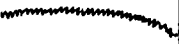





SCRATCH GAGE TARGETS (Page 4)					
No.	STATION (Longitud. Location)	PERIOD From - To	PATTERN		COMMENTS
1	2	3	4	5	6
28	FB17 -Bot	15JAN75 -19JUN75		*	Daily thermal stress changes recorded, but slow target advancement
29	FB27 -Top	17JAN75 -9JUN75		*	Daily thermal stress changes recorded
30	FB27 -Bot	15JAN75 -19JUN75		*	Daily thermal stress changes recorded, but target surface is corroded
31	FB42 -Top	15JAN75 -9JUN75			No scratch on target
32	FB42 -Bot	16JAN75 -9JUN75		*	Good record: Daily thermal stress changes.
33	FB57 -Top	15JAN75 -9JUN75			One blob, no advancement
34	FB57 -Bot	15JAN75 -9JUN75		**	Irregular trace, scribe slipped off
35	FB87 -Bot	16JAN75 -19JUN75		**	Series of blobs (Target corroded)
* - Approximate Magnification = 50					
** - Approximate Magnification = 200					
NOTE: Gage Extensions in Place at all Locations.					

Table 2.3 Reading Periods of Mechanical Gage

General Reading Period Number	Mech. Gage Reading Number	Date and Start Time	Loading Condition	Locations Read (Refer to Figs. 2.8, 2.9)
1	2	3	4	5
3	1	27SEP73 5:00	Stat. Det. on Jetties	6,7,8,6b,8b,14,15,16,14b,15b, 16b,20,21,20b,21b,27,28,28b, 35,36,34b,36b
3	2	30OCT73 1:00	Stat. Det. on Jetties	1,3,5,9,11,13,17,18,19,22, 24,26,31,33
3	3	30OCT73 3:00	Stat. Det. on Pontoon	6,7,8,14,15,16,20,21,27,28, 35,36
3	4	40OCT73 11:00	Stat. Det. on Pontoon	6,7,8,14,15,16,20,21,27,28, 35,36
3	5	50OCT73 4:00	Stat. Det. on Rings	6,7,8,14,15,16,20,21,27,28, 35,36
3.3	6	11OCT73 23:30	Stat. Det. on Pontoon	1,3,5,9,11,13,17,18,19,22, 24,26,31,33
3.4	7	12OCT73 5:00	Stat. Det. on Rings	1,3,5,9,11,13,17,18,19,22, 24,26,31,33
4.0	8	11DEC73	Stat. Det. on Piers Center Span in Water	1a,3a,5a,9a,11a,13a,11b*, 12b*,13b*,17a,18a,19a,17b*, 18b*,19b,22a,24a,26a,22b, 23b,24b,25b,29a,30a,31a,32a, 33a,29b*,30b*,32b,33b*
4.1	9	13DEC73 14:00	Stat. Det. on Piers Center Span out of water	1a,3a,5a,9a,11a,13a,11b*, 12b*,13b*,17a,18a,19a,17b*, 18b*,19b,22a,24a,26a,22b, 23b,24b,25b,29a,30a,31a, 32a,33a,29b*,30b*,32b,33b*

*Asterisks indicate locations where temperature compensating bars were read.

Table 2.3 (Cont.) Reading Periods of Mechanical Gage

General Reading Period Number	Mech. Gage Reading Number	Date and Start Time	Loading Condition	Locations Read (Refer to Fig 2.8,2.9)
1	2	3	4	5
Between 5 and 6	10	28MAR74 16:00 (NORTH) 1APR74 (9:00) (SOUTH)	Stat. Indet.	1a, 1b, 2b, 3b, 5b, 6b, 8b, 9a, 11a, 13a, 9b*, 10b*, 11b*, 12b*, 15a, 14b, 15b, 16b, 17b*, 18b*, 19b, 20a, 21a, 20b, 21b, 22a, 24a, 26a, 22b, 23b, 24b, 25b, 28b, 29a, 30a, 31a, 32a, 33a, 29b*, 31b*, 33b*, 34a, 36a, 36b
6.2	11	11JUN74 14:00	Stat. Indet.	1a, 2a, 3a, 4a, 5a, 1b, 2b, 3b, 5b, 9a, 11a, 13a, 9b, 10b, 11b, 12b, 17b, 18b, 19b, 22a, 24a, 26a, 22b, 23b, 24b, 25b, 29a, 30a, 31a, 32a, 33a, 29b, 30b, 31b, 33b
7.1	12	14JAN75 8:30 (NORTH) 15JAN75 14:00 (SOUTH)	Stat. Indet.	1a, 3a, 5a, 1b, 3b, 5b, 6a, 7a, 8a, 6b, 8b, 9a, 11a, 13a, 11b*, 13b, 15a, 14b, 16b, 17a, 18a*, 19a*, 18b*, 19b*, 20a, 21a, 20b, 21b, 22a, 24a, 26a, 24b, 25b, 26b, 29a, 30a, 31a, 32a, 33a, 33b*, 35a, 36a, 36b
After 7	13	19JUN75 10:00	Stat. Indet.	1a, 2a, 3a, 4a, 5a, 1b, 3b, 5b, 9a, 11a, 13a, 9b*, 10b*, 11b*, 12b, 13b*, 17a, 19a, 17b, 19b*, 22a, 26a, 23b, 25b, 29a, 31a, 33a, 29b, 31b, 32b*, 33b*

*Asterisks indicate locations where temperature compensating bars were read.

Table 2.4 Gage Types and Locations on Deck at FBI7

Lane	Transverse Section	Gage Number	Gage Type	Gage Location	
CURB	A-A	24	Single	Deck - between stiffeners	
		25*	Single	Deck - between stiffeners	
		26	Single	Side of stiffener	
		27*	} Rosette	Deck { transverse 45°	
		28			} longitudinal
		29			
		30	} Rosette	Web { horizontal 45° vertical	
		31			
	32*				
	B-B	14	Single	Deck - between stiffeners	
		15*	Single	Deck - beside stiffener	
		16*	Single	Side of stiffener	
		17*	Single	Deck - beside stiffener	
18*		Single	Side of stiffener		
33*		Single	Bottom of stiffener		
MIDDLE	A-A	19*	Single	Deck - beside stiffener	
		20*	Single	Side of stiffener	
		21*	Single	Deck - beside stiffener	
		22*	Single	Side of stiffener	
		23	Single	Deck - between stiffener	
	B-B	6	Single	Bottom of stiffener	
		7*	Single	Side of stiffener	
		8*	Single	Deck - beside stiffener	
		9*	Single	Deck - beside stiffener	
		10*	Single	Side of stiffener	
		11	} Rosette	Deck { longitudinal 45° transverse	
		12			
		13			
	C-C	1	} Rosette	Deck { longitudinal 45° transverse	
		2			
3					
4		Single	Web of floorbeam 17-vertical		
5*		Single	Bottom of stiffener		

*Gage used during random traffic study May-June 1974 (see Art. 6.4)

Table 2.5 DNER Vehicle Classification








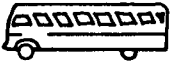
Cate- gory	No. of Axles	
1	2	
2	2	
3	3	
4	3	
5	4	
6	5	
7	6	
8	2	

Table 2.6 USA Truck Classification


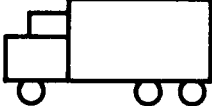
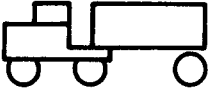

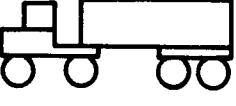
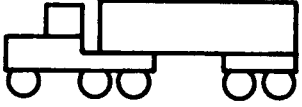
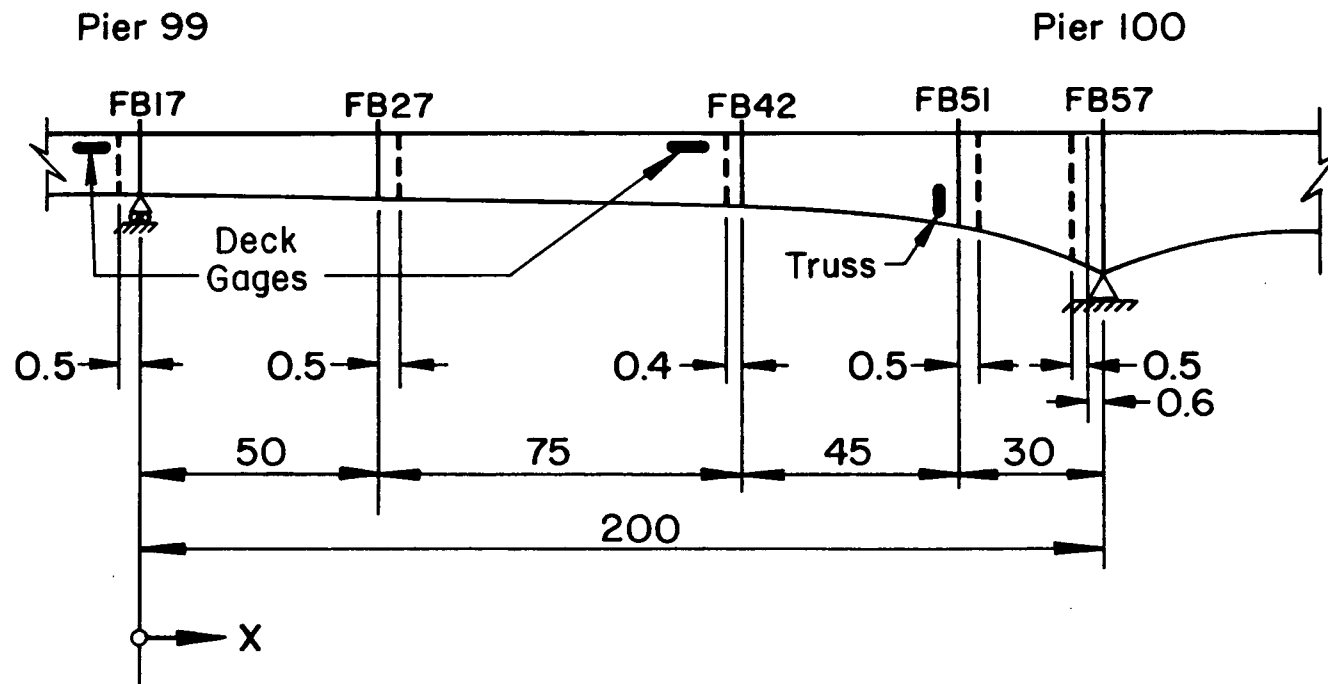
Category	Number of Axles	
B		BUS
2D	2	
3	3	
2S-1	3	
4	4	
2S-2	4	
3S-2	5	

Table 2.7 Chronological Record of Strain Data Acquisition

Date (1974)	Traffic Status	Period	Interval (Hours)	No. of Vehicles Recorded
Feb. 25	None	3:00 pm - 4:00 pm	1.0	Test Truck
May 30	Normal	11:00 am - 4:30 pm	5.5	120
May 31	Normal	1:30 pm - 4:00 pm	2.5	117
June 3	None	9:30 am - Noon	2.5	Test Truck Crawl Runs
June 3	Normal	2:30 pm - 4:30 pm	2.0	120 plus Seven Test Truck Speed Runs
June 4	Normal	9:30 am - Noon	2.5	105
June 4	Normal	2:30 pm - 4:30 pm	2.0	117
June 5	Normal	10:00 am - 11:00 am	1.0	63 plus Seven Test Truck Speed Runs



Dashed Lines Indicate Location Of Instrumented Sections
All Dimensions In Meters

Fig. 2.1 Location of Instrumented Sections
in Rio Side Span

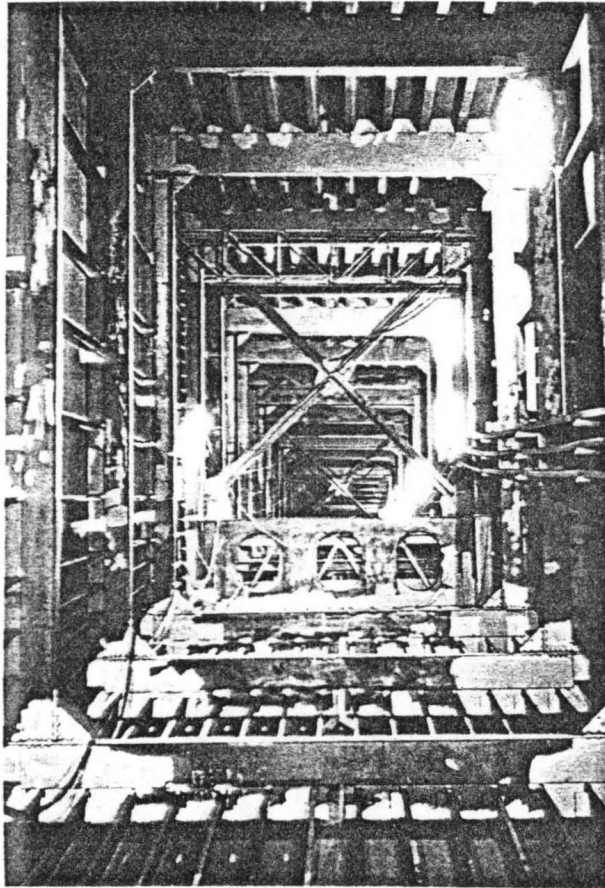


Fig. 2.2 View Inside North Box and of Instrumented Section at FB51 (First Section with Cross Bracing and Oval Holes in Transverse Girder)

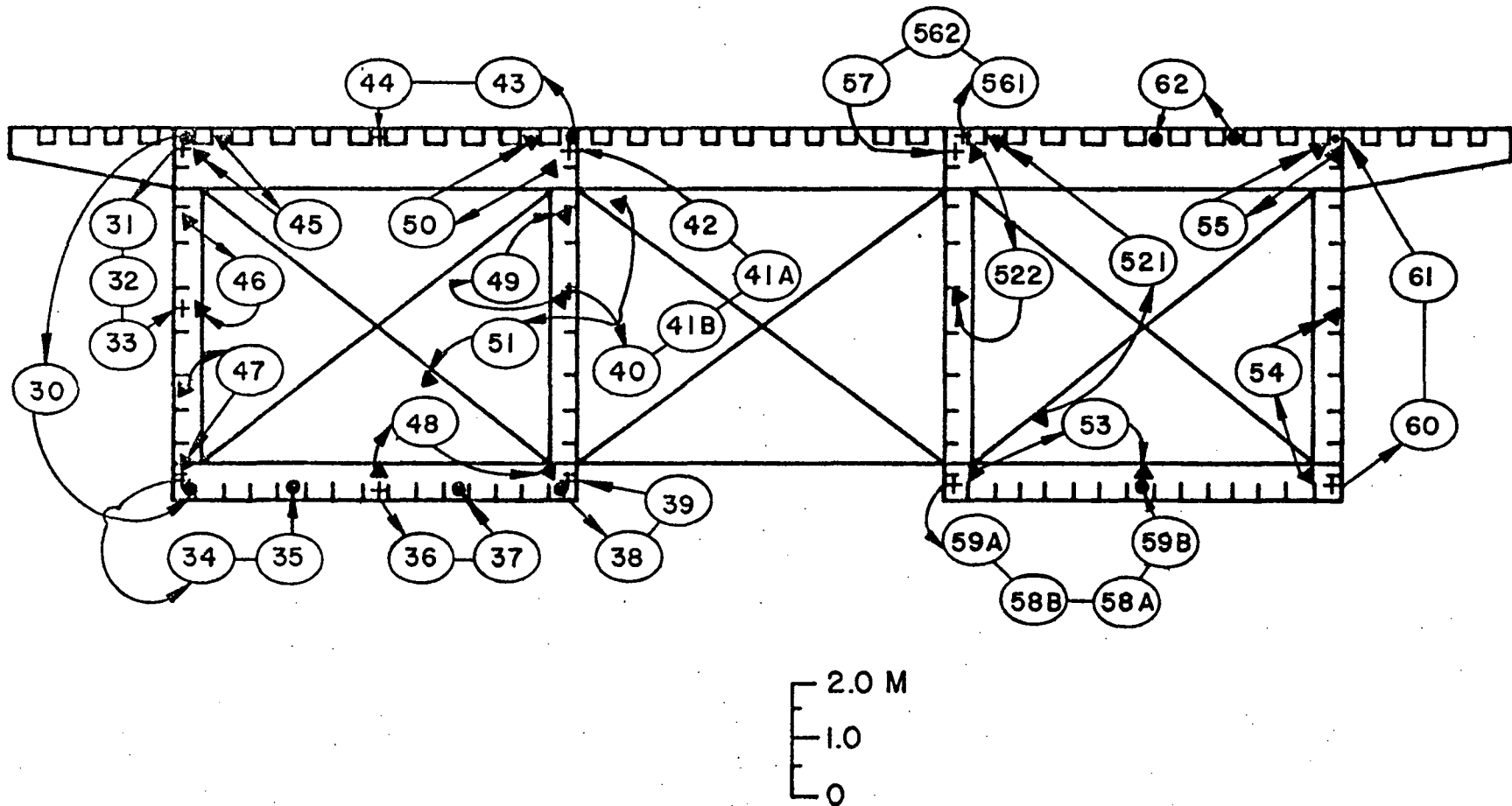
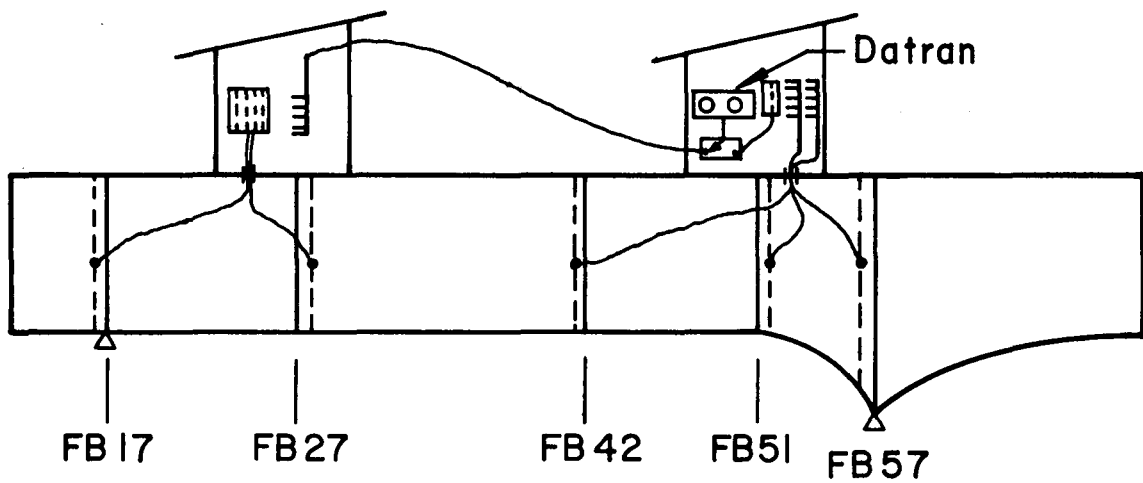
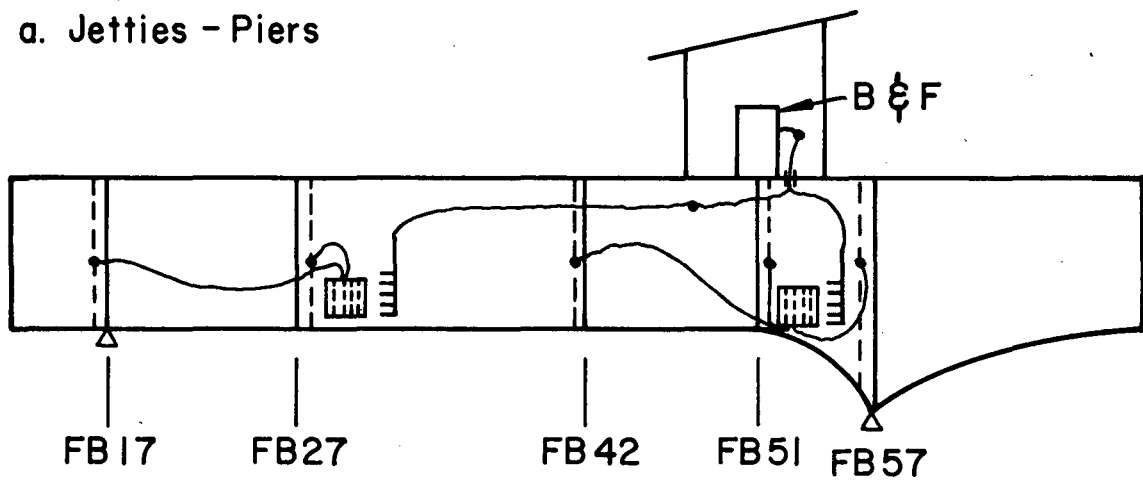


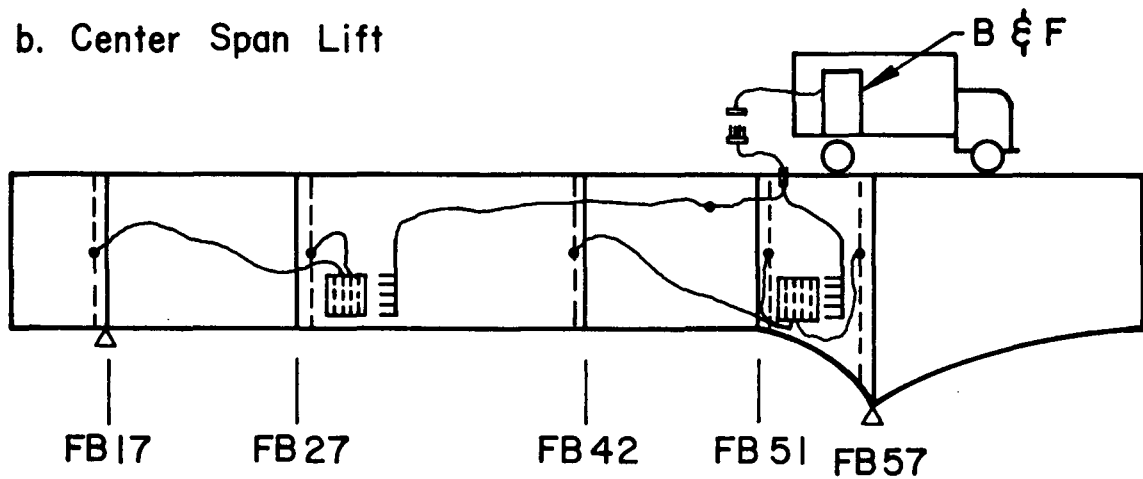
Fig. 2.3 Sample of DiStribution of Strain and Temperature Gages in a Cross Section (FB27)



a. Jetties - Piers

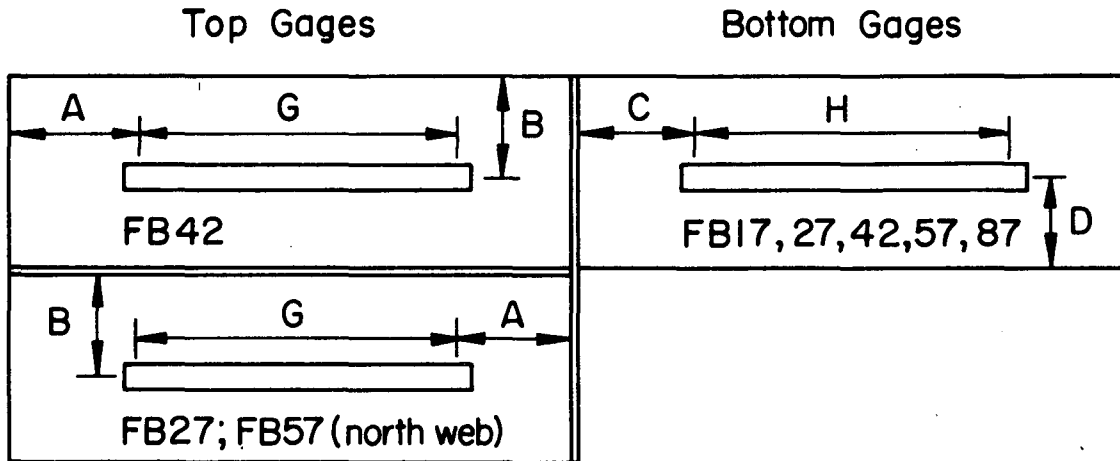


b. Center Span Lift



c. Completed Bridge

Fig. 2.4 Strain Gage Wiring Systems on Rio Side Span



	TOP GAGES			BOTT. GAGES		
	A	B	G	C	D	H
FB17	-	-	-	40.0	32.0	100.0
FB27	25.0	26.5	100.0	23.0	20.0	100.0
FB42	30.0	15.5	100.0	20.0	26.0	100.0
FB57	25.0	31.0	90.0	31.5	20.0	100.0
FB87	-	-	-	21.0	25.0	100.0

All Dimensions In cm.

All gages on south web, except as noted.

A = Distance from attachment screws to floor beam

B = Distance from center of gage to top flange

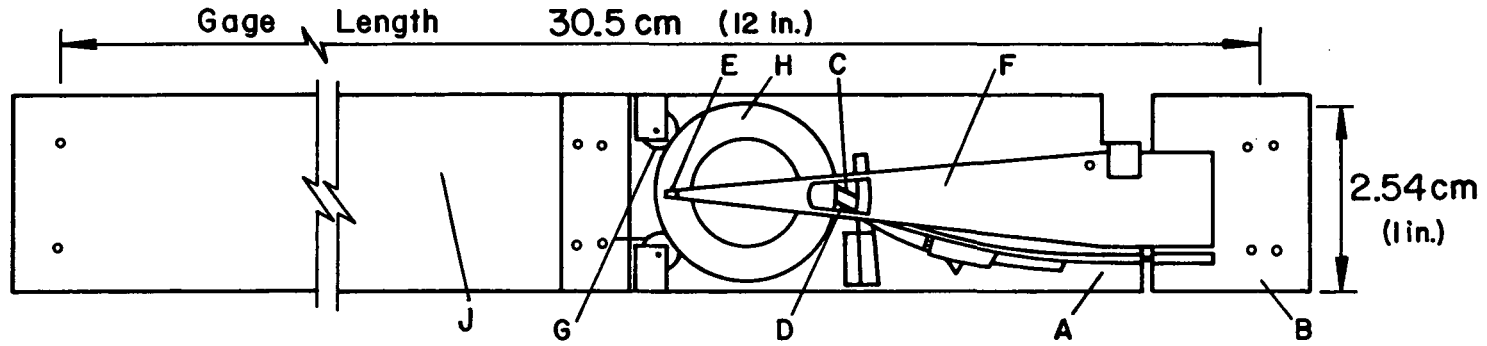
C = Distance from attachment screws to floor beam

D = Distance from center of gage to bott. flange

G = Gage length

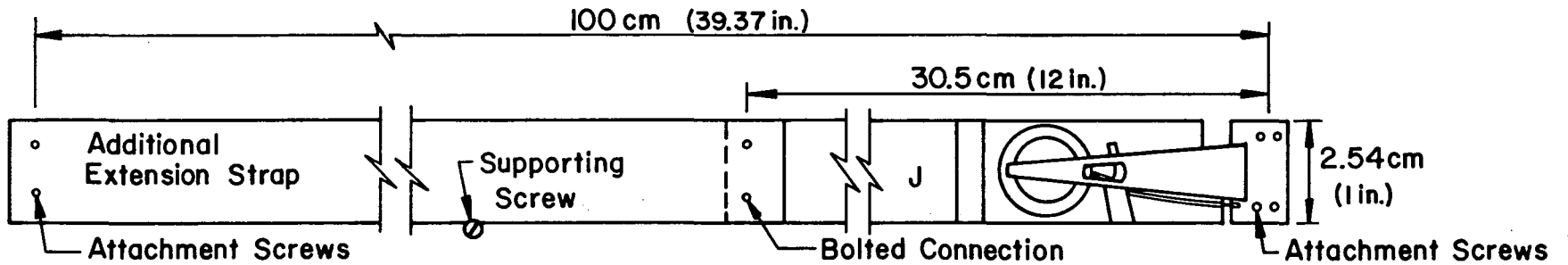
H = Gage length

Fig. 2.5 Location of Scratch Gages



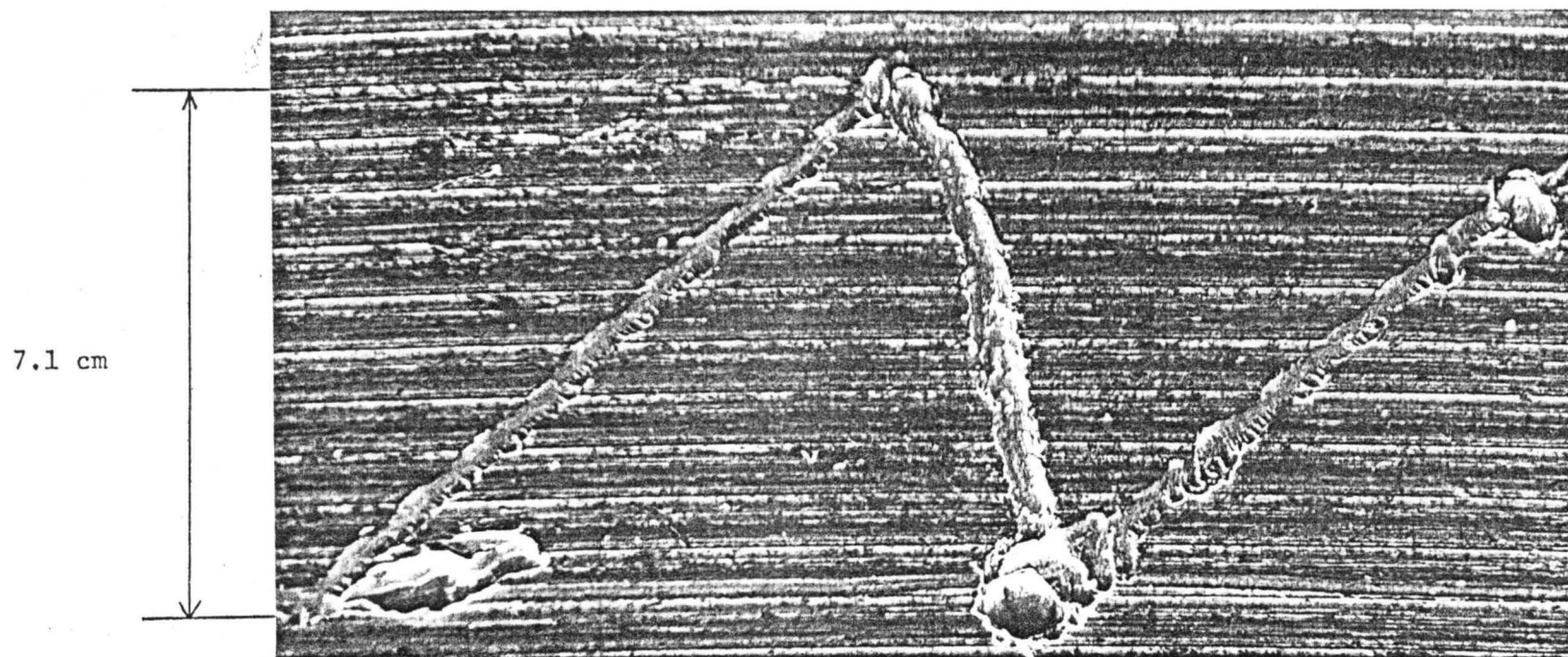
- | | | | |
|---|------------------|---|-----------------|
| A | Large Base Plate | E | Scribe Point |
| B | Small Base Plate | F | Scribe Arm |
| C | Driver Brush | G | Rollers |
| D | Retainer Brush | H | Target |
| | | J | Extension Strap |

(a)



(b)

Fig. 2.6 Scratch Gage Mechanism



$$\Delta\sigma = \frac{AE}{MG} = \frac{(7.1 \text{ cm})(2.1 \times 10^6 \text{ kg/cm}^2)}{(215)(30.5 \text{ cm})} = 2250 \text{ kg/cm}^2$$

FIG. 2.7 SAMPLE COMPUTATION OF STRESS CHANGE FROM SCRATCH GAGE TRACE

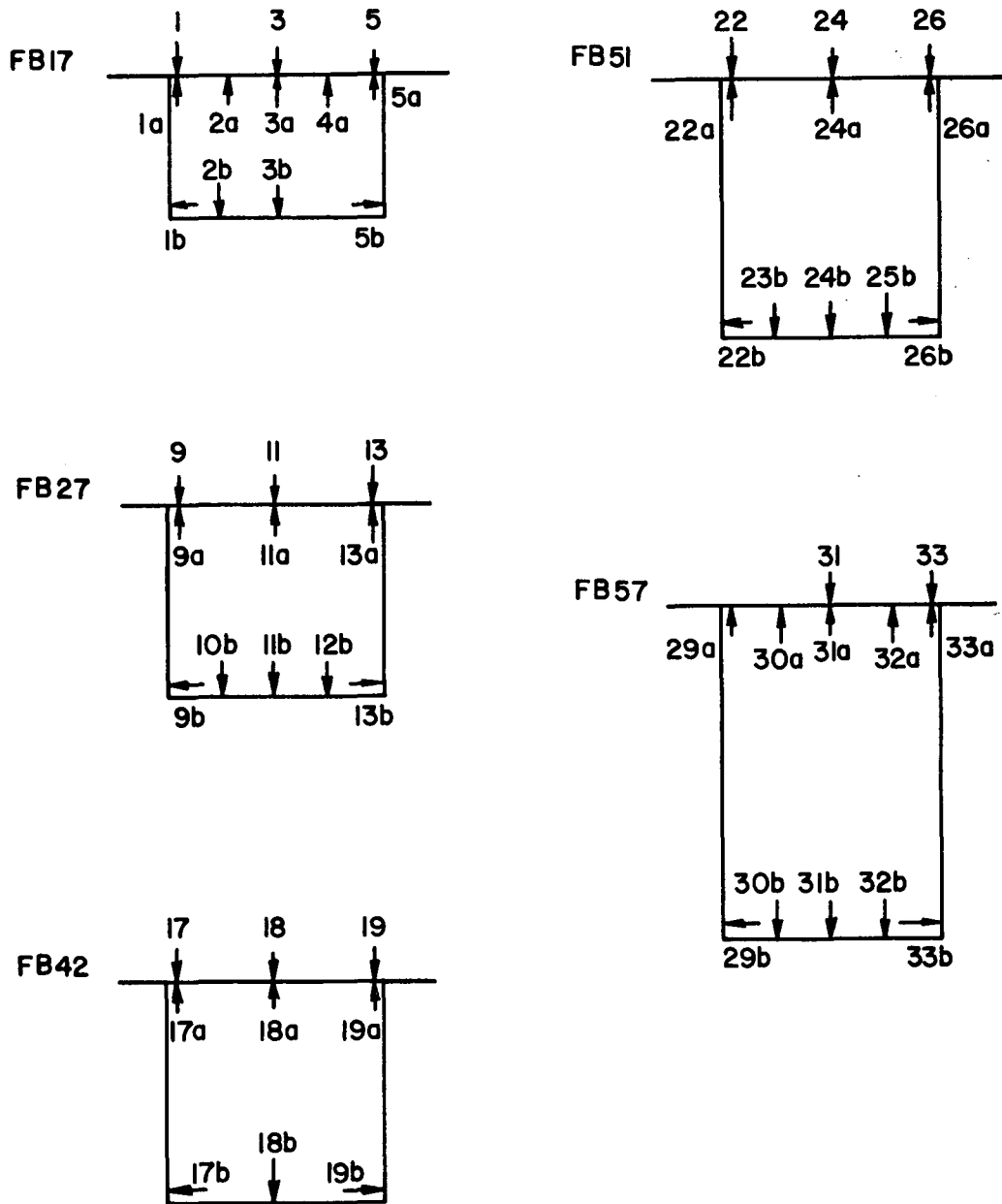


Fig.2.8 Mechanical Gage Hole Locations (North Box)
(View toward Niteroi)

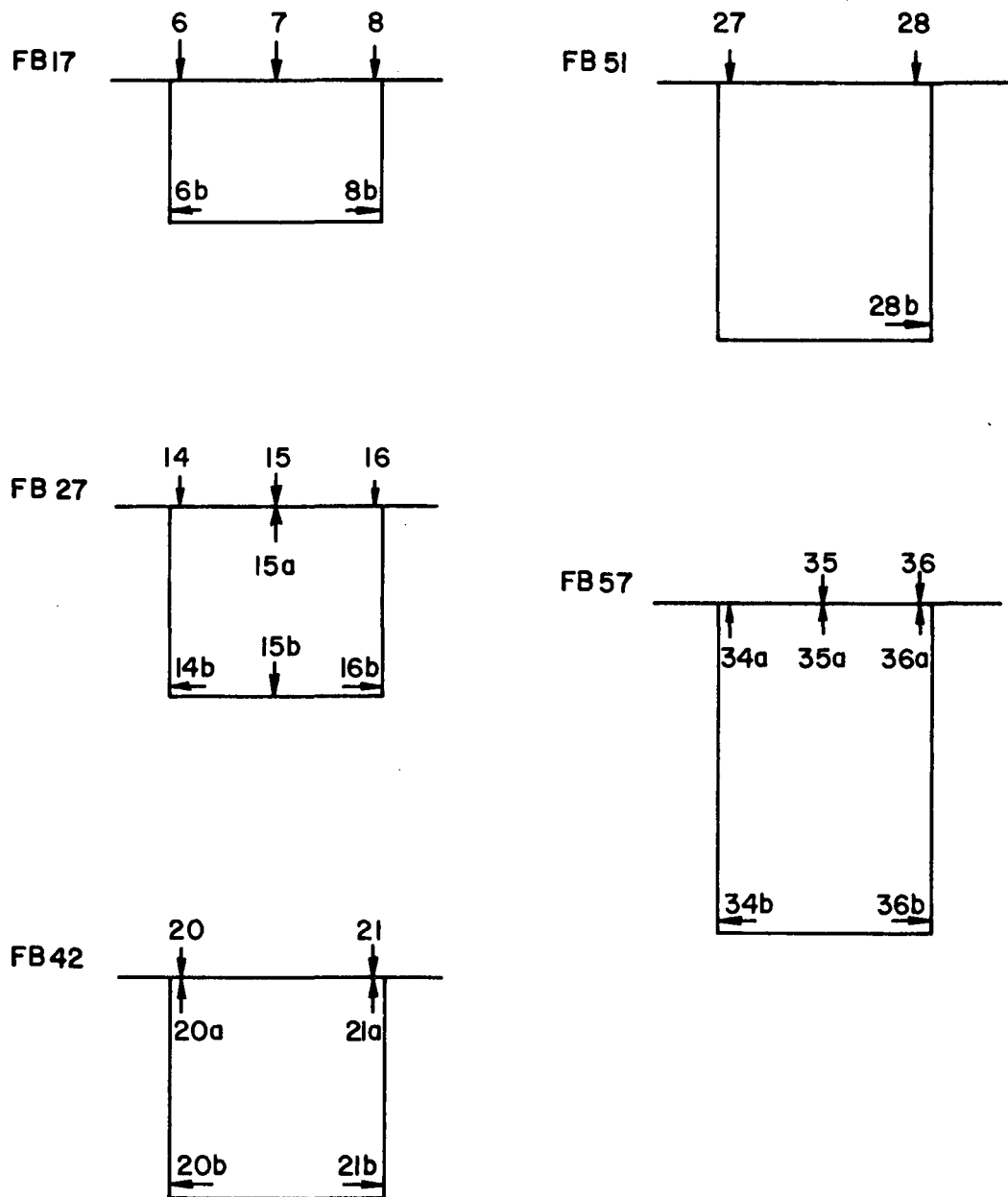


FIG.2.9 Mechanical Gage Hole Locations (South Box)
(View toward Niteroi)

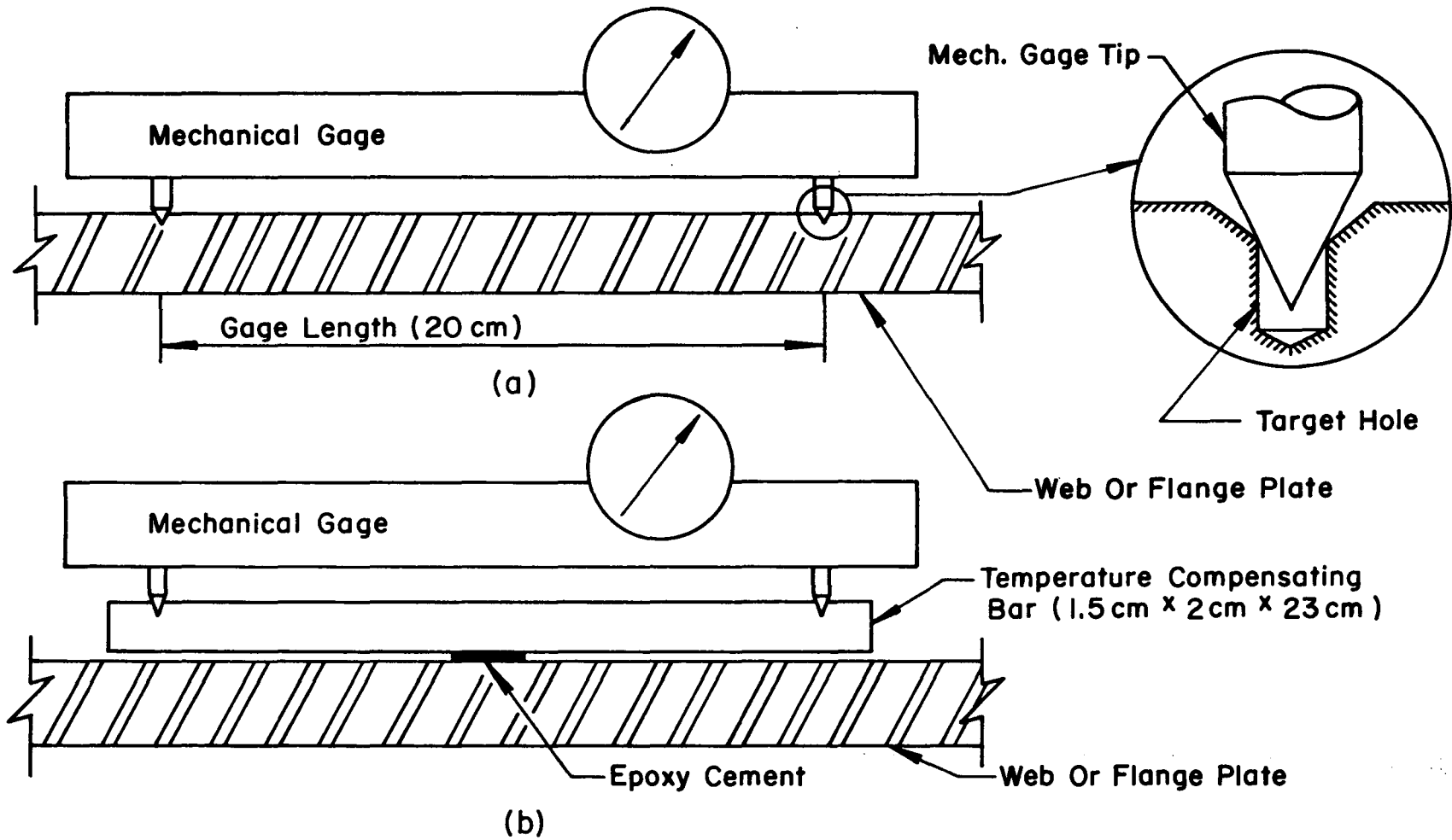
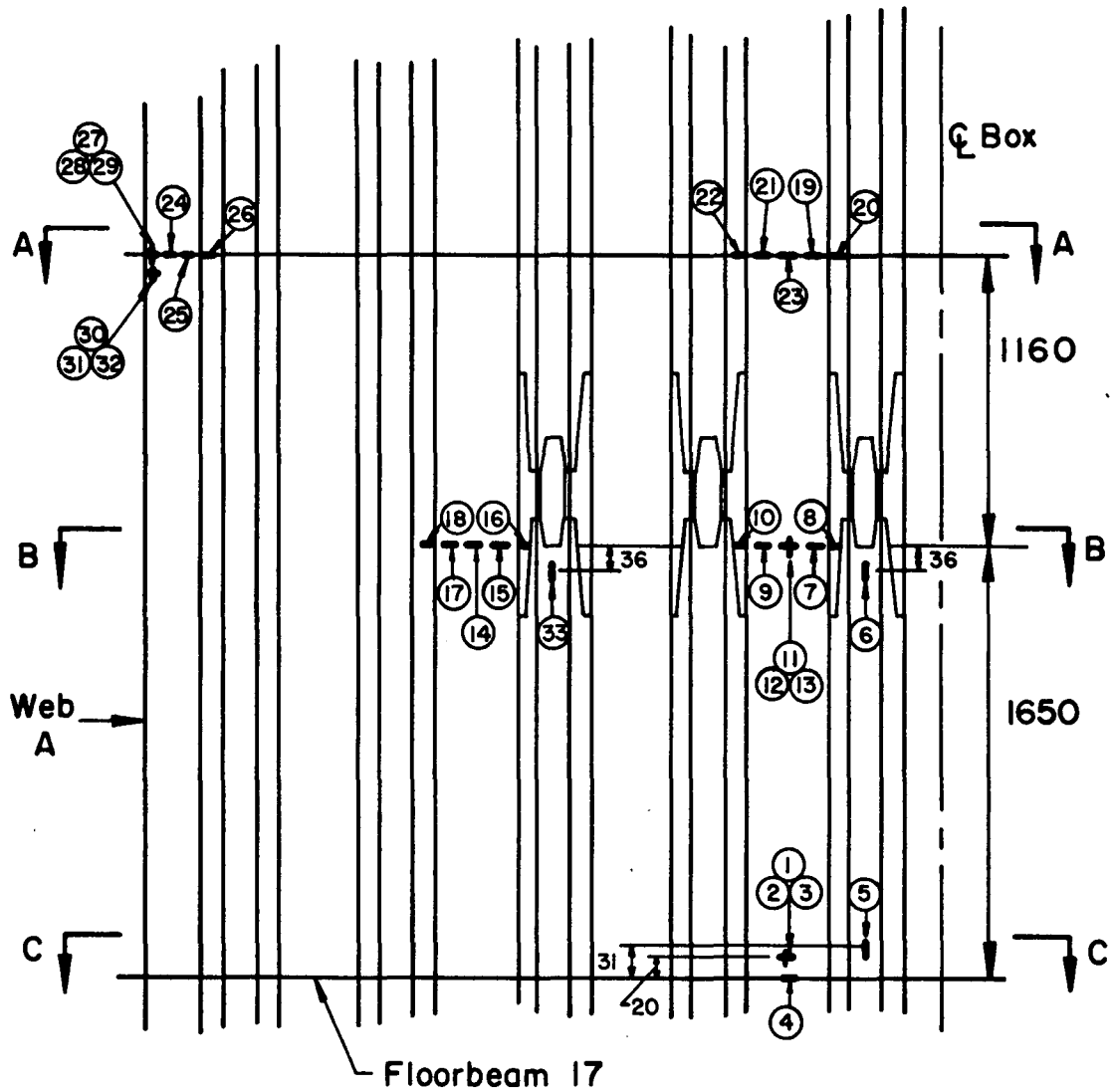
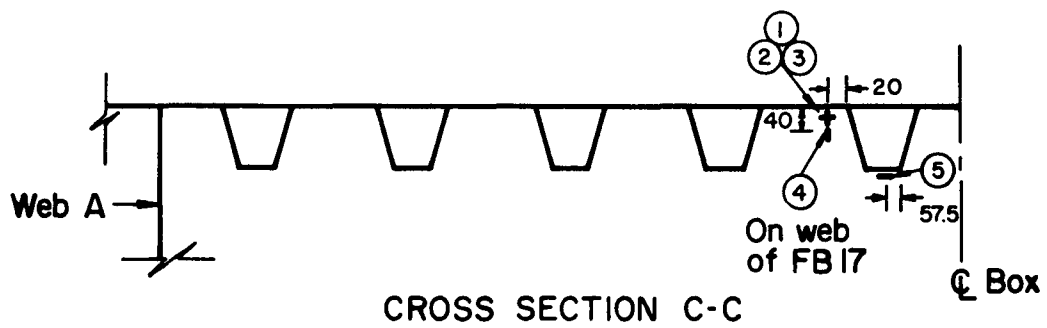
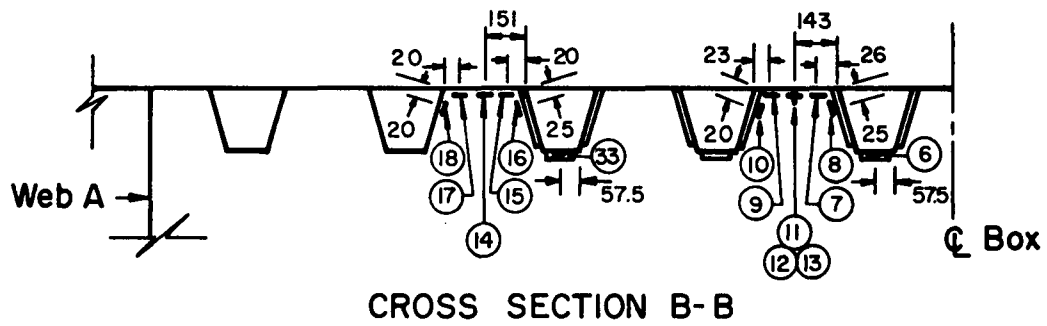
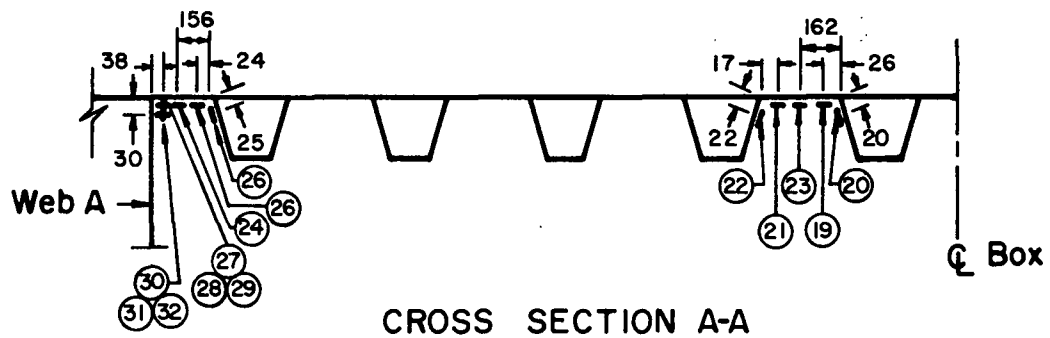


Fig. 2.10 Mechanical Gage System



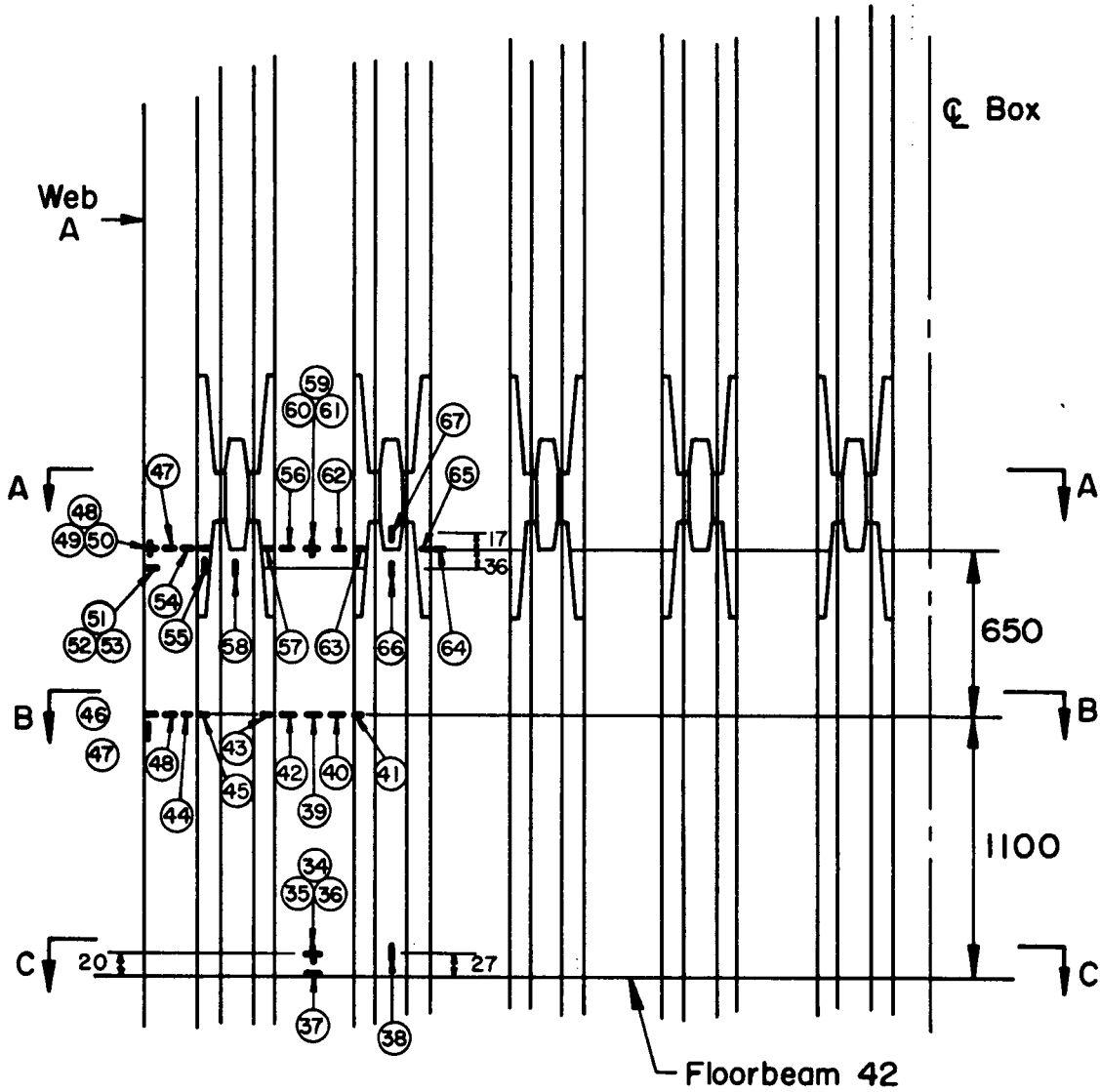
- Notes: 1. View from Below
 2. - Single Gage
 3. + Rosette Gage

Fig. 2.11 Layout of Strain Gages Near Floorbeam 17



- Single Gage
 + Rosette Gage

Fig. 2.12 Location of Strain Gages on Cross Sections Near Floorbeam 17



- Notes: 1. View from Below
 2. - Single Gage
 3. + Rosette Gage

Fig. 2.13 Layout of Strain Gages Near Floorbeam 42

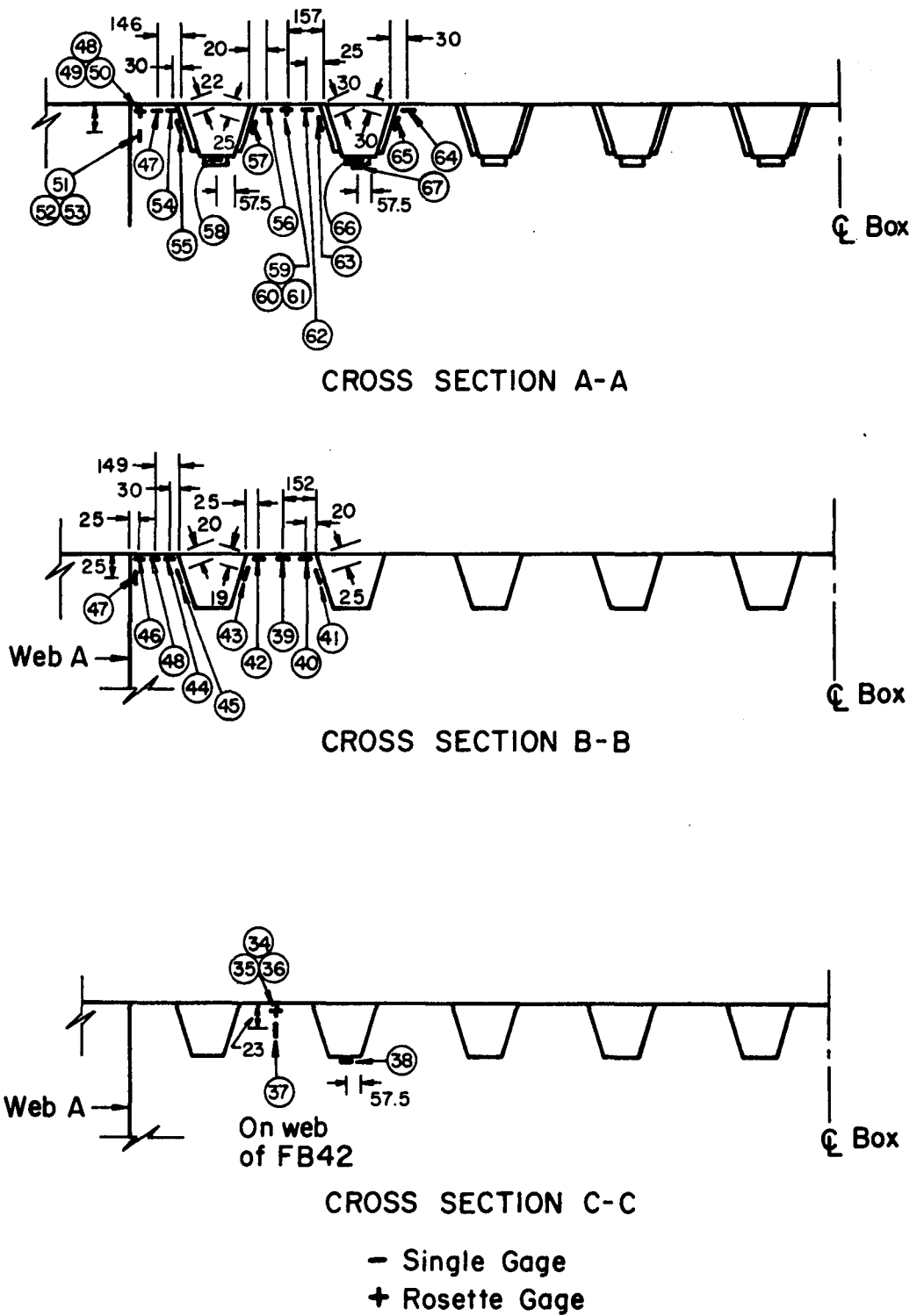


Fig. 2.14 Location of Strain Gages on Cross Sections Near Floorbeam 42

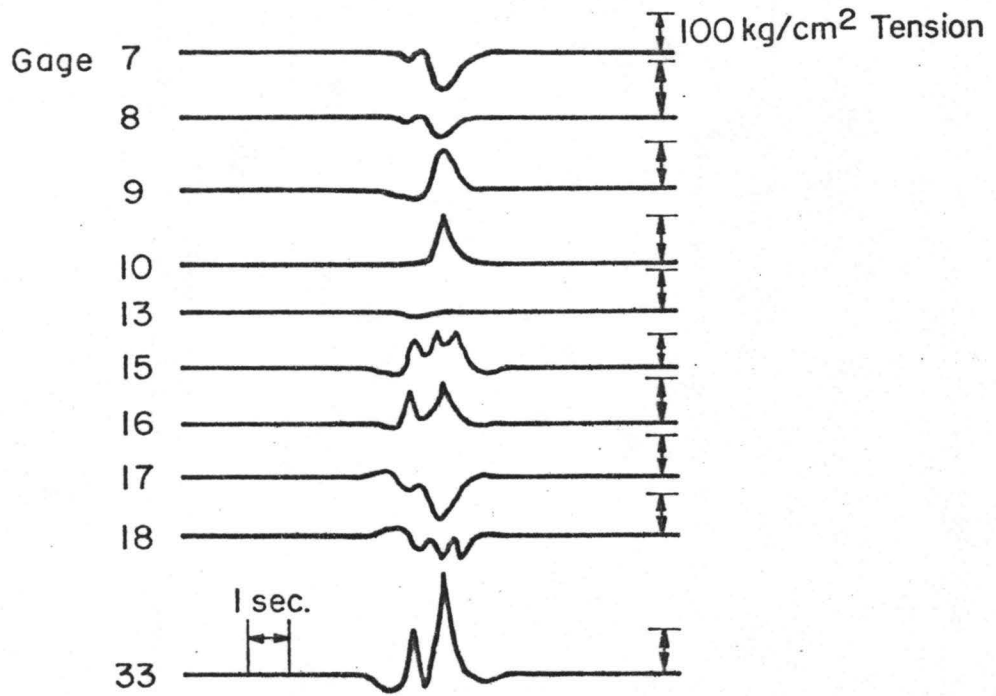


Fig. 2.15 Typical Analog Trace from Oscillograph Recorder

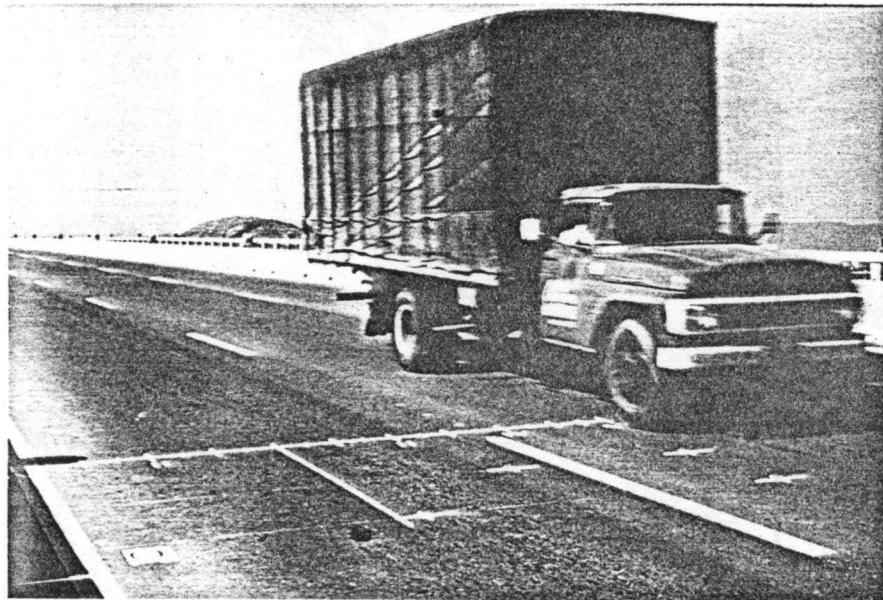


Fig. 2.16 Typical Truck

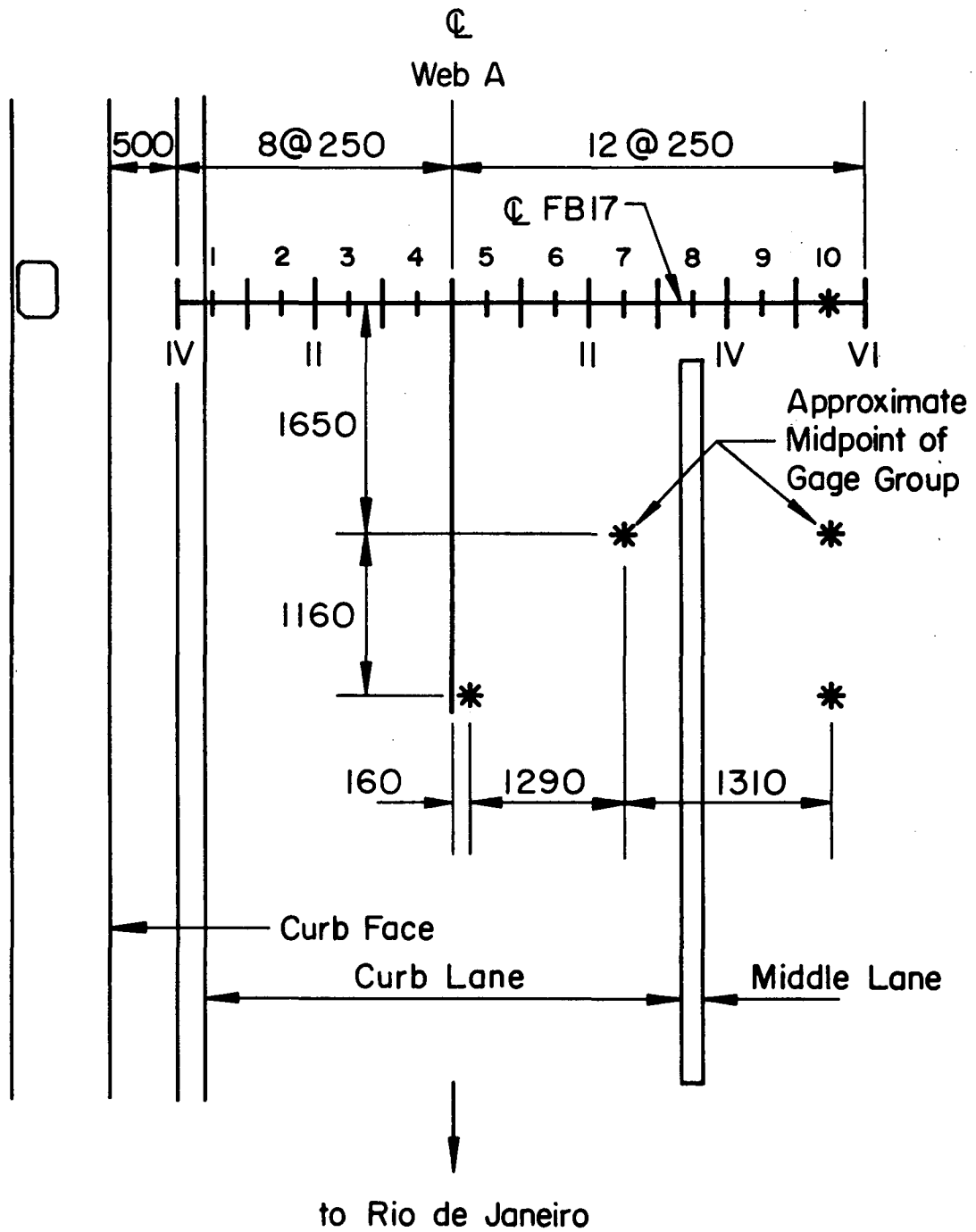


Fig. 2.17 Layout of Deck Markings

3. STATIC STRESSES AND FORCE HISTORY (A. Ostapenko and D. H. DePaoli)

3.1 General

Since the actual stress levels at the beginning of the readings were not known - they could be only assumed to be as computed in design analysis, the measurements gave just the changes of stresses for the particular cases investigated. Thus, often when reference is made in the text to "stress", "stress change" should be understood. The construction stages, for example, led to stress changes during the following conditions: (1) transfer of a side span from the jetties to the pontoon, (2) transfer from the pontoon to the pier rings, and (3) the stress change between the time when the center span (pontoon) was in the water and the time immediately after it was lifted out of the water (the center span lift stage). A comparison of the measured stress changes with the stress changes computed according to the theory used in design gave an indication of the accuracy and reliability of the design computations, not only for these stress changes but also for other conditions, such as dead and live load effects.

3.2 Observations During Construction

One of the principal purposes of the instrumentation was to monitor stress changes at some specific locations during the construction phases. If the observed stresses exceeded the design values, this would have indicated the development of some unforeseen situation and corrective measures could be taken before anything serious occurred.

The monitoring operation involved a reduction of the raw readings as they were taken, computation of the stresses and a comparison with the precalculated design values. The main intent was to check the bending stresses in the cross sections where the stresses were believed to be the greatest. In some instances a spot check was made at locations not originally planned and then the comparison was made with allowable stresses.

The period in which the first monitoring checks were made was the transfer of the south box of the Rio side span from the pontoons to the pier rings. Only a mechanical gage was used then to measure stresses in the outside surface of the top flange. The stress over the inner web at FB27 (Location 14) was found to be 1905 kg/cm^2 which is less than 12% different from the design value of 2172 kg/cm^2 . A check at FB42 over the inner web (Location 20) revealed a stress of (-1890 kg/cm^2) (compression) as compared to the design stress of (-1838 kg/cm^2) , a deviation of only 3%. Such close correlation (12% and 3%) was taken as quite acceptable.

When the north box was being erected, electrical strain gages were connected to a data acquisition unit and the checks were made using the strain gage readings. The checking computations were made again at FB27 and FB42.

During the transfer of the girder from the jetties to the pontoon the representative bending stress changes were the following: at FB27 (bottom flange) $(-)$ 2121 kg/cm^2 vs. the design stress of $(-)$ 2164 kg/cm^2 , at FB42 (top) $(+)$ 1705 kg/cm^2 vs. the design stress of $(+)$ 1751 kg/cm^2 , and at FB42 (bottom) $(-)$ 2427 kg/cm^2 vs. $(-)$ 2482 kg/cm^2 . Thus, the agreement was within about 3% and on the safe side.

However, when some spot readings of the transverse gages in the north end of the top floor beam at FB42 were reduced in the field, the stresses turned out to be quite substantial in comparison to the essentially zero stresses expected. With $(+)$ 470 kg/cm^2 at the top and $(+)$ 132 kg/cm^2 at the bottom of the floor beam, they indicated a bending moment where none should have been. At first these stresses were assumed to have resulted from an inadvertent twisting of the girder as it was jacked horizontally on the jetties and then transferred to the pontoon. However, when a moment of the same direction was detected at the other end of the floor beam, the phenomenon became even more puzzling because a twisting of the girder should have produced an opposite moment at that end of the floor beam. Still, since the stresses were only a fraction of the allowable stress level, there was no immediate concern. Later analysis of these bending stresses lead to a conclusion that the stresses apparently had been caused by Poisson's effect rather than by twisting of the girder. This topic is discussed in Chapter 5.

A spot check of the girder stresses in the north box when it was transferred from the pontoon to the pier rings showed that the stresses did not deviate from the design values more than 3% and even then they were on the safe side. These were in the bottom flange at FB27, $(-)$ 2425 kg/cm² vs. design $(-)$ 2465, and in the top and bottom flanges at FB42: $(-)$ 1780 kg/cm² vs. design $(-)$ 1957 kg/cm² and 2564 kg/cm² vs. design 2856 kg/cm², respectively.

The next stage of construction at which readings were monitored was the center span lift. The strain gages checked were the bottom longitudinal gages at FB42 and 57. Since the stresses again deviated very little from the design stresses, no additional checks were made.

As the construction stresses (stress changes) were the greatest of those induced in the girder when this study was conducted, and they showed good agreement with the design stresses, only a superficial spot check was made at the time of the test loads during the February 1974 sequence.

In summary, the monitoring of the construction stresses has indicated that the box girder developed stresses which were very close to the design stresses.* The only really puzzling observation was that

*Later reduction and analysis of all field data detected larger, but still experimentally acceptable, deviations of some individual readings. (See Art. 3.3, etc.)

of the bending stresses in the floor beam at FB42. Although not of dangerous level, these stresses were at first suspected of having been caused by the twisting of the girder. Eventually, they were found to be the result of the Poisson's ratio effect of the primary stresses in the girder.

3.3 Analysis of Strain, Scratch and Mechanical Gage Readings for Construction Phases

Only a few readings could be reduced and judged in the field in the course of the monitoring procedure. All the others were reduced later at Lehigh University. Since the major stress changes occurred during the construction stages, the analysis of these readings is presented here first. In many instances the readings from different gage systems and for both single-box half-sections are averaged in order to achieve greater statistical accuracy. However, in most of the discussion only the more accurate readings from the electrical and mechanical gages are utilized.

The reduced strain readings for the construction stages are plotted as stresses in Figs. 3.2, 3.3 and 3.6. The stresses computed from the mechanical gage readings are listed for all sets of readings in Table 3.2 and are plotted for the construction stages in Figs. 3.4, 3.5 and 3.6.

3.3.1 Maximum Stresses for Construction Stages

Jetties - Pontoon

The first major stress change was during the transfer of the single-box units from the jetties to the pontoon (Reading Nos. 3.0 to

3.2 of Table 2.1). The support points of the units were moved (Fig. 3.1) from FB17 + 8 meters and FB57 (192-meter span) to FB27 + 7.5 meters and FB51 - 2.5 meters (110-meter span). The stresses from the strain and mechanical gage measurements for this stage are shown in Figs. 3.2 and 3.4. The stresses measured at FB17 and FB57 resulted from other effects, such as temperature or experimental error, since from the transfer they should have been zero. The stress diagrams at FB27, FB42 and FB51 are the ones directly produced by this construction stage. The highest intensity is in the bottom flange at FB42. Table 3.1 shows that the average stress for this location from the strain and mechanical gage systems was compressive $(-)$ 2380 kg/cm². The highest tensile stress was recorded at top of FB27 with the average value from Table 3.1 being $(+)$ 1960 kg/cm².

Pontoon - Pier Rings

Transfer of the side span units from the center span pontoon to the pier rings resulted in the second major stress change (Reading Nos. 3.3 and 3.4 of Table 2.1). As shown in Fig. 3.1, the support conditions changed from a 110-meter span to a 200-meter span at FB17 and FB57. The stresses as recorded by the strain and mechanical gages are shown in Figs. 3.3 and 3.5. The maximum stress is tensile again at FB42 bottom, with the average for all gage systems from Table 3.1 being $(+)$ 2484 kg/cm². High compression was at FB27 top. The average from Table 3.1 is $(-)$ 2230 kg/cm².

Center Span Lift

All the measured stresses for the center span lift (Readings 4.0 and 4.1 in Table 2.1) are shown in Fig. 3.6, including the mechanical and scratch gage data. These stresses were produced by the center span weight on the cantilever beyond FB57 (Fig. 3.1) causing tension in the top flange. The highest stresses are seen to be at FB42, (+)1320 kg/cm² in the top and (-)1915 kg/cm² in the bottom flange.

It should be again remembered that all stresses given are stress changes, and in the most cases discussed so far, they lead to a change in the sign of the actual stress. For example, the stress change at FB27 top for the transfer from pontoon to pier rings was (-)2230 kg/cm² (compression). This means that the tensile stress at this point of approx. (+)1130 kg/cm² when the unit was on the pontoon was changed to compression of (-)1100 kg/cm² when the unit was transferred to the pier rings.

3.3.2 Scratch Gage Records for Construction Stages

Scratch gages were not expected to be as accurate as strain and mechanical gages, but they provided a continuous record as well as a check on the other gage systems. A full listing of the scratch gage records obtained in this study is given in Table 2.2. Five of the target records (Nos. 1, 2, 3, 7 and 8 in Table 2.2) have traces produced by the construction stages. The most complete record covering all the erection phases and the subsequent placement of the parapets and paving as well

as covering the test loads and the time till February 28, 1974, that is, shortly before the opening of the bridge to traffic is record No. 8 shown in Fig. 3.7.

A portion of this record is also reproduced in Fig. 3.8 together with the photographs of the other three clearest records (Nos. 1, 2 and 7) covering the construction phases. All four are shown to the same magnification. The target at FB27 top recorded the first two construction stages (it was removed prior to the center span lift), while the targets at FB27 bottom, FB42 top and FB42 bottom have all three construction stages. The trace for FB42 top is defined by the line connecting the "blobs" in a zig-zag pattern; the two thin intersecting scratches were made accidentally and are not part of the record.

The method of analysis of the target traces is discussed in Chapter 2 with reference to Fig. 2.7 which is an enlarged version of the right bottom trace (FB42 bottom) in Fig. 3.8. In order to make a comparison of the resulting stress changes with the stress changes measured by the mechanical and strain gages it is necessary to adjust for the fact that the scratch gage is located closer to the centroid of the section than the mechanical gage target holes and strain gages. The corrected values are computed in Table 3.3 for the traces of Fig. 3.8.

The stress changes computed from the scratch gages can in most cases only be found within a range due to "blobbing" on the targets (shiny areas caused by the scribe moving back and forth on the target without advancement). For example, the scratch gage trace at FB42 top (in Fig. 3.8) can be read for the transfer of the box unit from the jetties to the pontoon (the first downward zig) only within about $\pm 6\%$ accuracy. Thus, the figure of 1680 kg/cm^2 in Col. 3 of Table 3.3 actually could be anywhere between 1580 and 1780 kg/cm^2 . The average, adjusted to the extreme fiber (Table 3.3), is 1768 kg/cm^2 which still compares quite well with the strain and mechanical gage average of 1760 kg/cm^2 (Table 3.1).

One of the best defined traces suitable for an accurate comparison is the trace at FB42 bottom in Fig. 3.7 (also in Figs. 3.8 and 2.7). As shown below, the agreement between the three systems of gages is quite close (within 2%).

	Mech. & Strain (Table 3.1)	Scratch (Table 3.4)	Percent Difference
Jetties to Pontoon	-2380 kg/cm^2	-2405 kg/cm^2	1.0
Pontoon to Piers	$+2484 \text{ kg/cm}^2$	$+2456 \text{ kg/cm}^2$	1.0
Center Span Lift	-1880 kg/cm^2	-1846 kg/cm^2	2.0

A graphical comparison of the scratch gage readings with the readings from the strain and mechanical gages can be seen in Figs. 3.9 and 3.10 for the jetties-to-pontoon and pontoon-to-piers construction stages and in Fig. 3.6 for the center-span-lift stage. The general agreement is not as optimistic as in the listing above, but it still is well within the experimental accuracy that can be expected under field conditions.

3.3.3 Adjustment of Section Properties

In order to perform an analysis and a comparison of the measured stress values with the theory, design values of the cross-sectional properties were computed for the locations of the instrumented sections by parabolic or linear interpolation from the data which were supplied by the designer (HNTB) for the full 10 or 20-meter intervals. The new data are listed in Table 3.4.

The stresses averaged in Table 3.1 from the strain and mechanical gage readings for the jetties-to-pontoon and pontoon-to-piers construction stages were found to deviate relatively little from the design stresses. However, a trend was detected that the ratios of the top to bottom flange stresses were consistently different for the measured and theoretical values. As a result, the moments computed using the design values of section moduli S_T and S_B (from Table 3.4) were different for the top and bottom measured stresses whereas they should have been the same. For example, considering the transfer from pontoon to piers, the moment at FB27 is $[2230 \text{ (Table 3.1)} \times 1.6180 \times 10 \text{ (Table 3.4)}] = 36,081 \text{ tm}$ for the top flange stress and $[2410 \times 1.4257 \times 10] = 34,359 \text{ tm}$ for the bottom flange stress, as compared to the design moment change of 35,146 tm. The fact that the ratio of the moments (or stresses) remained the same at a particular section for all stages of construction, indicated an effective change in the cross-section properties.

Assuming that neither the girder depth nor the moment of inertia were affected -- only the location of the centroid, the adjusted location is computed in Table 3.1 from the ratios of the top to bottom

stresses. The stress ratio gives the ratio of C_T to C_B , the centroidal distances to the extreme fibers of the top and bottom flanges. Then, C_T is obtained from the design depth $d_{Des.} = C_T + C_B$. Table 3.5 gives a comparison of the adjusted and design C_T 's. The percent shift of the centroid is seen to be from 2 to 4.5% of C_T at the investigated sections of FB27,42 and 51.* The adjusted section moduli S_T and S_B are then obtained for further analysis from the design values of moments of inertia.

The results of adjusting location of the centroid is demonstrated by entering in Fig. 3.6 the stresses computed from the design moments of the center span lift (from Table 3.4) using the adjusted section moduli (from Table 3.5). A comparison with the measured stresses from the strain, mechanical and scratch gages in the figure leads to the following observations:

(1) At FB27 and FB51, the computed stress levels fall in the middle of the scattering of the measured values and, thus, the adjusted S 's can be accepted as more accurate than the design S 's.

(2) At FB42, however, the computed stresses are higher than the measured averages by essentially equal amounts at the top and bottom. The equal amounts indicate that the adjusted neutral axis (centroid) is in the correct position, and the discrepancy in the stress levels points to a higher actual moment of inertia, I , than computed. This,

*As the shift of the centroid (N.A. - neutral axis) at each of the three locations is downward, toward the midheight of the girder section, causing a reduction of the larger C (C_B), the shift is on the safe side.

of course, means that the actual section is stronger than considered in design both due to the downward shift of the neutral axis and due to a greater actual moment of inertia, I . In fact, were I taken 1.11 of the design value, the computed stresses would fall directly within the scattering of the measured stresses.

The above observations were confirmed by computing the moments for the center span lift from the average measured stresses and the adjusted section moduli (See Table 3.6) and plotting these moments together with the design moment diagram as shown in Fig. 3.11. The agreement at FB27 is excellent. The averages at FB51 and FB57 also agree with the design moment diagram. However, at FB42, although the computed moments closely bunch together, they fall below the design moment by about 10% indicating a stronger section than assumed in design.

Figure 3.12 shows the similarly computed moments for the jetties-to-pontoon and pontoon-to-piers construction stages (Computations in Table 3.7). The overall agreement is quite good, but the computed moments at FB42 again tend to fall below the design moments.

3.3.4 Conclusions

Analysis of the field readings made during the three construction stages and a comparison of the data with the design values lead to the following conclusions:

1. The stresses monitored in the field during construction deviated little from the design stresses thus verifying reliability of the construction procedure and of the relevant computations.

2. The generally close agreement between the measured stress changes and the design stress changes indicates that the method of analysis used in design was accurate for computing stresses. Thus, the actual stresses due to the dead, live and thermal loads can be also assumed to be equal to the stresses computed, and the method of analysis used can be accepted as sufficiently accurate for this type of structure.

3. The fact that the measured stresses tended to be lower than the design stresses, such as at FB42, seems to mean that the actual plate thicknesses probably were somewhat greater than specified thus leading to a safer structure. Apparently this was also the reason for the downward shift of the effective neutral axis which resulted in an additional reduction of the maximum stress in the cross section (in the bottom flange).

3.4 Test Loading Stresses and Distribution of Loads Between Boxes

3.4.1 Test Load Program

A test load program was conducted on the steel girder spans in conjunction with a similar program on the concrete spans. The objectives of the tests on the steel structure were the following:

- 1) Verification that the stresses produced in the girder by live loading placed at critical locations were in agreement with the stresses computed theoretically.
- 2) Verification that the behavior of the completed bridge -- a statically indeterminate three-span girder -- was as predicted in the analysis performed for design.
- 3) Determination of the distribution between two boxes of the loading placed on one box. Theoretical analysis indicates a 55% to 45% distribution between the loaded and unloaded boxes. (3.2)

In addition to meeting the three objectives listed above, some of the test load positions could be used for:

- 4) Measurement of stresses in the components of the orthotropic deck structure as part of the study of the effects of regular traffic on the deck structure discussed in detail in Chapter 6.

Four alternate test load schemes (versions) were proposed to ECEX to achieve these objectives. Each scheme consisted of four to six positions of test truck convoys on the bridge, determined

by using influence lines for the moments at the instrumented sections and a requirement that the average loading should not exceed the intensity stipulated by the DNER Specification. (3.1) The schemes differed from each other by the number of positions, the weights of individual trucks, the lengths of the loaded portions and the total numbers of trucks.

Scheme (Version):	1	2	3	4
No. of Ld. Positions:	6	6	4	4
Total No. of trucks:	48	42	24	21
Weight of each truck (t):	18.9	17.5	18.9	17.5

Scheme No. 4 shown in Fig. 3.13, requiring the smallest number of trucks -- 21, was approved mainly because its basic arrangement of 21 trucks distributed over 80 meters of one trunk (one-half of the bridge width) was perfectly suited for the tests on the concrete spans. However, with a smaller total load this scheme gave lower measured stresses which were adversely affected by the degree of accuracy of the measuring system to a greater extent than would have been for the other schemes (versions).

The testing period was scheduled between the completion of the bridge and opening it to traffic. Since at the time the freshly deposited Epoxy asphalt wearing surface still required curing and had to be protected, 5 cm-thick wooden boards were placed under the truck wheels when the trucks were positioned on the bridge for taking readings.

The gravel loaded trucks were weighed prior to the test. The method was to weigh the front axle, the two rear axles and the whole

truck. The truck weights did not deviate more than 0.10 tons from the specified 17.5 tons and the total aggregate weight was equal to 367.71 t, just 0.21 t over the intended 367.5 t.

The trucks were placed in the three lanes facing in the direction of traffic, seven trucks per lane as shown by heavy lines in Fig. 3.13. Only in Load Position 3, the trucks were arranged differently since for a maximum moment it was necessary to keep the trucks within the 74 meters of the 30-meter cantilever plus the 44-meter suspended span. Six trucks were in each of the three north lanes and three trucks in the south lane against the median and straddling the joint between the cantilever and the suspended span. The exact location of trucks for Positions 2 and 3 is shown in Fig. 6.1.

All readings were taken during the night as indicated by the starttimes listed in Table 2.1, Readings 5.0 to 5.5. Thus the effect of temperature was reduced. Yet, since considerable time elapsed between the individual sets and the zero reading, some effect of temperature and of voltage fluctuation was expected to detract from the accuracy of the readings, especially for Load Positions 1 and 2 for which the zero reading could not be started till 6:45 hours and ended when the sun was already coming up.

3.4.2 Stresses due to Test Loads

The moments due to the four positions of the test loading were computed from influence lines and are listed in Table 3.8. The stresses in the top and bottom flanges were obtained using the section moduli adjusted on the basis of the measurements during the construction stages as shown in Table 3.5 for the sections at FB27, 42 and 51 and the design section moduli of Table 3.4 for the sections at FB17 and FB57.

As anticipated, the accuracy of some of the readings was plagued by occasional vehicles crossing the bridge, voltage fluctuations, and unsteady temperature conditions resulting from the changes in weather and from the length of time needed for repositioning the trucks. Thus, the stresses, computed theoretically to be of the order of 200 kg/cm^2 , were often overwhelmed by the deviations of the same order of magnitude, and in these cases the resultant readings could give no more than a qualitative indication that the stresses were close to the expected range.* However, there were still enough good readings to meet the stated objectives.

Figure 3.14 shows the flange stresses computed from the strains measured at the FB42 section for Load Positions 2, 4 and 1. Since these stress changes include not only the bending stresses caused by the test loads but also the stresses equivalent to the changes in temperature between the zero and the load readings, a comparison with the theoretical stresses could not be made directly. The following assumptions were made to obtain the load stresses:

- (1) The temperature change between the zero and the load readings was the same over the full cross section of a box. This assumption was relatively reasonable since most of the readings were made at night.

* A statistical system analysis of the doubtful readings could not be performed due to a lack of time. Furthermore, its usefulness at this point is debatable. However, such a study may be a follow-up of this project.

- (2) Test loads produced only bending stresses and the ratio between the bottom and top flange stresses was the same as the ratio between the adjusted section moduli for the top and bottom flange
- (3) In each box, the strains (and stresses) vary linearly from top to bottom and are constant across the width. Thus, bending or variation of temperature in horizontal transverse direction would result in different effective temperature (axial stress) changes between the north and south boxes.

With these assumptions, the following formulas for computing the bending stresses in each box due to the test loads were derived:

$$\sigma_{Tb}^N = \frac{1}{(1-S_T/S_B)} (\sigma_T^N - \sigma_B^N) \quad (3.1)$$

$$\sigma_{Bb}^N = (S_T/S_B) \sigma_{Tb}^N \quad (3.2)$$

$$\sigma_a^N = \sigma_T^N - \sigma_{Tb}^N \quad (3.3)$$

with assumption (2) in equation form being

$$\frac{\sigma_{Bb}^N}{\sigma_{Tb}^N} = S_T/S_B \quad (3.4)$$

Where

S_T, S_B = section moduli for the top and bottom flanges, adjusted on the basis of the stresses measured for construction stages and listed in Table 3.5 (Table 3.4 for FB17 and 57).

σ_T^N = Average stress in the top flange of the north box, computed from the field readings.

σ_B^N = Average stress in the bottom flange of the north box, computed from the field readings.

σ_{Tb}^N = Stress in the top flange of the north box due to the bending produced by test loads.

σ_{Bb}^N = Stress in the bottom flange of the north box due to the bending produced by test loads.

σ_a^N = Axial stress uniform over the box cross section which is equivalent to a change in temperature between the zero and the load strain readings. The corresponding temperature change ΔT^N in °C is

$$\Delta T^N = (\sigma_a^N) / (E \times \alpha) = (\sigma_a^N) / 25.33 \quad (3.5)$$

with

E = Modulus of elasticity.

α = Coefficient of thermal expansion, for steel

$$= 12.06 \times 10^{-6} \text{ cm/cm/}^\circ\text{C.}$$

In the above, superscript "N" designates the north (Paqueta) box, but the formulas are equally valid for the south (Cidade) box if superscript N is replaced with S.

A sample computation of the bending stresses in the section of FB42 for Load Position 4 will illustrate the procedure. The average flange stresses are found from Fig. 3.14b.

$$\sigma_T^N = -(1/4)[197 + (2) 185 + 168] = -183.8 \text{ kg/cm}^2$$

$$\sigma_B^N = +(1/3)[(2) 164 + 139] = +155.5 \text{ kg/cm}^2$$

Here, the measured stress of 840 kg/cm^2 was omitted because it obviously had a gross error being completely out of range with the other values.

$$\sigma_T^S = -(1/2)(256 + 185) = -220.5 \text{ kg/cm}^2$$

$$\sigma_B^S = +(1/2)(189 + 179) = +184 \text{ kg/cm}^2$$

With $S_T/S_B = -(2.523/1.8468) = -1.366$ (section moduli from Table 3.5), the load bending stresses are computed from Eqs. 3.1 and 3.2.

$$\sigma_{Tb}^N = -143.5 \text{ kg/cm}^2$$

$$\sigma_{Tb}^S = -170.0$$

$$\sigma_{Bb}^N = +196.0$$

$$\sigma_{Bb}^S = 233.0$$

These stresses are within 10% of the theoretical stresses in Table 3.8.

Equations 3.3 and 3.5 give

$$\sigma_a^N = -40.3 \text{ kg/cm}^2$$

$$\sigma_a^S = -49 \text{ kg/cm}^2$$

and the corresponding temperature changes

$$\Delta T^N = -1.6 \text{ }^\circ\text{C}$$

$$\Delta T^S = -1.9 \text{ }^\circ\text{C}$$

It is remarkable how small a change in temperature ΔT , of less than 2°C , may lead to a stress deviation of more than 30% ($\sigma_{Tb}^N = -143.5$ vs. $\sigma_T^N = -183.8$ with $\sigma_a^N = -40.3$) for these low bending stresses.

The above results for Load Position 4 and the analogous ones for Load Positions 1 and 2 are summarized on Lines 1 to 12 of Table 3.9. The deviations of the computed σ_{Bb} from theory are shown in parentheses below Lines 4 and 10.

A summary of the pertinent results for all other sections is given in Table 3.10. Since σ_{Tb} is related directly to σ_{Bb} through (S_T/S_B), only the larger σ_{Bb} is listed for each case. In Figure 3.15, a plot of σ_{Bb} in both boxes at all sections is shown for each Test Load Position. For some sections the readings were completely erratic and they were not analyzed, e.g., FB27 for Ld. Position 4. A few stresses have substantial unexplainable deviations from the theoretical values, e.g., 75 kg/cm^2 for $\sigma_{Bb}^N = -87.9 \text{ kg/cm}^2$ at FB51 - Ld. Position 2, and these should be disregarded in drawing conclusions.

Since the accuracy of the strain gage system of instrumentation itself, even under good laboratory conditions, cannot be expected to be better than $10 - 20 \text{ kg/cm}^2$, that is, about 10% of the higher readings analyzed here, the stresses computed here can be accepted as adequately confirming validity of the analytical methods used in design.

3.4.3 Scratch Gage Record for Test Loads

The maximum stress changes caused by the test loads being barely 200 kg/cm^2 -- the theoretical margin of sensitivity of the scratch gages, it was doubtful that they would be recorded by the scratch gages. However, the gage at FB42 bottom, worked exceptionally well exhibiting much greater sensitivity, and its target trace for this period (No. 8 in Table 2.2) shows some zig-zags which may have been caused by the test loads. The whole trace is shown in Fig. 3.7, and the zig-zags pertaining to the time of test loads are the last ones at the right end. However, it is essentially impossible to distinguish them from the preceding and concurrent zig-zags of the same order of amplitude caused by the daily temperature fluctuations.*

Figure 3.16 shows an enlargement of the pertinent portion. It appears that the series of zig-zags labeled (1) to (9) may have been produced by the test loads in the following sequence:

- (1) to (2) - application of test load 1 (-178 kg/cm^2)
- (2) to (3) - removal of test load 1 and application of test load 2
($178 + 213.7 \cong 390 \text{ kg/cm}^2$)
- (3) to (4) - removal of test load 2
- (4) to (7) - thermal stress changes from 6:00 hrs to 24:00 hrs on 25 Feb.
- (7) to (8) - application of test load 3 (-18.6 kg/cm^2)
- (8) to (9) - removal of test load 3 and application of test load 4
(230 kg/cm^2)

*Thermal stresses are discussed in Art. 3.5 and Chapter 4.

(9) to (end) - removal of test load 4 at 5:00 hrs on 26 February and subsequent thermal and construction traffic effects till the removal of the target at about 14:00 hrs on 28 February, 1974.

The argument against fully accepting this interpretation is the difficulty of explaining the number of blobs and zigs after point (9) which must have been recorded within the two days before the removal of the target.

Another possibility is that the segment labeled (1) to (9) was wholly produced by temperature variations and construction traffic and only the very end portion of the trace was affected by the test loads. Then,

- (A) to (B) - application of test load 1,
- (B) to (C) - removal of test load 1 and application of test load 2,
- (C) to (end) - test loads 3 and 4 and the concurrent and subsequent thermal effects.

In both cases the principal stroke is the tension downward stroke approaching 400 kg/cm^2 thus potentially representing the reloading from Position 1 to 2. However, as can be seen in Fig. 3.7, there are a number of similar strokes produced by the changes of temperature and thus there can be no full certainty which are which.

The above discussion leads to the conclusion that only unusually high live loads resulting in stress over 400 kg/cm^2 can be expected to leave a record on the scratch gage target which can be separated with certainty from the thermal effects.

3.4.4 Distribution of Loads Between Boxes

Although this bridge was designed to carry a full live load by each box in conformance with the DNER Specification (3.1), in actuality the load may be applied mainly to one box and not over all six lanes. The bracing inside and between the boxes was designed for such cases, and the pertinent analysis established that a load applied to one box would be distributed in a ratio 55% to 45% between the loaded and the unloaded boxes, respectively. The test load program presented an opportunity to check this analysis experimentally.

Taking the load contribution to a box to be proportional to the moment and the resultant bending stress, the share of the load taken by the south box is given in per cent by

$$\% \text{ Distr.} = \frac{100}{1 + (\sigma_{Bb}^N / \sigma_{Bb}^S)} \quad (3.6)$$

where the bending stresses of the north and south boxes are taken in the bottom flange since they are larger than in the top flange. The other box then takes the remainder.

The ratios of $\sigma_{Bb}^N / \sigma_{Bb}^S$ are computed on line 13 in Tables 3.9 and 3.10 for each Test Load Position and for each section where there are sufficiently reasonable data. The corresponding distribution percentages are listed on lines 14 and 15; on line 14 for the box loaded in a particular position and on line 15 for the unloaded box.

Although many values on lines 14 and 15 of Table 3.10 may be debatable because of the significant discrepancies between some measured stresses as, for example, can be detected from the inconsistent deviations between the stresses in the north and south boxes

shown on lines 4 and 10, some conclusive observations can still be made. For Test Load Position 1 (the trucks in the central span), the loaded north box had higher stresses near the support (57 and 62(?)% at FB57 and 51). It seems as if a countertwisting moment developed within the span to counteract an uneven moment at the intermediate support (FB57). Although no rigorous analysis was performed, it appears that this kind of behavior should have been expected.

Load Position 2 (the trucks within the side span) resulted in consistently higher stresses in the loaded north box although the difference at FB27 is only 2%. A similar observation can be made also for Test Load Positions 3 and 4 if the two sections indicated by question marks are disregarded as unrealistic. Then, the average percentage for the loaded box from Load Positions 2, 3 and 4 becomes

$$(1/7)(51 + 55 + 54 + 53 + 53 + 54 + 56) = 53.7\%$$

which is only slightly below the theoretical value of 55%.

The most consistent values of the measured stresses due to the test loads were at FB42 for Load Positions 2 and 4 (shown in Fig. 3.14). The load distribution percentages for these two cases average from the values given in Table 3.9 to 54%. This is even closer to the theory than the average for all sections, but still 1% below.

From the above discussion it can be concluded that the load distribution can be taken as 54 vs. 46% between the loaded and unloaded boxes and that the theoretical method used in Ref. 3.2 can be trusted to give accurate results.

3.5 Force History

The term force history refers to a continuous record of the change of internal forces in the bridge during construction and after completion. A record of stresses at a few locations was sufficient to establish the forces once the applicability of the analytical methods was verified by evaluating the construction stresses. Thus in the following all attention is on the record of stress changes. The prime means of obtaining a continuous record were the scratch gages. Mechanical gage readings also served for relating a state of stress at one time with a state of stress at another time period several months later by comparing the respective sets of readings with the readings on an Invar bar. On the other hand, the electrical resistance gages can be reliably used only over the short time period they are connected to a data acquisition unit.

The force history study can be subdivided into the following three periods: (1) Erection, (2) Placement of pavement and parapets, and (3) Service.

3.5.1 Erection

This period covers the major construction stages -- the erection of the bridge girder segments. It consisted of the transfer from the jetties to the pontoon, from the pontoon to the pier rings, and the center span lift. The period extends until the time when the center span was permanently connected to the side spans, thus transforming the structure from a statically determinate system into a three-span continuous girder.

The stresses for these construction stages are discussed in Art. 3.3. The large amplitude stress changes of the four scratch gage traces for this period shown in Fig. 3.7 are compared there with the stresses measured by other systems (electrical and mechanical). The blobbed portions at the ends and between the large zig-zags represent a record of the interim periods between the transfers. For example, in the right bottom photograph, FB 42 Bott., the first top blob is a record of the two days between the transfer of the side span from the jetties to the pontoon and the transfer from the pontoon to the pier rings. Apparently the stress changes were too small, not only to advance the target but even to really blob it up.

The next blob between the transfer to the pier rings on 14 October 1973 and the center span lift on 12 December 1973 is much more pronounced. However, although the stress changes during the intervening two months were larger, there still was no target advancement. This means that the stresses, which during this period could have been caused only by temperature variation and repositioning of construction equipment, remained below approximately 200 kg/cm^2 -- the apparent sensitivity of this particular gage.

The complete trace recorded by this target before its removal is shown in Fig. 3.7. The blobbed area at the end of the large trace produced by the center span lift (the third one in sequence) was developed while the bridge was still statically determinate and the stresses were due to the hoisting of the center span and the thermal effects.

Again, there was no advancement till the center span was bolted to the side span cantilevers on 5 January 1974.

3.5.2 Placement of Pavement and Parapets

The low amplitude zig-zag trace shown in Fig. 3.7 for the period after 5 January 1974 until 28 February 1974, right before the opening of the bridge to traffic, covers the construction period after the bridge was joined into a statically indeterminate continuous girder structure. Due to the indeterminacy the day-night thermal stress changes became large enough to advance the target and the blobs developed only when the temperature changes were too small.* The last few zig-zags took place when the load testing was conducted as discussed in Art. 3.4.2.

The recorded daily stress changes are of approximately 350 kg/cm^2 and they are given by the amplitude of the zig-zags. However the overall lowering or rise of the trace could be explained only by considering the stresses caused by construction operations.

Figure 3.17 shows this portion of the trace in conjunction with the stress changes computed for the placement of parapets, median barrier and pavement and plotted to the same stress scale. The time scale was judiciously established by counting the daily zigs and assigning the remaining days to the slight blobs which developed when the temperature variation as given by the meteorological records was too small. These periods are marked in the figure by dashed lines.

* Thermal stress analysis is discussed in detail in Chapter 4.

A direct correlation between the overall pattern of the scratch gage trace and the stress plot can be observed. For example, between the 15th and 21st January (7 days), a theoretical stress change of 175 kg/cm^2 was calculated as depicted by the gradual dip in the plot. This corresponds to an overall stress change of about 175 kg/cm^2 recorded by the trace over 7 zigs made in 7 days.

Other scratch gage traces for this period (Nos. 7 and 9 of Table 2.2) are not as clear as the trace discussed above (No. 8) -- they were less sensitive and have more blobbed areas making it difficult or impossible to pinpoint specific dates. However, they still exhibit the general stress change pattern of this construction period.

3.5.3 Service

The regular service period started when the bridge was opened to traffic on 4 March 1974. It can be considered to consist of two parts: one extending to January 1975 and the other from January 1975 on after the gage length was changed from 30.5 cm to 100 cm, thus making the gages more sensitive.

The gage traces of the first part are Nos. 12 to 22, 24 and 25 in Table 2.2. Of these, Nos. 15, 20, 22 and 24 are the clearest for analysis.

Figure 3.18 shows the trace No. 22 which gives a record of the stress changes at FB42Bott from 6 June 1974 till 9 January 1975. As in Fig. 3.17, the zig-zags are produced by the daily temperature changes, and except for some blobbed and indistinct areas resulting from more even temperature conditions, a day-to-day correspondence can be established between the

zigs and specific dates. (Daily meteorological records of temperature and humidity can be very helpful for this purpose.*)

The establishment of such a correlation provides a means for pinpointing the date of some event should this event produce an unusually large stress change. However, no such stress changes are discernible either in Fig. 3.18 or in any other scratch gage traces, thus indicating that no incident of overstressing has taken place during this period.

Another important observation was made from the trace of Fig. 3.18 in conjunction with the traffic records supplied by DNER. The traffic records show an average traffic count of 20,000 vehicles per day during the week (Monday through Friday) and a double that, approximately 40,000 per day, for Saturday and Sunday. However, no such weekly periodicity can be detected in the trace of the stress changes. Thus, the stresses caused by regular traffic are apparently so low that they are completely overshadowed by the thermal stress changes.

An estimate of the gross bending stresses produced at FB42Bottom by the present traffic was made utilizing information from the DNER traffic count and some plausible assumptions with respect to the weight and speed of particular types of vehicles. A summary of the highest hourly traffic counts, of the assumptions and of the resultant stresses is given in Table 3.11. The weekday traffic was chosen with the highest hourly truck count of 37 and the Sunday traffic with the highest car count of 3263.

*Such correlation is discussed later in connection with the larger amplitude scratches obtained after January 1975.

The Sunday stress of 64 kg/cm^2 hardly differs from the weekday stress of 60 kg/cm^2 , and this confirms the observations made for Fig. 3.17 of the absence of any weekly changes of the amplitude of the scratch gage trace. Realistically assuming that instead of one truck and one bus two of each are on the side span, the resultant bending stress of 122 kg/cm^2 is still quite low in comparison with the live load design stress of approximately 700 kg/cm^2 . Of course this situation may change with an increase of the truck traffic in the future.

The scratch gage traces covering the period from January 1975 till June 1975 are Nos. 28 to 35 of Table 2.2 with the traces No. 28 and 32 being the best. With the gage length extended from 30.5 cm to 100 cm the amplitude significantly increased in comparison with the amplitude of the traces for the previous periods. There is a zig for essentially every day.

A comparison of the improved accuracy is illustrated in Figure 3.19 where two segments of scratch gage traces, one for the gage length of 30.5 cm and the other for the gage length of 100 cm, are shown. A zig corresponding to a stress change of 280 kg/cm^2 is pointed out in each segment. It is obvious that the trace for the 100 cm gage length is defined much more clearly and can be evaluated with greater precision. The larger thickness of it was apparently produced by smaller zig-zags generated by traffic superimposed on top of the general large trace caused by diurnal changes of temperature.

Figure 3.20 shows a parallel presentation of a scratch gage trace (a segment of No. 32 of Table 2.2) and of a meteorological temperature record for the same period. In correlating the two curves, the low points of the scratch gage trace (high tension) should be matched with the high points of the temperature curve. Since the forward motion of the scratch gage target is somewhat irregular for it depends on the magnitude of the stress changes rather than on time, the matching points of the two curves are not exactly above each other. Furthermore, the temperature record was taken at the meteorological station many kilometers away and thus only approximately represents the temperature conditions at the bridge. Still, there is a relatively close agreement between the daily fluctuations of the stress and temperature.

A violent storm at 17:00 hours on May 17, 1975, with wind gusts up to 94 km/h, caused a sudden reduction in temperature from 26° to 17°. This was not recorded by the scratch gage. However, the subsequent leveling of the temperature (see the horizontal portion between 17th and 18th of May) led to a stabilization of the scratch gage trace with the advancement apparently caused only by the traffic.

Although a detailed analysis of scratch gage traces in conjunction with the meteorological (temperature, humidity, solar radiation) and traffic data promises to yield considerable benefits in understanding the bridge behavior and the forces to which the bridge may be subjected, this is a very time consuming and demanding activity which could be only initiated within the scope of this project.

3.5.4 Mechanical Gage Readings

The mechanical gage readings made after the erection of the bridge were intended to indicate any permanent gross stress changes in the life of the bridge as would have been caused by pier settlements or some other unforeseen effects. The readings on the bridge were taken at three to six month intervals and each time they were compared to the readings on the same Invar bar used as a standard reference. In this manner it was possible to establish absolute strain changes from one reading to the next.

The first reading of this series was taken in December 1973 (Reading No. 9 in Table 2.3) after the central span was lifted out of the water but not yet connected to the side spans. All other readings were made on the completed bridge under regular traffic in March 1974, June 1974, January 1975 and June 1975 (Reading Nos. 10 to 13 in Table 2.3).

At first the data from different reading periods made no sense; there was considerable scatter and no logical correlation seemed to exist. Apparently, this scatter was due to the following causes:

- a) Damage to the gage holes due to rust, dirt, paint, mechanical disturbance (stepping on), etc.
- b) Temperature variations in the bridge during the several hours needed to take readings and from location to location in the bridge cross sections.
- c) Changes in the traffic and wind conditions during a reading period and between the readings.

- d) Human errors in reading, recording and identification of gage locations.

Application of careful judgement, especially in correcting human errors in the identification of gage hole locations and recording which may have resulted from the changes of personnel, eliminated many inconsistencies and the data could be analyzed.

Figure 3.21 gives some typical plots of the mechanical gage readings at four cross-sectional locations for the five reading times. Whereas the period from December 1973 to March 1974 does not show any logical pattern in the changes of readings -- apparently due to the structural changes resulting from the bolting of the central span, the other periods have each a definite trend as indicated by the lines sloping up or down. For example, the readings tend to increase from June 1974 to January 1975, and decrease from January 1975 to June 1975. Analogous observations were also made for other sections and gages.

A summary of the strain changes at all measured sections in the completed bridge is shown for the three periods in Fig. 3.22. Included are both the top and bottom flange readings. There is considerable scatter for the first two periods (March 1974 - June 1974 and June 1974 - January 1975, but the last period (January 1975 - June 1975) shows much more consistent strain changes.

Statistical analysis was made to determine the following characteristics of the strain changes for a particular period:

- Difference of strain changes between the top and bottom flanges in a cross section. This would have indicated a bending moment.
- Variation of the top-to-bottom flange strain differences along the girder from one instrumented section to another. A linear variation of the moments computed from the strain differences would have pointed to a permanent moment.
- Average strain change in a cross section corresponding to a gross elongation or shortening of the girder.

As can be observed in Fig. 3.22, especially in the most consistent plot (c), no definite bending effects, neither from section to section nor in individual sections, could be detected conclusively. However an overall uniform shift is quite obvious.

Table 3.12 summarizes the statistical analysis of the average strain changes based on the data plotted in Fig. 3.22. In order to minimize the effect of the extreme random errors, the range of data was reduced after obtaining the first mean and standard deviations to $R = \text{Mean} \pm \text{Standard Deviation}$. The new mean and standard deviation were taken then as the indicators of the strain change in a particular period.

Since the only plausible cause for these gross strain changes appears to be the seasonal change of temperature, the strains converted to the corresponding temperature changes are entered on the last line

of Table 3.12 with the standard deviation giving the range of accuracy. The meteorological records show the average air temperature changes between the readings to be about 4 to 5° lower than the values in Table 3.12. This agrees with the observations that the average temperature increase in the bridge relative to the temperature in the air is higher during the day than at night and with the fact that the readings were taken at different times.

For example, the period from January 1975 to June 1975 has a temperature change of -19.4°C and the meteorological records indicate a change of -13°C .

In summary, a conclusion can be reached that, although the mechanical gage readings on the completed bridge are subject to some scatter, they are sufficiently accurate to measure average strains caused by temperature changes and thus have the capability to detect gross changes in bridge forces which may take place between the readings due to pier settlements or other unforeseen causes.

3.5.5 Conclusions

The following general conclusions can be reached from the force history study:

- 1) The forces produced by the erection stages and the placement of the parapets, median barrier and pavement could be recorded by the scratch gages with adequate accuracy.
- 2) The gross bending stresses caused by the present level of traffic are too small (about 120 kg/cm^2) to be recorded distinctly with the scratch gages.

3) Stress changes due to the daily temperature fluctuations leave a continuous trace on the scratch gage targets and may be used to pinpoint the date of a particular event.

4) Mechanical gage readings can reliably provide a check on the gross force changes in the bridge caused by seasonal temperature changes or some unforeseen occurrences such as settlement of a pier. A six-month interval between readings should be sufficient.

3.6 Chapter 3 - Tables and Figures

Table 3.1 Stress Changes (kg/cm²) Jetties to Pontoon - Pontoon to Piers
and Effective Location of N.A.

1) FB27

1.1) Jetties to Pontoon

Top Flange

$$\left. \begin{array}{l} \text{Strain } [1920 + 1939(2) + 2003]/4 = 1950 \\ \text{Mech } [1890 + 1995(2) + 1995]/4 = 1970 \end{array} \right\} 1960$$

Bottom Flange

$$\text{Strain } [2222 + 2081 + 2191 + 2089 + 2121 + 2040]/7 = 2120$$

$$1960/2120 = 0.925$$

1.2) Pontoon to Piers

Top Flange

$$\left. \begin{array}{l} \text{Strain } [2215 + 2209 + 2300]/3 = 2240 \\ \text{Mech } [2101 + 2208(2) + 2247]/4 = 2220 \end{array} \right\} 2230$$

Bottom Flange

$$\text{Strain } [2358 + 2355 + 2425 + 2504]/4 = 2410$$

$$2230/2410 = 0.925$$

$$C_T/C_B = 0.925; C_T + C_B = 634.7 \text{ cm} = d_{\text{Des.}}$$

$$C_T = 305.0 \text{ cm}$$

2) FB42

2.1) Jetties to Pontoon

Top Flange

$$\left. \begin{array}{l} \text{Strain } [1740 + 1799(2) + 1705]/4 = 1760 \\ \text{Mech } [1734 + 1785]/2 = 1760 \end{array} \right\} 1760$$

Bottom Flange

$$\text{Strain } [2427 + 2427 + 2326 + 2326]/4 = 2380$$

$$1760/2380 = 0.739$$

2.2) Pontoon to Piers

Top Flange

$$\left. \begin{array}{l} \text{Strain } [1797 + 1835(2) + 1780]/4 = 1810 \\ \text{Mech } [1691 + 1779(2) + 1916]/4 = 1790 \end{array} \right\} 1800$$

Table 3.1 (Cont'd) Stress Changes (kg/cm²) Jetties to Pontoon -
Pontoon to Piers

Bottom Flange

$$\text{Strain } [2436 + 2467(2) + 2564] / 4 = 2484$$

$$1800/2484 = 0.725$$

$$[.725 + .739] \frac{1}{2} = .732 = C_T/C_B; C_T + C_B = 731.1 \text{ cm} = d_{\text{Des.}}$$

$$C_T = 309.0 \text{ cm}$$

3) FB51

3.1) Jetties to Pontoon

Top Flange

$$\left. \begin{array}{l} \text{Strain } [1094 + 1100(2) + 1089] / 4 = 1095 \\ \text{Mech } [892 + 1102] / 2 = 1000 \end{array} \right\} 1047.5$$

Bottom Flange

$$\text{Strain } [1044 + 1029 + 1064] / 3 = 1040$$

$$1047.5 / 1040 = 1.0072$$

3.2) Pontoon to Piers

Top Flange

$$\left. \begin{array}{l} \text{Strain } [1096 + 1069(2) + 1096] / 4 = 1080 \\ \text{Mech } [990 + 1034] / 2 = 1010 \end{array} \right\} 1045$$

Bottom Flange

$$\text{Strain } [1037 + 1034 + 1075] / 3 = 1050$$

$$1045 / 1050 = .9952$$

$$[1.0072 + .9952] / 2 = 1.00 = C_T/C_B$$

$$C_T + C_B = 918.8 \text{ cm} = d_{\text{Des.}}$$

$$C_T = C_B = 459.4 \text{ cm}$$

Table 3.2 Stress Changes (kg/cm²) - Mechanical Gage Readings

LOCATION	G A G E	JETTIES TO PONTOON (SOUTH)	PONTOON TO PIERS (NORTH)	CENTER SPAN LIFT (NORTH)	ON JETTIES TO BRIDGE COMPLETION (SOUTH)	JAN75-JUN75 (NORTH)*
1	2	3	4	5	6	7
FB17 TOP	1		-26.7			
	3		-73.9			
	5		-51.3			
	1a			- 140.6		
	3a			- 63.3		-200*
	5a			- 118.0		
	6	- 105				
	7	- 262				
FB17 BOTT.	8	- 105				
	1b					-195*
	2b					
	3b					-200*
	4b					
	5b					-188*
	6b				+ 897	
	7b					
FB27 TOP	8b				+1421	
	9		-2101			
	11		-2208			
	13		-2347			
	9a			+ 892.8		-195*
	11a			+ 970.1		
	13a			+1040.4		-163*
	14	+1890				
	15	+1995				
	16	+1995				
FB27 BOTT.	14a					
	15a					
	16a					
	9b					
	10b					
	11b			- 984.2		
	12b			- 871.7		
	13b			-1377.9		
14b				+ 704		
15b				+ 599		
16b				+ 939		

*Strain Changes (10⁻⁶ cm/cm)

Table 3.2 (Cont'd) Stress Changes (kg/cm²) - Mech. Gage Readings

LOCATION	G A G E	JETTIES TO PONTOON (SOUTH)	PONTOON TO PIERS (NORTH)	CENTER SPAN LIFT (NORTH)	ON JETTIES TO BRIDGE COMPLETION (SOUTH)	JAN75-JUN75 (NORTH)*
1	2	3	4	5	6	7
FB42 TOP	17		-1691			
	18		-1779			
	19		-1916			
	17a			+1321.6		-263*
	18a			-3859.6		
	19a			+1251.3		-200*
FB42 BOTT.	20	+1732				
	21	+1785				
	20a					
	21a					
	17b			-1659.1		
	18b			-1982.5		
FB42 BOTT.	19b			-1926.2		
	20b				+2293	
FB51 TOP	21b				+1596	
	22		-2031			
	24		- 511			
	26		-1034			
	22a			+ 864.7		
	24a			+1054.5		
	26a			+1068.8		-170*
	27	+ 892				
FB51 BOT	28	+1102				
	28a					
	22b			-1160.0		
	23b			-1138.9		
FB51 BOT	24b			-1181.0		
	25b			-1448.2		
	26b					-250*
	28b				+1533	

*Strain Changes (10⁻⁶ cm/cm)

Table 3.2 (Cont'd) Stress Changes (kg/cm²) - Mech. Gage Readings

LOCATION	G A G E	JETTIES TO PONTOON (SOUTH)	PONTOON TO PIERS (NORTH)	CENTER SPAN LIFT (NORTH)	ON JETTIES TO BRIDGE COMPLETION (SOUTH)	JAN75-JUN75 (NORTH)*
1	2	3	4	5	6	7
FB57 TOP	29					
	31		-144			
	33		-129			
	29a			+688.9		-200*
	30a			+822.5		
	31a			+921.0		-225*
	32a			+745.2		
	33a			+820.0		-225*
	34					
	35	+ 52				
	36	+262				
	34a					
35a						
36a						
FB57 BOTT.	29b			-921.0		
	30b			-829.5		
	31b					
	32b			-836.6		
	33b			-829.5		
	34b				+ 851	
	35b					
36b					+1481	

*Strain Changes (10⁻⁶ cm/cm)

Table 3.3

Stress Changes from Scratch Gage Targets - Construction Stages

LOCATION	CONSTRUCTION SEQUENCE	STRESS CHANGE (kg/cm ²)	$\frac{C_{FL.}}{Y_{S.G.}}$	EXTRAPOLATED STRESS CHANGE IN FLANGE (kg/cm ²)
1	2	3	4	5 = 3 x 4
FB27 TOP	Jetties - Pontoon	1970	1.095	2156
	Pontoon - Piers	2210	1.095	2418
FB27 BOTT	Jetties - Pontoon	2060	1.065	2198
	Pontoon - Piers	2210	1.065	2351
	Center Span Lift	820	1.065	869
FB42 TOP	Jetties - Pontoon	1680	1.053	1768
	Pontoon - Piers	1680	1.053	1768
	Center Span Lift	1440	1.053	1516
FB42 BOTT	Jetties - Pontoon	2250	1.066	2405
	Pontoon - Piers	2300	1.066	2456
	Center Span Lift	1730	1.066	1846

$\frac{C_{FL.}}{Y_{S.G.}}$ = $\frac{\text{Distance from centroid to extreme fiber of flange}}{\text{Distance from centroid to scratch gage}}$

Table 3.4 Cross-Sectional Properties Used in Analysis

Instrumented Section at Floor Beams						
FB	17	27	42	51	57	
1	x (m)	-0.5	50.5	124.6	170.5	198.9
Column	1	2	3	4	5	
2	I (m ⁴)	3.371	4.811	7.796	20.366	42.064
3	d (cm)	568.3	634.7	731.1	918.8	1286.8
4	C_T (cm)	243.7	297.3	302.8	439.5	619.2
5	C_B (cm)	324.6	337.4	428.3	479.3	667.6
6	S_T (m ³)	1.3832	1.6180	2.5751	4.6336	6.7938
7	S_B (m ³)	1.0385	1.4257	1.8200	4.2498	6.3001
8	ΔM : J-P	0	-30,855	-45,169	-46,398	-1730
9	(tm) P-PR	0	+35,146	+47,333	+47,245	+1,762
10	C.Span Lift	0	-15,079	-37,206	-50,911	-59,392

- Notes:
- 1) Depths, d, were computed by parabolic interpolation between the values at neighboring 10-m stations supplied by the designer (HNTB).
 - 2) Moments of inertia, I, were computed by parabolic interpolation except at FB42 where cross-sectional dimensions were used.
 - 3) Moment changes, ΔM , were computed by linear interpolation from the moment diagrams supplied by the designer (HNTB).

Table 3.5 Cross-Sectional Properties Adjusted
on Basis of Field Readings

	FB	27	42	51
	1	2	3	4
1	Depth $d_{Des.}$ (cm)	634.7	731.1	918.8
2	$(C_T)_{Des.}$ (cm)	297.3	302.8	439.5
3	$(C_T)_{Adj.}$ (cm)	305.0	309.0	459.4
4	Shift of N.A. e (cm)	7.7	6.2	19.9
5	% (e/C_T)	2.6	2.0	4.5
6	$(S_T)_{Adj.}$ (m ³)	1.5773	2.5230	4.4332
7	$(S_B)_{Adj.}$ (m ^{3/4})	1.4595	1.8468	4.4332

Table 3.6 Computation of Moment Changes - Center Span Lift
(Adjusted Location of Neutral Axis)

LOCATION		MECHANICAL GAGES	STRAIN GAGES
1		2	3
FB17	Top	1 (100 kg/cm ²)(1.3832 x 10) = +1,383 tm*	0.0 tm
	Bottom	2 NO READINGS	NO READINGS
FB27	Top	3 (970 kg/cm ²)(1.5773 x 10) -15,300 tm	(980 kg/cm ²)(1.5773 x 10) = -15,458 tm
	Bottom	4 (1050 kg/cm ²)(1.4595 x 10) = -15,325 tm	(1123 kg/cm ²)(1.4595 x 10) = -16,390 tm
FB42	Top	5 (1290 kg/cm ²)(2.5230 x 10) = -32,493 tm	(1350 kg/cm ²)(2.5230 x 10) = -34,004 tm
	Bottom	6 (1880 kg/cm ²)(1.8468 x 10) = -34,660 tm	(1950 kg/cm ²)(1.8468 x 10) = -35,950 tm
FB51	Top	7 (1050 kg/cm ²)(4.4332 x 10) = -46,549 tm	(1243 kg/cm ²)(4.4332 x 10) = -55,105 tm
	Bottom	8 (1160 kg/cm ²)(4.4332 x 10) = -51,425 tm	(1176 kg/cm ²)(4.4332 x 10) = -52,134 tm
FB57	Top	9 (811 kg/cm ²)(6.7938 x 10) = -55,098 tm	(1212 kg/cm ²)(6.7938 x 10) = 82,341 tm**
	Bottom	10 (848 kg/cm ²)(6.3001 x 10) = -53,425 tm	(1003 kg/cm ²)(6.3001 x 10) = -63,190 tm

*This moment change apparently corresponds to equivalent temperature change.

**This stress was affected by stress concentrations and system problems.

Table 3.7 Computation of Moment Changes - Jetties to
Pontoon - Pontoon to Piers
(Adjusted Location of Neutral Axis)

LOCATION		JETTIES - PONTOON	PONTOON - PIERS	
FB27	Top	1	(1960 kg/cm ²)(1.5773 x 10) = -30,915 tm	(2230 kg/cm ²)(1.5773 x 10) = +35,174 tm
	BOTT	2	(2120 kg/cm ²)(1.4595 x 10) = -30,941 tm	(2410 kg/cm ²)(1.4595 x 10) = +35,174 tm
FB42	TOP	3	(1760 kg/cm ²)(2.5288 x 10) = -44,330 tm	(1800 kg/cm ²)(12.5288 x 10) = +45,338 tm
	BOTT	4	(2380 kg/cm ²)(1.8437 x 10) = -43,880 tm	(2500 kg/cm ²)(1.8437 x 10) = +46,090 tm
FB51		5	Avg. ΔM^* = (1045 kg/cm ²)(4.4332 x 10) = 46,330	

*Stress changes for all four cases at FB51 TOP, Jetties-Pontoon, BOTT, Jetties-Pontoon, TOP, Pontoon-Piers, BOTT, Pontoon-Piers, were very close to each other and an average stress change was taken for the moment computation.

Table 3.8 Theoretical Moments per Box and Stresses for Test Loads
(Moments from Influence Lines)
(50-50% distribution of total moment between boxes was
assumed)

M in tm, σ in kg/cm²

Load Position		FB				
		17	27	42	51	57
1	2	3	4	5	6	7
1	M	0	-7333.5	-3290.1	-4502.0	-5281.0
2	1 σ_T	0	+84.5	+130.4	+101.6	+77.7
3	σ_B	0	-91.4	-178.1	-101.6	-83.8
4	M	0	+3616.9	+3947.4	-587.5	-3947.4
5	2 & 4 σ_T	0	-229.3	-156.5	+13.3	+58.1
6	σ_B	0	+247.8	+213.7	-13.3	-62.7
7	M	-2879	-1891.5	-344.1	+614.4	+1207.4
8	3 σ_T	+208.1	+119.9	+13.6	-13.8	-17.8
9	σ_B	-277.2	-129.6	-18.6	+13.8	+19.1

Table 3.9 Bending Stresses and Load Distribution at FB42
(From stresses in Fig. 3.14)

		Load Position			
		1	2	4	
	1	2	3	4	
1	North Box	σ_T^N	+175.8	-94	-183.8
2		σ_B^N	-113.7	+252	+155.7
3		σ_{Tb}^N	+136.4	-146	-143.5
4		σ_{Bb}^N	-186.4 (+8)	+200 (-14)	+196.0 (-18)
5		σ_a^N	+39.4	+52.2	-40.3
6		ΔT^N	+1.5	+2.1	-1.6
7	South Box	σ_T^S	+187	-75.5	-220.5
8		σ_B^S	-156.5	+210	+184
9		σ_{Tb}^S	+145.2	-121	-170
10		σ_{Bb}^S	-198.3 (+20)	+165 (-49)	-233 (+19)
11		σ_a^S	+41.8	+45	-49
12		ΔT^S	+1.7	+1.8	-1.9
13	$\sigma_{Bb}^N / \sigma_{Bb}^S$		0.940	1.212	0.841
14	% Distr. on Ld. Box		48.4	54.7	54.3
15	% on Unld. Box		51.6	45.3	45.7

The numbers in parentheses below lines 4 and 10 give deviations of σ_{Bb} from the theoretical values.

Table 3.10 Bending Stresses due to Test Loads

		Test Load Position 1					
Floor Beam		17	27	42	51	57	
1		2	3	4	5	6	
0	(S_T/S_B) Adj	-1.332	-1.0807	-1.366	-1.0	-1.07836	
1	North Box	σ_T^N	+55.1	+120	+175.8	+117	+171.8
2		σ_B^N	+34	-34	-113.7	-124.8	-104.4
3		σ_{Bb}^N	-12.1	-80.0	-186.4	-120.9	-143.3
4		Dev.	(+12)	(-11)	(+8)	(+19)	(+60)
5		σ_a^N	+46.1	+46.0	+39.4	-3.9	+38.9
6		ΔT^N	+1.8	+1.8	+1.5	-0.2	+1.5
7	South Box	σ_T^S	+13.5	+88	+187	+77	+185.3
8		σ_B^S	+65	-100	-156.5	-69	-27.8
9		σ_{Bb}^S	+29.4	-97.6	-198.3	-73	-110.6
10		Dev.	(+29)	(+6)	(+20)	(-29)	(-27)
11		σ_a^S	+35.6	-2.4	+41.8	+76.5	+82.8
12		ΔT^S	+1.4	-0.1	+1.7	+3.0	+3.3
13	$\sigma_{Bb}^N / \sigma_{Bb}^S$	N.G.	0.820	0.940	1.656?	1.30	
<u>Load Distr.</u>							
14	% Ld. Box		45?	48	62?	57	
15	% Unld. Box		55	55	38?	43	

Notes: N.G. = No Good, i.e., completely misleading because of large errors relative to values.

Lines 4 and 10: Deviation from the theoretical stress of Table 3.8 in absolute value
 $= |\sigma_{Bb}^N| - |(\sigma_{Bb}^N)_{Theor.}|$

Table 3.10 (Cont. 1) Bending Stresses due to Test Loads

		Test Load Position 2					
Floor Beam		17	27	42	51	57	
1		2	3	4	5	6	
0	$(S_T/S_B)_{Adj}$	-1.332	-1.0807	-1.366	-1.0	-1.07836	
1	North Box	σ_T^N	+94.5	-136.3	-94	+113.4	+142.6
2		σ_B^N	+12.0	+283.7	+252	-62.7	-33.9
3		σ_{Bb}^N	-47.1	+218.1	+200	-87.9	-91.6
4		Dev.	(+47)	(-30)	(-14)	(+75)	(+29)
5		σ_a^N	+59.1	+65.6	+52.2	+25.2	+57.7
6		ΔT^N	+2.3	+2.6	+2.1	+1.0	+2.3
7	South Box	σ_T^S	N.G.	-111	-75.5	N.G.	+140.3
8		σ_B^S		+296	+210		-13.0
9		σ_{Bb}^S		+211	+165		-79.5
10		Dev.		(-38)	(-49)		(+17)
11		σ_a^S		+84.6	+45		+66.5
12		ΔT^S		+3.3	+1.8		+2.6
13	$\sigma_{Bb}^N / \sigma_{Bb}^S$	N.G.	1.034	1.202	N.G.	1.152	
	<u>Load Distr.</u>						
14	% Ld. Box		51	55		54	
15	% Unld. Box		49	45		46	

Notes: See the table for Load Position 1

Table 3.10 (Cont. 2) Bending Stresses due to Test Loads

		Test Load Position 3					
Floor Beam		17	27	42	51	57	
1		2	3	4	5	6	
0	(S_T/S_B) Adj.	-1.332	-1.0807	-1.366	-1.0	-1.07836	
1	North Box	σ_T^N	+226.7	+20	+13.7	-20	-114.5
2		σ_B^N	-172.5	-66	-58.9	-31.4	-74.4
3		σ_{Bb}^N	-228.0	-44.7	-41.9	-5.7	+20.8
4		Dev.	(-49)	(-85)	(+23)	(-8)	(+2)
5		σ_a^N	55.5	-21.3	-17.0	-25.7	-95.2
6		ΔT^N	+2.2	-0.8	-0.7	-1.0	-3.8
7	South Box	σ_T^S	+100.9	+200	+14.7	-39	-36.5
8		σ_B^S	-260.0	+71	-50.5	+103	-59.4
9		σ_{Bb}^S	-206.1	-67.0	-37.6	+32	-11.9
10		Dev.	(-71)	(-62)	(+19)	(+18)	(-31)
11		σ_a^S	-53.9	+138	-12.9	+71	-47.5
12		ΔT^S	-2.1	+5.4	-0.5	+2.8	-1.9
13	$\sigma_{Bb}^N / \sigma_{Bb}^N$	1.106	0.667	1.114	N.G.	N.G.	
	<u>Load Distr.</u>						
14	% Ld. Box	53	40?	53			
15	% Unld. Box	47	60?	47			

Notes: See table for Load Position 1

Table 3.10 (Cont. 3) Bending Stresses due to Test Load

		Test Load Position 4				
Floor Beam		17	27	42	51	57
1		2	3	4	5	6
0	$(S_T/S_B)_{Adj}$	-1.332	-1.0807	-1.366	-1.0	-1.07836
1	σ_T^N	-48	N.G.	-183.8	+17.5	+61
2	σ_B^N	-34.3		-155.7	-59.1	-64.5
3	σ_{Bb}^N	+7.8		+196.0	-38.3	-65.1
4	Dev.	(+8)		(-18)	(+25)	(+2)
5	σ_a^N	-42.1		-40.3	-20.8	+0.61
6	ΔT^N	-1.7		-1.6	-0.8	0
7	σ_T^S	-107	N.G.	-220.5	-38	+61.3
8	σ_B^S	-122		+184	-134	-174.4
9	σ_{Bb}^S	-8.6		+233	-48	-122.3
10	Dev.	(+9)		(+19)	(+35)	(+59)
11	σ_a^S	-113.4		-49	-86	-52.1
12	ΔT^S	-4.5		-1.9	-3.4	-2.1
13	$\sigma_{Bb}^N / \sigma_{Bb}^S$	N.G.	N.G.	0.841	0.80	0.53
	Load Distr.					
14	% Ld. Box			54	56	65?
15	% Unld. Box			46	44	35?

Notes: See the table for Load Position 1

Table 3.11 Bending Stresses at FB42 Bottom
due to Present Traffic

		Car (DNER Categ. 1,2,3,9,10)	Truck (DNER Categ. 4,5,6,7)	Bus (DNER Categ.8)
1	Weight (kg.)	2000	55,000*	8000
2	Velocity (km/h)	90	50	70
	<u>Weekday (15Jan75, Total 26,400)</u>			
3	Max. No. per hr. (at 18 hrs)	1640	37	83
4	Spacing (m)	55	1350	800
5	No. in 200m (Rio side span)	3.64	1	1
6	Bending Stress (kg/cm ²)	3.4	50	7.3
7	Total Stress (kg/cm ²)		--60--	
	<u>Weekend (1Sep74, Total 35,420)</u>			
8	Max. No. per hr. (at 18 hrs)	3263	9	104
9	Spacing (m)	27.5	5000	700
10	No. in 200m (Rio side span)	7.3	1	1
11	Bending Stress (kg/cm ²)	6.9	50	7.3
12	Total Stress (kg/cm ²)		--64--	

*Maximum truck weight was estimated from the deck strain gage readings described in Chapter 6.

Notes:

- 1) The days were selected to give maximum observed hourly traffic rates.
- 2) Spacing = (Velocity)/(Hourly Rate)
- 3) Bending stress for cars was computed using the worst distribution of cars according to the design influence line for the moment at FB42.
- 4) Bending stress for trucks and busses was computed using the moment influence line for FB42.

Table 3.12 Adjusted Mean Strain and Temperature Changes
from Mechanical Gage Readings

Period	Mar. '74 to June '74	June '74 to Jan. '75	Jan. '75 to June '75
Mean (No. of Data) $M_1 (N_1)$	(Strain x 10^{+6}) 29.1 (28)	(Strain x 10^{+6}) 147.4 (24)	(Strain x 10^{+6}) -250 (19)
Std. Deviation (SD_1)	181.1	124.8	65.0
New Range $R = M_1 \pm SD_1$	-152 to 210	23 to 272	-315 to -185
Adj. Mean (No. of Data) $M_2 (N_2)$	14.0 (21)	134.3 (17)	-226.4 (16)
Std. Deviation SD_2	86.5	52.9	28.0
Temperature Change $\Delta^{\circ}C = \frac{1}{11.7} (M_2 \pm SD_2)$	$1.2^{\circ} \pm 7.4^{\circ}C$	$11.5 \pm 4.5^{\circ}C$	$-19.4^{\circ} \pm 2.4^{\circ}C$

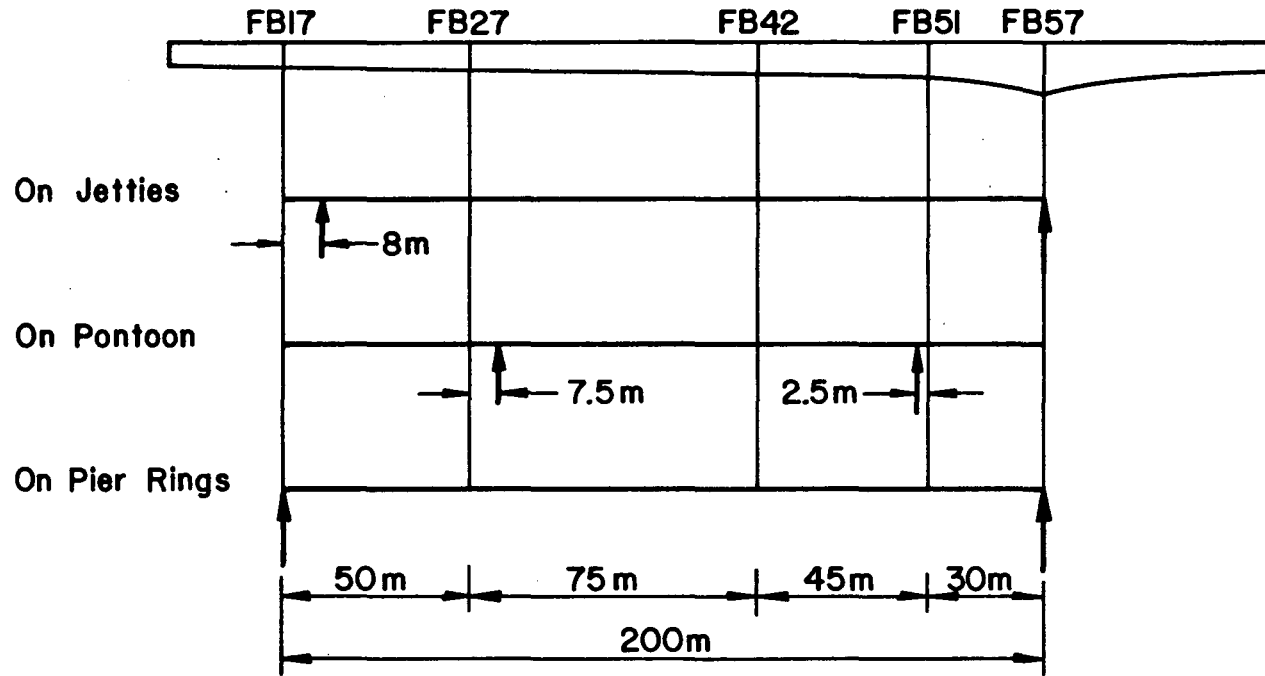


Fig. 3.1 Support Points - Rio Side Span Units

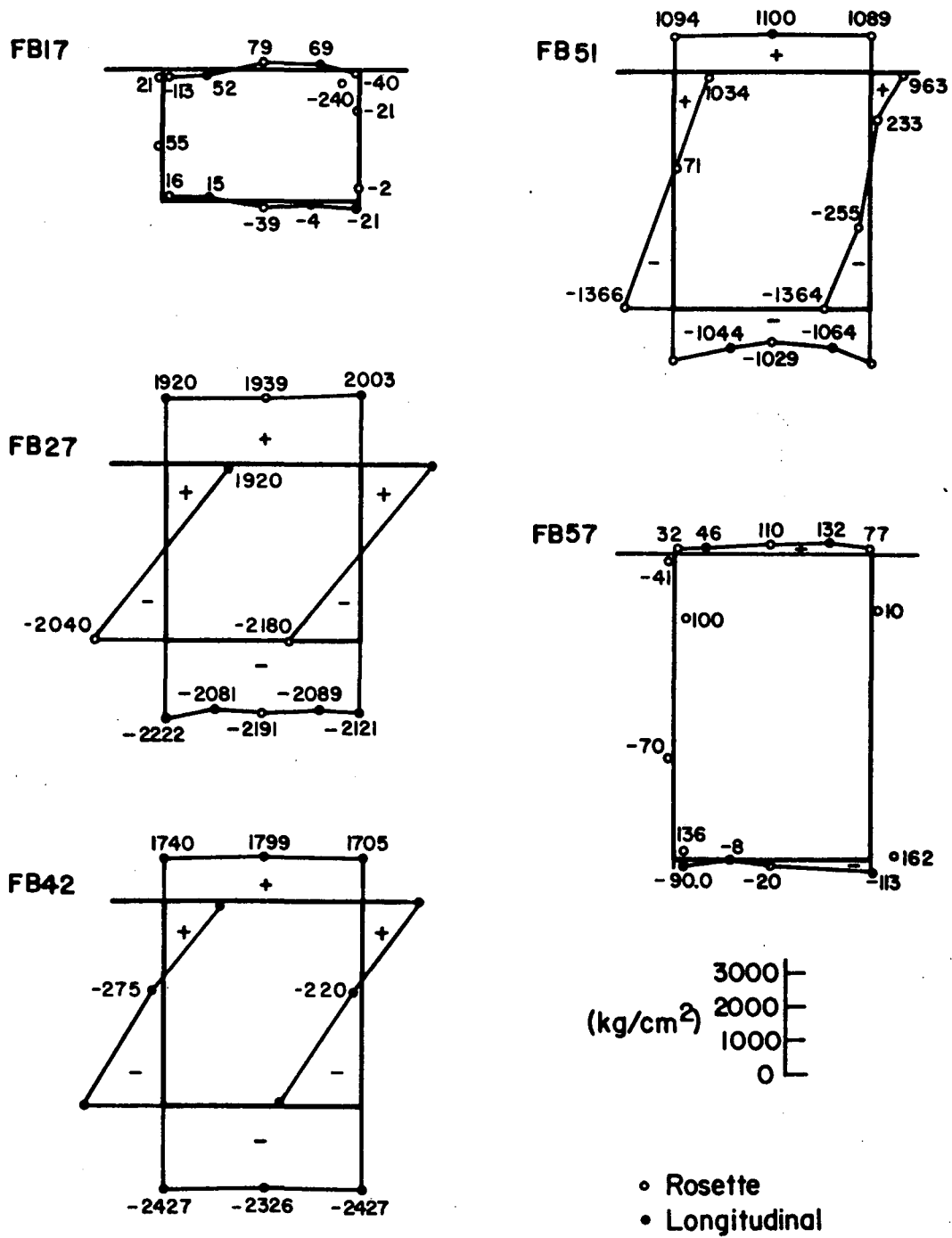


Fig. 3.2 Stress Changes (Strain Gage Measurements) - Jetties to Pontoon

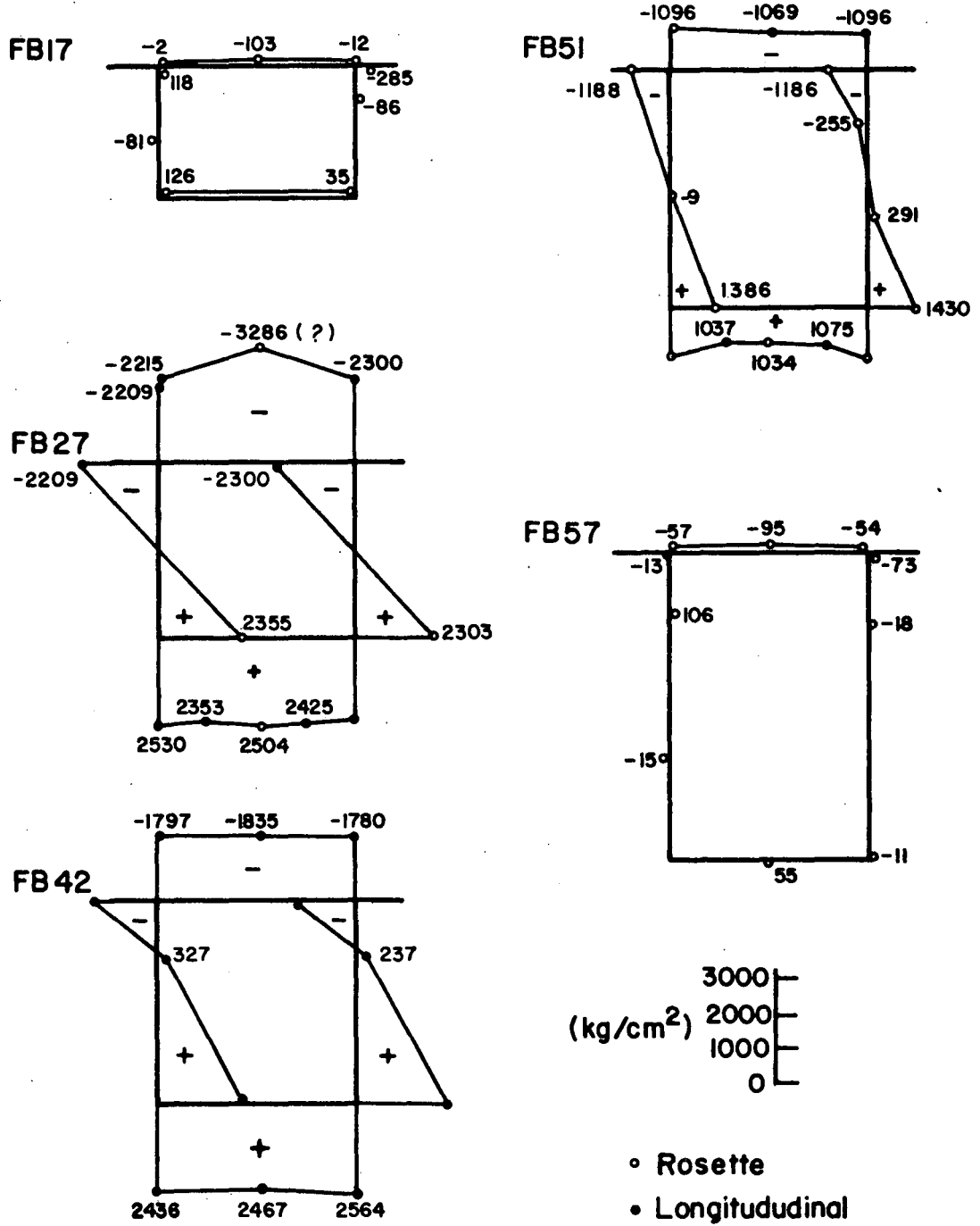


Fig. 3.3 Stress Changes (Strain Gage Measurements) - Pontoon to Piers

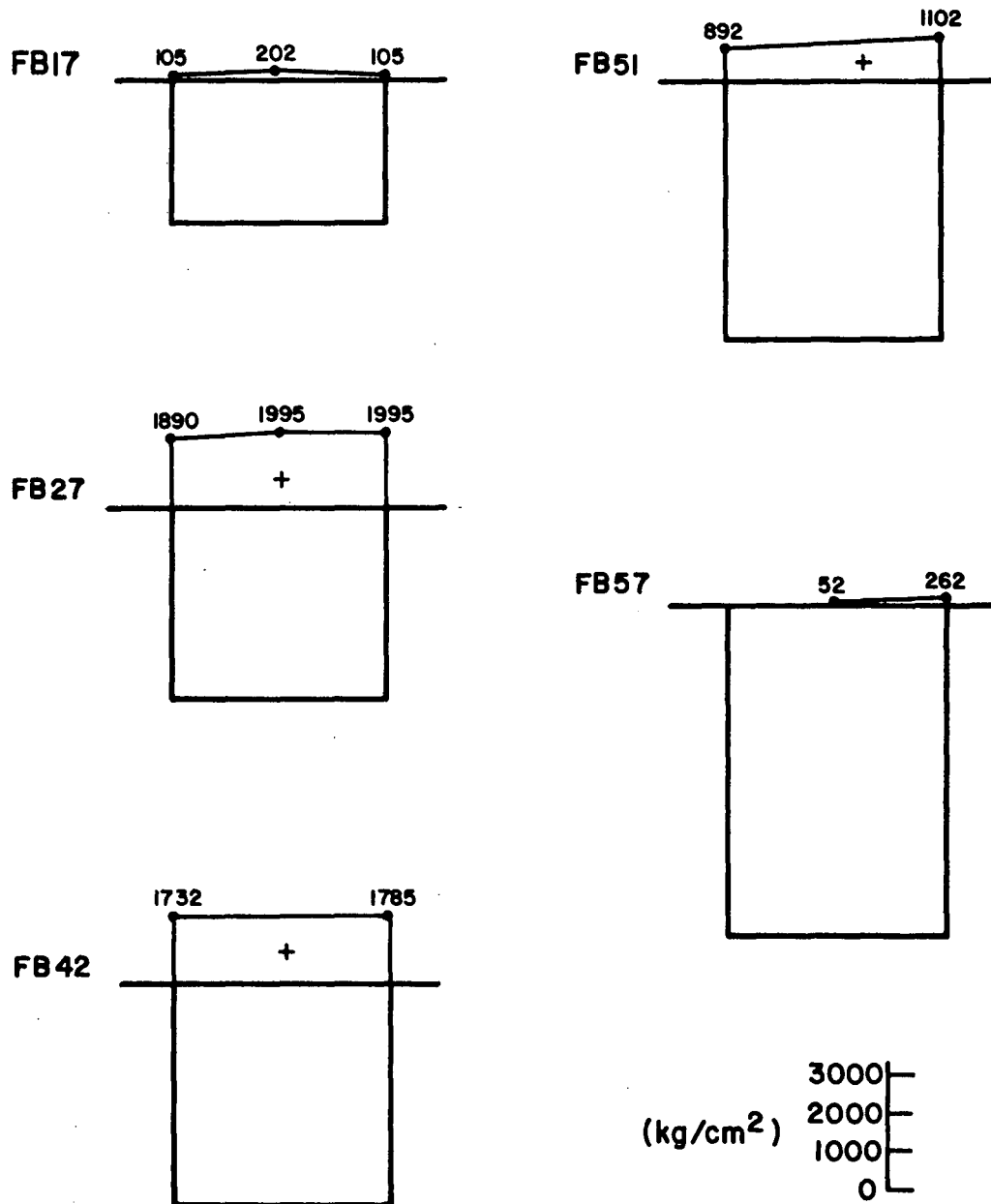


Fig. 3.4 Stress Changes (Mechanical Gage Measurements) Jetties to Pontoon

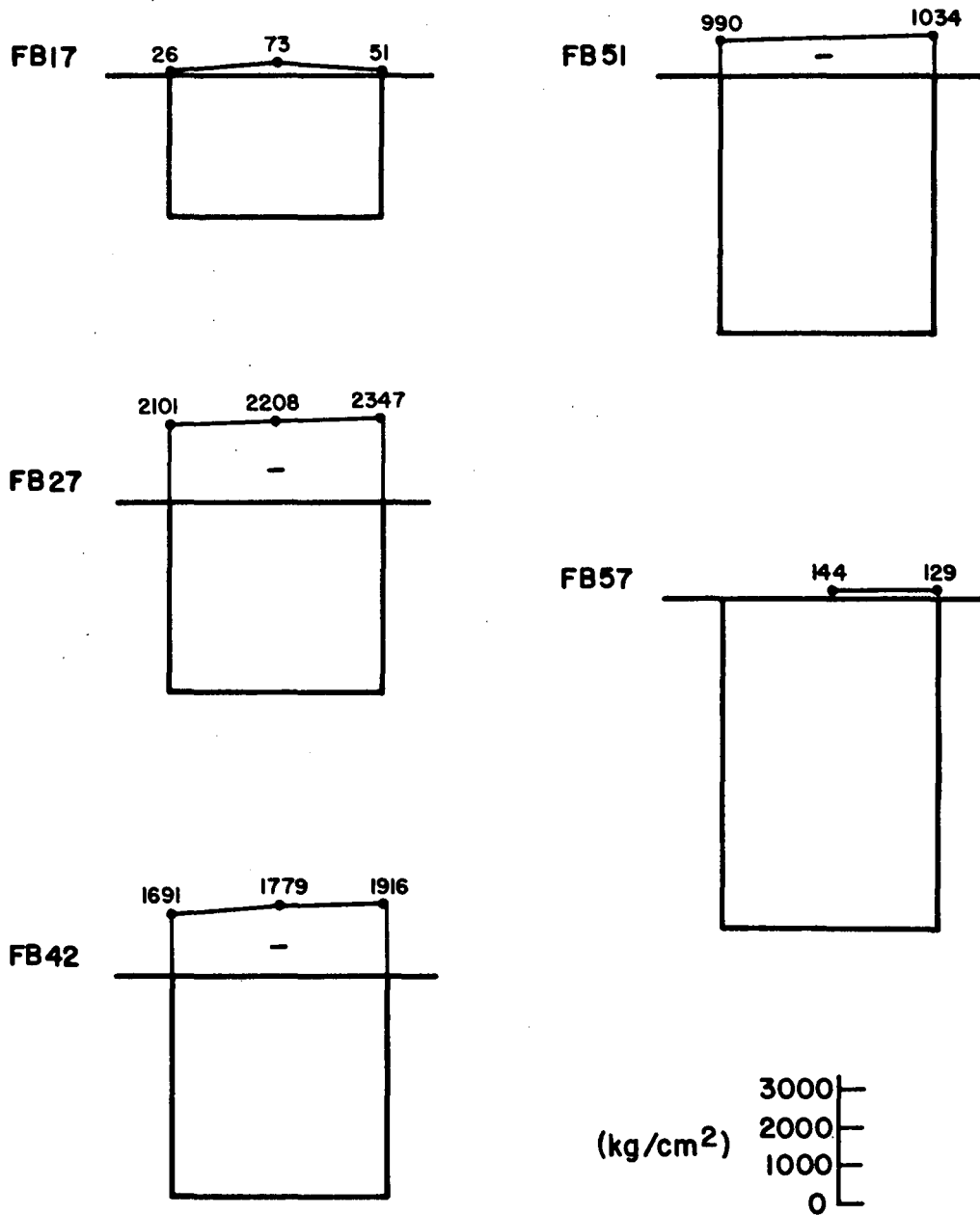


Fig.3.5 Stress Changes (Mechanical Gage Measurements) - Pontoon to Piers

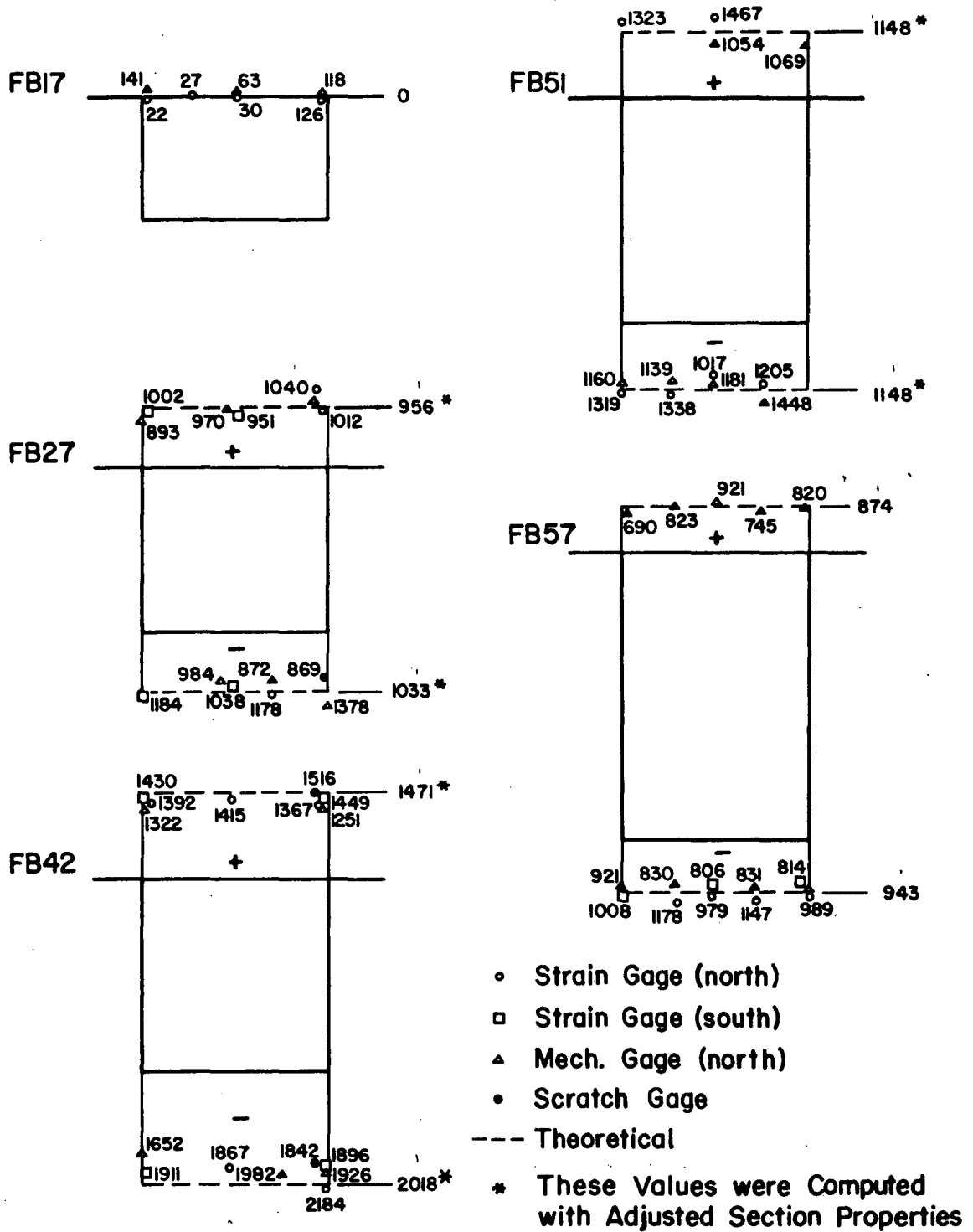


Fig. 3.6 Stress Changes - Center Span Lift

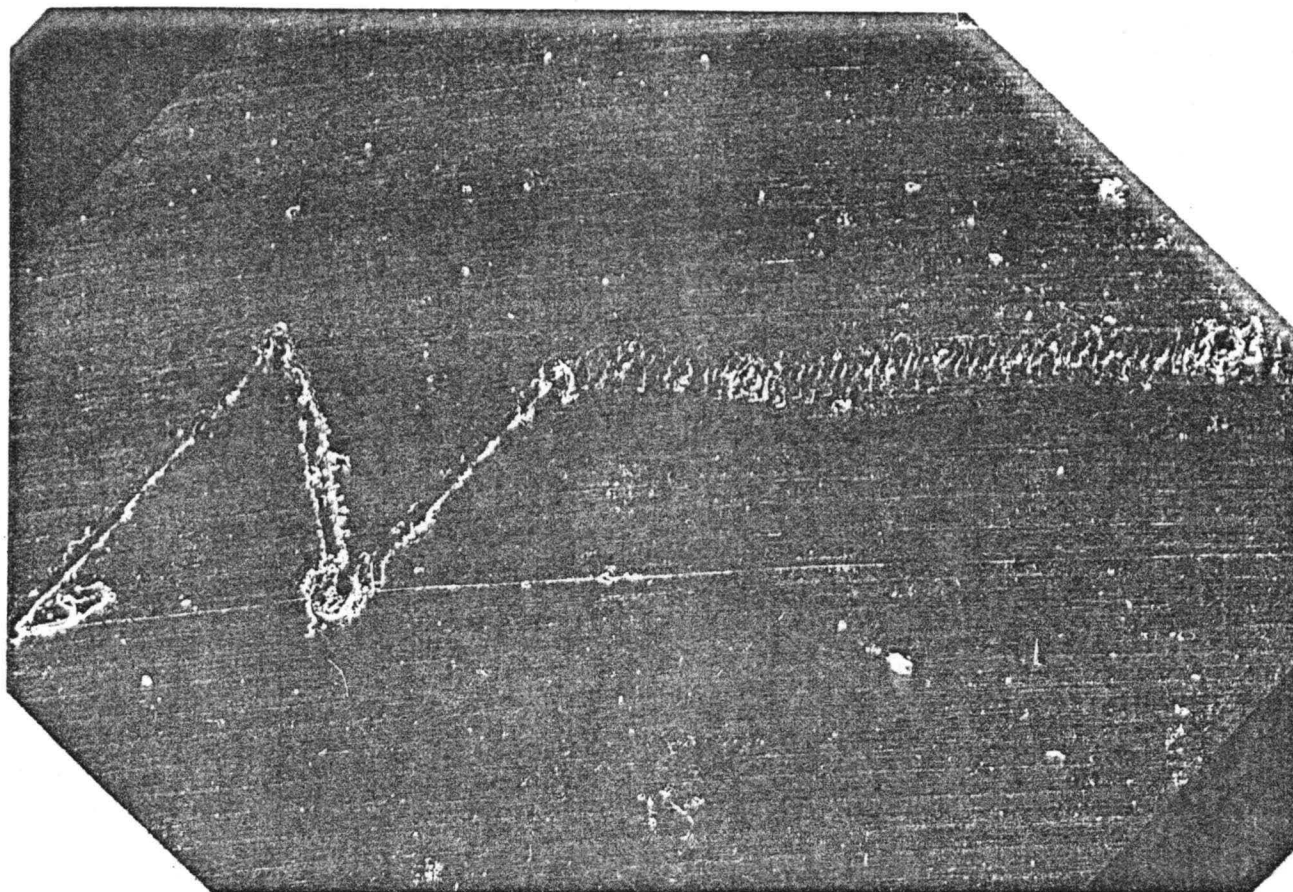
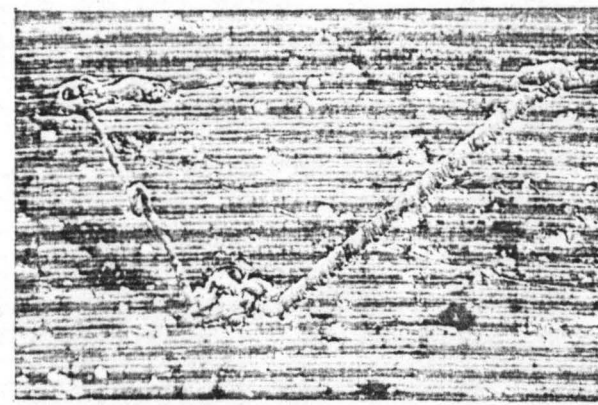
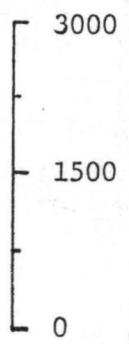
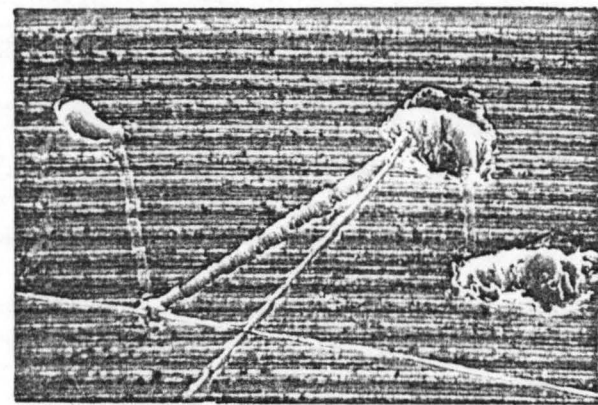


Fig. 3.7 Scratch Gage Trace No. 8 (FB42 Bottom) Covering Construction Phases and the Subsequent Period till shortly before Opening the Bridge to Traffic

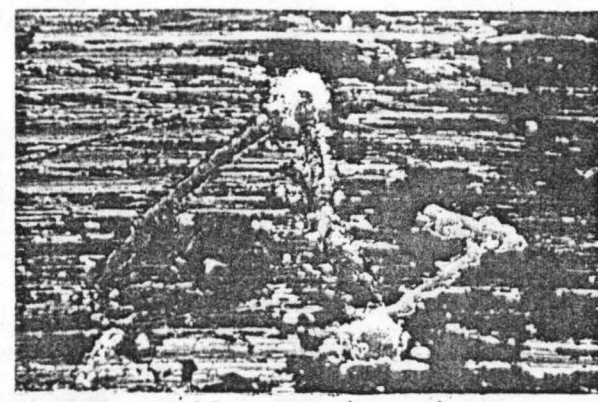
SCALE
(kg/cm²)



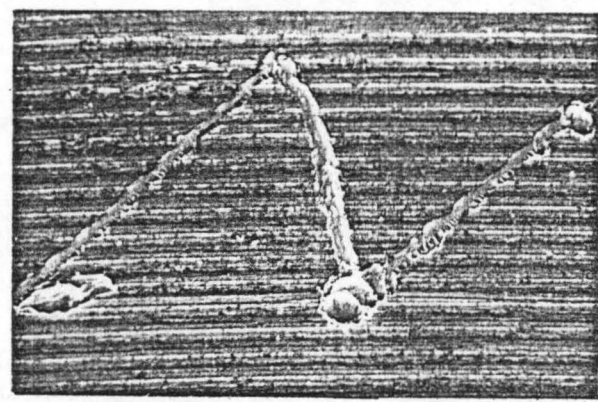
FB27 TOP (No. 2)



FB42 TOP (No. 7)



FB27 BOTT (No. 1)



FB42 BOTT (No. 8)

Fig. 3.8 SCRATCH GAGE TRACES (90X) - CONSTRUCTION STRESS CHANGES

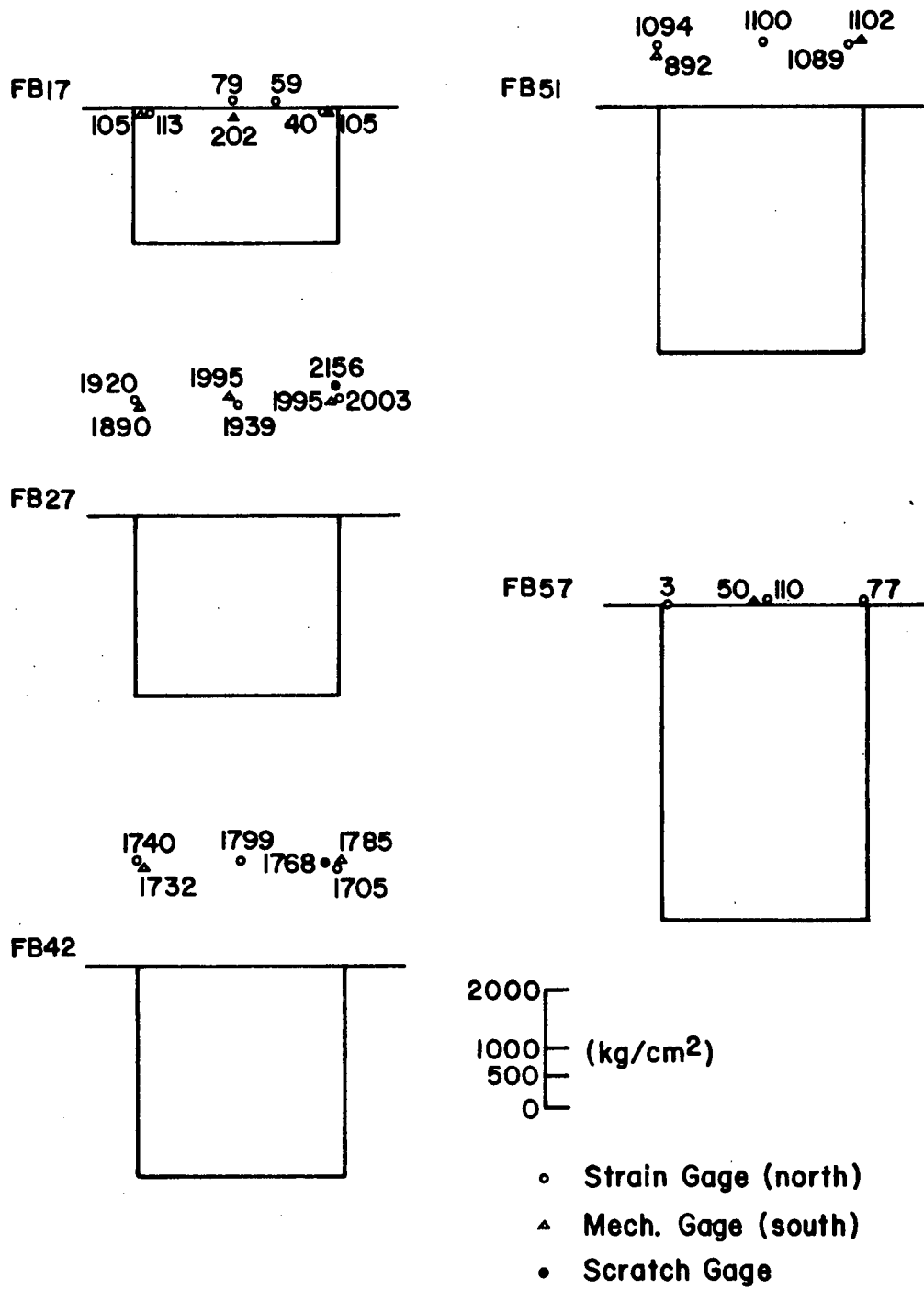


Fig. 3.9 Top Flange Stress Changes - Jetties to Pontoon
 (Rio Side Span)

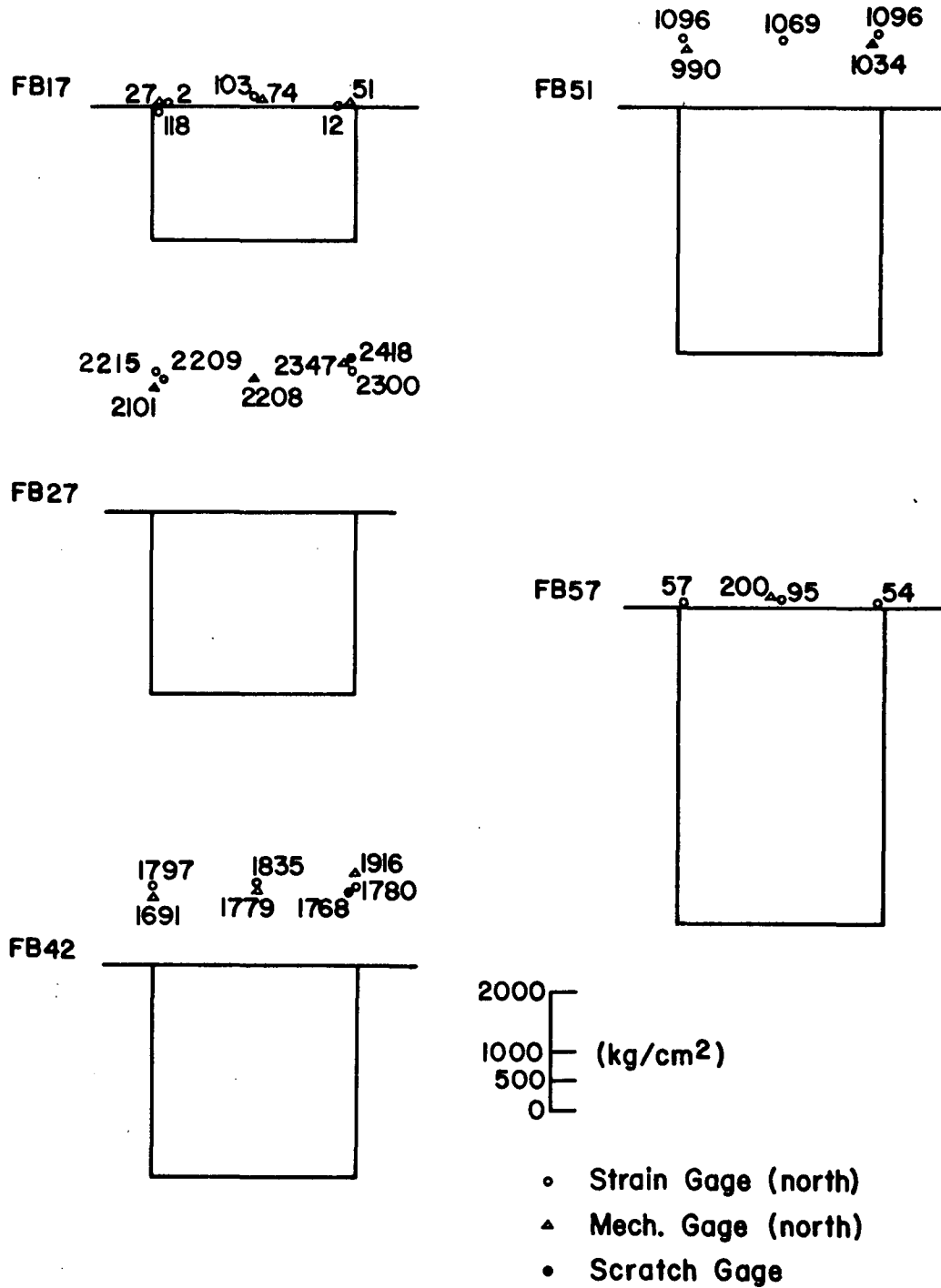


Fig.3.10 Top Flange Stress Changes - Pontoon To Piers (Rio Side Span)

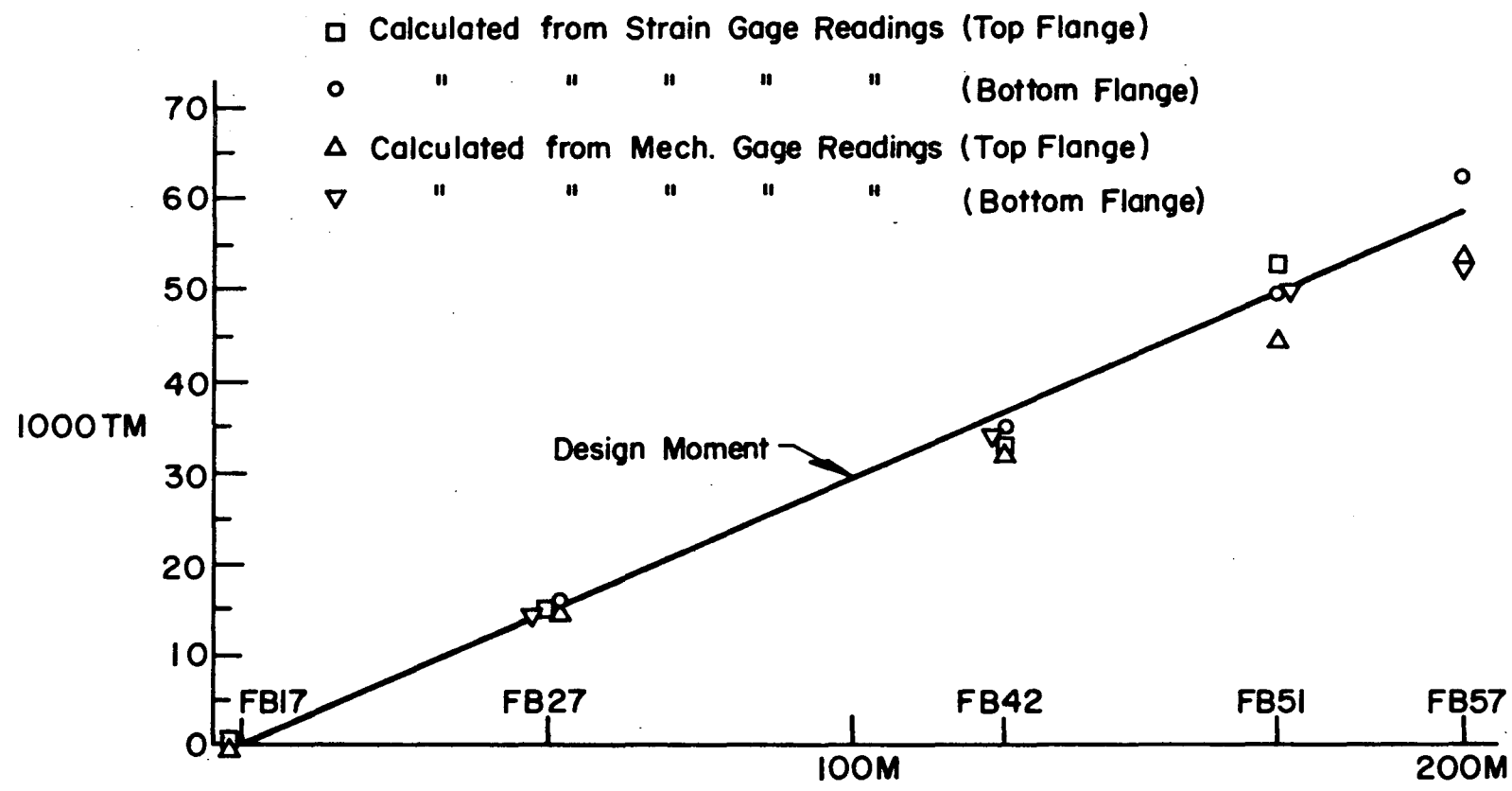


Fig. 3.11 Moment Change - Center Span Lift

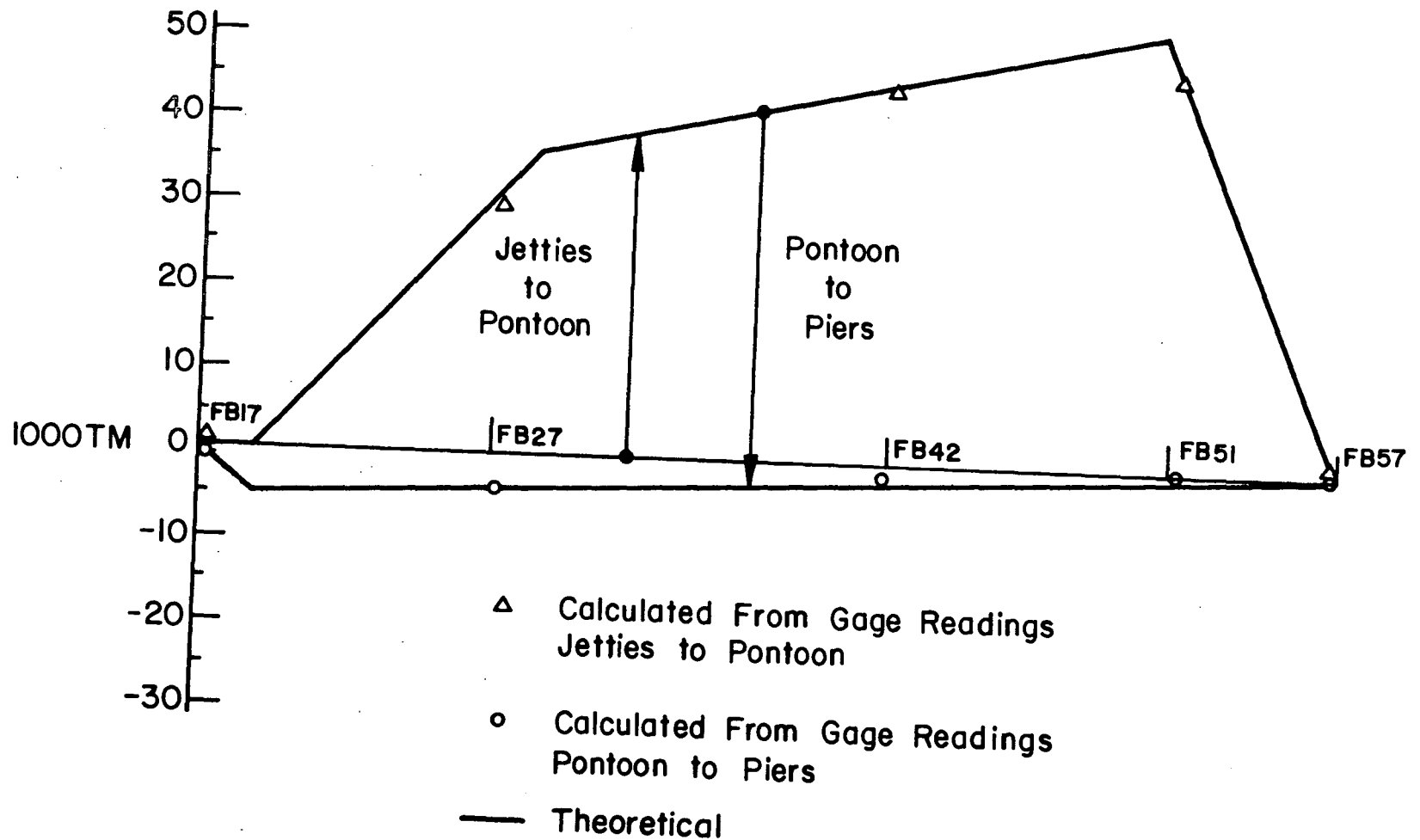


Fig. 3.12 Moment Changes - Rio Side Span Boxes

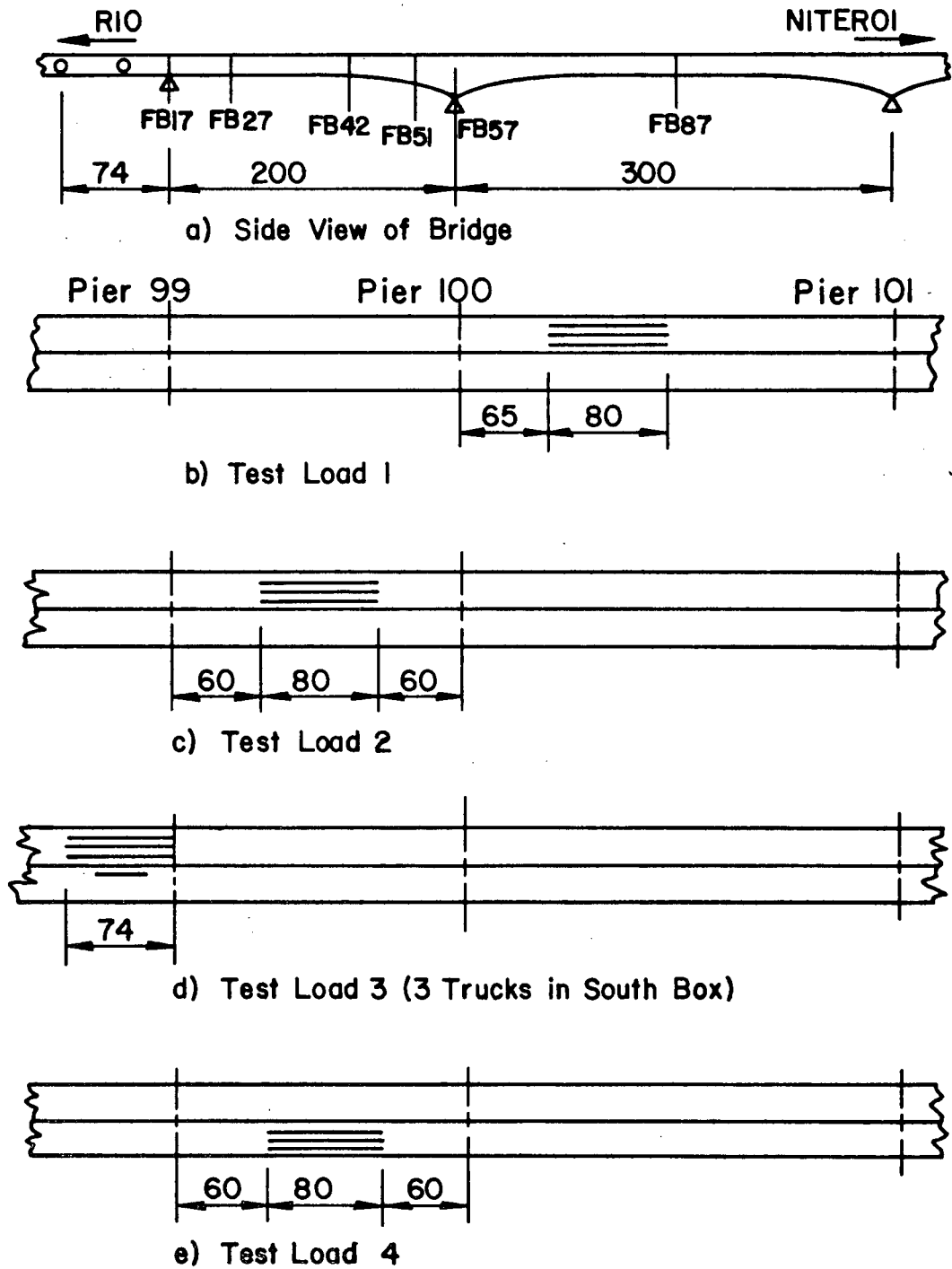
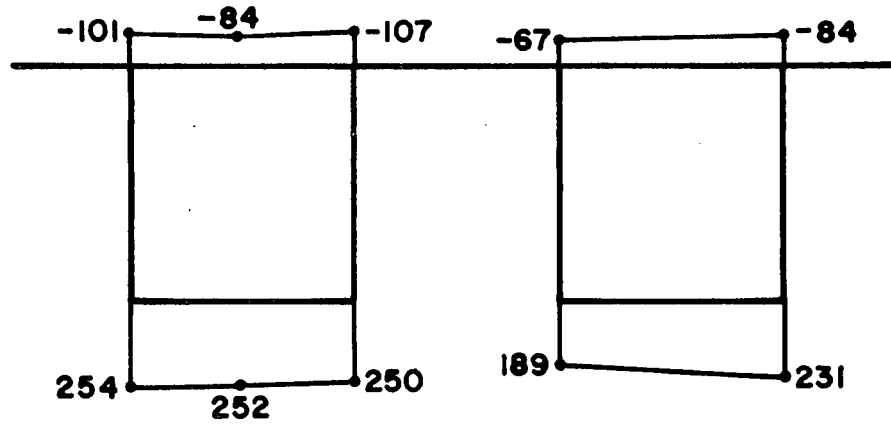
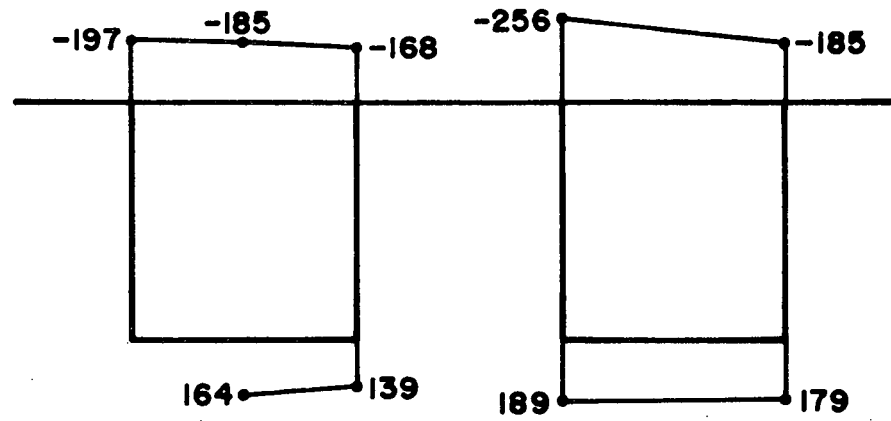


Fig. 3.13 Test Load Positions (21 17.5-Ton Trucks) - Scheme 4
 (All Dimensions in Meters)

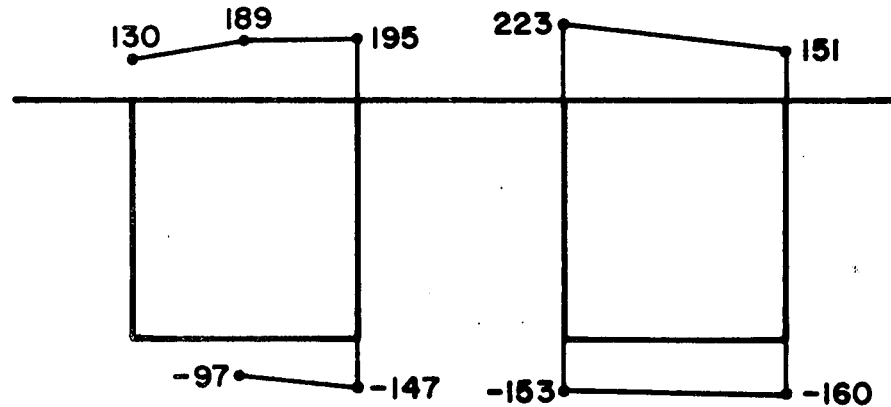
a. Position 2



b. Position 4



c. Position 1



(kg/cm²)

400
200
0

Fig. 3.14 Stress Changes at FB42 due to Test Loads

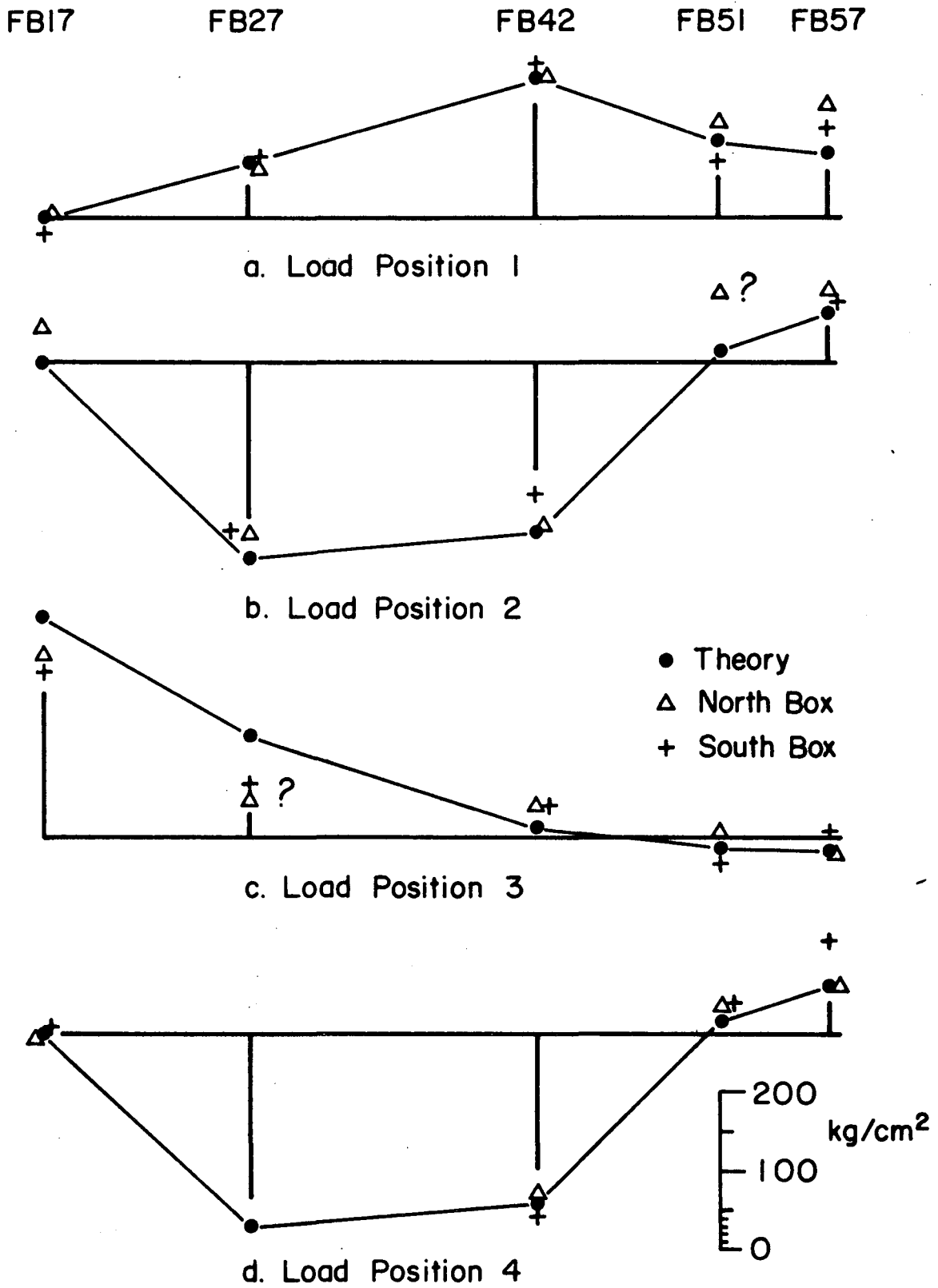


Fig. 3.15 Bending Stress in Bottom Flange of Rio Side Span due to Test Loads

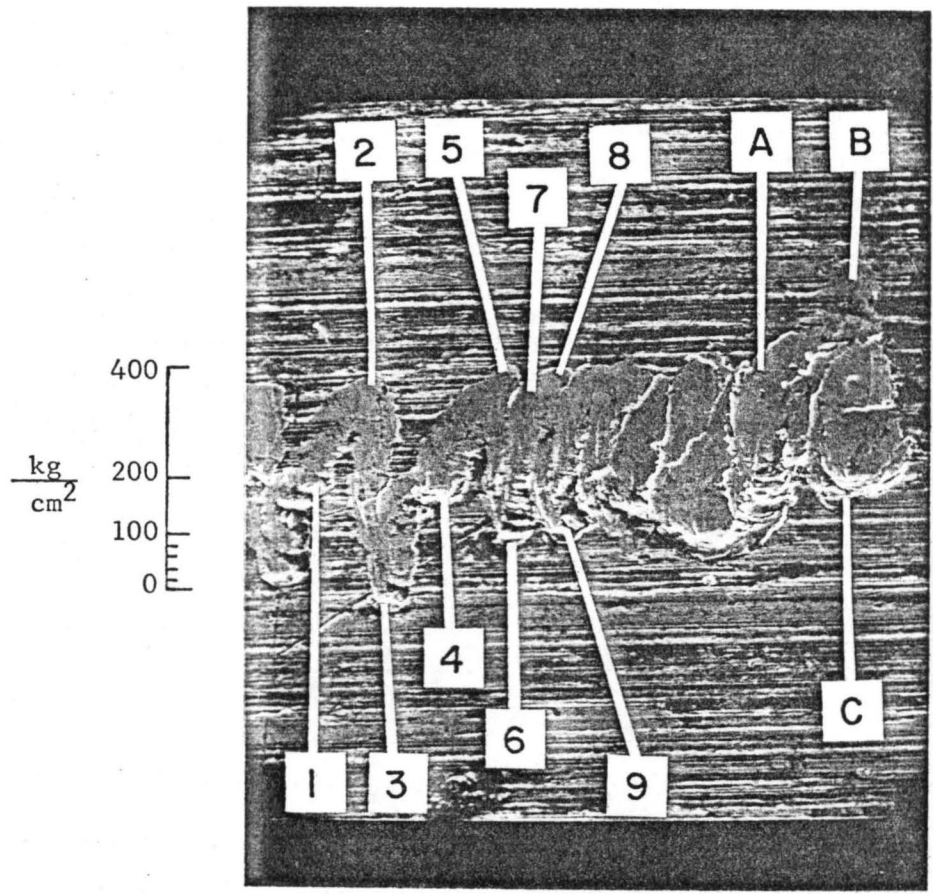


Fig. 3.16 Scratch Gage Trace for Test Loads

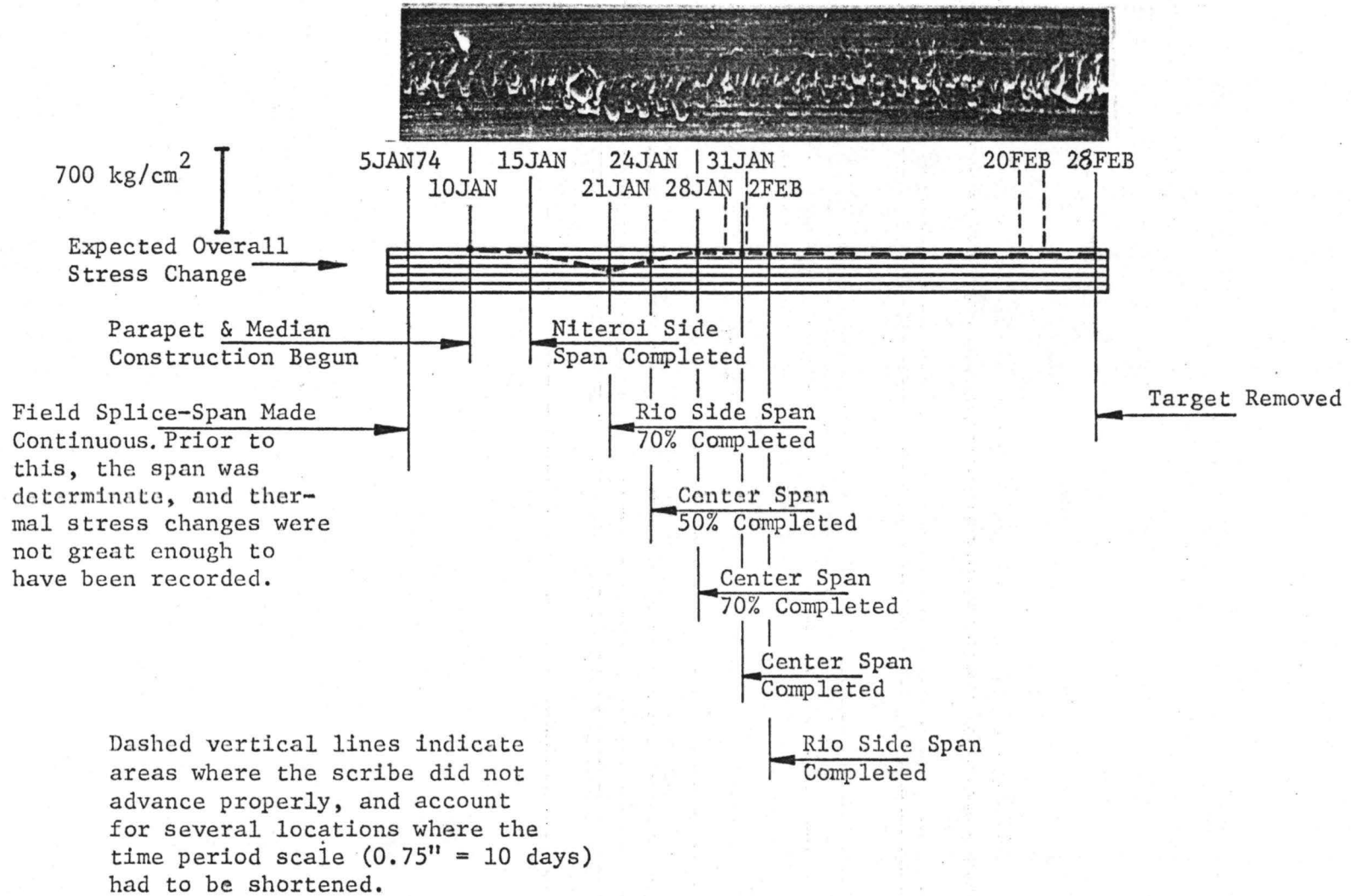


Fig.3.17 Parapet and Median Construction - Scratch Gage Trace vs. Theoretical Values

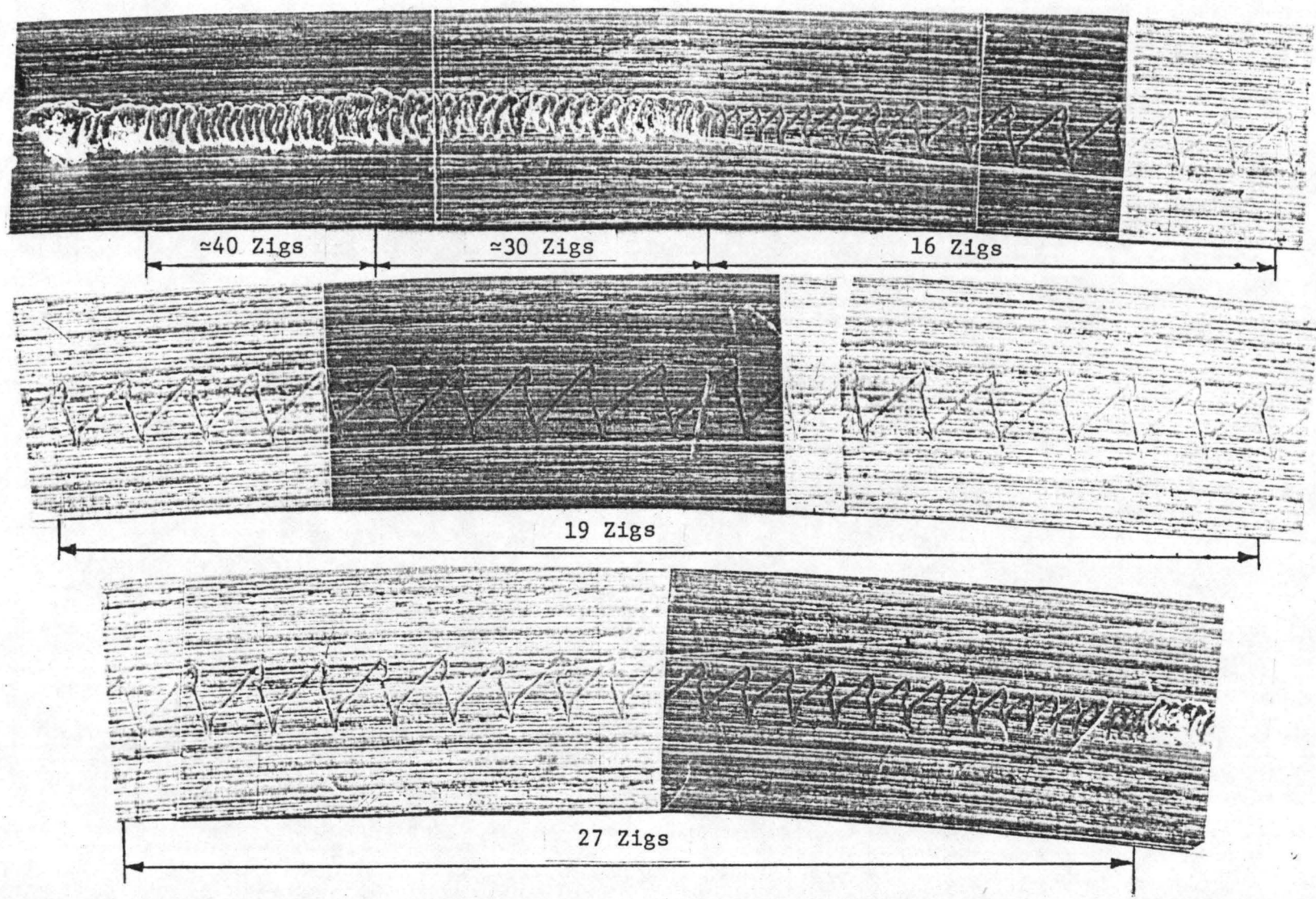
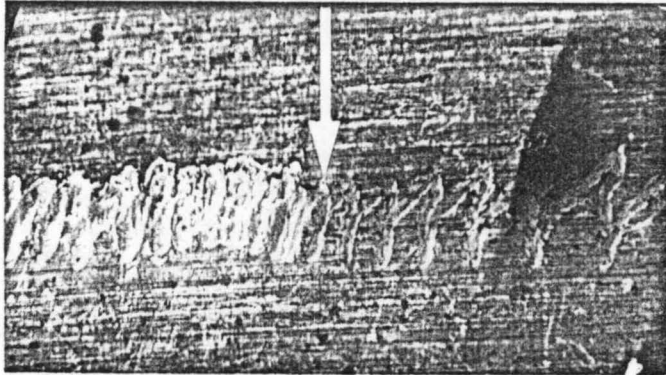
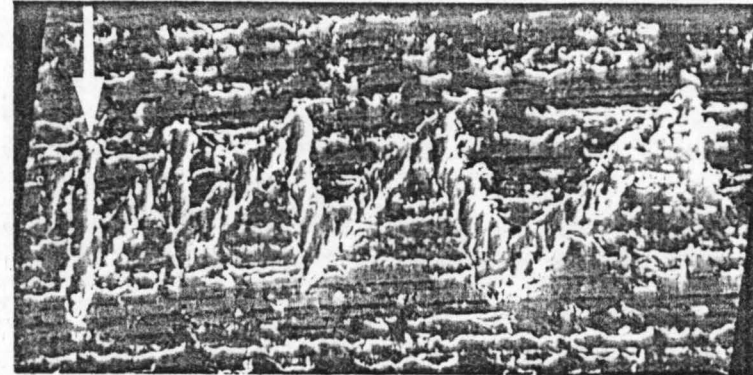


Fig. 3.18 Scratch Gage Trace--FB42 Bottom--6June1974 to 9Jan1975 (Trace No. 22 of Table 2.2)



Scratch Gage Target No. 20
(A Portion)

Gage Length = 30.5 cm
Stress Change = 300 kg/cm²
(At Arrow)



Scratch Gage Target No. 23

Gage Length = 100 cm
Stress Change = 205 kg/cm²
(At Arrow)

Fig. 3.19 Comparison of Scratch Gage Traces for Different Gage Lengths
(Magnification = 210X)

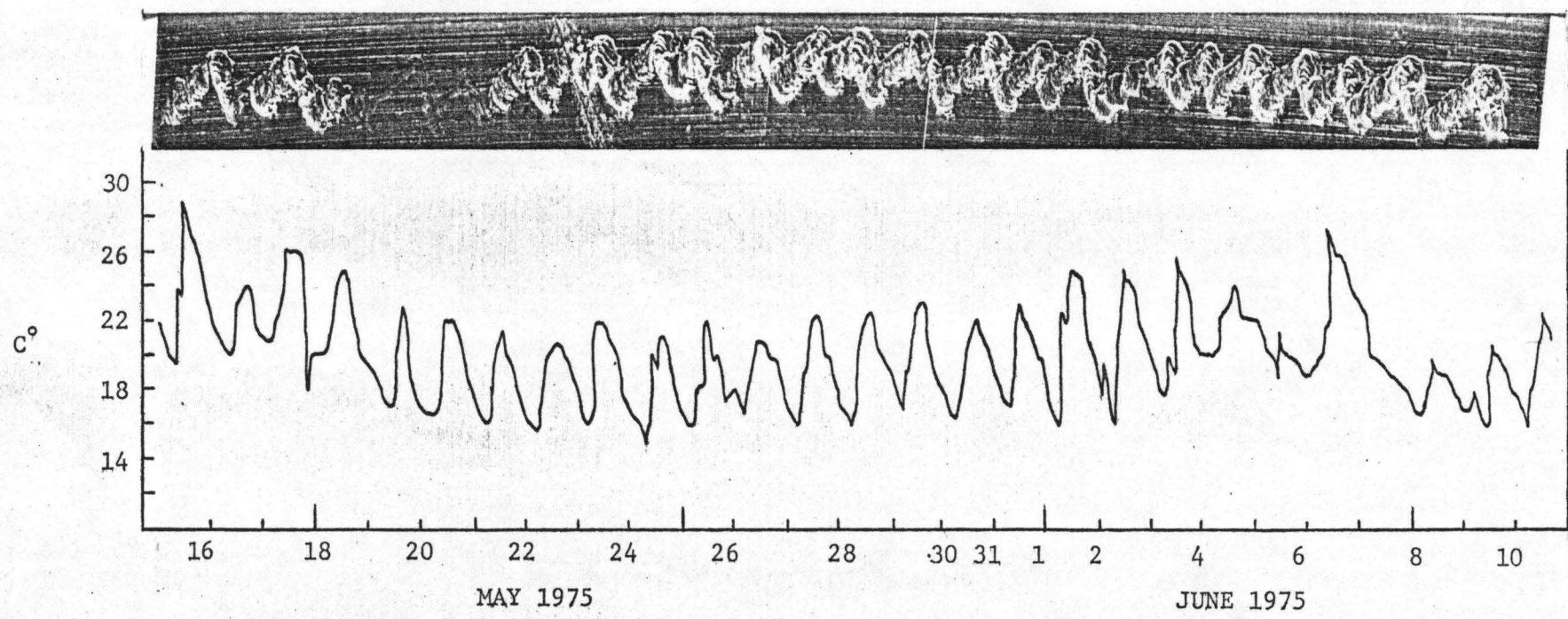


FIG. 3.20 SCRATCH GAGE TRACE (FB.42 BOTTOM) VS. AIR TEMPERATURE

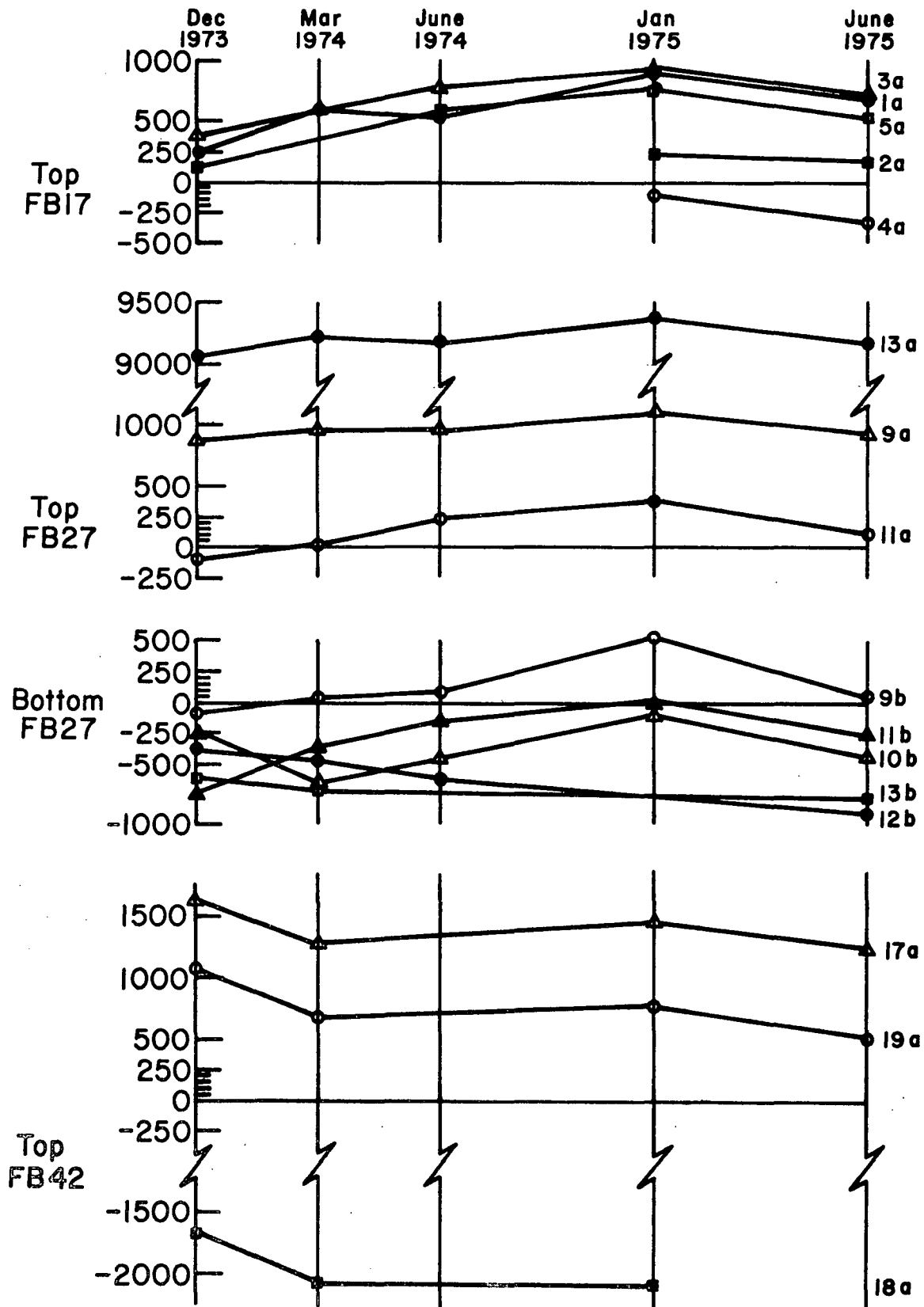
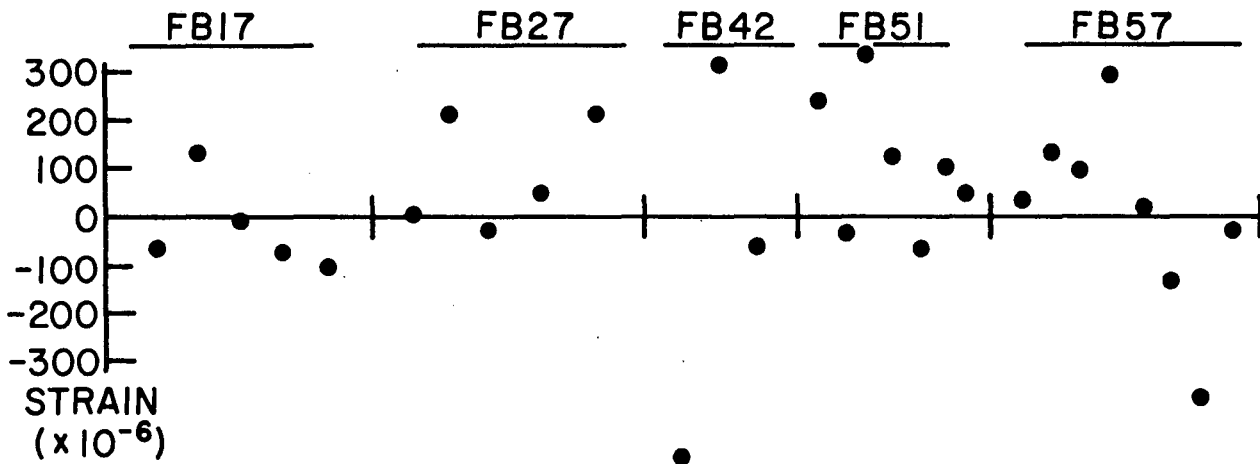
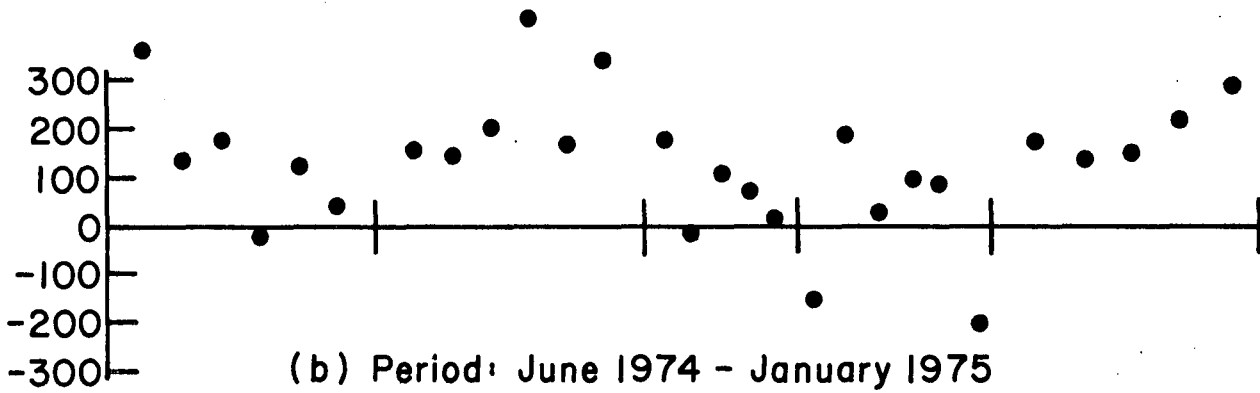


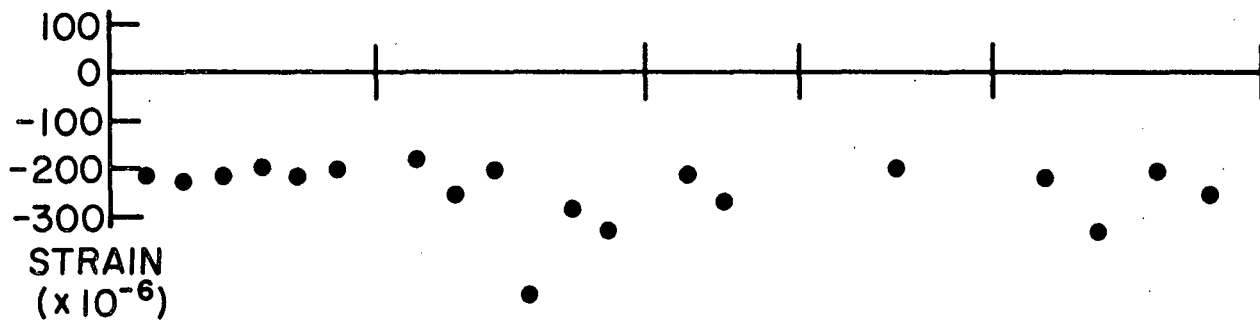
Fig. 3.21 Mechanical Gage Readings for Some Locations



(a) Period: March 1974 - June 1974



(b) Period: June 1974 - January 1975



(c) Period: January 1975 - June 1975

Fig. 3.22 Strain Changes from Mechanical Gage Readings
(Completed Structure)

4. TEMPERATURE STUDIES

(M.E. Bhatti, D.H. DePaoli and A. Ostapenko)

4.1 Instrumentation and Schedule

4.1.1 Need for Temperature Studies

Most commonly the effect of temperature on bridge girders has been considered by providing adequate travel at the expansion joints and bearings. This has been accomplished either by allowing the travel to be a certain percentage of the span length or by specifying a mandatory temperature change and coefficients of thermal expansion. The temperature gradient from the top of the roadway to the bottom fiber of the girder has been generally considered to be linear. Most specifications permit greater allowable stresses when the effect of temperature is included. (4.1) Probably the most important consequence of temperature effects has been the deformations which must be accurately considered in construction.

It is only in very recent years that the attention of engineers has been drawn to the thermal phenomena in conjunction with the universal trend toward better understanding of the behavior and strength of bridges with the purpose of more efficient utilization of construction materials.

Most field measurements of temperature distribution have been conducted on prestressed concrete bridges. Also a few studies have been made on steel and composite bridges. (4.2) A theoretical approach

has been proposed for computing the temperature distribution in a bridge girder from the ambient conditions.(4.3) These studies have shown that the temperature in a bridge cross section may deviate considerably from the linear pattern assumed in design. An interesting work has been recently (1975) reported on the measurement of reactions in a redundant concrete bridge girder in France.(4.4) The thermal stresses due to the redundancy were calculated in that study using a simplified version of the method of Ref. 4.3 and they were found to be of potential intensity to induce cracking of concrete.

Although the differential equations and principles of thermo-elastic analysis are well established (4.5), their application to bridge girders is hampered by the complexity of the cross sections, uncertainties of thermal material properties, lack of knowledge about the actual temperature and wind conditions and, most of all, insufficient field measurements of temperature distribution in bridges for confirmation of the theoretical results since many simplifying assumptions must be made without which the problem is unmanageable. For these reasons, only some simpler cases have been analyzed so far.* (4.3)

The instrumentation program of the President Costa e Silva Bridge presented a fortuitous opportunity of obtaining extensive

*Up to 1973. However, an article appeared at the time of writing this report (Sept. 1975) which describes a somewhat more refined method than in Ref. 4.3, applied to a concrete section. The method is favorably compared with tests on a small-scale model.(4.6) Some sample concrete bridges were analyzed for the North American climatic conditions.(4.7)

temperature and stress data on a steel box girder bridge of unprecedented dimensions. Of particular interest was the variation of the temperature pattern through the day and the stresses induced by such variation. The analytical work concentrated on the development of a computer method for determining thermal stresses and on the interpretation of field observations.

4.1.2 Instrumentation for Measurement of Temperature

As described in Art. 2.2, two cross sections were selected for mounting temperature gages. The reason for the selection was to provide a comparison between a relatively shallow section, FB27, within the span and thus exposed to wind, with the deepest cross section of the bridge, FB57, which was also partially shielded from the direct effect of wind by the turbulence created by the pier shafts below it.

The temperature gages were of the electrical resistance type and were read using the strain recording equipment with the pertinent circuits slightly modified. The principle of a temperature gage is that the metal of which it is made changes its resistance with temperature. In the bridge cross section the gages were placed so as to obtain as complete a picture of temperature distribution as was possible under the field conditions and in the time available. The actual location of the temperature gages (symbolized by triangles) is shown in Figs. A.2 and A.6 of Appendix A.

Important information on the day to day thermal effects was provided by the scratch gages.

A few thermocouples were also installed but most of them were damaged during construction stages and no systematic readings could be taken.

4.1.3 Schedule of Readings

Readings of temperature gages were made every time strain gages were read as shown in Table 2.1. However, all construction and test load readings (Readings No. 3.0 to 5.5) were taken almost fully during the night time when the temperature in the bridge was essentially uniform and thus the thermal stresses were small.

In February 1974, readings 5.6 and 5.7 were taken of all temperature and strain gages to establish the temperature distribution pattern typical for the bridge on a hot summer day. Unfortunately, the sky was partially overcast on these two days, and due to the closeness of the opening of the bridge to traffic, the readings could not be repeated.

In June 1974, the temperature study concentrated on determining the temperature variation in the cross section with time (Readings 6.1 and 6.2). The gages were not switched and the same group of 12 gages was read over and over again at short time intervals.

The last set of temperature readings was made in January 1975 (Reading 7). These readings covered a period from deep in the night till the end of the next day to determine not only the temperature variation at certain locations, but also a full temperature distribution at times several hours apart.

4.2 Thermal Stress Analysis

4.2.1 General

Thermal stresses develop due to differential thermal expansion (or contraction) in a body. For a wide range of temperature, this expansion is directly proportional to the temperature change. The coefficient of linear expansion is defined as the change in length which a bar of unit length undergoes when its temperature changes by one degree. If free expansion and contraction is permitted (unrestrained body) no stress is caused by a planar change in temperature. However when the temperature change in a homogeneous body is non-planar, different elements of the body tend to expand by different amounts and this conflicts with the requirement that the body strains remain continuous. As a consequence, the elements exert a restraining action against each other. The system of strains produced by the restraining action cancels out all, or part of, the free thermal expansion and a system of self-equilibrating stresses, known as thermal stresses, is developed.

4.2.2 Thermo-Elastic Analysis of Beams

1) Thermal Stresses due to Non-Linear Temperature Distribution

A change in length of a bar due to a temperature change is:

$$\Delta L = \alpha L T \quad (4.1)$$

where: ΔL = change in length of a bar,
 T = temperature change = $T_f - T_o$
 α = coefficient of thermal expansion,
 T_o = initial temperature,
 T_f = final temperature.

In the above case, only the axial change in length is considered and for simplification, the change in sectional dimensions of the bar is ignored. If each fiber of the body was free to expand or contract, no stress would be produced by the temperature change. However, expansion or contraction cannot proceed freely in a continuous body, and stresses are produced. In other words, the strains in the body which prevent a change in length due to a change in temperature also produce thermal stresses.

To relate the stresses due to the restraint with a temperature change in a fully restrained body, consider that the elongation of a bar of length L due to a uniform stress σ across the section is given by

$$\Delta L = \frac{\sigma L}{E} \quad (4.2)$$

where E is the modulus of elasticity of the material. In general, the value of E varies with temperature but in many engineering problems, where relatively small variation in temperature are encountered, E can be considered constant.

If the bar is completely restrained so that it does not change length and it does not bend or buckle, then the sum of the elongations given by Eqs. 4.1 and 4.2 must be equal to zero and the resultant thermal stress is

$$\sigma = -\alpha E T \quad (4.3)$$

where the negative sign on the right hand side indicates that the stress is compressive to resist a thermal expansion of the bar.

Consider a rectangular beam of constant width b and depth h , as shown in Fig. 4.1a, and a temperature change T uniform through the depth. For a restrained beam, the stress (compressive if the change of temperature results in expansion of body) is given by Eq. 4.3. On the other hand, if the beam is unrestrained, that is the supports move out by a pull of $\alpha E T A$, then at some distance from the end of member, the net stress is:

$$\sigma = -\alpha E T + \frac{1}{A} \iint \alpha E T dA \quad (4.4)$$

which is equal to zero. Thus, in the case of a uniform temperature distribution, there is no stress in an unrestrained body.

When the temperature distribution is non-linear, (Fig. 4.1b), there is a differential expansion in adjoining layers of the body which results in the warping of the sections of the beam. This, however, violates the basic assumption of bending theory that a plane section should remain plane after deformation of the member. In order to keep the sections plane, some forces P and M , must be applied in such a manner that they cancel out the thermal expansion of the body.

But these imaginary forces disturb the static equilibrium of the body. Hence, to establish equilibrium, a set of equal and opposite forces must be applied on the section as shown in Fig. 4.1c.

The net stress in an unrestrained beam then becomes

$$\sigma = -\alpha ET(y) + \frac{P}{A} + \frac{M}{I} y \quad (4.5)$$

or in a more general form:

$$\sigma = -\alpha ET(y,z) + \frac{P}{A} + \frac{M_z}{I_z} y + \frac{M_y}{I_y} z \quad (4.6)$$

$$\text{where } P = \iint E \alpha T(y,z) dydz \quad (4.7a)$$

$$M_z = \iint E \alpha T(y,z) y dydz \quad (4.7b)$$

$$M_y = \iint E \alpha T(y,z) z dydz \quad (4.7c)$$

where $T(y,z)$ is the temperature change as a function of y and z , and σ is the axial stress, tensile if positive and compressive if negative.

2) Thermal Stresses in Indeterminate Structures

Indeterminate structures develop stresses due to temperature effect which consists of the stresses on an unrestrained beam (Eq. 4.6) and of the stresses produced by the redundants. Analysis of such a structure for the redundants is conveniently performed by the force method (otherwise known as the Superposition, Virtual Work, etc., method). (4.8) The concepts of it are demonstrated next by means of a one-degree redundant two-span beam of Fig. 4.2.

With the middle reaction as the redundant, the following compatibility equation for the deflection at the midpoint can be written:

$$u_1 = u_{10} + f_{11} X_1 = 0 \quad (4.8)$$

where u_1 is the total deflection at redundant X_1 , u_{10} - the deflection due to the effect of temperature on an unrestricted (statically determinate) beam, f_{11} - the deflection for the redundant equal to unity (flexibility coefficient), and X_1 is the true value of the redundant. Using the principle of virtual work,

$$u_{10} = \int \frac{1}{I} \left(\int \alpha T y dA \right) M_1 dx \quad (4.9)$$

where $T = T(y)$ and M_1 is the moment due to $X_1 = 1$ (in Fig. 4.2, $M_1 = -x/2$).

The solution for the redundant from Eq. 4.8 is

$$X_1 = -\frac{1}{f_{11}} (u_{10}) \quad (4.10)$$

The final stresses are found by adding the stresses produced by the non-linear distribution of temperature according to Eq. 4.5 and the stresses due to redundant reaction X_1 .

$$\sigma = \sigma_t + \sigma_r = -\alpha ET + \frac{P}{A} + \frac{M}{I} y + \frac{M_1 X_1}{I} y \quad (4.11)$$

If the beam has a variable cross section, for example, as shown in Fig. 4.3, direct integration along the beam indicated in

Eq. 4.8 may no longer be feasible and numerical integration would have to be used. The beam then is subdivided into segments as shown in Fig. 4.3 and the individual contributions summed up. Furthermore, integration over the cross section at each station may also have to be performed numerically such as for the Section A-A in Fig. 4.3. Then, Eq. 4.8 becomes

$$u_{10} = \sum_i \frac{M_i}{I_i} \left(\sum_j \alpha_j T_j y_j \Delta A_j \right) \Delta x_i \quad (4.12)$$

and

$$f_{11} = \sum_i \frac{M_i^2}{I_i} \Delta x_i \quad (4.13)$$

where the i 's sum along the beam and the j 's over the cross section. The subscript j for α_j takes care of the possibility that the cross section may consist of materials with different coefficients of thermal expansion.

For structures of more than one degree of indeterminacy, the solution for redundants can be generalized from Eq. 4.8 to

$$X = -F^{-1} U \quad (4.14)$$

where X and U are the column matrices of the redundants and of the deflections of the primary structure, and F^{-1} is the inverse of the flexibility matrix. (4.9)

The individual elements of the k - th row of the U and F matrices are by numerical integration:

$$\begin{aligned}
 u_{ko} = & \sum_i \frac{M_{ki}}{I_i} \left(\sum_j \alpha_j T_j y_j \right) \Delta x_i \\
 & + \sum_i \frac{N_{ki}}{A_i} \left(\sum_j \alpha_j T_j \Delta A_j \right) \Delta x_i
 \end{aligned} \tag{4.15}$$

$$\text{and } f_{kp} = \sum_i \frac{M_{ki}}{I_i} M_{pi} \Delta x_i + \sum_i \frac{N_{ki}}{A_i} N_{pi} \Delta x_i \tag{4.16}$$

Where subscripts k and p designate the k - th and p - th redundant reactions, N_{ki} is the axial force produced by $X_k = 1$, and M_{pi} and N_{pi} are the moment and axial force due to $X_p = 1$. For a one-degree indeterminate structure subjected to bending only, $N = 0$, $k = p = 1$, and Eqs. 4.15 and 4.16 reduce to Eqs. 4.12 and 4.13.

In the case of deformation about both y and z axes, Eqs. 4.15 and 4.16 should be expanded analogously to Eqs. 4.6 and 4.7a,b,c to include the moments about y - axis. Then, the thermal stress formula becomes

$$\begin{aligned}
 \sigma = \sigma_t + \sigma_r = & \left[-\alpha ET + \frac{P}{A} + \frac{M_z}{I_z} y + \frac{M_y}{I_y} z \right] + \\
 & \left[\frac{1}{A} (\{N\}^T \{X\}) + \frac{y}{I_z} (\{M_z\}^T \{X\}) + \frac{z}{I_y} (\{M_y\}^T \{X\}) \right]
 \end{aligned} \tag{4.17}$$

In these equations, the superscript T means the transpose of a matrix. The first bracketed expression gives the thermal stress in the statically determinate primary structure, σ_t , and the second bracketed term the stress produced by the redundants, σ_r . Braces { } indicate column matrices of the moments M_{zk} and M_{yk} and of the axial forces N_k produced by the unit redundants X_k .

Of course many other methods may be used for indeterminate structures, such as the displacement methods, but the above formulation was chosen due to its simplicity in application to the thermal analysis of the President Costa e Silva Bridge. (4.10)

4.3 Method of Thermo-Elastic Analysis of the President Costa e Silva Bridge

4.3.1 Structural System

1) Structure and Assumptions

As shown in Fig. 1.2f and described in Art. 1.3, the steel portion of the President Costa e Silva Bridge is a three-span continuous girder with two suspended portions in the adjoining spans. The two middle supports of the three-span continuous girder have fixed bearings on top of the piers and are thus elastically restrained from horizontal motion. The ends are free to expand horizontally (assuming frictionless rollers at the end piers). Thus, for the deformations in the vertically longitudinal plane, the structure has three degrees of indeterminacy - two vertical and one horizontal. Due to the symmetry of the structure and of the thermal field distribution in this plane, the redundancy can be reduced to two degrees.

The amount of the horizontal movement at the intermediate piers depends on their stiffness. During the erection of the center span, one of the piers was pulled at the top to ease the erection and the deflection and the force were recorded. The pier stiffness thus was found to be 56.3 ton/cm. The axial shortening of the piers was not considered in the analysis.

As the temperature distribution can be unsymmetrical in the transverse horizontal direction, analysis for the horizontal plane was also formulated. The girder was idealized as a three-span continuous beam supported on four elastic reactions provided by the transverse bending of the piers. The pier stiffness in this direction was taken to be eight times of the longitudinal direction. Since the girder reactions in this case are not at the shear center, but at the bottom of the girder, torsion of the girder had to be considered.

The method developed for the thermo-elastic analysis of the bridge is based on the following assumptions:

- (a) Material properties, such as the modulus of elasticity, coefficient of thermal expansion and Poisson's ratio are constant within the temperature range under consideration.
- (b) Variation of the cross section and temperature distribution along the bridge is continuous and smooth.
- (c) Shear deformations are ignored in analysis.
- (d) Warping stresses due to warping torsion and shear lag are neglected.

- (e) The effect of thermal deformation of the cross bracing, floor beams and vertical stiffeners is neglected.

The methodology of the method followed the concepts formulated by Eqs. 4.14 to 4.17 and required a subdivision of the structure into elements for performing numerical integration and knowledge of the temperature throughout the bridge.

2) Subdivision of Bridge Girder into Segments and Elements

Since the girder of the President Costa e Silva Bridge has a variable cross section, it was necessary to use numerical integration in the analysis as indicated by Eqs. 4.15, 4.16 and 4.17. The full length of the three-span portion of 700m was subdivided into 35 20-meter long segments. For the purpose of integration, each segment was assumed to be prismatic (constant cross section) with the properties as given at the midpoint.

Due to the symmetry of the structure and of the thermal distribution, only one-half of the girder, from the Rio pier to the midspan, that is, eighteen segments, had to be considered.

Figure 4.4 gives an isometric view looking toward Niteroi of a typical cross section of the bridge. The global coordinate axes X, Y and Z are located at the north top edge of the section. The origin of the X-axis is placed at Pier 99 (Rio side pier), and the X-coordinate defines the distance of the midpoint of each segment along the girder from the origin. The Y and Z-coordinates define the location of an

element in the cross section. The centroidal axes y and z are computed for the cross section at midpoint of each segment in terms of Y and Z .

For the purpose of numerical integration and computation of the cross-sectional properties, each cross section is subdivided into a maximum of 171 elements as shown in Fig. 4.5 for FB57 (the deepest section). The first 55 elements pertain to the plates of the top and bottom flanges and of the four webs. The remaining elements cover the longitudinal stiffeners of the flanges and webs. Other, shallower sections are generated by modifying some of the original elements to have zero area. For example, the FB27 section of Fig. 4.6 has zero area for web elements 7 to 9, 15 to 17, 30 to 32, and 38 to 40.

In the initial formulation, the computer program was intended to be completely general and the discretization of the cross sections was made arbitrary. One inadvertent carry-over of this earlier formulation into the final program is that the flange plates, for both the top and bottom flanges, retained their unsymmetrical subdivision. For example, this can be observed in Fig. 4.5 for elements 48, 49 and 50 of the north box versus elements 52, 53 and 54 of the south box. The consequence of this deviation from symmetry in subdivision is that some computed values, such as thermal stresses, become slightly unsymmetrical.

4.3.2 Generation of Thermal Distribution in the Bridge from Field Measurements

In order to perform thermo-elastic analysis of the bridge, it was necessary to know the temperature, or more precisely the change of temperature, in each element of the girder. Thus, it was necessary to have a procedure for generating these temperature values from the readings made at the limited number of points in the cross sections of

FB27 and FB57. The computerized procedure developed consisted of two parts: one part for establishing the temperature in all the elements at FB27 and FB57 from the measured values and the other part for generating the temperature in the elements of all the other sections.

1) Temperature Distribution in Sections at FB27 and FB57

The field readings for the sections at FB27 and FB57 were plotted on the cross section outlines. After some judicious smoothening, the points were connected by a line to establish a realistically continuous pattern of distribution. The values at the centroids of the first fifty-five elements were then scaled off and used for further calculations on a computer. (The computer program is given in Appendix B).

In the computer, the fifty-five temperature values were used to calculate the values for elements 56 through 171 by using simple proportionality relationships. It was thus assumed that the temperature is distributed linearly between adjoining elements although the overall distribution over the cross section may be linear or non-linear depending on the field data.

2) Temperature Distribution Along the Bridge

The generation of the temperature distribution in the first 55 elements at sections other than FB27 and FB57 was programmed according to the following rules:

1. No variation of temperature between FB17 and FB27, the values for the elements of the same size and location at each section are taken to be the same as for particular elements at FB27.

2. Variation of temperature between the corresponding elements of the same number in the sections at FB27 and FB57 is linear.
3. The temperature of the web plate elements which are below the center line of element No. 6 on the north web*, that is, elements 7, 8 and 9 is completed by creating a smooth temperature surface between element No. 6 and the imaginary line which is established 55.65 cm above and parallel to the bottom edge of the web plate. The temperature along this line is taken to vary linearly from FB27 to FB57. The temperature in the wedge-like portion between this line and the center line of element No. 6 connecting FB27 and FB57 is linear in each vertical section.
4. At the center of the bridge, FB87, the same temperature distribution is assumed over the section as at FB27, except that the web portion between element No. 6 and the point 55.65 cm above the bottom of the web is filled in linearly since the depth at FB87 is greater than at FB27. The temperature distribution for the sections between FB87 and FB57 is estimated in the same way and with the same pattern and assumptions as for the temperature between FB27 and FB57, except in a reverse order.

*The elements of the other three webs corresponding to No. 6 are Nos. 18, 29 and 41.

The temperature of a stiffener element (Nos. 56 to 171) is obtained by linear interpolation between the temperatures at the plate element centroids between which the stiffener is located.

The temperature field beyond the bridge center, FB87, is assumed to be symmetrical.

4.4 Field Measurements of Temperature

4.4.1 Temperature Data of February 1974

The readings on 26 and 27 February 1974 (Reading Nos. 5.6 and 5.7 of Table 2.1) were taken with the purpose of establishing the temperature distribution in the bridge cross sections on a typical hot Summer day. Although the conditions were not ideal due to variable cloudiness and technical delays, some useful data was still obtained.

The temperature measured at FB57 on 27 February 1974 between 11:05 and 13:15 hrs. is shown in Fig. 4.7 as a representative sample. The heavy solid circles and solid ordinates indicate the places where particular gages were located. The small circles with dashed ordinates give the values transferred from an adjoining plate where the gage was actually located. All ordinates are shortened by 20°C for a better presentation. Thus, a scaled value should be increased by 20° . The readings indicate some scatter, but this can be readily ascribed to the only later recognized fact that the temperature-time gradient in the period from 11 to 13 hrs. during which the readings were taken is quite steep and can readily account for variations of $3\text{-}4^{\circ}\text{C}$. The apparent

symmetry of the pattern results from the east-west orientation of the bridge and from the February sun passing essentially overhead.

Keeping the above in mind, the following observations can be made from the figure:

1) The temperature in the top flange plate is the highest in the middle of a box (up to over 42°C) and then drops a few degrees at the webs, due to their heat-sink action.

2) The flange tips have markedly lower temperature than the rest of the flange (reduction by over 10°C) due to the concrete curb and railing over them. However, the gradient of variation from the edges to the higher flange temperature in the unprotected flange is indefinite.

3) The temperature on each of the four webs is essentially constant over the full depth except for a very sharp increase at the top, to the temperature of the top flange.

4) The temperature in the two outside webs is equal to each other and is approximately 4°C higher than in the two inner webs.

5) The air temperature in the boxes at the lower levels, as measured by the gages on the bracing diagonals, is approximately equal to the temperature of the outside webs, but at the top it is higher and equal to the air temperature between the boxes.

A comparison of the FB57 temperatures shown in Fig. 4.7 with the temperatures measured at the shallower section of FB27 lead to a conclusion that no recognizable difference between them could be detected which could be ascribed to their different locations along the girder -- FB57 at the pier and FB27 within the span.

Since there were no night readings on the same day, temperature change for the 27 February 1974 readings was found by taking the

difference between the temperatures shown in Fig. 4.7 and the temperatures measured at night during the test load studies two days earlier. In order to have a conservative and general pattern, the values were liberally adjusted to accentuate the irregularity and severity of the conditions possible at other times. A similar reduction was also made for FB27. The resultant temperature changes are shown in Fig. 4.8 and 4.9 for FB27 and FB57, respectively. (The values shown are some of those needed for computer analysis.) The plots exhibit essentially the same characteristics as the temperature distribution shown in Fig. 4.7, but they should be considered as a sample of the temperature change rather than the actual change for 27 February 1974.

4.4.2 Temperature Data of June 1974

The June 1974 readings (Nos. 6.1 and 6.2 in Table 2.1) were taken from a small group of twelve gages in the north box which were read at short time intervals. The gages for this group were selected considering that the sun at this time of the year is low in the north and is able to strike the outside north web. Although not all gages worked every time, it was still possible to obtain the temperature variation in the bridge cross section through the day.

The temperature readings for 10 June 1974 in the top flange and the adjoining webs at FB27 are plotted in Fig. 4.10 against time. The period extends from the condition of essentially uniform temperature equal to the air temperature at about 9:00 hrs. to the highest value at about 14-15:00 hours and then to the subsequent temperature reduction toward 17:00 hrs. Only the gage at the inner web deviates from this

pattern by apparently giving erroneous readings before 12:00.

It is seen in the plot that although the air temperature changes only 5°C , the bridge temperature increases by up to 14°C . The two observations, relevant to the readings made in February 1974, are that the temperature varies quite rapidly during the 11:00 to 13:00 hr. period, but contrary to what was intuitively expected, the greatest temperature difference between the individual points develops only later, at 14-15:00 hrs. when the peak is attained for the most exposed points in the top flange.

Figure 4.11 of the temperature variation at FB57 on the same day depicts a very similar pattern of temperature variation and supplies some additional information. First of all, the gage at the bottom of the north web (hollow circles) shows a very dramatic temperature increase under the early exposure to sun rays. Already at 9:00 when the top flange was still at the air temperature, the bottom of the web was already 5°C higher and warming up faster than other components. Gradually, the temperature in the web levelled off and started declining at 14:00, that is before the other points reached their maxima.

The gage at the left tip of the top flange (hollow triangles) hardly warmed up, developing a temperature differential with the flange itself of about 10° - the same as was observed in February 1974.

The plot in Fig. 4.12 shows the temperature variation measured at FB57 on 11 June 1974. This time the gage at the bottom of the north web did not work and thus the effect of early sun rays could not be

recorded as was done in Fig. 4.11. All other observations made for Figs. 4.10 and 4.11 are supported by Fig. 4.12.

Although the temperature difference in Figs. 4.10, 4.11 and 4.12 between the points on the flange and immediately under it on the web is only about one-third or one-half of that observed in February, even though in February it had not yet reached its maximum, the patterns are very consistent.

The February observation of the top flange temperature in the middle of the box being higher than at the webs is also confirmed by the June readings at FB57 made on 10 and 11 June 1974 (Figs. 4.11 and 4.12).

4.4.3 Temperature Data of January 1975

The January 1975 testing program (Reading No. 7 of Table 2.1) was designed to make up for the deficiencies of the two previous temperature measurements. It was not certain that the February 1974 readings gave the maximum day temperature and also there were no readings made on the preceding night. The June 1974 readings gave a picture of the temperature vs. time variation, but had only a small number of gages read.

The readings covered a period from 23:00 hours on 16 January 1975 till 17:00 hours the next day in order to determine not only the temperature variation at certain preselected locations, but also the temperature distribution over the full sections at times several hours apart. The most important result of these readings was the establishment

of the lowest and highest levels of the temperature variation through the day and, thus, of the maximum temperature change. This change was needed for the thermo-elastic analysis.

Figures 4.13 and 4.14 show the maximum diurnal temperature changes at FB27 and FB57 between 6:30 and 15:00 on 17 January 1975. The solid dots and ordinates designate the readings. In comparison with Fig. 4.7 for February 1974, Fig. 4.14 has somewhat fewer readings since a number of gages had been damaged in the interim time. Specifically, the readings at the flange tips are absent. However, the pattern of temperature distribution and the ordinates differ relatively little.

The smoothed curve of the temperature change in Figs. 4.13 and 4.14 was determined by utilizing previous observations and the readings made in January 1975 at various times during the day. Thus, recognizing the symmetry of the temperature changes about the vertical axis and the equivalence of temperatures at FB27 and FB57, all the readings shown in Figs. 4.13 and 4.14 were combined in Fig. 4.15 on an outline of the north box (the flange tip is on the left side). A pattern of the maximum temperature change was then approximated from this composite plot. This pattern was then superimposed on the cross sections of Figs. 4.13 and 4.14 for a direct comparison with the readings plotted on them.

The highest change of temperature is in the top flange with a maximum of 17.5° . At the webs the temperature rapidly drops to 9° in the outside

webs and to 6° in the inside webs. Then the temperature remains constant in each web till the bottom flange where there is a gradual transition between the outside and inside webs.

Since the meteorological records indicate 17 January 1975 to be the day with the highest air temperature for the period of this study since 1973, the pattern of temperature change in Figs. 4.13 and 4.14 may be accepted as a maximum typical pattern. In comparison with Figs. 4.8 and 4.9 for the conservative approximations of the February 1974 conditions, the distributions of Figs. 4.13 and 4.14 are much more regular and have smaller values.

4.5 Analysis of Thermal Stresses

The computer program, based on the method of Art. 4.3 and described in Appendix B, was used to analyze the bridge for the temperature changes measured in February 1974 and January 1975.

4.5.1 Thermal Stresses for Sample Data of February 1974

Figures 4.16, 4.17 and 4.18 show the representative plots of the thermal stresses computed from the changes given in Figs. 4.8 and 4.9. Since the computer program, in accordance with Art. 4.3.1, analyzes only the sections at mid-points of 20-meter segments, these do not necessarily coincide with the instrumented sections. The thermal stresses of Fig. 4.16 are exactly at FB27 ($x = 50\text{m}$), but the stresses shown in Fig. 4.17 are at $x = 130\text{m}$, that is, 5m beyond FB42 and in Fig. 4.18 (at $x = 190\text{m}$), 8.9m before the instrumented section at FB57.

A comparison of the thermal stress distribution pattern of Figs. 4.16 and 4.18 with the respective temperature change distributions of Figs. 4.8 and 4.9 indicates a good correlation although it may not be immediately obvious. For example, the reduction of the top flange stress in Fig. 4.18 from -206.9 kg/cm^2 and 173.6 kg/cm^2 to -70.4 kg/cm^2 at the center is equivalent to a temperature drop of $(206.9 + 173.6 - 2 \times 70.4) / 2 \times 25.1 = 4.8^\circ\text{C}$. This corresponds to the reduction in the top flange temperature pattern of Fig. 4.9.

The typical characteristics of the thermal stress patterns in Figs. 4.16 to 4.18 are the following:

- The maximum compressive stress is in the top flange. It increases from FB27 toward the section at the intermediate pier, FB57. The increase is mainly due to the effect of the redundant reactions.
- The stress reversal in the webs immediately below the top flange gives the highest tensile stresses corresponding to the drastic reductions in the temperature change pattern of Figs. 4.8 and 4.9. It is important that these high tensile stresses are in the vicinity of the centroid where the bending stresses from dead and live loads are very small or zero.
- The tensile stresses in the bottom flange are not the greatest in the cross section. The maximum values occur in the middle portion of the span, Fig. 4.17 - FB 42, where the live load stresses are also expected to be the highest.

Since the sample temperature change patterns in Figs. 4.8 and 4.9 were possibly made more conservative than can be realistically expected, the stress values shown in Figs. 4.16 to 4.18 should also be viewed as conservatively high.

4.5.2 Thermal Stresses for January 1975 Data

The thermal stresses computed from the temperature changes measured in January 1975 and plotted in Figs. 4.13 and 4.14 are shown in Figs. 4.19, 4.20 and 4.21. The sections are at or near FB27, FB42 and FB57, respectively.

In comparison to the case for February 1974, the temperature changes and stresses are much more regular and symmetrical. The numerical stress values are lower, but the characteristics of the pattern are the same. The maximum compression in the top flange is 120 to 140 kg/cm². The tension in the web below the top flange is about 120 kg/cm². The tension in the bottom flange is about 76 kg/cm², again the highest at FB42 in the middle of the span.

Since the stress distribution in these figures was obtained for the temperature values scaled at the centroids of the elements rather than immediately at the junction, the stresses at the junctions of the top flange plate with the web do not always agree. For example, the stresses at the top web edges in Fig. 4.20 appear to be greater than the corresponding stresses in the top flange. However, since the discrepancy is not more than 25 kg/cm², it is readily explainable by a scaled temperature differential of only 1°C.

The thermal stresses in Figs. 4.19 to 4.21 were computed for a typical observed pattern of temperature change (see the last paragraph of Art. 4.4.3). Thus, the stress levels can be accepted as representative of the maximum thermal stresses that can be expected in the bridge structure. With 150 kg/cm^2 maximum compression in the top flange, 120 kg/cm^2 maximum tension at the top of the webs and 80 kg/cm^2 maximum tension in the bottom flange, these stresses are readily covered by the 25 to 33% increase in allowable stresses, generally permitted when thermal effects are added to the effects of dead and live loads.

4.6 Scratch Gage Record of Thermal Effects

The scratch gage traces discussed in Art. 3.5 in connection with the force history contained a record of diurnal stress changes in the form of a zig-zag scratch - one cycle for each day.

The initial interpretation, prior to the computer analyses presented above, was that the scratch trace amplitude was primarily a measure of the stresses produced by the redundant reactions developing due to temperature changes. Stress changes of the order of 200 to 400 kg/cm^2 are mentioned in Art. 3.5 in conjunction with the traces shown in Figs. 3.7 and 3.17 to 3.20. For example, specific values of 205 and 300 kg/cm^2 are pointed out in Fig. 3.19.

There are, however, a number of arguments which make it impossible to ascribe the zig-zags to thermal stresses only. The maximum thermal stress change computed in Art. 4.4 for the location of the scratch gage at FB42 Bottom (Fig. 4.20) is approximately $64\text{--}70 \text{ kg/cm}^2$, which is considerably smaller than the apparent stress recorded by a scratch gage for this location. For example, the right photograph of

Fig. 3.19 indicates a zig equivalent to 205 kg/cm^2 (for 12 January 1975). Considering that the five zig tops in this figure correspond to the five days this target was in the bridge and that the live load stresses are superimposed on the zig-zag line and only increase its thickness (see discussion in Art. 3.5.3), there must be some not-yet-considered phenomenon which leads to the discrepancy between the computed thermal stresses and the daily strain fluctuation recorded by the scratch gages.*

Another observation pertinent to proper interpretation of scratch gage traces is the appearance of the daily fluctuation only after the bridge girder was joined into a three-span continuous structure as illustrated in Fig. 3.7 and noted in Chapter 3. However, this fact cannot be explained by the stresses from the redundants since the redundants produce a stress change of only about 200 kg/cm^2 which is too small to be the cause.

After a careful search, the explanation for the discrepancy between the computed and measured thermal stresses was found to lie in the difference of temperature between the girder plate and the scratch gage.

The original analysis assumed that the temperature of the scratch gage is the same as the temperature of the steel plate to which it is attached. However, the field observations have shown first qualitatively then approximately quantitatively, that there exists a difference due to the unequal air temperature inside and outside the box, the effects of wind and direct solar radiation, as well as due to the insulating barrier between the gage and structure provided by the paint and the clearance.

*The initially mistrusted computer results were confirmed by approximate manual calculations and by the strains measured in the structure.

For example, considering the scratch gage location at FB42 Bottom on the inner web, the early afternoon temperature inside the box at the bottom is several degrees lower than the temperature of the web steel. The scratch gage, although attached to the web, is still separated from it by the paint and an air gap and thus has its temperature closer to the temperature of the air inside the box than of the web steel. Therefore, the gage, expanding less than it should, would record a longer tensile scratch than the scratch produced by the tensile stresses developing in the steel at this time. On the other hand, at night, the inside air temperature, and thus the temperature of the scratch gage, is higher than the temperature of the web. Thus, the gage, being longer than it should, would record a greater compressive stress than occurs in reality. The net effect of these two compounding deviations is that the stress change recorded is greater than the actual one.

What is significant is that the combined temperature deviation which can explain the discrepancies between the computed and measured stresses is so realistically small. For example, the above-mentioned scratch gage value of 205 kg/cm^2 is reduced to the computed value of 65 kg/cm^2 (within the 64 to 70 range) by a temperature deviation of only 5.6°C . Actually, this is lower than the differences of eight or more degrees which were felt or approximately measured in the field. Apparently, the plastic covers which were taped over the scratch gages did help to some extent, but they were not fully adequate to eliminate this effect.

The absence of the daily zig-zags for the period the bridge girder was still statically determinate resulted from the cancelling rather than the amplifying effect of the temperature differentials on the thermal stresses described above. For example, with the redundant stresses being zero, the thermal stress at FB42 Bottom in the early afternoon was compressive and thus, the relative shortening of the gage led to a reduction of the compressive scratch amplitude to the extent that it was recorded only as a blob without advancing the target. The possibility of an overcompensation was apparently reduced by a better ventilation of the open end box during construction than has been available in the completed bridge.

Since the temperature differential between the scratch gage and the structure may vary from day to day, and thus cannot be quantified, the principal value of the daily zig-zag trace provided by the scratch gages is in being able to pin-point the date of some unusual stress events rather in the evaluation of the actual thermal stresses.*

4.7 Summary and Recommendations

4.7.1 Summary

The thermal study conducted on the President Costa e Silva Bridge gave the following principal results:

- 1) The temperature measurements on the bridge established that the greatest temperature change in a bridge cross section occurs between 6:30 and 15:00 hours and is of the pattern shown in Fig. 4.14.

*The accuracy of the scratch gages in the bridge may be improved by shielding them, for example, with hollowed-out styrofoam panels taped over the gages.

- 2) The computer program developed for thermo-elastic analysis of the bridge gave a typical maximum thermal stress distribution as shown in Fig. 4.20 for the section near FB42. The stresses are below 150 kg/cm^2 in tension or compression and thus are sufficiently small not to endanger the bridge.
- 3) The scratch gages have recorded larger than actual thermal stress changes due to inadvertent temperature difference between the gage and the structure, and thus cannot be relied upon to give accurate stress readings unless they are better insulated. However, they can be trusted to monitor the bridge for the occurrence of some unforeseen stress changes (higher than about 300 kg/cm^2) and to be able to pinpoint the date of such an occurrence.

4.7.2 Recommendations

Although the thermal stresses in the President Costa e Silva bridge have been found not to be of dangerous levels, the results of this study provide valuable material for formulating some specific recommendations on the treatment of thermal effect in steel bridges.

- 1) Temperature Change for Design of Steel Bridges under Rio de Janeiro Conditions

The temperature change distribution measured on the President Costa e Silva Bridge can be considered as representative of the temperature changes in steel box and plate girders under the Rio de Janeiro climatic conditions. However, in deference to the temperature gradient in the girder plates between the

outside and inside surfaces and the fact that the measurements were made only on the inside surface, the following prudently conservative temperature change distribution is recommended for use in design of similar steel bridges:

+ 20°C in the top flange plate,

+ 20°C to +5°C, linear reduction from the top flange plate to a point on the webs and stiffeners 25 cm below the flange,

+ 5°C in the remainder of the cross section.

Figures 4.22 and 4.23 show this recommended temperature change pattern and the resultant thermal stresses for the President Costa e Silva Bridge.

2) Thermo-Elastic Analysis of Steel Bridges

The computer program developed for thermo-elastic analysis of the President Costa e Silva Bridge (see Appendix B) can be modified for other girder structures. Thermal stresses in statically determinate girders are expected to be safely low but in continuous, indeterminate girders they may be of significant magnitude and thus an analysis should be always performed.

3) Scratch Gages

Scratch gages are recommended as reliable devices for monitoring unforeseen stress conditions in important bridge structures. In selecting the location and the gage length, careful attention should be given to the expected stress changes produced by regular traffic and daily temperature fluctuations. The gages should be thermally insulated from the surrounding

air in order to reduce the temperature differential between the gage and the structure surface on which it is installed.

4) Future Use of Instrumentation in the President Costa e Silva Bridge

The electric and mechanical gage systems in the bridge will be functional for a number of years and additional readings should be taken in order to refine the information obtained so far and to clarify some of the plausible approximations made in the present study. Specifically, mechanical gage readings at FB42 and FB27 (or FB17) taken on the same summer day one to two hours apart from 6:00 till 18:00 hours would be helpful.

The scratch gage monitoring should be continued, but the number of gages can be reduced from eight to the following four: one at FB87 (mid-length of the bridge, two at FB42 (top and bottom), and one at FB17 Bottom. The remaining scratch gages can then be removed and installed on some other structures.

4.8 Chapter 4 - Tables and Figures

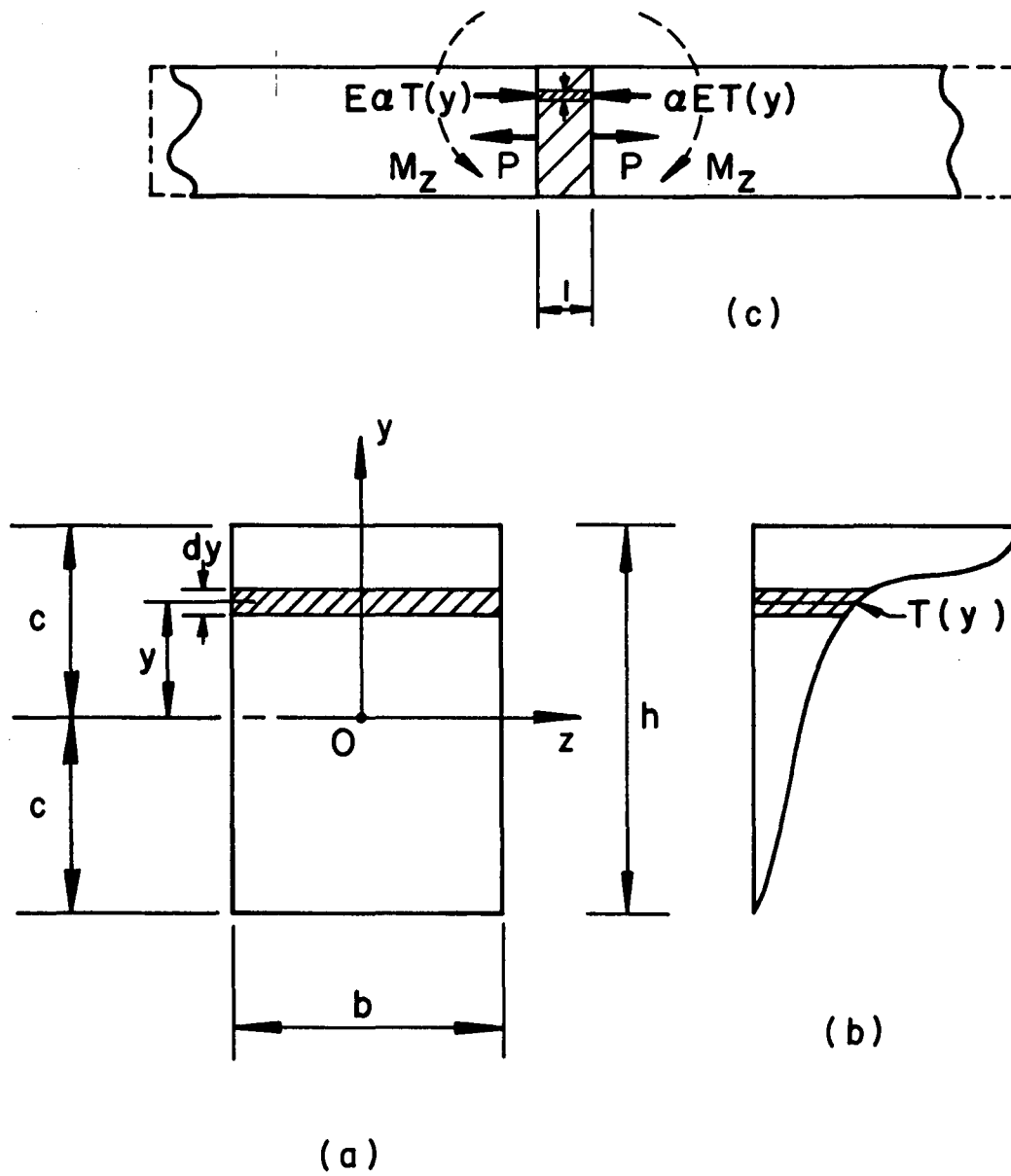


Fig. 4.1 Rectangular Beam Section Under Non-Linear Temperature Change.

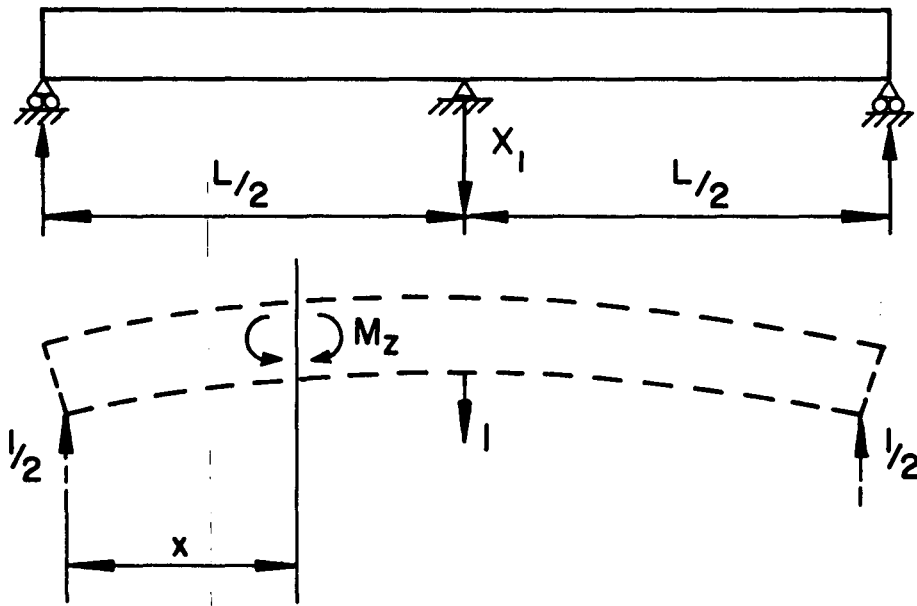


Fig. 4.2 Two-Span Beam Under Effect of Temperature.

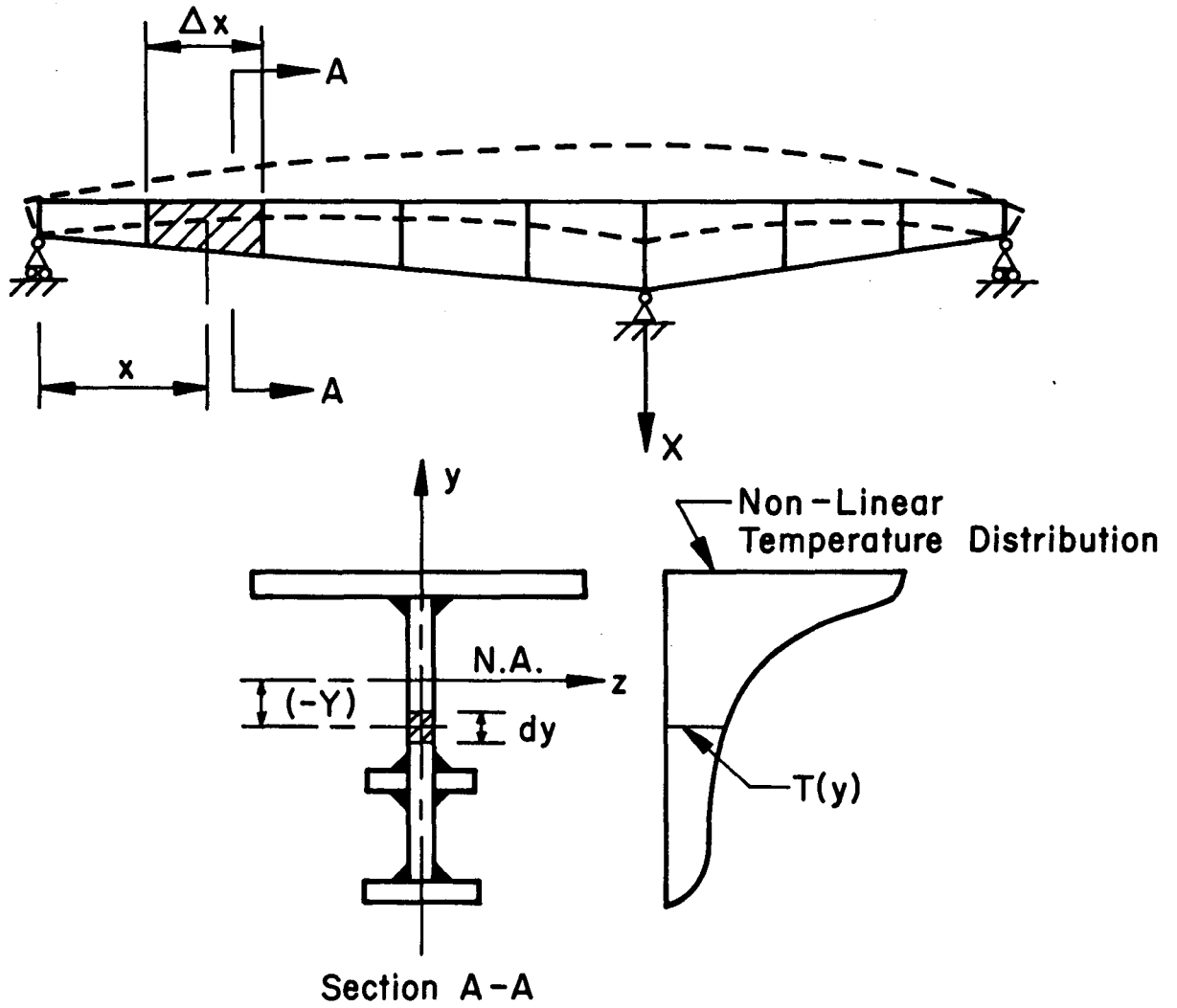


Fig. 4.3 Non-Prismatic Indeterminate Beam Under Non-Linear Temperature.

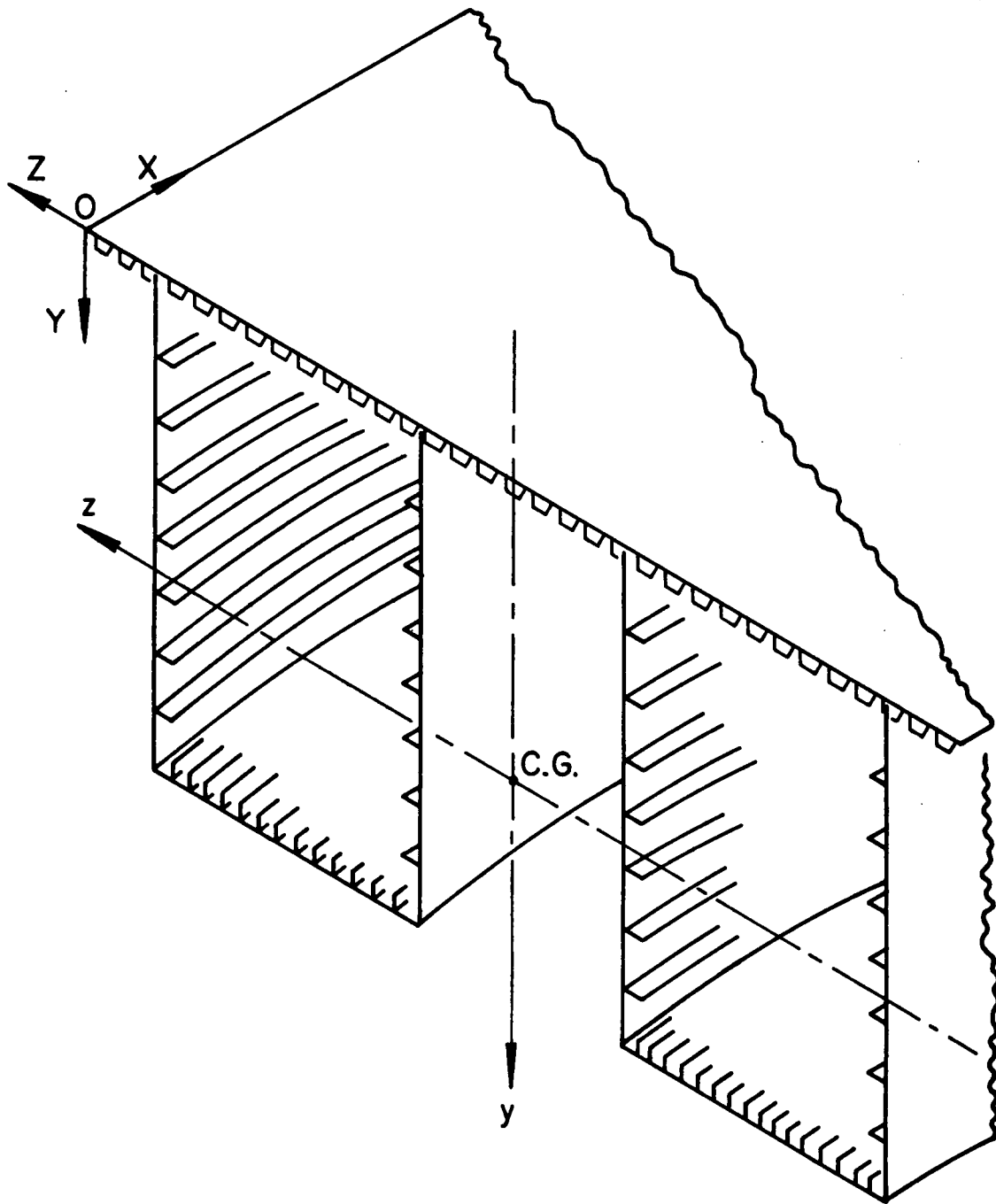


Fig. 4.4 Coordinate Axes in a Typical Bridge Cross Section.

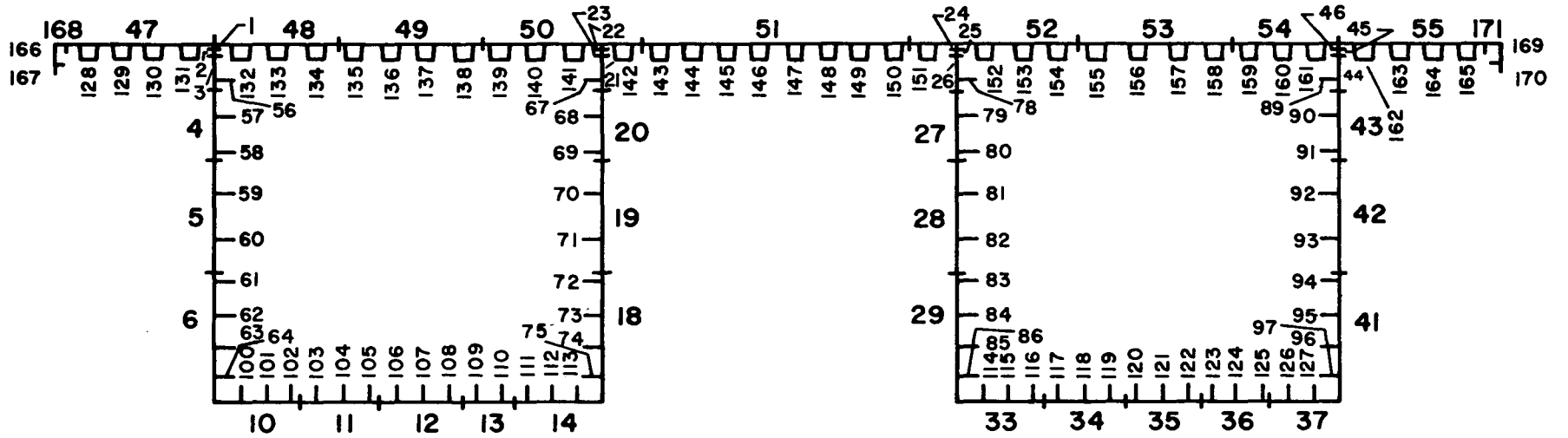


Fig. 4.6 Subdivision of Section at FB27 into Elements.

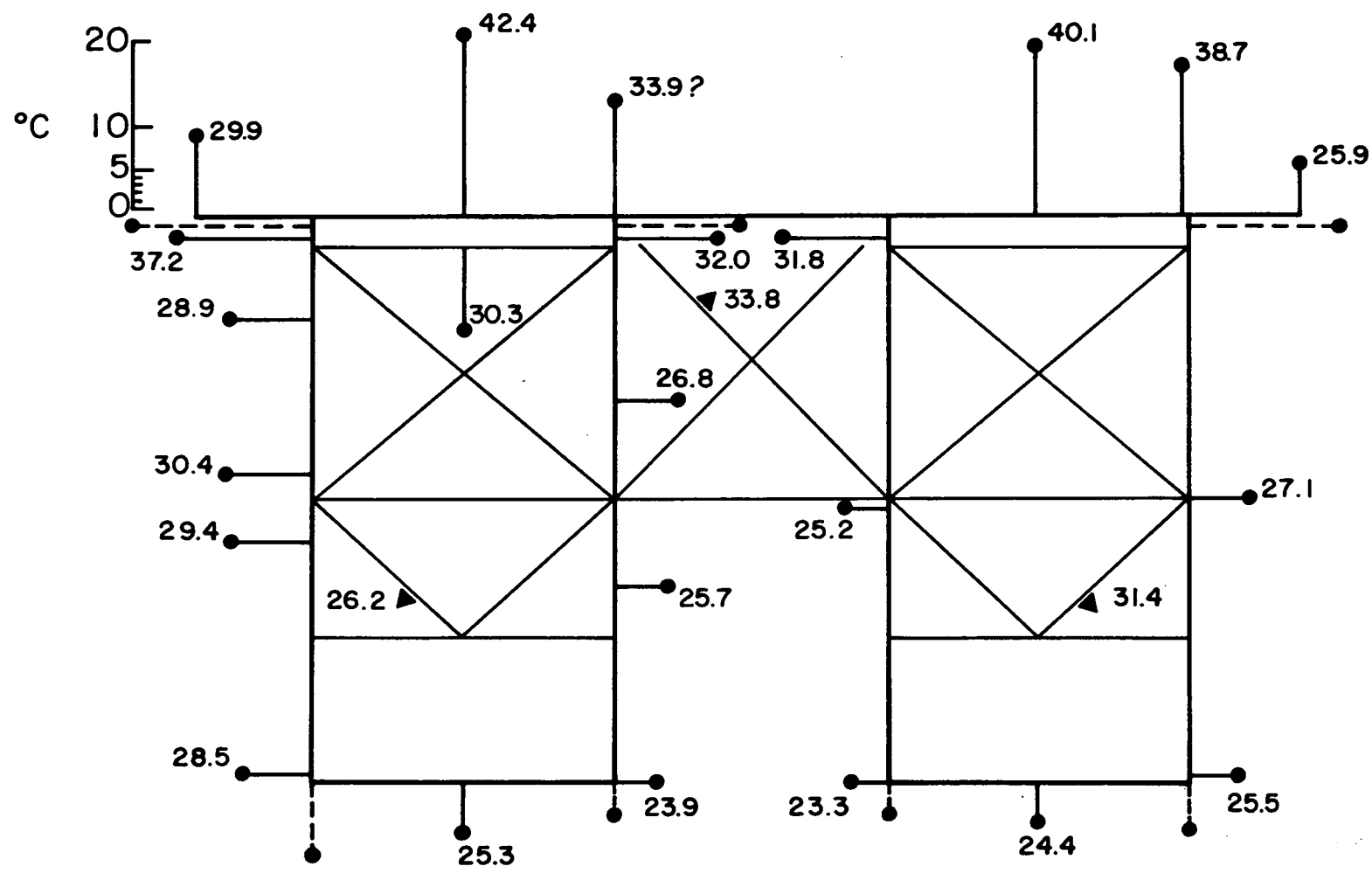


Fig. 4.7 Temperature Distribution Measured on 27 February 1974.

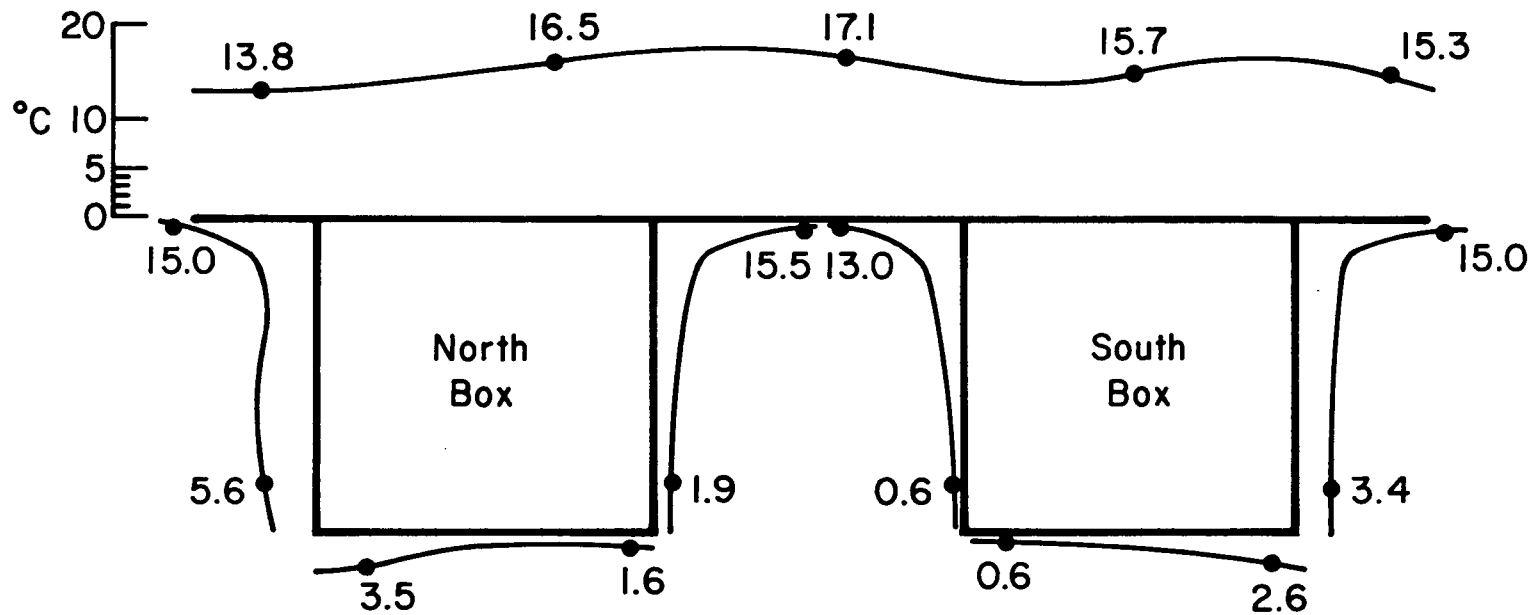


Fig. 4.8 Sample of Temperature Change at FB27 Based on February 1974 Readings.

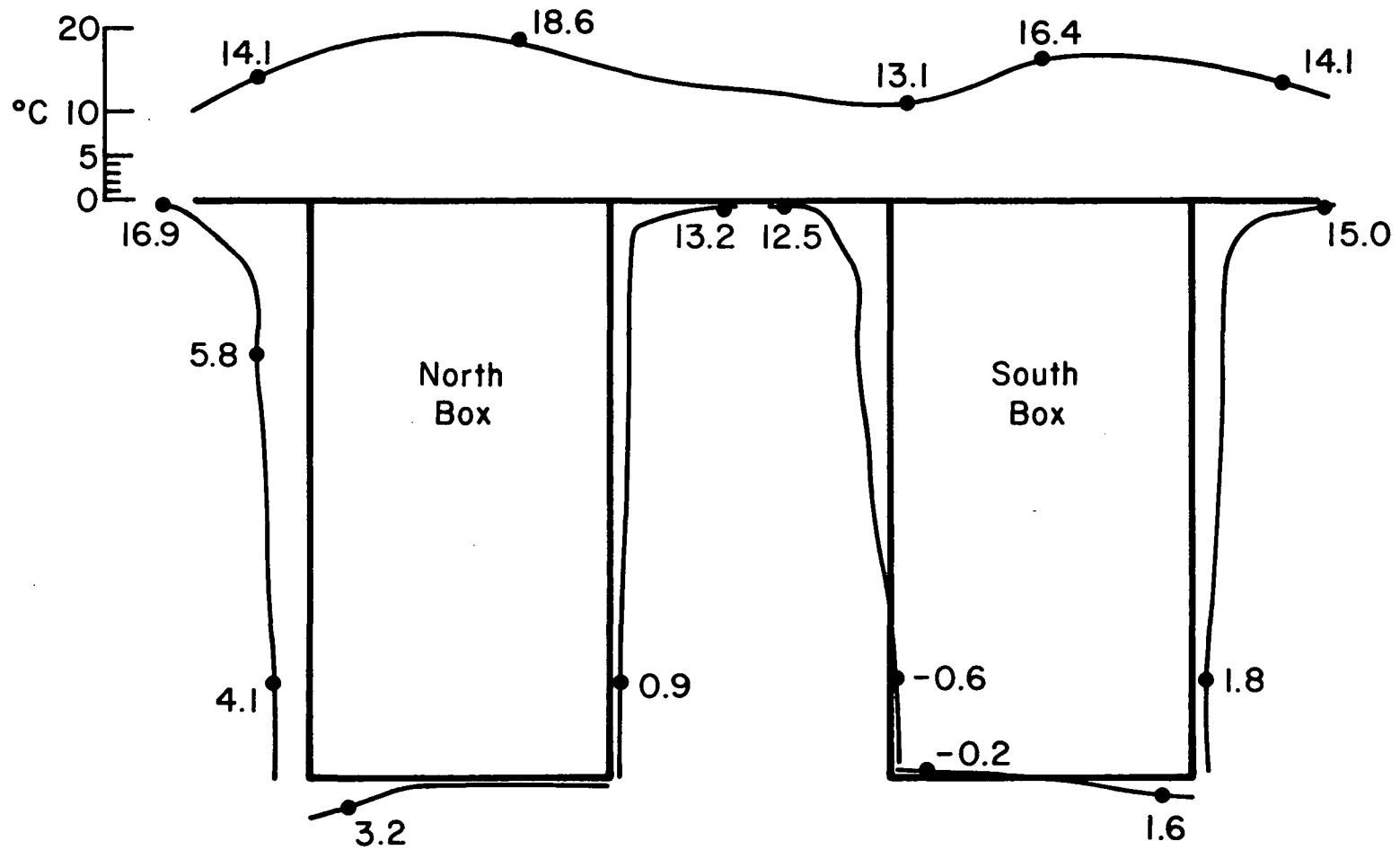


Fig. 4.9 Sample of Temperature Change at FB57 Based on February 1974 Readings.

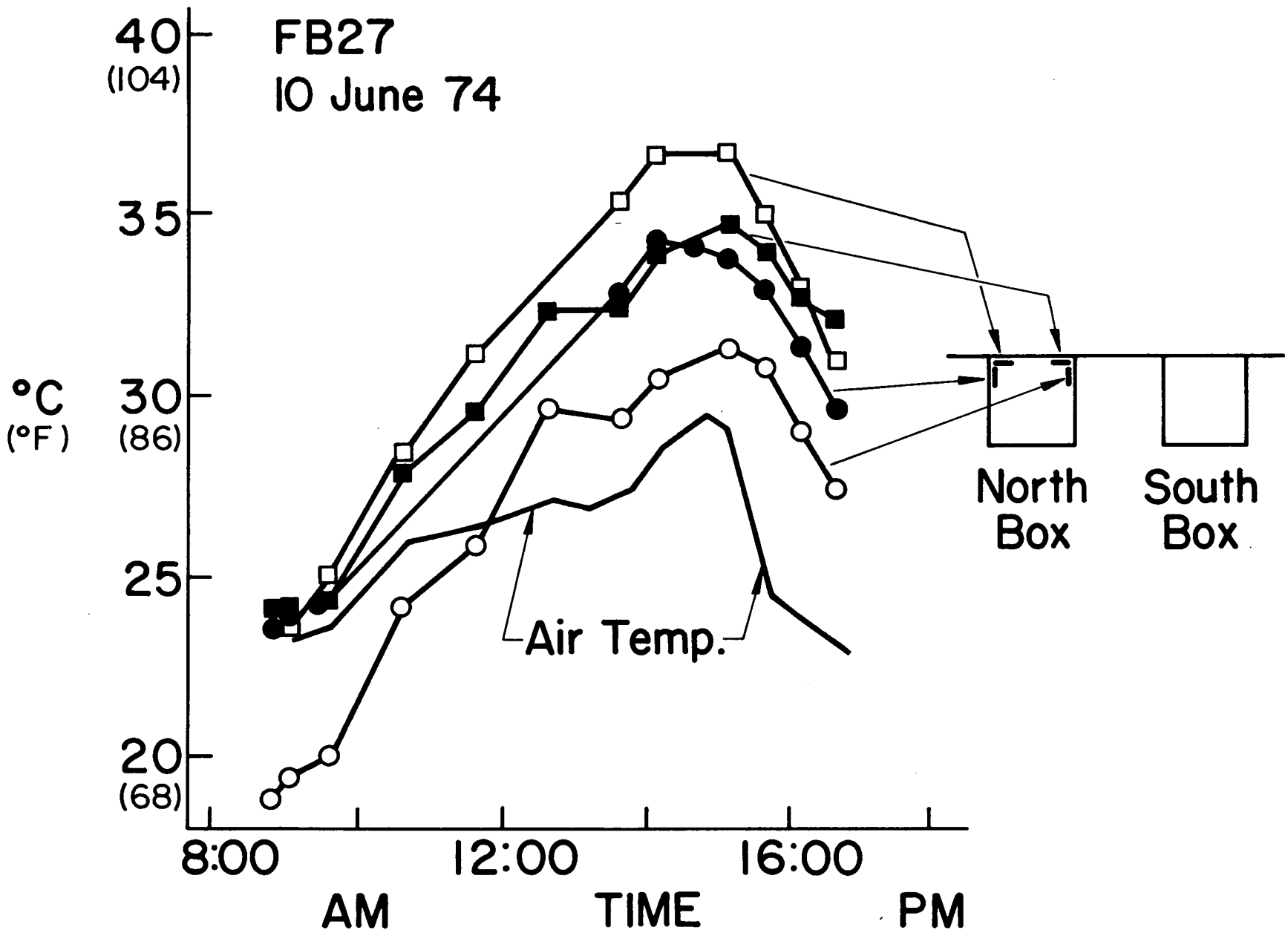


Fig. 4.10 Temperature Variation with Time at FB27 on 10 June 1974.

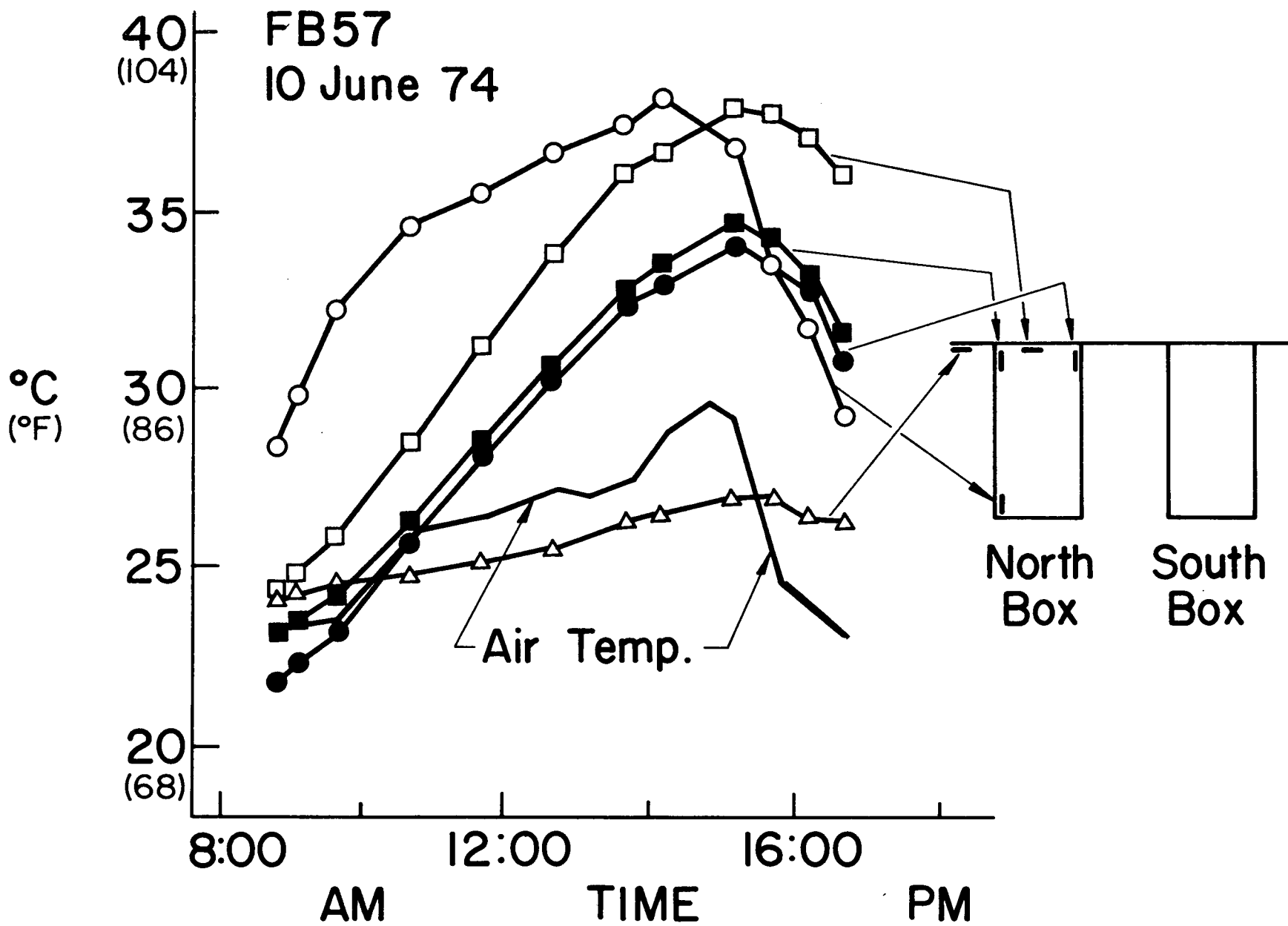


Fig. 4.11 Temperature Variation with Time at FB57 on 10 June 1974.

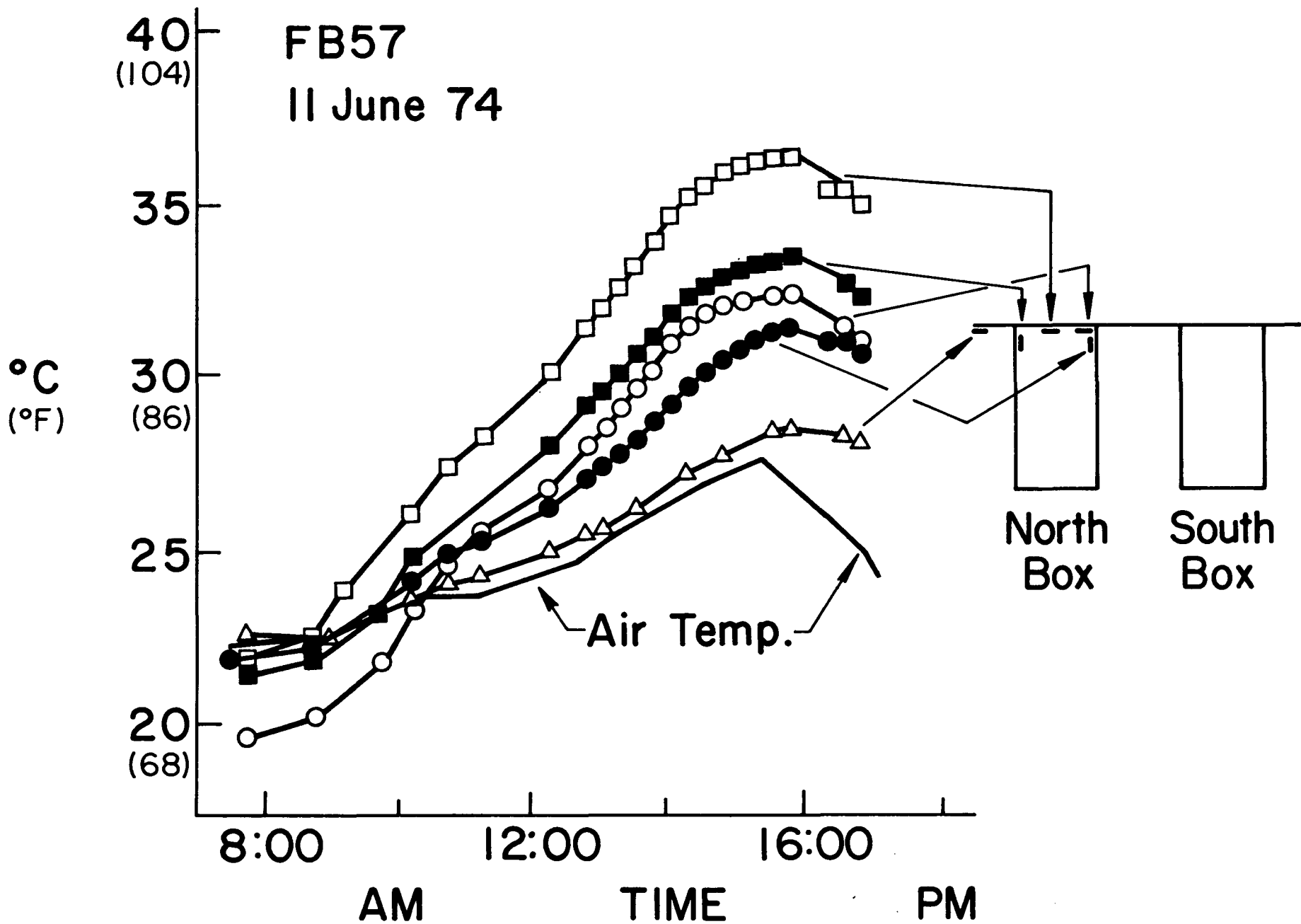


Fig. 4.12 Temperature Variation with Time at FB57 on 11 June 1974.

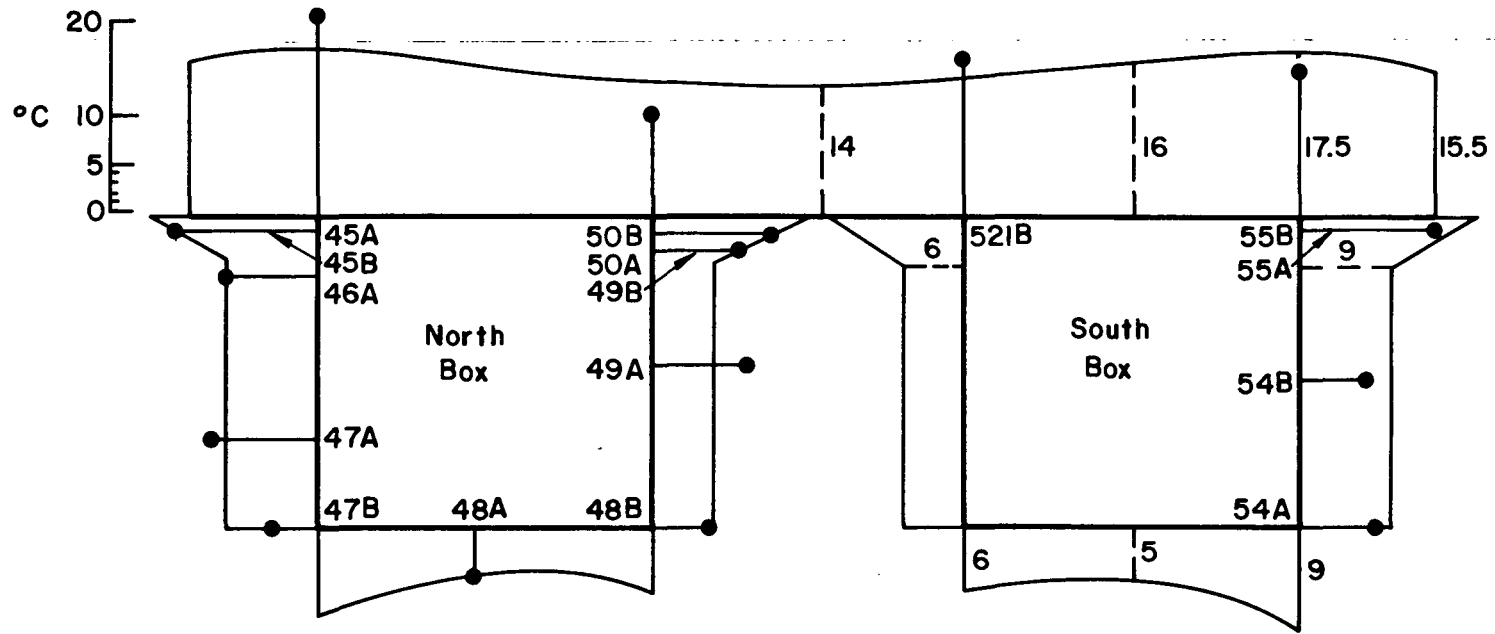


Fig. 4.13 Maximum Temperature Change at FB27 on 17 January 1975 (6:30 - 15: hrs).

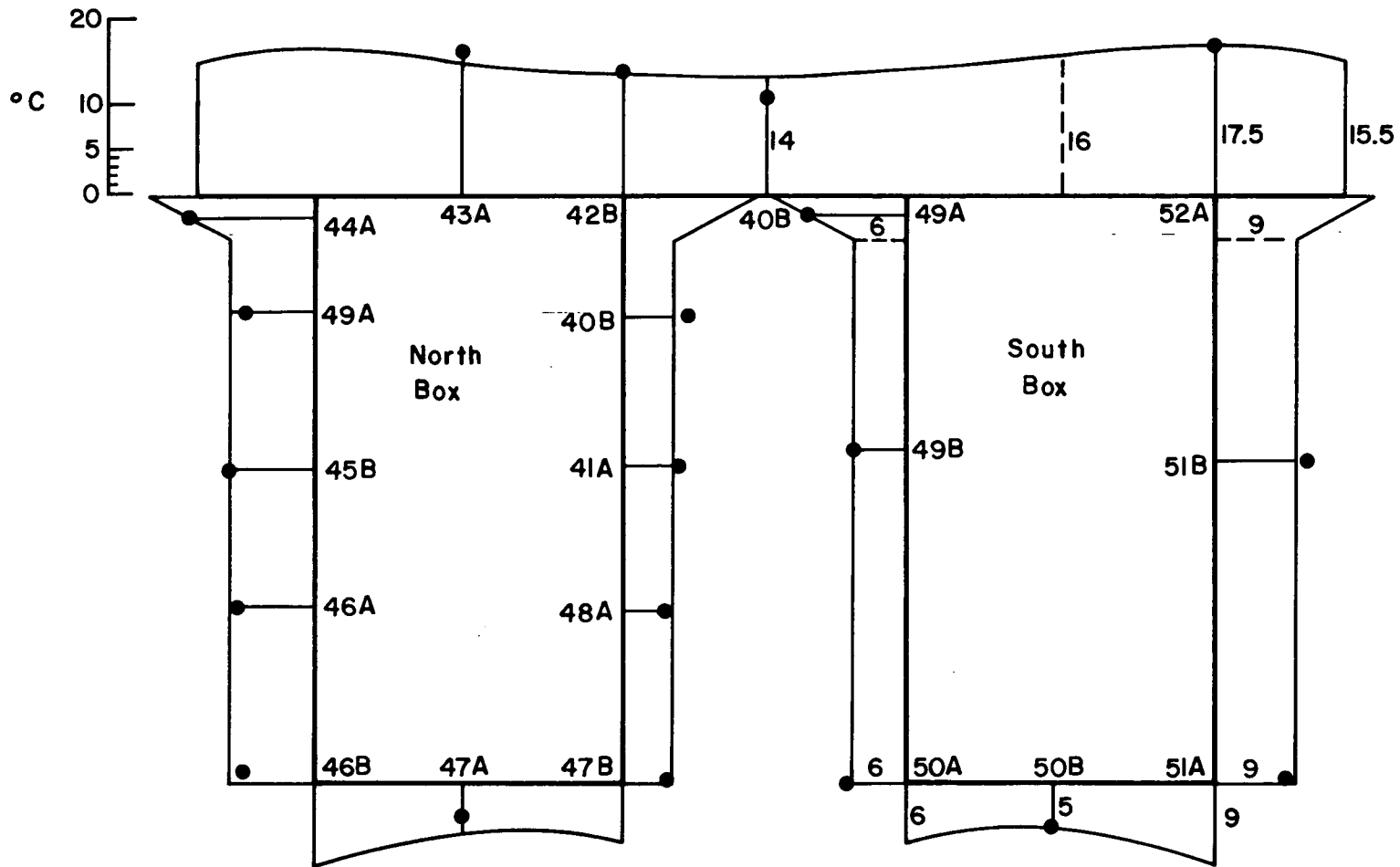


Fig. 4.14 Maximum Temperature Change at FB57 on 17 January 1975 (6:30 - 15:00 hrs).

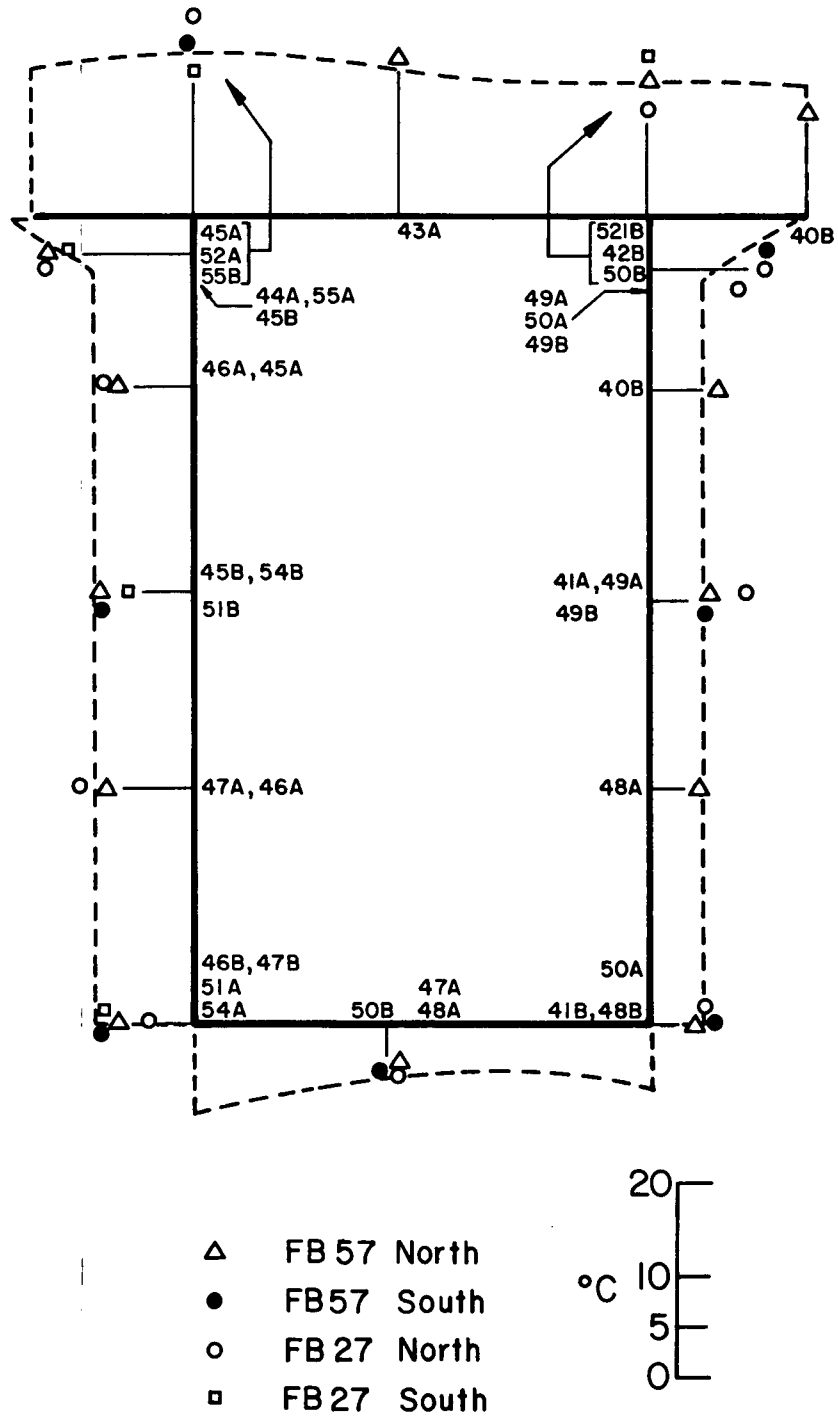


Fig. 4.15 Composite of Temperature Changes on 17Jan75 (6:30 - 15:00 hrs) (shown on the Outline of the North Box).

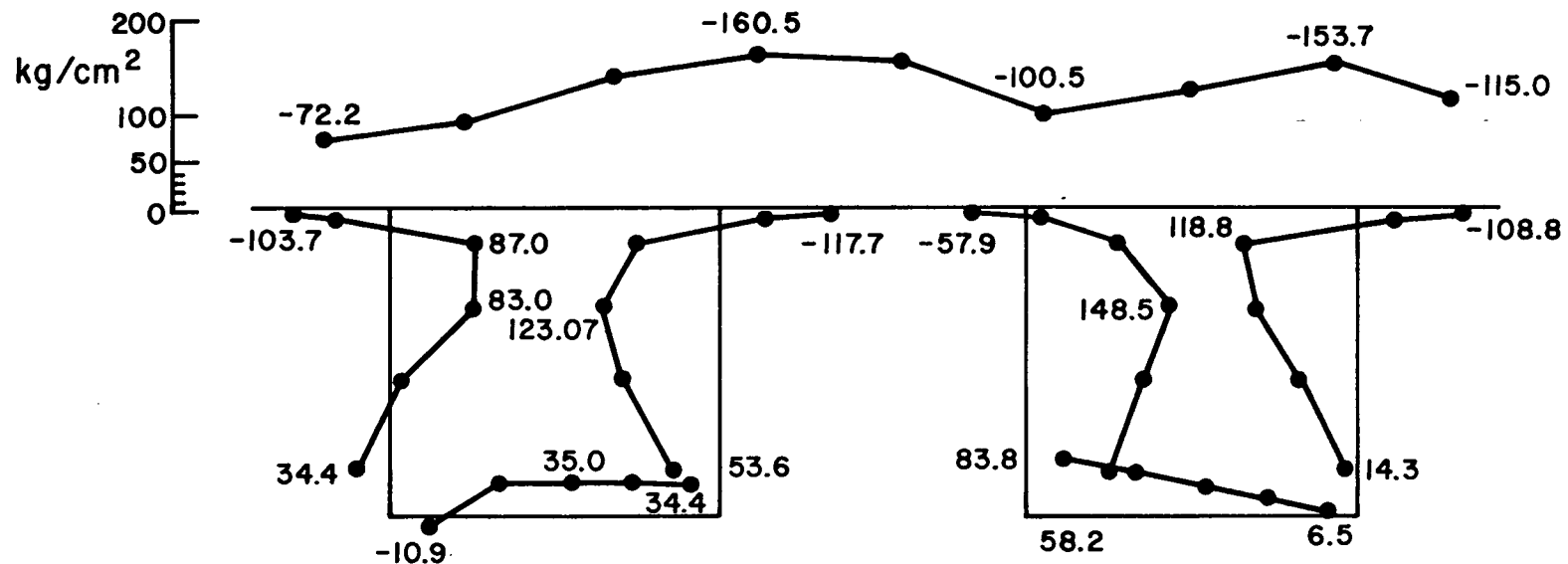


Fig. 4.16 Thermal Stresses at FB27 (x = 50m) for Sample Data of February 1974.

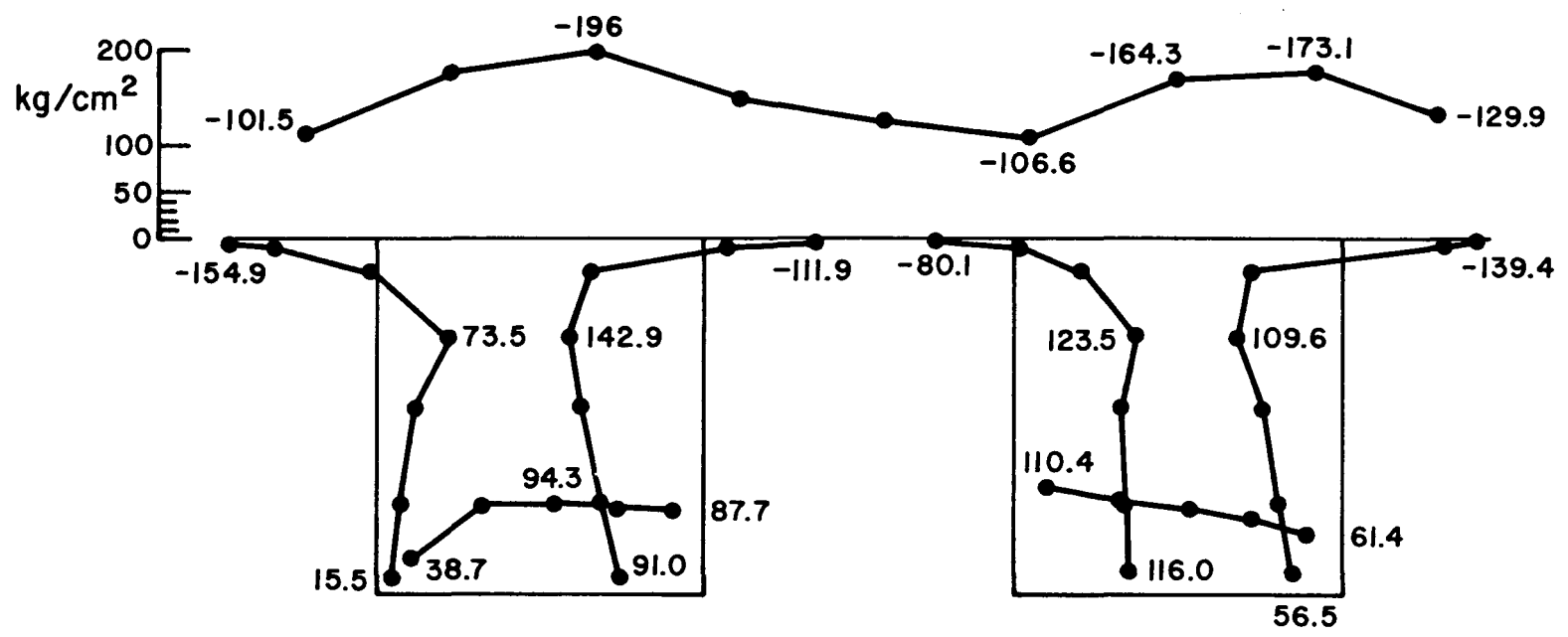


Fig. 4.17 Thermal Stresses near FB42 (x = 130m) for Sample Data of February 1974.

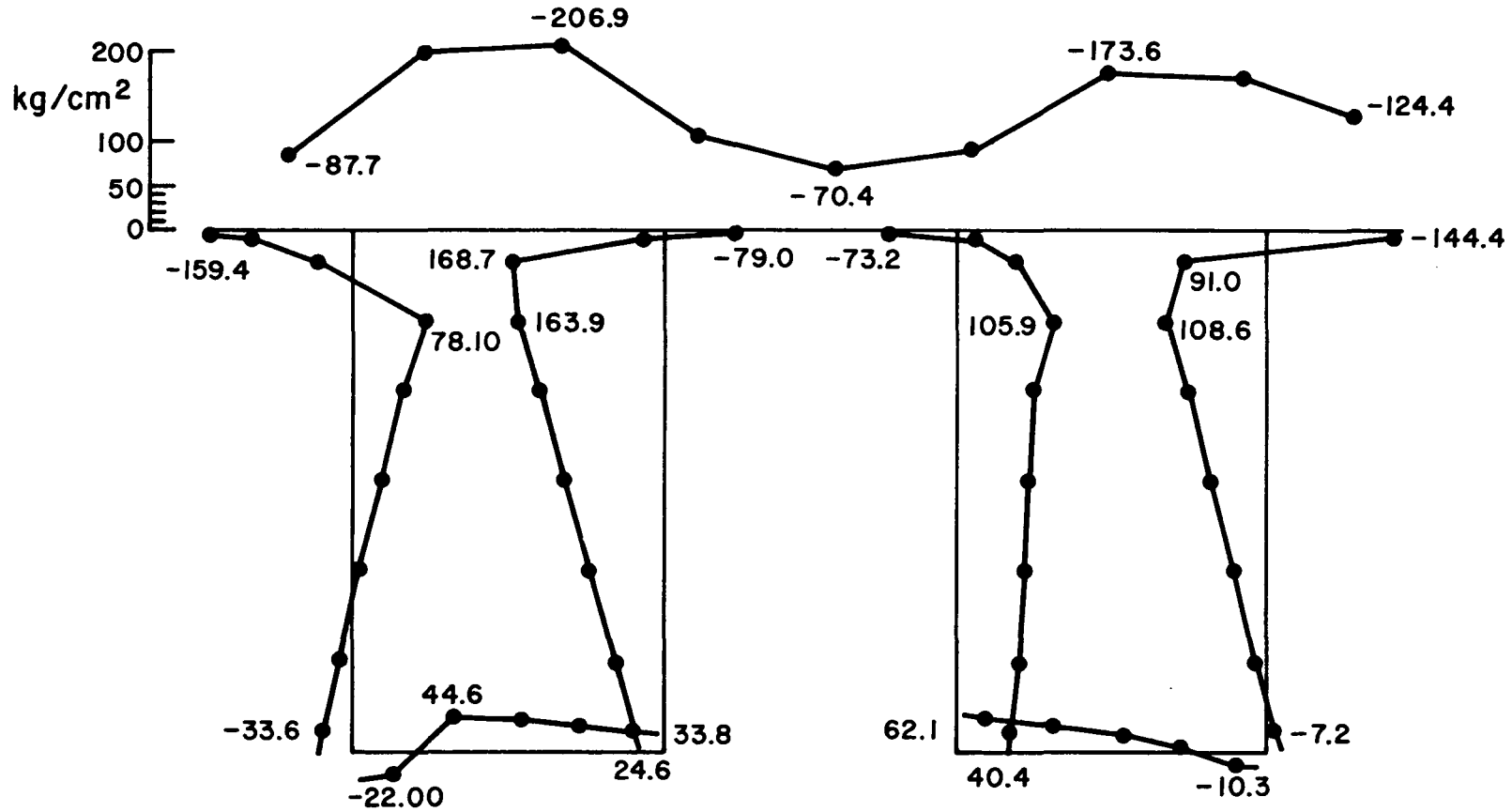


Fig. 4.18 Thermal Stresses near FB57 (x = 190m) for Sample Data of February 1974.

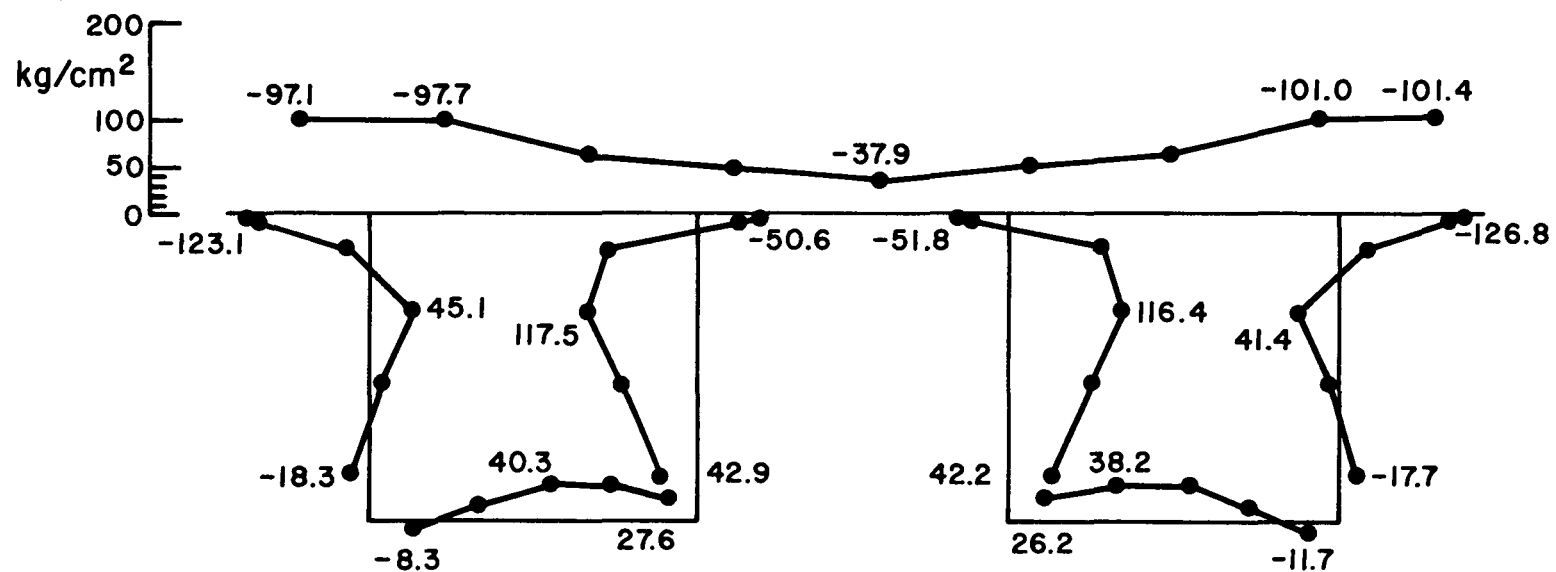


Fig. 4.19 Thermal Stresses at FB27 (x = 50m) for January 1975 Data.

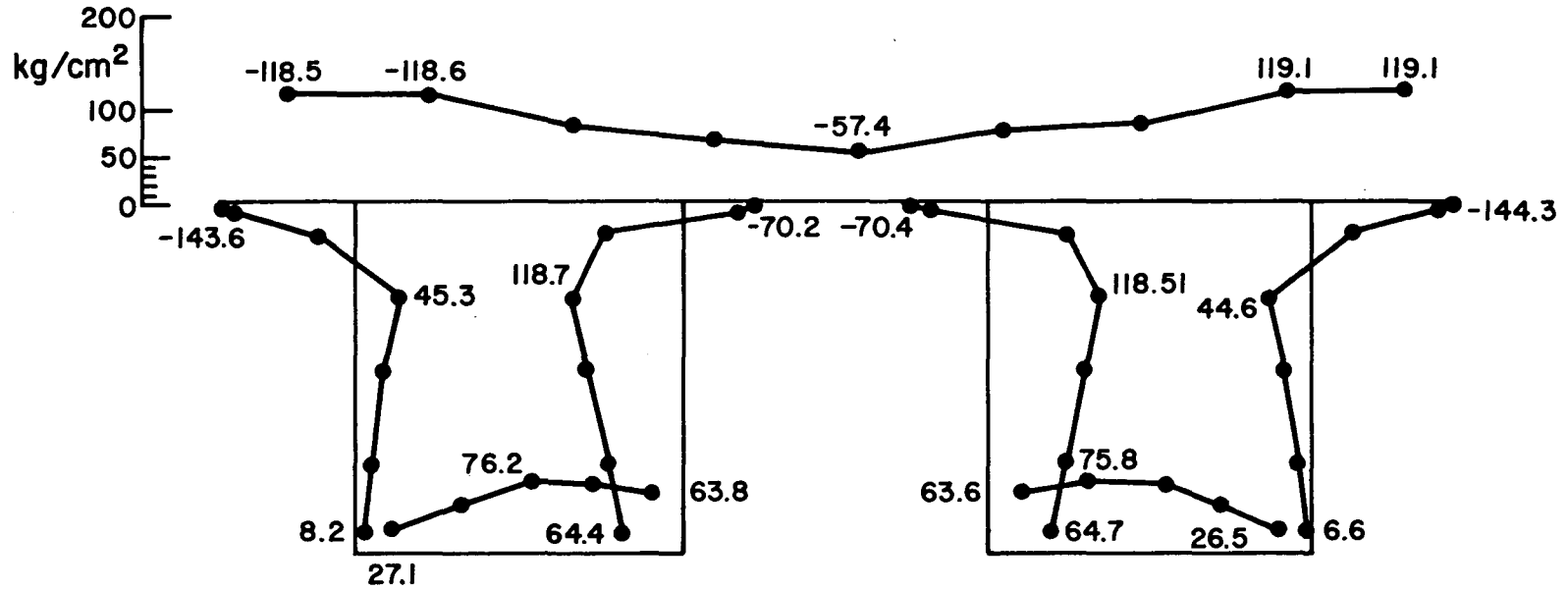


Fig. 4.20 Thermal Stresses at FB42 (x = 130m) for January 1975 Data.

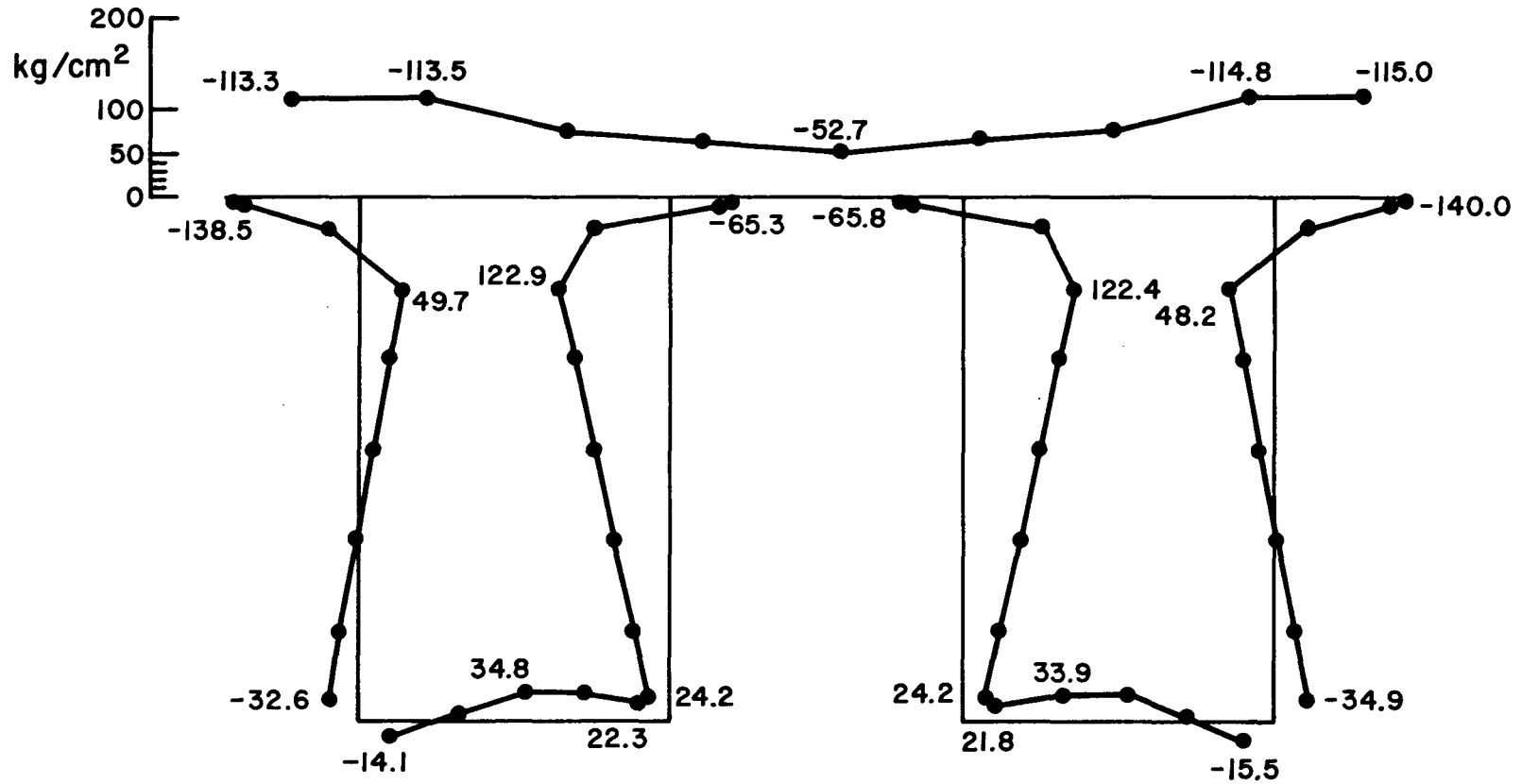


Fig. 4.21 Thermal Stresses at FB57 (x = 190m) for January 1975 Data.

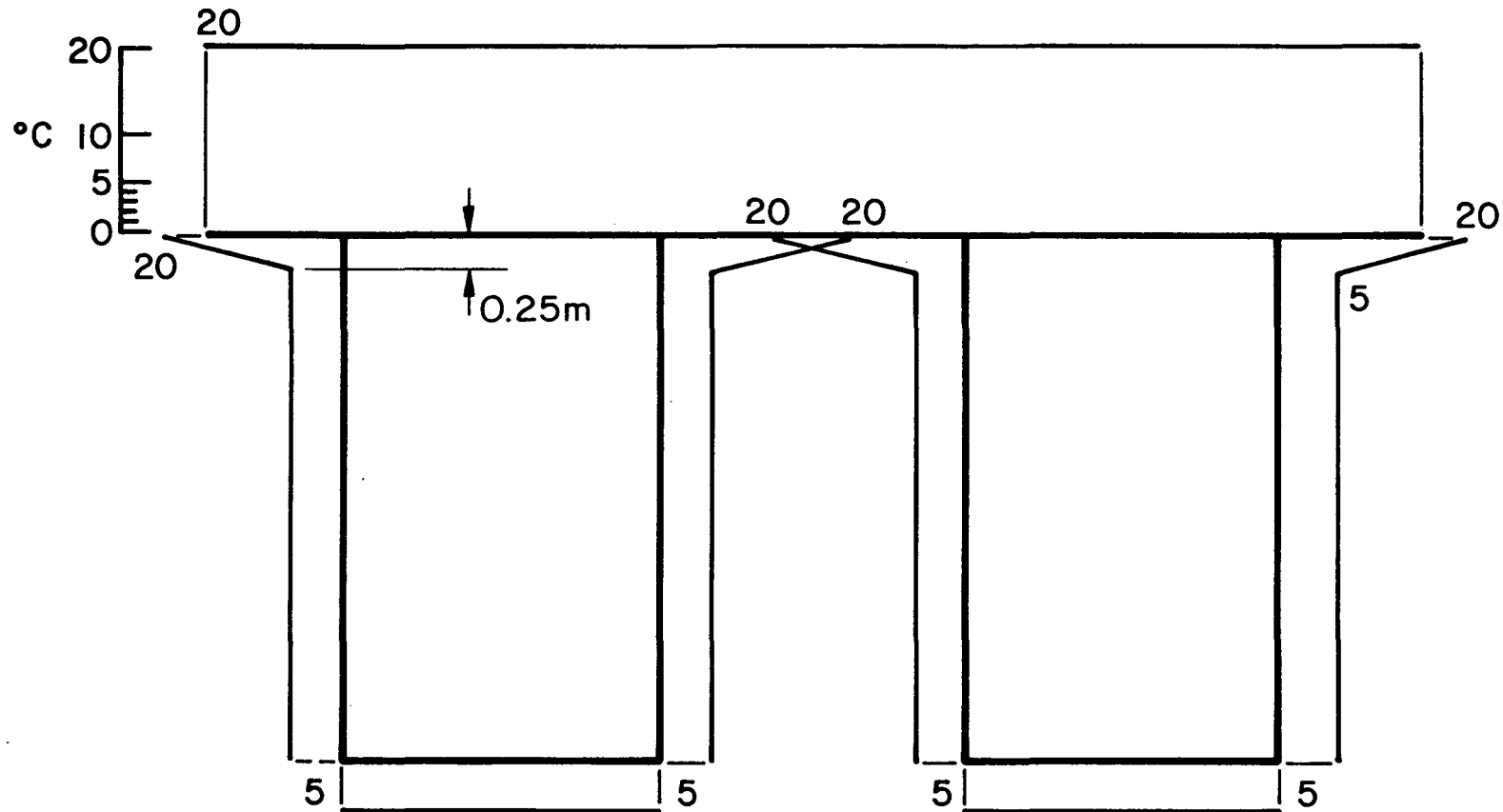


Fig. 4.22 Temperature Change Distribution Recommended for Design of Steel Box and Plate Girder Bridges Under Rio de Janeiro Climatic Conditions (shown on Cross Section at FB57)

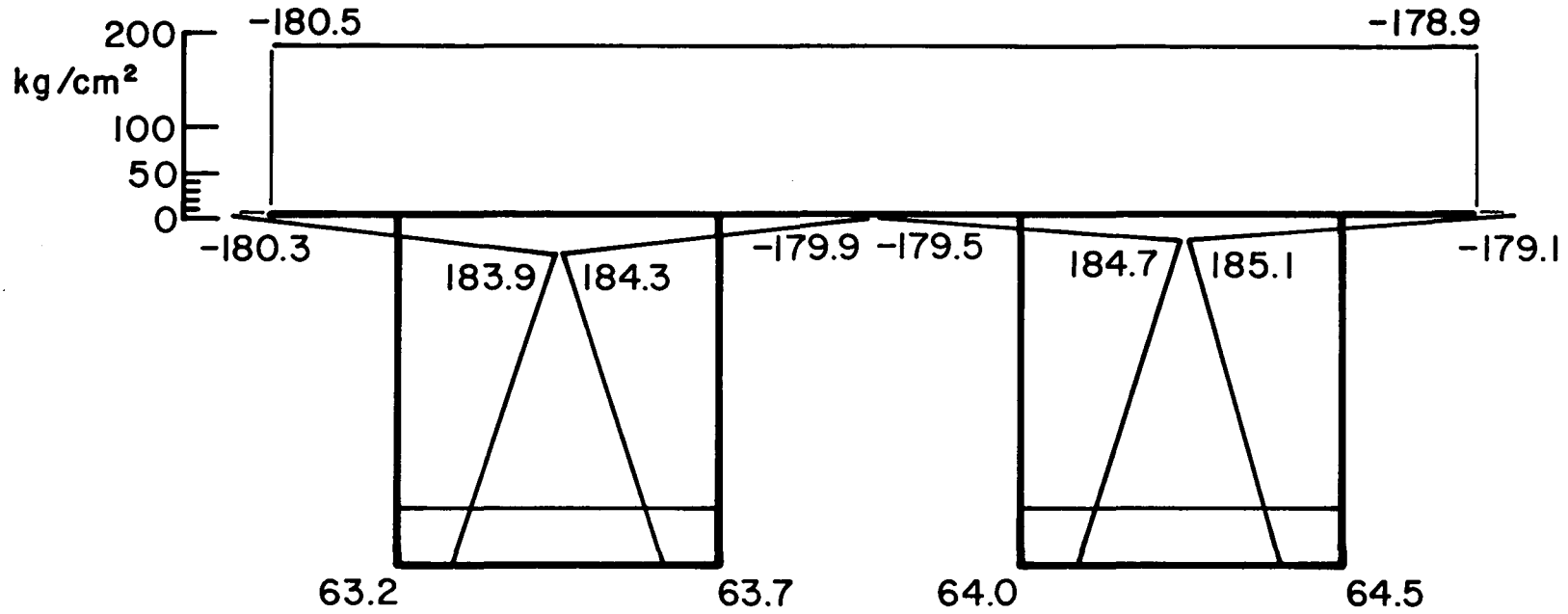


Fig. 4.23 Thermal Stresses in the President Costa e Silva Bridge Near FB42
(x = 130 m) due to Temperature Change of Fig. 4.22

5. EFFECTIVE PLATE WIDTH AND TRANSVERSE STRESSES
DUE TO POISSON'S RATIO EFFECT

(J. E. O'Brien and A. Ostapenko)

5.1 Observed Transverse Strain Patterns and Possible Causes

To study forces and stresses in the transverse bracing frames, strain gages were placed on the flanges of the floor beams and transverse stiffeners and on the flange or web plate of the box shell at opposite locations. These gages measured strains in the direction perpendicular to the longitudinal axis of the bridge.

Figure 5.1 (transverse strain changes at FB27 during the transfer from jetties to pontoon) shows a pattern across the member cross sections of large strains of the same sign, but of varying magnitude. This pattern indicates the presence of moment and axial force despite the absence of vertical loads. Similar patterns are also shown in Figs. 5.2 to 5.6 for FB42 and for other cases of loading. These strains could not have been caused by temperature changes. For example, in the case of Fig. 5.3 both readings were taken at night when the variation in temperature was less than 2°C between any two points in the frame. The only other explanation is in the development of transverse stresses due to longitudinal stresses, that is, Poisson's effect. Poisson's effect occurs when large changes in strain in the longitudinal direction attempt to create a corresponding opposite transverse strain in the plates of the girder. This tendency for shrinkage or expansion (equivalent

to 30% of the longitudinal strain) is resisted by floor beams and stiffeners and thereby the patterns of stress are created as if produced by a moment and an axial force.

Figures 5.1 to 5.6 (6 cases of data) show a number of strain readings with a magnitude of up to 300 micro-cm/cm (equivalent to a stress change of 600 kg/cm^2). These strains offer an opportunity to investigate Poisson's effect phenomenon since its proper understanding is important for the evaluation of possible stress levels in a realistic analysis and design of similar bridge structures. This data can also serve as a tool for establishing the values of effective widths in stiffened plates affected by Poisson's effect.

5.2 Analysis

5.2.1 Assumptions and Procedure

Analysis of the transverse frames was made using the following assumptions:

1. The effective width is constant over the length of each frame member.
2. The vertical members of both boxes have the same constant effective width.
3. The gross normal stress varies linearly from top to bottom of the box girder.

Thus, there are three unknown widths (effective widths of the top, vertical and bottom members).

Since any method of indeterminate analysis can only handle as many unknowns as there are redundants and the three unknown effective widths are additional unknowns, the problem cannot be solved directly. The additional needed relationships are established by utilizing the transverse strain readings.

The approach is based on the requirement that at the correct values for the effective widths, the calculated strain for the points of measurement should be as close as possible to the measured values. Thus, the process consists of minimizing the error between the calculated and measured strains. This minimization is started by assuming random values for the three effective widths.

Using the initial random effective widths, the strains due to Poisson's effect on the frame are calculated at the points of measurement. Then, the error is computed as the sum of squared differences between the calculated and the measured strains. Next, the effective width for the top member is increased by a certain increment and the analysis repeated giving a new value of the error. If the new error is less or equal to the previous error, the effective width of the vertical member is then incremented. If the new error is greater than the previous error, the previous effective width of the top member is decreased by the increment and a new error calculated. If the new error is still not less or equal to the value of the error for the unincremented width for the top

member, the unincremented effective width for the top member is kept and then the effective width for the vertical member is incremented. When this process is completed with the effective width of the vertical member, the effective width of the bottom member is incremented and then the process is returned back to the effective width for the top member. This technique is repeated over and over until the error cannot be decreased any further.

With these final effective width values, stresses can be obtained at various points in the frame. Figure 5.7 is the general flow chart of the computer program that performs the process of calculating effective widths and corresponding stresses. After solving all six cases of data in the same manner (Figs. 5.1 to 5.6), the resultant effective width values were compared and appropriate conclusions drawn.

5.2.2 Method of Analysis and Computation of Stresses

The force method was chosen for analyzing the transverse frames primarily because of its ability to handle any of the six sets of data and geometry with very few modifications. (5.1) Another reason for the selection was that the matrix form of the force method was suitable for the available computer (CDC 6400).

The first step in the analysis was to decide on the primary structure and redundants of the transverse frame of the completed bridge. Due to the symmetry of the cross section and primary normal

stresses, only one-half of the section needed to be analyzed. The transverse frame was idealized as shown in Fig. 5.8a with the resultant primary structure (statically determinate) as given in Fig. 5.8b (5 redundants). In this primary structure, the frame can be represented as a series of cantilevers (Fig. 5.9). Acting at the free end of each of the cantilevers is a moment, a shear, and an axial force denoted by M , S , and P , respectively. These bar forces are listed in matrix C in order of member number, and sublisted in order of M , S , and P . The sign convention is indicated by the positive directions shown in Fig. 5.9. This model can be readily modified to represent a single box case (existing during construction) by eliminating redundants 4 and 5.

In general, the elements for the C matrix are found from

$$C = B_0 \cdot R + B_1 \cdot X \quad (5.1)$$

where

R = matrix of external loads applied to the nodal points.

X = matrix of the values of redundants.

B_0 = matrix of bar forces due to real external loads
on the primary structure.

B_1 = matrix of bar forces due to unit redundant forces
applied on the primary structure.

C = matrix of all bar forces.

Since the internal forces of the frame are a result of Poisson's effect only, R matrix equals zero. Consequently, Eq. 5.1 reduces to

$$C = B_1 \cdot X \quad (5.2)$$

The values of the redundants are found from the matrix equation

$$X = -[(B_1)^T \cdot F \cdot B_1]^{-1} \cdot (B_1)^T \cdot V \quad (5.3)$$

where the additional notation is

V = deflections created at the end of each cantilever
by Poisson's effect when the member is released.

F = total flexibility matrix.

The total flexibility matrix F of a structure is composed of the basic element flexibility matrices (f_i), one for each member.

For a cantilever the basic element flexibility matrix is

$$f_i = \begin{bmatrix} \frac{L_i}{EI_i} & \frac{L_i^2}{EI_i} & 0 \\ -\frac{L_i^2}{EI_i} & \frac{L_i^3}{EI_i} & 0 \\ 0 & 0 & \frac{L_i}{EA_i} \end{bmatrix} \quad (5.4)$$

where:

L_i = length of the i^{th} member.

A_i = area of the i^{th} member.

I_i = moment of inertia of the i^{th} member.

E = modulus of elasticity.

The total flexibility matrix F is shown in Fig. C-2 of Appendix C.

The derivation of the B_1 matrix is facilitated by drawing the M , S , and P diagrams for the redundants of unit value applied on the primary structure (Fig. 5.10). Then, the elements of the B_1 matrix are found as the forces on the ends of the released cantilevers. The complete B_1 matrix is shown in Fig. C-1 of Appendix C.

The derivation of the V matrix is facilitated by drawing the longitudinal stress, deflected shape, basic curvature, and basic axial strain diagrams for the primary structure due to Poisson's effect (Fig. 5.11). In this derivation, the first items that need to be known are the changes in transverse strain in the top and bottom flange plates of the box girder as if the plates were unstiffened. These changes are found from the longitudinal stress in the respective flanges (σ_T and σ_B) as follows:

for the top flange -

$$\epsilon_T = (-\mu)\sigma_T/E \quad (5.5a)$$

for the bottom flange -

$$\epsilon_B = (-\mu)\sigma_B/E \quad (5.5b)$$

where μ = Poisson's ratio ($\mu = 0.3$ is used).

The corresponding strains in the web plates are a linear variation from ϵ_T to ϵ_B according to Assumption 3 in Art. 5.2.1.

The axial strain and curvature in the primary structure are found from the following equations:

The axial strain in the floor beam

$$\epsilon_t = \epsilon_T \cdot t_t \cdot b_{et}/A_t \quad (5.6a)$$

The curvature in the floor beam

$$\phi_t = \epsilon_t \cdot e_t \cdot A_t/I_t \quad (5.6b)$$

The axial strain in the bottom stiffeners

$$\epsilon_b = \epsilon_B \cdot t_t \cdot b_{eb}/A_b \quad (5.6c)$$

The curvature in the bottom stiffeners

$$\phi_b = \epsilon_b \cdot e_b \cdot A_b/I_b \quad (5.6d)$$

The axial strain at the top of the vertical stiffeners

$$\epsilon_{vt} = \epsilon_T \cdot t_v \cdot b_{ev}/A_v \quad (5.6e)$$

The curvature at the top of the vertical stiffeners

$$\phi_{vt} = \epsilon_{vt} \cdot e_v \cdot A_v/I_v \quad (5.6f)$$

The axial strain at the bottom of the vertical stiffeners

$$\epsilon_{vb} = \epsilon_B \cdot t_v \cdot b_{ev}/A_v \quad (5.6g)$$

The curvature at the bottom of the vertical stiffeners*

$$\phi_{vb} = \epsilon_{vb} \cdot e_v \cdot A_v/I_v \quad (5.6h)$$

In the above expressions, t_t , t_v , t_b , are the thickness of the top, vertical, and bottom plates of the girder, respectively.

*Values of the axial strains and curvatures between the top and bottom of the vertical stiffeners have a linear variation.

b_{et} , b_{ev} , b_{eb} are the effective widths of the top, vertical, and bottom plates of the girder. e_t , e_v , e_b are the eccentricities from the center of the plate of the top, vertical, and bottom members of the frame to their respective centroidal axes. A_t , A_v , A_b are the areas of the top, vertical and bottom members of the frame. I_t , I_v , I_b are the moments of inertia of the top, vertical, and bottom members of the frame.

The V matrix is thus calculated by finding the deflections at the end of each released cantilever element due to these strains and curvatures (See Appendix C.1 for the details of calculations).

Once the B, F, and V matrices have been computed, the redundants can be solved using Eq. 5.3. Then the member bar forces (C matrix) are obtained from Eq. 5.2

The strains at the points of measurements are computed from the forces in the C matrix. These are the calculated strains that are compared to the measured strains. (See Section 5.2.1). The calculated strains (ϵ_c) are equal to the sum of the strain produced by the redundants (ϵ_R) and the strain produced by Poisson's effect on the primary structure (ϵ_p). The equations for finding ϵ_R and ϵ_p are

$$\epsilon_R = \frac{P}{A \cdot E} + \frac{M \cdot c}{I \cdot E} \quad (5.7)$$

$$\epsilon_p = \epsilon + \phi \cdot c \quad (5.8)$$

where for a particular point M and P are the moment and thrust created by the redundants, A and I are the area and moment of inertia for the particular member, c is the distance from the centroidal axis, E is the modulus of elasticity, and e and ϕ are the axial strain and curvature calculated in Eqs. 5.6

Once the final effective widths are found by the error minimization process described in Section 5.2.1, the stresses can be calculated. The strains across the depth of a member must be linear and continuous. The stresses are linear, however they are not continuous. There are three places in the cross section of a frame member where the stresses reach local maxima or minima:

- σ_1 in the exterior fiber of the plate,
- σ_2 in the web of the member at the plate interface,
- σ_3 in the flange of the floor beam or stiffener.

The stress across the cross section is a function of three effects as shown in Fig. 5.12; the stress required to restrain the top flange from Poisson's effect ($-P_p/A_f$), the stress from Poisson's effect on the released member ($P_p/A + \frac{M_p c}{I}$), and the stress created by the redundants ($P_R/A + \frac{(S_R \cdot x - M_R) c}{I}$). From this, the important stresses in the section in question become:

$$\sigma_1 = -P_p/A_f + (P_p/A - \frac{M_p \cdot c_1}{I}) + (P_R/A + \frac{(S_R \cdot x - M_R) c_1}{I}) \quad (5.9a)$$

$$\sigma_2 = (P_p/A - \frac{M_p \cdot c_2}{I}) + (P_R/A + \frac{(S_R \cdot x - M_R) c_2}{I}) \quad (5.9b)$$

$$\sigma_3 = (P_p/A + \frac{M_p \cdot c_3}{I}) + (P_R/A - \frac{(S_R \cdot x - M_R) c_3}{I}) \quad (5.9c)$$

where A is the total area of the member; A_f is the effective area of the flange comprised of the plate, and x is the distance from the free end of the cantilever; c_1 , c_2 , c_3 are the distances to the centroidal axis from stress points 1, 2, and 3, respectively. The subscripts R and P indicate whether the bar force subscripted is from a redundant or from Poisson's effect on the released structure.

5.3 Effective Width and Resultant Stresses

The first results from the single box data analyzed using the original model of Article 5.2 (a three-redundant single box), showed that the effective width is dependent on the length of a member and independent of the plate thickness. As seen in Table 5.1, Column 8, the b_e/L ratios for the top members are almost the same for two locations (FB42 and FB27) and two cases of loads (Jetties to Pontoon and Pontoon to Pier Rings) (0.332, 0.294, 0.327, 0.231). Also, the vertical and bottom members both have nearly the same average b_e/L ratios, though lower ones than the top members. On the other hand, the b_e/t ratios listed in Column 7 of Table 5.1 vary very substantially, especially for the top members. Yet, using the effective width equal to a specific multiple of the plate thickness is an approach often used in design.

The b_e/L ratios for the vertical members at FB27 are slightly larger than for the vertical members at FB42. To make the analysis for FB27 more realistic, a new model was introduced (a five-redundant single box, having both braces). The results became even more consistent with those of the FB42 (three-redundant) model which has no braces.

Three different models were tried in the analysis of the data for the center span lift (double box section). The data for FB27 and FB42 was analyzed using the model of Fig. 5.8 in Article 5.2 (five-redundant, double box). The data for FB27 was also analyzed using a six-redundant model of Fig. 5.13 in which both cross braces are considered. The data of FB42 was similarly analyzed in a four-redundant model without cross bracing.

Apparently, because of the errors introduced by instrument drift and voltage fluctuations, the readings for the center span lift (complete structure - double box) gave no conclusive results by any of the analytical models used.

Much of the measured data indicated stresses of the order of 600 kg/cm^2 , and the analytical results from the programs for the single box section showed calculated strains that were in agreement with the measured values. The effective plate width was found to be $b_e/L \approx 0.30$ for the top members, and $b_e/L \approx 0.19$ for the vertical and bottom members. This result, implying that the effective width is a function of length, is based on the following two observations. First, the top members (the floor beams) at FB27 and FB42 have the same length but different plate thicknesses, 10mm and 16mm, respectively, and the results in Column 8 of Table 5.1 show that the b_e/L ratios for the top members are essentially the same (0.3) at both FB42 and FB27 despite this large difference in plate thickness. Secondly, the vertical and bottom members, although having different section properties and lengths, have nearly the same average

b_e/L ratios equal to 0.19. The difference between the floor beam value and the vertical and bottom member value seems to be primarily due to the restraint of the lateral movement of the plate of the floor beam provided by the cantilevering portion of the top flange plate.

Data smoothening was tried in order to improve the single box results and to obtain consistent results from the center span lift data. The strains at the points of measurements were calculated using the effective widths of $0.30L$ for the top member and $0.19L$ for the vertical and bottom members. These calculated strains were then compared to the measured strains and the extreme values which deviated by more than 20% were eliminated. The data smoothened in this way was then used to reevaluate the effective width and the results are listed in Columns 9 to 11 of Table 5.1. For the single box data this process used the five-redundant FB27 program and the three-redundant FB42 program. For the double box structure, smoothening was performed on the six-redundant FB27 program and both the four and five-redundant FB42 programs. The results confirmed the initial single box observations of average $b_e/L = 0.30$ and 0.19 for the top and vertical (and bottom) members, respectively.*

*The adjusted mean value changed from 0.308 to 0.295 (standard deviation change from 0.011 to 0.003) for the top members and from 0.197 to 0.186 (standard deviation change from 0.031 to 0.018) for the vertical and bottom members. The adjusted mean and the corresponding standard deviation were obtained from the data within the range of (first mean) \pm (first standard deviation) as also used in Table 3.12.

The reason the data from the center span lift gave inconsistent results was apparently the time period between the zero and final readings. One day elapsed between the readings, and this enabled the amplifier of the data acquisition device (B&F) to drift. A noticeable voltage fluctuation during this period may also have contributed to the poor readings.

Some of the changes in stresses produced by Poisson's effect in this structure were as high as 600 kg/cm^2 . Being approximately 20% of the yield stress, these stresses could be significant when taken into account with other stresses due to dead load, traffic loads, impact, and wind loads.

5.4 Conclusions

In this bridge the governing factor for the effective plate width for members perpendicular to the girder axis was found to be the length of the member. The specific values for the effective width are $b_e = 0.19L$ for the vertical and bottom stiffeners, and $b_e = 0.30L$ for the floor beams. The larger value for the floor beams is due to two reasons: one, the floor beams are restrained on both ends from axial movement by the cantilever flange plate of the girder; two, the top flange of the girder is more heavily stiffened in the longitudinal direction than the webs and bottom flange.

It is recommended that Poisson's effect should be considered in design of steel box girders. The stresses due to this phenomenon

in long span structures with high dead load moment could be significant and should be added to other stresses. Poisson's effect could also increase the possibility of fatigue failure in short span structures with large cyclic moment changes due to live loads.

5.5 Chapter 5 - Tables and Figures

MEMBER	FLOOR BEAM No.	TEST*	t (mm)	L (mm)	NUMBER OF REDUND.	INITIAL DATA			SMOOTHENED DATA		
						b_e (mm)	b_e/t	b_e/L	b_e (mm)	b_e/t	b_e/L
COLUMN	1	2	3	4	5	6	7	8	9	10	11
TOP	42	J to P	16	6860	3	2278	142.375	.332	2278	142.375	.332
	42	P to P	16	6860	3	2014	125.875	.294	2003	125.188	.292
	42	C	16	6860	4				See Section 5.3		
	42	C	16	6860	5						
	27	J to P	10	6860	3	2242	224.2	.327	--	---	--
	27	P to P	10	6860	3	1586	158.6	.231	--	---	--
	27	J to P	10	6860	5	2116	211.6	.308	2015	201.5	.294
	27	P to P	10	6860	5	1555	155.5	.227	2053	205.3	.299
	27	C	10	6860	5	2054	205.4	.299	--	---	--
	27	C	10	6860	6	2127	212.7	.310	1762	176.2	.257
Vertical	42	J to P	12	7280	3	1251	104.25	.172	1215	101.25	.167
	42	P to P	12	7280	3	1173	97.75	.161	1256	104.67	.173
	42	C	12	7280	4				See Section 5.3		
	42	C	12	7280	5						
	27	J to P	12	6310	3	1647	137.25	.261	--	---	--
	27	P to P	12	6310	3	1350	112.5	.213	--	---	--
	27	J to P	12	6310	5	1517	126.42	.240	1674	139.5	.265
	27	P to P	12	6310	5	1265	105.42	.200	1058	88.17	.168
	27	C	12	6310	5	2705	225.42	.429	--	---	--
	27	C	12	6310	6	2615	217.92	.414	918	76.5	.145
Bottom	42	J to P	20	6860	3	1426	71.3	.208	1426	71.3	.208
	42	P to P	20	6860	3	1271	63.55	.185	1417	70.85	.207
	42	C	20	6860	4				See Section 5.3		
	42	C	20	6860	5						
	27	J to P	18	6860	3	986	54.78	.144	--	---	--
	27	P to P	18	6860	3	1332	74.00	.194	--	---	--
	27	J to P	18	6860	5	1200	66.67	.175	1192	66.22	.174
	27	P to P	18	6860	5	1428	79.33	.208	1395	77.5	.203
	27	C	18	6860	5	846	47.00	.123	--	---	--
	27	C	18	6860	6	817	45.39	.119	871	48.39	.127

*J to P - Jetties to Pontoon
P to P - Pontoon to Pier Rings
C - Center Span Lift

Table 5.1: Effective Widths Computed from Transverse Strains

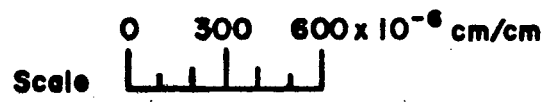
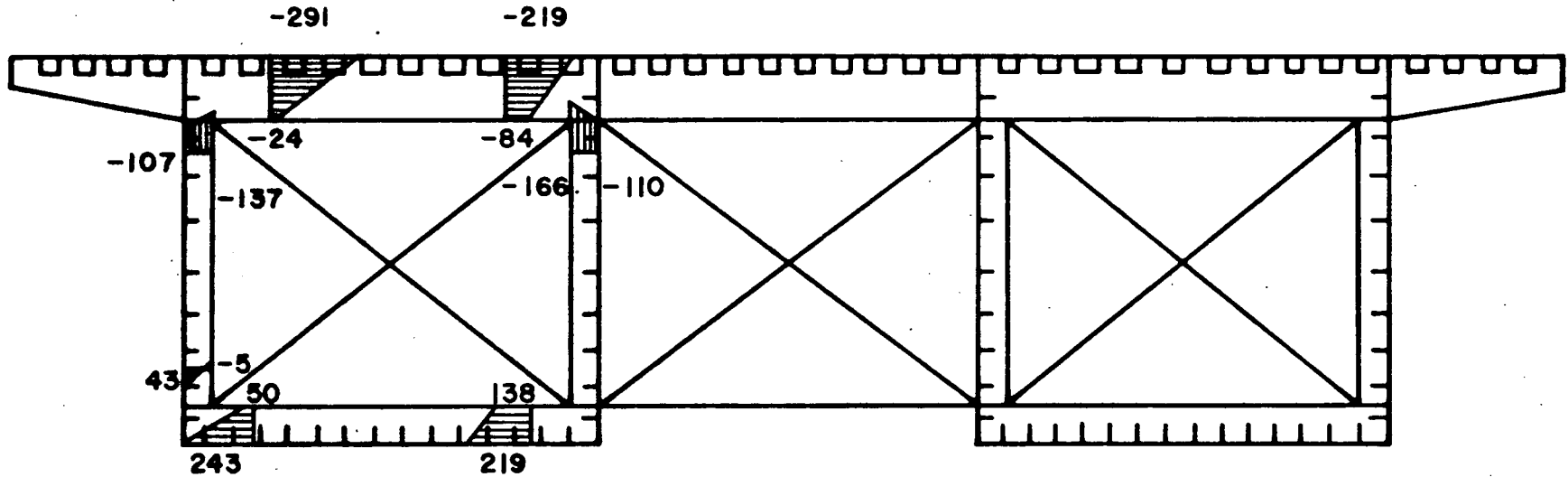


Fig. 5.1 Transverse Strains at FB27 due to Transfer of North Box from Jetties to Pontoon

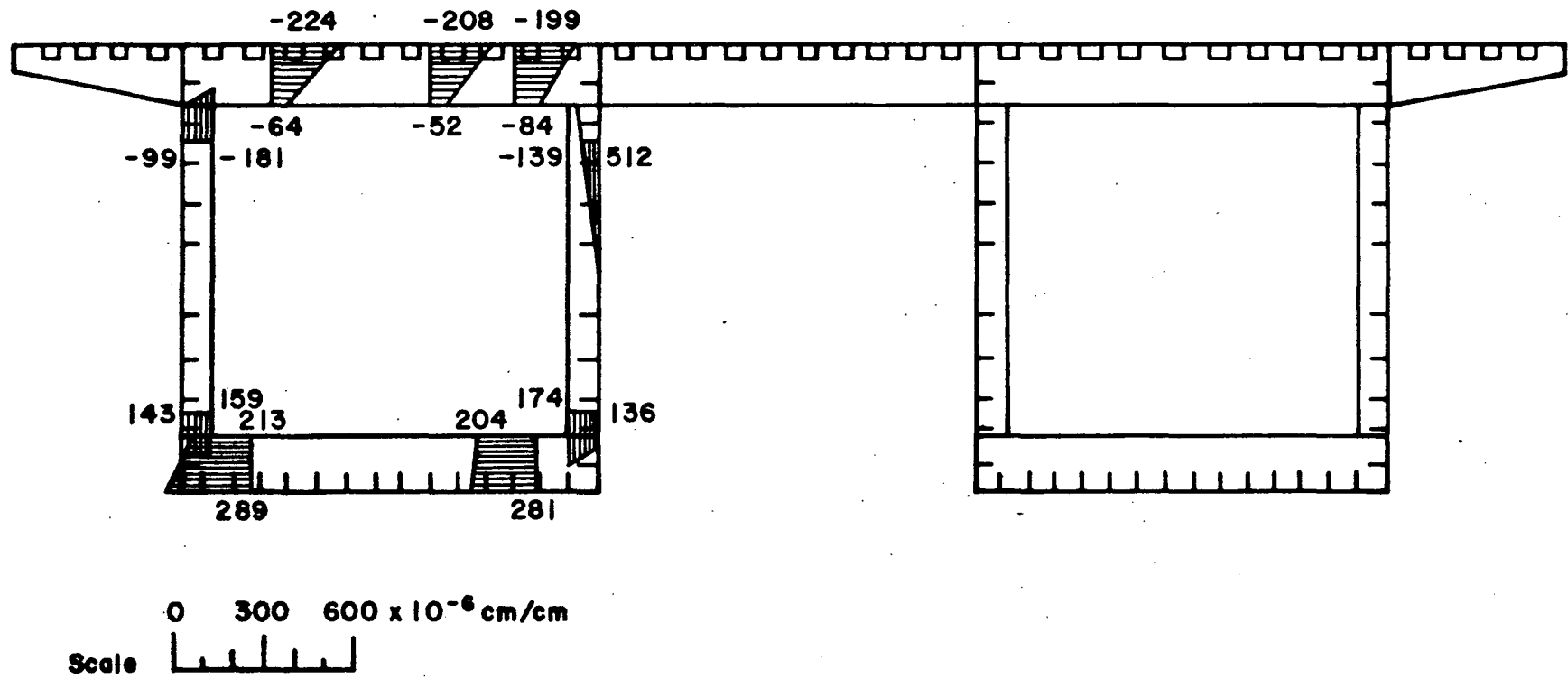
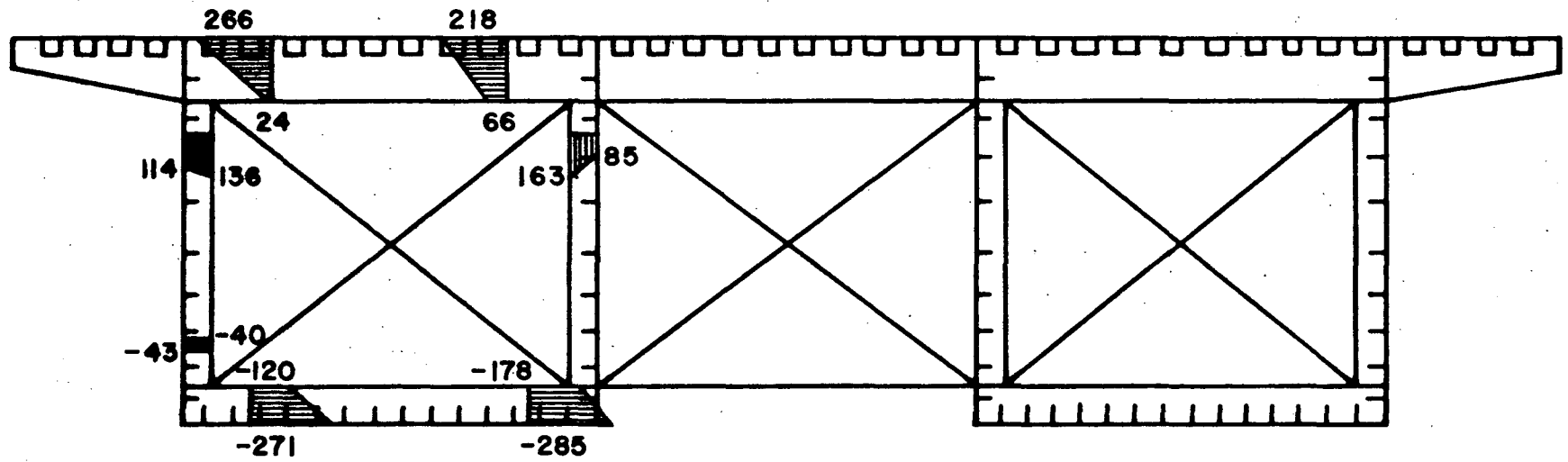


Fig. 5.2 Transverse Strains at FB42 due to Transfer of North Box from Jetties to Pontoon



0 300 600 x 10⁻⁶ cm/cm
Scale

Fig. 5.3 Transverse Strains at FB27 due to Transfer of North Box from Pontoon to Pier Rings

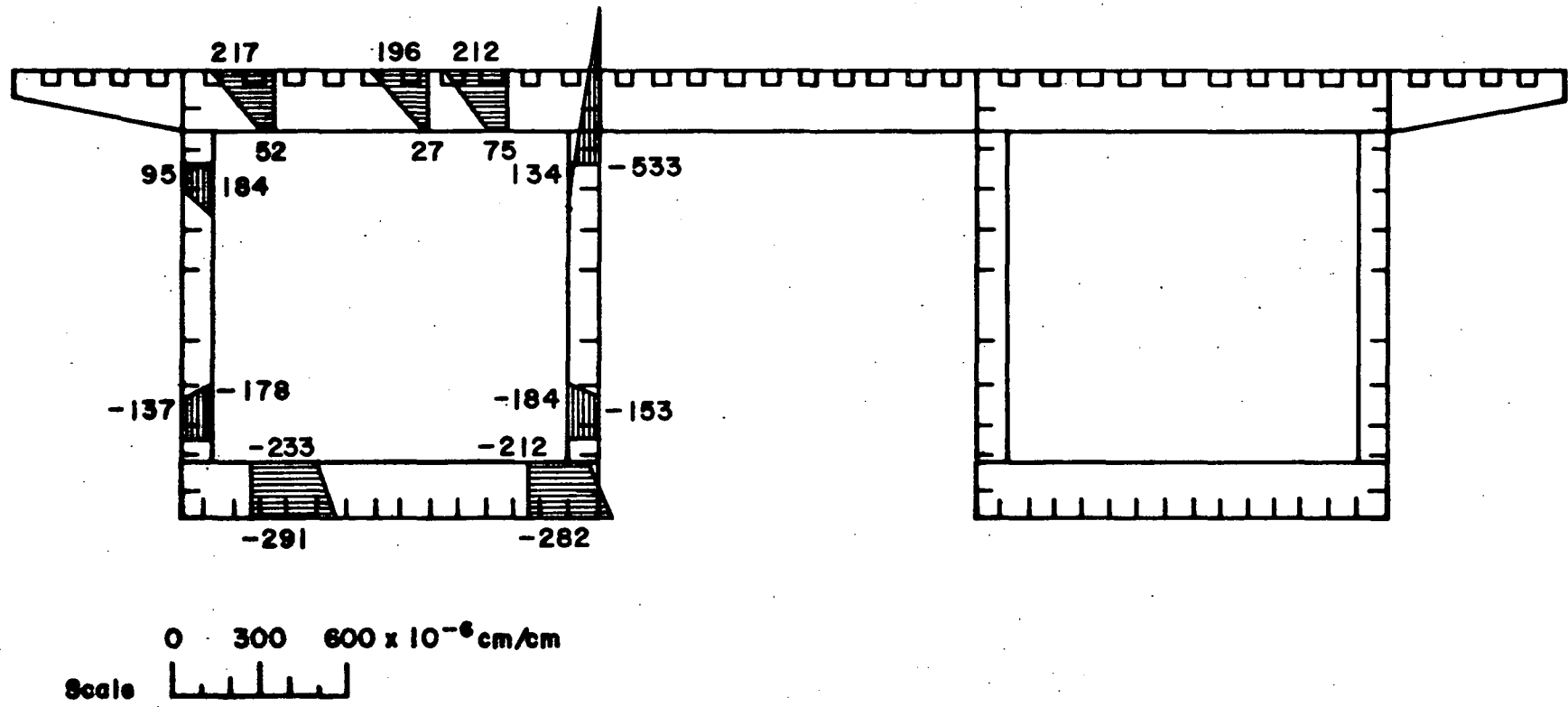


Fig. 5.4 Transverse Strains at FB42 due to Transfer of North Box from Pontoon to Pier Rings

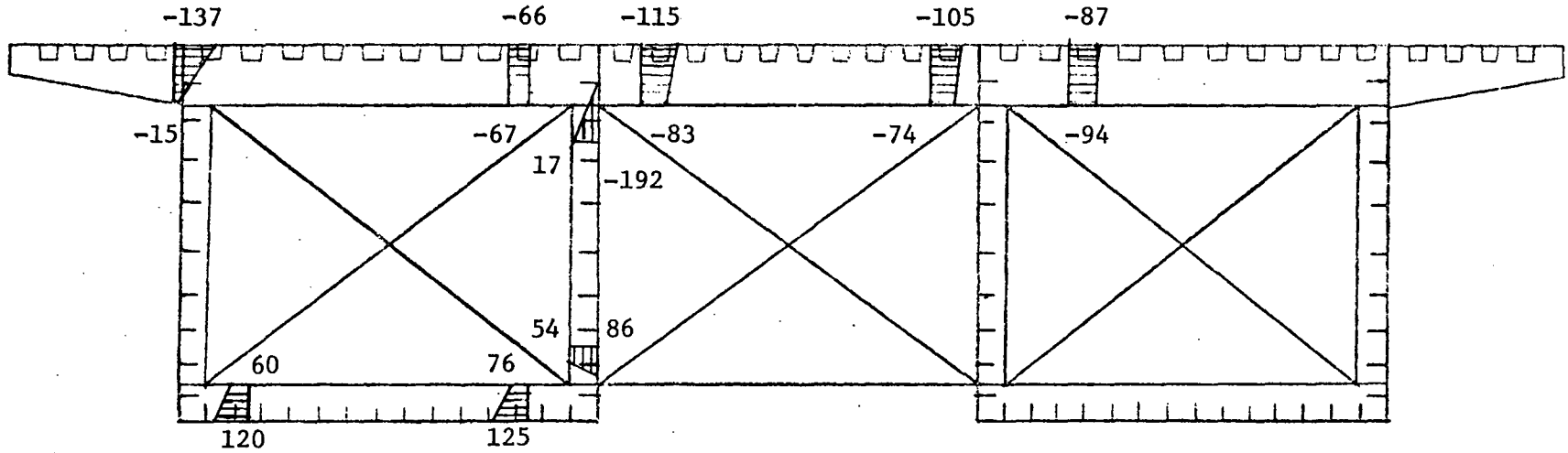
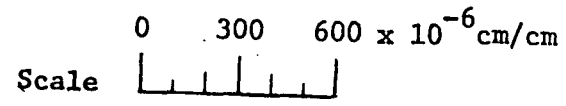


Fig. 5.5 Transverse Strains at FB27 in Double-Box Section due to Center Span Lift



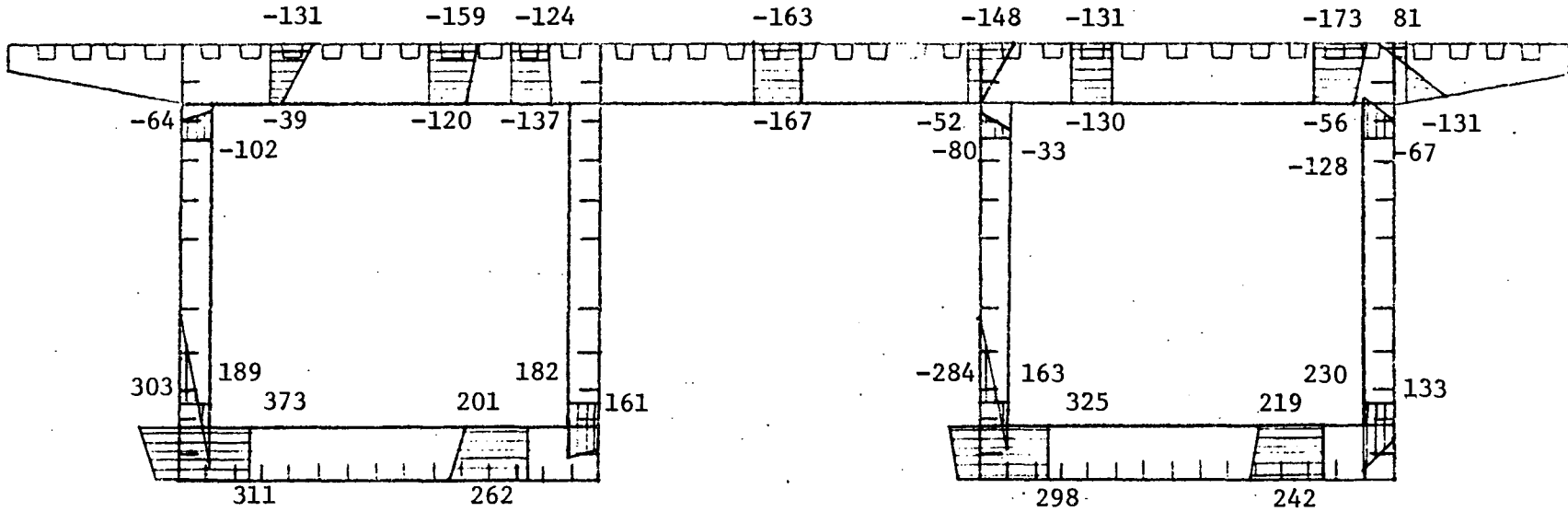
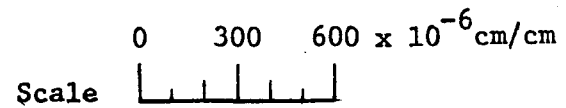


Fig. 5.6 Transverse Strains at FB42 in Double-Box Section due to Center Span Lift



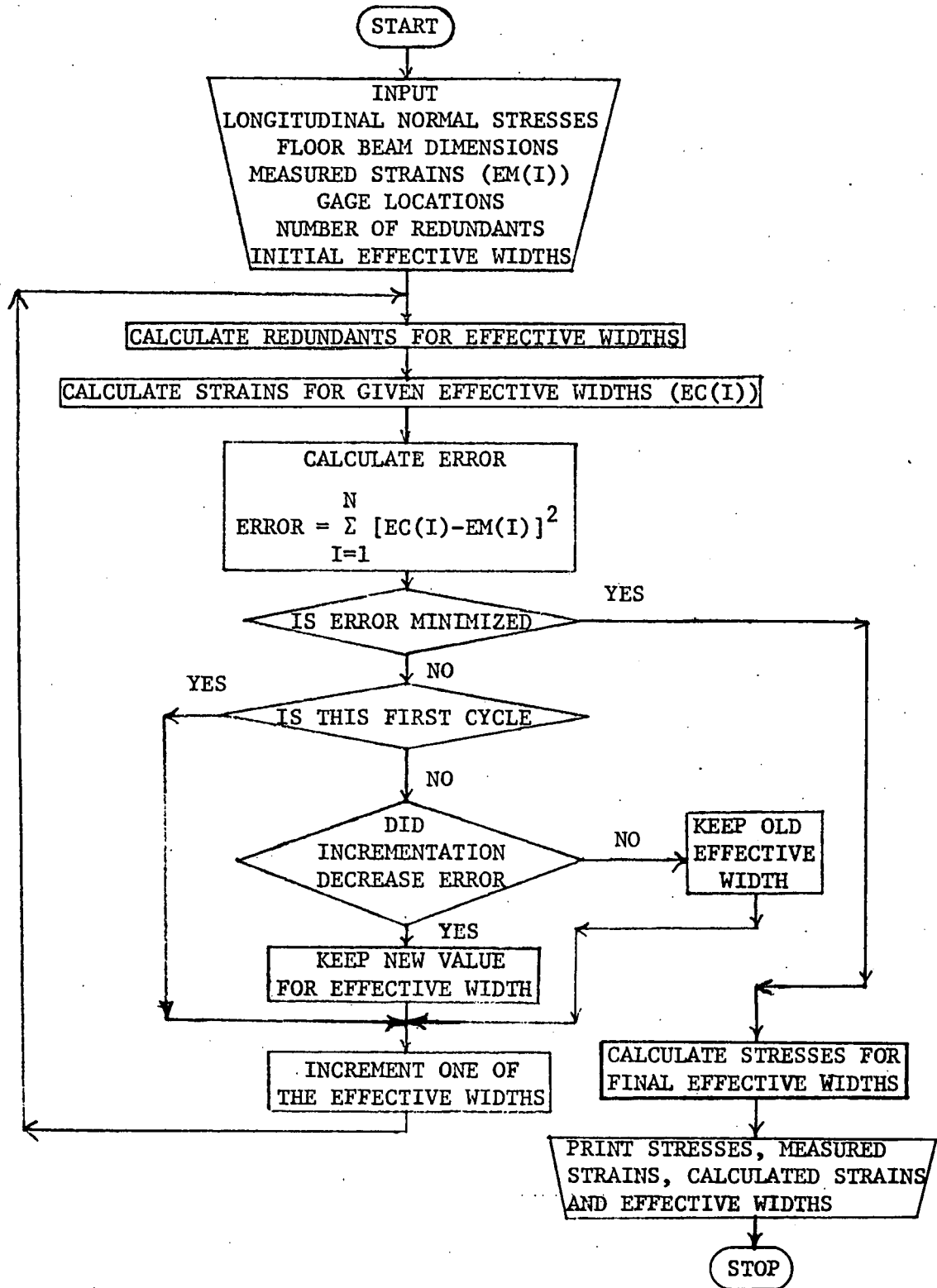


Fig. 5.7 Flow Chart of Computer Program for the Determination of Effective Widths

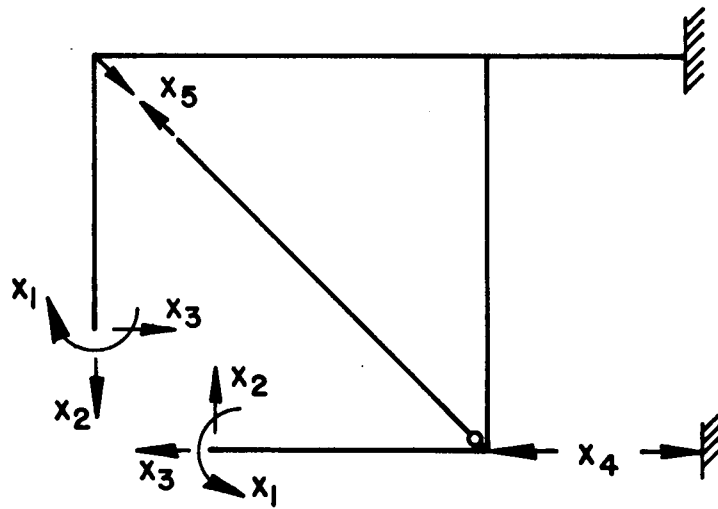
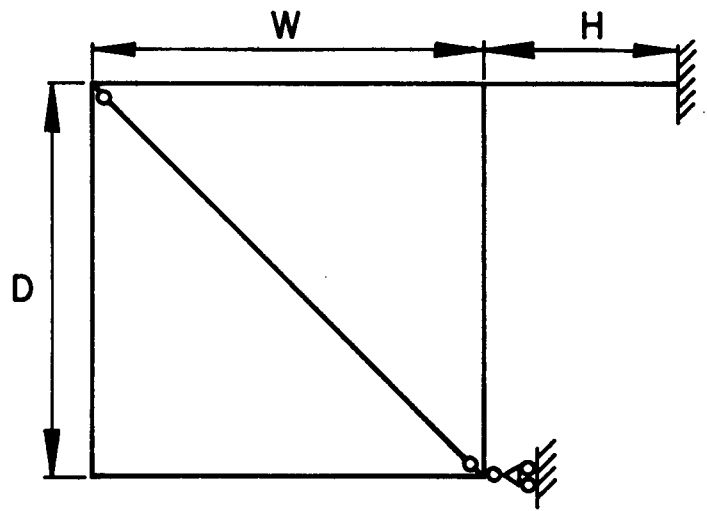


Fig. 5.8 Model of Typical Transverse Frame for Analysis

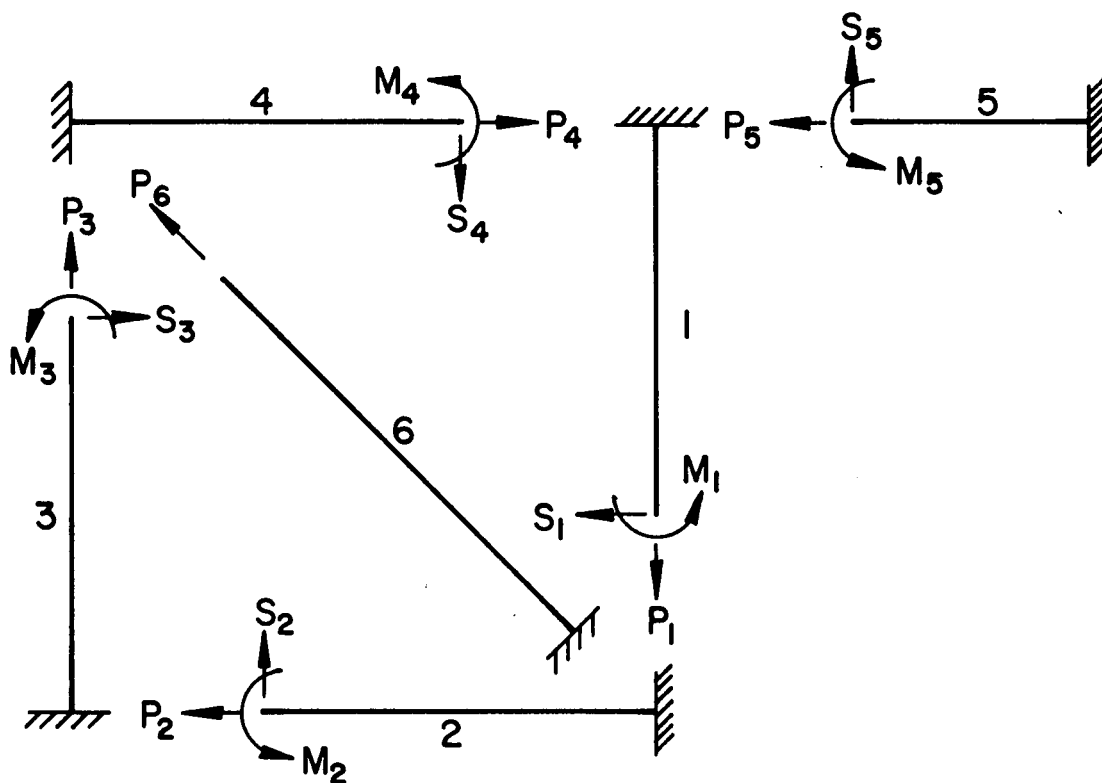
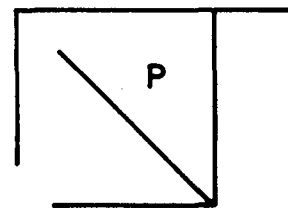
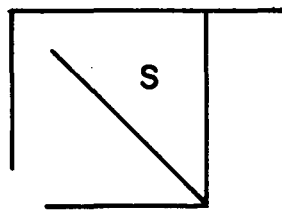
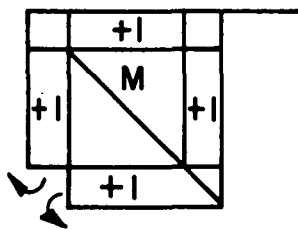
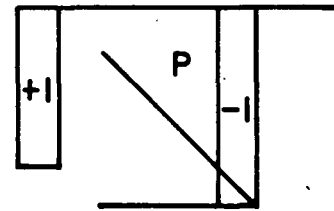
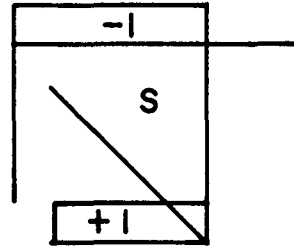
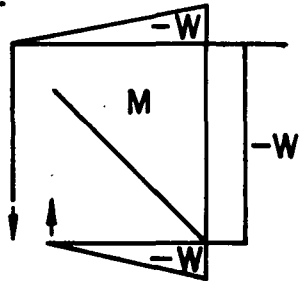


Fig. 5.9 Cantilever Idealization of Structure for Force Method

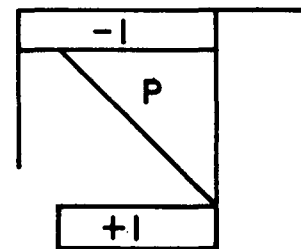
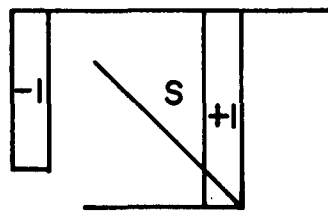
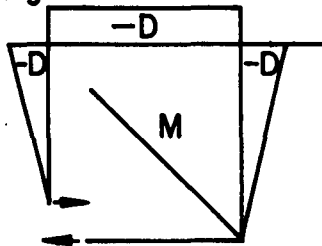
$X_1 = 1$



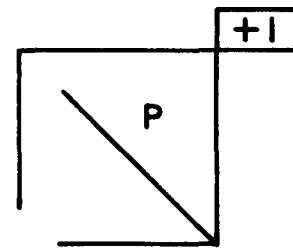
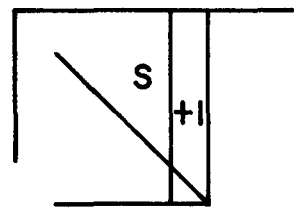
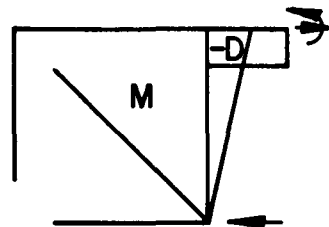
$X_2 = 1$



$X_3 = 1$



$X_4 = 1$



$X_5 = 1$

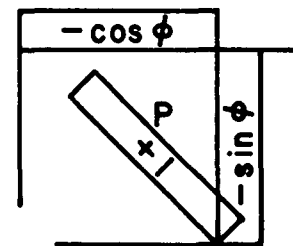
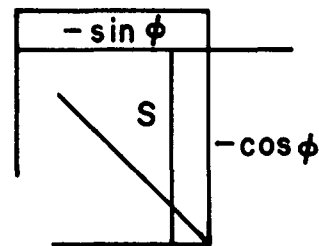
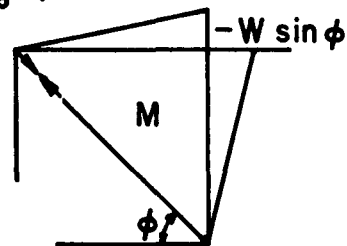


Fig. 5.10 Moment (M), Shear (S), and Thrust (P) Diagrams for Unit Redundants

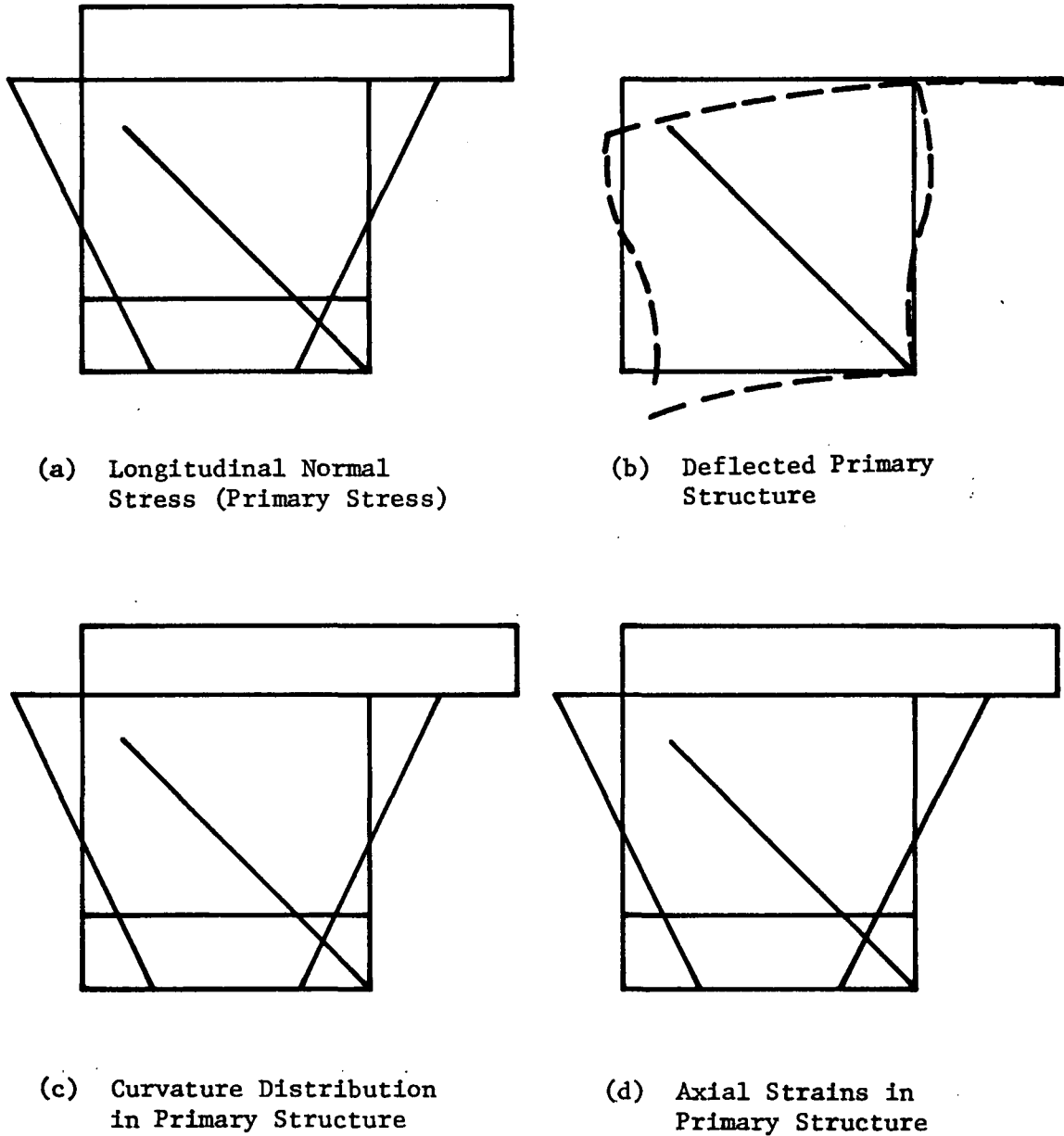
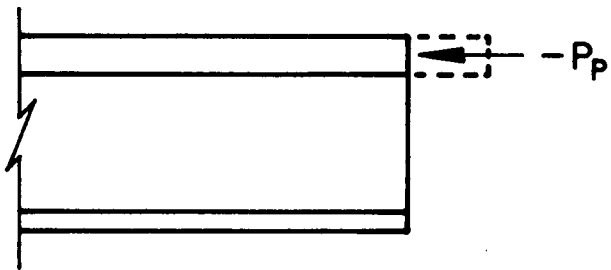
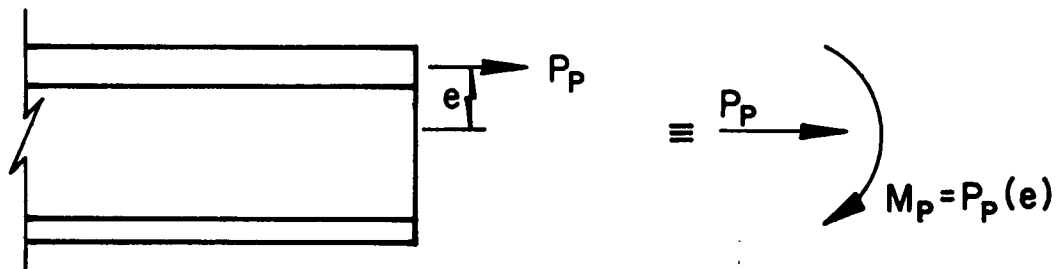


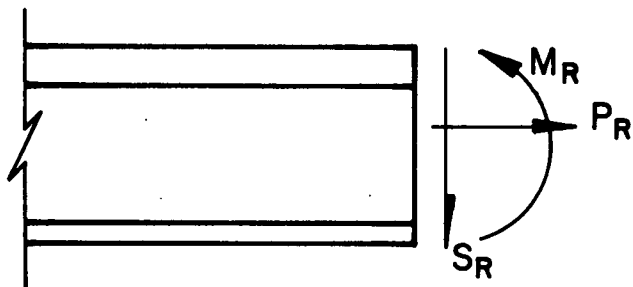
Fig. 5.11 Secondary Stress Effects



Force to Restrained Flange Plate

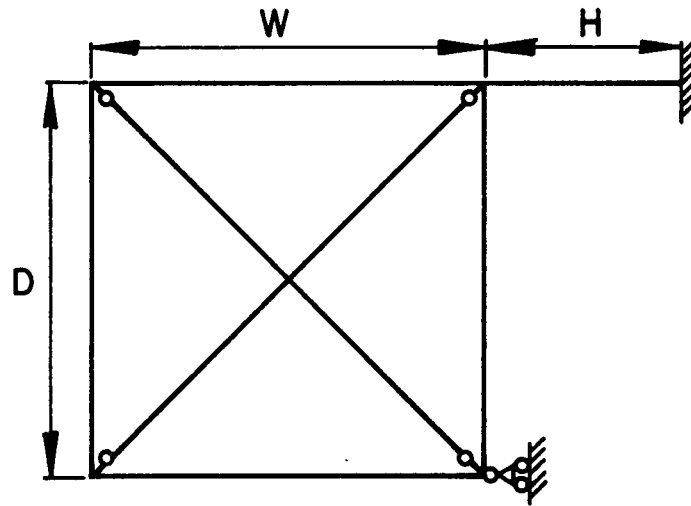


Force on Unrestrained Member

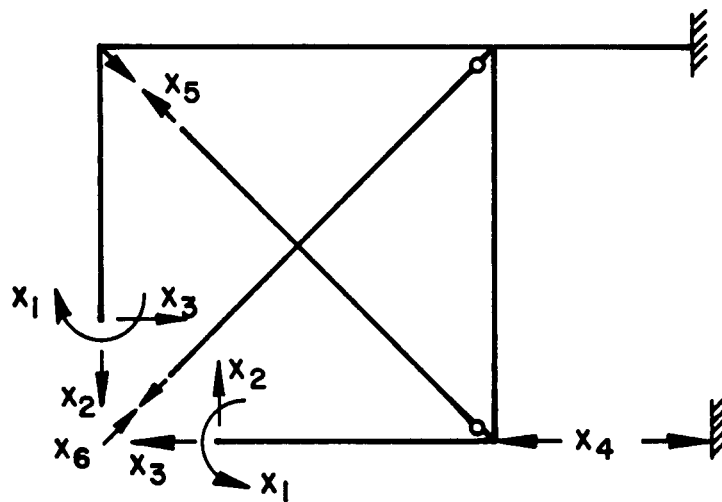


Forces Caused by Redundants

Fig. 5.12 Forces Acting on a Cross Section



a) Idealization of Actual Structure



b) Primary Structure

Fig. 5.13 Revised Model of Typical Transverse Frame for Analysis

6. STRESS HISTORY - ORTHOTROPIC DECK
STRESSES UNDER TRAFFIC

(J. H. Daniels, B. T. Yen and J. W. Fisher)

6.1 Introduction

As part of the investigation into the service life behavior of the steel orthotropic deck of the Rio-Niteroi Bridge, it was necessary to determine the local stresses generated in the deck under vehicular traffic with particular attention to various welded details in the steel deck and its stiffening elements.

Studies in England on experimental orthotropic bridge deck panels have demonstrated the possibility of fatigue cracks being generated in the stiffener-to-floorbeam welds.(6.1) Tests were therefore carried out on the Rio-Niteroi Bridge in February and again in May and June of 1974, to ascertain the stress magnitudes under controlled test truck loads and the stress history under a random traffic sample so that the fatigue susceptibility of various welded details can be assessed. Studies in the U.S. during the past 15 years have demonstrated the applicability of stress measurements obtained in the field when assessing the serviceability of highway bridge structures.(6.2)(6.3)(6.4)(6.5) Furthermore, such field tests have been very useful in the development of criteria and specifications for fatigue design.(6.6)

Since the loading spectrum for highway bridges in Brazil is not well defined, the tests of the Rio-Niteroi bridge deck can also serve as a calibration to assist in defining the loading spectra.(6.7)

Controlled load tests were initially made in February 1974 at locations near floorbeams 17 and 42, in order to establish the more probable regions of higher stress range in the steel deck and its stiffening elements. More extensive tests were then made in May and June 1974 near floorbeam 17, consisting of controlled load tests and stress history tests under random traffic. The severity of the various welded details at these locations was estimated from existing data and detail classifications.(6.8)

Special tests were also made near floorbeam 42 in February 1974 to evaluate the probable influence of pot holes or other surface irregularities in the deck pavement which can greatly amplify the dynamic stress due to inertia forces. This was accomplished by running a truck of known weight over plank runways placed longitudinally on the deck. The runways had transverse cleats nailed to the planks at intervals. The cleats were therefore used to simulate a surface roughness condition. The difference in strain response from passes over the runways, and on the smooth deck adjacent to the runways, provides a qualitative evaluation of the effect of surface roughness on strains in the orthotropic deck.

6.2 Field Testing

6.2.1 Controlled Load Tests - Feb. 26, 1974

A description of the static load tests of the box girders in the vicinity of Piers 99 and 100 is given in Article 3.3. In those tests, a group of 21 loaded three axle gravel trucks was placed in four different positions on the deck and strain data from all deck gages recorded (Figs. 2.11 - 2.14). In two of the positions one of the trucks was placed directly above the groups of deck gages near floorbeam 17 and 42.

Figure 6.1 shows the location of the test truck in the vicinity of the gages near floorbeams 17 and 42. The truck directly over the deck gages at each of the two locations is shown shaded in the figure. Figure 6.2 shows a cross section of the deck and the positions of the rear wheels relative to the trapezoidal stiffening elements at both locations. The wheel and axle spacings of the trucks are given in Art. 3.3 together with the axle and truck weights.

The asphalt surface on the north box was placed just a few days prior to the static load tests. Consequently, to prevent damage to the surface from the wheel loads, the trucks were parked on plank runways. The runways consisted of pairs of planks approximately 6.5 to 7.5 cm thick and 30 to 35 cm wide running continuously in the longitudinal direction of the bridge for the total length of the loaded area. The planks were spaced apart as shown in Fig. 6.2 and connected by 2 x 5 cm cleats nailed to the planks. The cleats were spaced about 2 to 3 meters apart on the average.

Following the static load tests described in Art. 3.3, truck No. 14 was used to provide dynamic strain data from six gages at each of the floorbeam 17 and 42 locations. At each location the truck was run back and forth several times on the runways as well as on the smooth deck between the runways. Figure 6.3 shows the truck positions during the several runs at each location. Since the speedometer on the truck did not work the truck speed was estimated to be as follows: about 8 to 11 kilometers per hour when travelling on the runways and about 24 to 32 kilometers per hour when travelling on the smooth deck between the runways. The truck speed when travelling on the runways was necessarily reduced because of the cleats connecting the planks. The cleats provided a fairly rough travelling surface resulting in significant bouncing of the truck wheels and movements of the runways. After each pass, the runways had to be re-aligned before the next pass could be made.

6.2.2 Controlled Load Tests - June 3 and 5, 1974

Based on the results of the controlled load tests described in Art. 6.2.1 a decision was made to confine the June controlled load tests to the location near floorbeam 17.

The controlled load tests at floorbeam 17 were made using a Euclid truck of known axle and total weight. The Euclid truck is shown in Fig. 6.4. The dimensions, axle weights and total weight of the truck are shown in Fig. 6.5.

The Euclid truck made 13 "crawl run" passes on the deck over the deck gage locations at floorbeam 17. The 13 positions are shown in Fig. 6.6. In each case the crawl run position, shown circled in the figure, identifies the nearly exact location of the centerline of the front right wheel of the Euclid truck. Each crawl run was made in the direction of normal traffic (towards Rio de Janeiro). The truck speed during each crawl run was approximately 2 to 3 kilometers per hour to simulate static load conditions. In each case the crawl run began about 15 to 20 meters east (towards Niteroi) of floorbeam 17 and finished about 15 to 20 meters west (towards Rio de Janeiro) of the centerline of floorbeam 17. During the crawl run tests, the traffic to Rio de Janeiro was detoured to the eastbound lanes to remove its influence on the crawl run results.

The Euclid truck also made 7 "speed run" passes on the deck over the deck gage locations at floorbeam 17. The 7 positions are shown in Fig. 6.7. In each case the speed run position, shown circled in the figure, identifies the approximate location of the centerline of the front right wheel of the Euclid truck. The speed runs were also made in the direction of normal traffic (towards Rio de Janeiro). The truck speed was approximately 55 to 60 kilometers per hour. Traffic over the test section near floorbeam 17 was not eliminated during the speed runs. The Euclid test truck paced itself so that it passed over the test section when no other truck type vehicles were in the vicinity. However, there usually was some light automobile traffic at the same time. Strain data under light traffic alone previously indicated that it would have no significant affect on the test truck results.

6.2.3 Random Traffic: May 30 - June 5, 1974

A total of 642 truck records were obtained during this interval of time as shown in Table 2.7. During the sample periods all truck and bus type vehicles and other heavy vehicles travelling towards Rio de Janeiro which fell within DNER classes 2 to 8 inclusive (see Table 2.5) were counted, the class recorded, and corresponding strain data at FB 17 recorded on the oscillograph equipment. No attempt was made to record or count other light vehicle traffic.

Each of the 120 vehicles recorded on May 30, 1974 was also photographed as it was about to cross the instrumented portion of the orthotropic deck near floorbeam 17 (see Fig. 2.16). The purpose of the photographs was basically two-fold: (1) to have a photographic record of a sample of the types of vehicles included within the total record and (2) for use in the analysis as part of the technique used to weigh the axles of each of these 120 trucks. This technique is described in Art. 6.5.3.

6.3 Results of Controlled Load Tests

6.3.1 Controlled Load Tests - Feb. 26, 1974

Figure 6.8 shows the strain variation with time for the six strain gages near floorbeam 17 as recorded by the oscillograph equipment for speed runs 1, 2 and 3 shown in Fig. 6.3(a) and described in Art. 6.2.1. Run 1 was made on the runway, while runs 2 and 3 were on the smooth deck between runways.

The maximum recorded stress ranges at the six gage locations for all six speed runs are shown in Table 6.1. Recorded strain values from the analog traces were converted to stresses assuming an elastic modulus of 2,109,200 Kg/cm².

Table 6.1 also shows the static stresses at all gage locations near floorbeam 17 which were obtained during the static load tests described in Art. 3.3.

Figure 6.9 shows the strain variation with time for the six strain gages near floorbeam 42 as recorded by the oscillograph equipment for speed runs 1, 2 and 4 shown in Fig. 6.3(b) and described in Art. 6.2.1. Run 1 was made on the runway while runs 2 and 4 were on the smooth deck between runways. The maximum recorded stress ranges at the six gage locations for all five speed runs are shown in Table 6.2. Table 6.2 also shows the static stresses at all gage locations near floorbeam 42 which were obtained during the static load tests described in Art. 3.3.

6.3.2 Significance of Results - Feb. 26, 1974

A comparison of the stress ranges shown in Table 6.1 indicates that the stress ranges for all passes of the truck over the runways were smaller than those corresponding to passes made on the smooth deck. There are three reasons for this difference: (1) the locations of the wheels with respect to the gage are different for passes on and off the runways; (2) the truck speed on the runway was substantially slower than that on the smooth deck as discussed in Art. 6.2.1; and (3) the wheel loads were distributed to the deck over a larger area when the truck was travelling on the runways.

In effect, when the truck was travelling on the runways, it was subjecting the deck to considerable impact loading as the wheels passed over the lateral cleats (Art. 6.2.1). The same kind of impact loading could be expected from a truck running on the deck if the deck were rough such as might result from potholes which were left to develop in the deck. In this case, the stress ranges probably would be at least equal to or greater than the maximum values shown in Table 6.1.

6.3.3 Controlled Load Tests - June 3 and 5, 1974

Figure 6.10 shows the typical strain variation with time for 9 strain gages near floorbeam 17 as recorded by the analog trace. The traces correspond to the crawl run of the Euclid test truck in position 11 shown in Fig. 6.6.

Figure 6.11 shows a similar strain variation with time for the same 9 strain gages near floorbeam 17 corresponding to the speed run of the Euclid test truck in position 5 shown in Fig. 6.7.

Tables 6.3 and 6.4 show the stress ranges obtained at the gage locations near floorbeam 17 corresponding to the crawl and speed runs of the Euclid truck for all positions shown in Figs. 6.6 and 6.7.

Figures 6.12 through 6.18 show the variation in stress ranges at 16 gage locations near floorbeam 17 for both front and rear axles corresponding to the 13 crawl run positions of the Euclid truck shown in Fig. 6.6. Figures 6.16 through 6.18 also show the variation in stress ranges at 7 gage locations for both front and rear axles corresponding to the 7 speed run positions of the Euclid truck shown in Fig. 6.7.

The results shown in Figs. 6.12 through 6.18 show two basic characteristics which are useful in the later analysis of the fatigue strength of welded details in the orthotropic deck, as follows:

(1) stress range at most details are primarily wheel (or wheel group) dependent rather than axle (or axle group) dependent (the exceptions being details near gages 5, 27 and 33) and (2) stress range is nearly independent of truck speed. This is primarily because of the smooth deck condition. Deck roughness can be expected to produce higher stress range with truck speed.

6.4 Results of Random Traffic Studies - May - June 1974

6.4.1 Stress Range Histograms

Figures 6.19 through 6.23 show typical stress range histograms at five gage locations near floorbeam 17 corresponding to passage of the 642 vehicles recorded in Table 2.7. The gage locations are identified in Table 2.4 and in Figs. 2.11 and 2.12. Table 6.5 summarizes the results obtained at other gages.

A stress range histogram depicts the percentage of occurrence between several stress range intervals. Stress range is the difference between a maximum stress and the following minimum stress as determined from the analog strain trace. It was observed that gages where high maximum stresses were observed were also subjected to high stress ranges.

6.4.2 Vehicle Position Histogram

Figure 6.24 shows the lateral vehicle position histogram for vehicles passing over floorbeam 17. The histogram was constructed by

observing the position of a vehicle in relation to the deck markings at floorbeam 17 (Fig. 2.17) as determined from the photographs of each of the 120 vehicles taken on May 30 and discussed in Art. 2.4.3.

A vehicle position histogram depicts the percentage of occurrence between several lateral location intervals at floorbeam 17.

6.5 Traffic Analysis

Since traffic loading from the vehicles crossing the Rio-Niteroi Bridge plays a major role in assessing the fatigue resistance, it is necessary to evaluate the frequency and weight distribution of traffic from the available records and field measurements. In this manner an approximate load spectrum can be developed for the orthotropic deck.

6.5.1 Traffic During Strain Recording Periods (May - June 1974)

During the in-service testing of the orthotropic deck in May and June of 1974, traffic counts and strain readings were taken simultaneously over selected time periods as discussed in Art. 2.4.4 and shown in Table 2.7. This record indicated that the distribution of vehicle categories is as shown in Fig. 6.25. The highest volume consisted of two axle trucks and buses. The frequency of occurrence of the various types of vehicles crossing the structure indicated that heavy wheel loads associated with 4, 5 and 6 axle trucks would be relatively infrequent.

6.5.2 Traffic During 1974-75

Since vehicles crossing the structure are charged tolls, daily records are available from DNER which describe the frequency of

the various categories of vehicles crossing the bridge. Results of the 15-month interval between March 4, 1974 and May 31, 1975 discussed in Art. 2.4.5 are summarized in Figs. 6.26 and 6.27. A comparison of the traffic during the strain recording period in May and June 1974 and that during the fifteen month interval (Fig. 6.25 and Figs. 6.26 and 6.27) show comparable distributions of south bound traffic from Niteroi to Rio de Janeiro. The northbound traffic distribution was also comparable as Fig. 6.26 and Fig. 6.27 demonstrate.

Hence it is reasonable to assume that the traffic composition sampled during the test intervals in May and June 1974 is typical for the entire structure during the fifteen month period up to May 31, 1975.

No loadmeter surveys are available for vehicle traffic in Brazil. Thus, it is not possible to determine directly the frequency of occurrence of vehicles by axle or gross weight.

6.5.3 Estimated Axle and Vehicle Weights

Wheel or axle loads of vehicles crossing the structure are not directly available for the traffic using the structure. Hence it is necessary to approximate this data from the field studies.

As discussed in Art. 2.4.3, 120 vehicles were photographed as they passed over a reference line at floorbeam 17 and simultaneous strain records were acquired. Since static and dynamic "influence lines" for selected gages were acquired through the positioning of the test vehicle as described in Art. 6.3.3 and shown in Figs. 6.12 to 6.18,

an estimate of the axle loads of the 120 trucks crossing the structure was made by assuming that the strain response from a vehicle is directly proportional to load. The position of the wheels of the 120 trucks passing over floorbeam 17 were determined from the photographs.

The results of this method of estimating axle group and vehicle weights are given in Figs. 6.28(a) and 6.28(b). Since it was observed that closely spaced axles caused a single response of stress at a point, axle group loads instead of individual axle weights are presented. The number of axle groups varied from one to three.

Figure 6.28(a) shows the estimated axle load distribution which has a skewed characteristic. This indicates that large numbers of relatively small axle loads can be expected. The larger axle loads decrease in frequency with increasing weight. Since the orthotropic deck is primarily responsive to axle loads (wheel loads), each vehicle crossing the orthotropic deck generates 2 or more stress cycles.

The frequency of occurrence of gross vehicle weight is given in Fig. 6.28(b). There are a larger number of buses and two axle trucks at 10 to 15 tons. The relative distribution of gross vehicle weight from the 1970 United States Federal Highway Administration Nationwide survey is given in Fig. 6.29 for comparison.(6.6) This figure, when compared with Fig. 6.28(b) shows that Brazilian traffic is not as frequent at the present time at the higher load levels. The small peak at 30 to 40 tons in Fig. 6.28(b) however, suggests that the load spectrum in the future probably will be comparable to those of the United States.

Experience with several bridges in the United States has shown that the average daily truck traffic can be expected to increase at an average annual rate of about 1.5% when the highways serving the bridge structure are not expressways. After all main arteries leading to the bridge are completed and opened to traffic, a substantial increase in average daily truck traffic can be expected.(6.7)

Since the approach arteries leading to the Rio-Niteroi Bridge are still being planned or under construction, it is assumed in this analysis that the average daily truck traffic (ADTT) will increase at an average rate of 1.5% during the next 10 year period as work on the transportation system within Rio de Janeiro and its surrounding environs continues. After approximately 10 years, the average rate of increase in truck traffic will in all probability increase at a higher rate. Figure 6.30 shows a plot of the estimated average daily truck traffic commencing with the observed volume in 1974 and projected into the future. A rate of 3.0% is used after 1984.

6.6 Analysis of Orthotropic Deck Welded Details for Fatigue Susceptibility

The field stress measurements during May and June 1974 provided a stress history over a random sample period for the selected gage locations. These stress history measurements are used to evaluate the fatigue behavior of several details in the welded orthotropic deck. The frequency of truck and bus traffic up to the year 2014 as shown in Fig. 6.30 was estimated so that the cumulative stress cycles can be determined.

To evaluate the adequacy of the measured stress range histograms, the lateral placement (position) of the random sample of trucks (Fig. 6.24) was combined with the "influence line" (Fig. 6.15) to estimate the probability density function $h(s)$ for unit stresses in the trapezoidal stiffening rib at gage 33. The function $h(s)$ and the axle weight probability density function $g(w)$ as shown in Fig. 6.28(a) were used to construct the probability density function for stress range, $p(s)$, by employing the formula

$$p(s) = \sum_w g(w) h(s) \frac{1}{W} \Delta W \quad (6.1)$$

The results of this estimation are compared with the measured stress range probability density in Fig. 6.31(a). The results are in reasonable conformity and suggest that the measured stress spectra are a reasonable estimate of the stresses generated by the truck and bus traffic on the bridge structure.

An examination of the orthotropic deck indicated that there were three major details that should be examined, as follows: (1) the end of the splice plate welded onto the trapezoidal stiffening ribs, such as that near floorbeam 17; (2) the partial-penetration rib-to-deck weld between the orthotropic plate and the trapezoidal stiffening ribs; and (3) the weld connecting the trapezoidal stiffening ribs to the floor beams.

6.6.1 Splices of the Trapezoidal Stiffening Ribs

The end of the splice plate represents a Category E condition according to the 1974 AASHTO fatigue provisions and is based on laboratory studies of welded attachments.(6.8) Figure 6.31(b) shows the splice details near floorbeams 17 and 42. The weld toe termination of the splice plate on the bottom of the trapezoidal stiffening rib constitutes an attachment plate over 30 cm long which places it into Category E.

The stress range spectrum for gage 33 near floorbeam 17 is shown in Fig. 6.31(a). Observations at the test site indicated that stress ranges less than 35 kg/cm^2 were generally caused by light trucks and some buses. These were ignored in evaluating the fatigue resistance of the detail.

Two methods were used to evaluate the cumulative damage due to the random application of stress range and its frequency of occurrence.

One procedure used was the root-mean-square method.(6.9)(6.10) In this method the root-mean-square of the stress ranges in a spectrum provides an equivalent constant cyclic stress range and can be correlated

directly with the number of stress cycles corresponding to the spectrum. The root-mean-square stress range is defined as

$$S_{rRMS} = (\sum \alpha_i S_{ri}^2)^{\frac{1}{2}} \quad (6.2)$$

where α_i is the frequency of occurrence of stress range S_{ri} .

A root-mean-square stress range of 222 kg/cm^2 results from the measured stress range spectrum shown in Fig. 6.31(a). This S_{rRMS} value is plotted in Fig. 6.32 and compared with the constant cycle stress range data from laboratory studies. (6.9) Recent studies on randomly applied loads have demonstrated that when some stress cycles exceed the fatigue limit (approximated by the horizontal line at 350 kg/cm^2 in Fig. 6.32) the fatigue strength relationship (S-N curve) continues to decrease. (6.10) Figure 6.32 indicates that the lower bound (99% survival) fatigue strength will be reached in about 40,000,000 cycles. If, on average, each truck is assumed to produce only one stress cycle, the fatigue strength will be reached in about 70 years if the current average daily truck traffic (ADTT) is maintained.

There are two conditions that suggest that this may be reached at an earlier date. First, it is probable that the frequency of occurrence (ADTT) will increase with passage of time. In addition, it is also probable that the frequency of occurrence of the heavier load vehicles will increase in the future. This latter tendency will cause an increase in the S_{rRMS} over the life of the structure. If the frequency of truck traffic increases an annual rate of 1.5%, the lower bound fatigue strength

will be approached in about 50 years; if the rate of increase is 3.0% after 1984, it will be in about 40 years. Higher rates of growth will obviously decrease the amount of time required to reach the lower bound fatigue strength.

The stress range histogram was also evaluated using Miners Hypothesis for cumulative damage.(6.11) By combining the relationships provided by constant cycle data and Miners rule, an equivalent stress range S_{rMINER} can be estimated as(6.10)

$$S_{rMINER} = (\sum \alpha_i S_{ri}^3)^{1/3} \quad (6.3)$$

This resulted in an equivalent stress range of 268 kg/cm^2 , corresponding to about 20,000,000 cycles of constant cycle stress range by the fatigue strength line of Fig. 6.32. This number of cycles will be reached in about 30 years based on the present frequency of truck traffic and an annual increase rate of 1.5%.

It is apparent that both the root-mean-square stress range and the Miners equivalent stress range suggest that fatigue cracks could develop in about 30-40 years at this splice (Gage 33) of trapezoidal stiffening rib near floorbeam 17.

Stress measurements made at a few other locations near floorbeam 17 and 42 indicated that the level of stress ranges at the ends of the splice plates at floorbeam 42 were slightly lower than that at Gage 33, but still exceeded the constant cycle fatigue limit. Consequently, it is also probable that fatigue cracks may develop at these locations,

depending on the frequency of stress range occurrence. However, a much longer life is expected.

6.6.2 Connection of Trapezoidal Stiffening Ribs to the Floor Beam

The trapezoidal stiffening ribs pass through the floor beams at cutouts in the floorbeam web. A coped area exists at the bottom face of the trapezoidal shape as shown schematically in Fig. 6.33(a). The floorbeam web is connected to the sloping sides of the trapezoidal shapes by fillet welds. These welded connections are directly analogous to a transverse stiffener attached to the web of a girder. It constitutes a non-load carrying connection and is classified as a Category C detail by the current AASHTO fatigue specification.

Experience on an experimental orthotropic bridge deck panel which had the trapezoidal stiffening ribs framing into the floor beams without a cope hole(6.1) had demonstrated that fatigue cracking could occur in the load carrying welds which connected the sloping webs and bottom flange of the trapezoidal ribs to the floorbeam web. Further studies on laboratory specimens were reported by Nunn(6.12) and confirmed that a load carrying rib-to-floorbeam connection needed to be assessed for fatigue in the weld. These types of joints do not exist in the Rio-Niteroi bridge. The welded connection has a cope hole and is a higher fatigue strength joint.

The results of stress range measurements obtained at gage 5 near floorbeam 17 are plotted in Fig. 6.33(b). This shows that the highest stress range in the bottom flange of the trapezoidal stiffening

rib near floorbeam 17 was about 602 kg/cm^2 . The root-mean-square stress range of the stress spectrum is 172 kg/cm^2 ; the Miners equivalent stress range is 213 kg/cm^2 .

The lower bound fatigue strength relationship for design of Category C details is plotted in Fig. 6.34. The highest recorded stress range and both the S_{rRMS} and S_{rMINER} for the bottom flange of the stiffening rib fall below the fatigue limit of 844 kg/cm^2 . Since the most critical point for fatigue is the weld toe termination which is on the sides of the trapezoidal shape 25mm above the bottom flange surface, the corresponding stress ranges at this most critical point are much less than the fatigue limit. Hence, even with substantial increases in magnitude of axle load and in truck traffic frequency, no fatigue damage is expected in this connection.

Since ranges at other trapezoidal stiffening ribs across the box girder should provide comparable stress histograms as for gage 5 because about the same bending stress is developed in the stiffening ribs under wheel loads. Those stiffening ribs located nearer the box girder webs will have even lower stress range since the relative deflections near the deck plate to box girder web junction will be less.

6.6.3 Connection of Stiffening Rib to Orthotropic Plate

The trapezoidal stiffening ribs used for preventing buckling of the thin deck plate and for distributing wheel loads provide good load distribution, high torsional rigidity and efficient longitudinal flexural behavior and generally less welding between the stiffening rib and deck. Their use does have disadvantages since the fabrication and

field splicing are more difficult, changes in rib cross section are more difficult to accommodate and the fatigue behavior may be more severe due to the transverse stresses under wheel loads.

Experience in England on the experimental orthotropic bridge deck panels showed that high compressive cyclic stresses transverse to the trapezoidal stiffener were occurring in the deck near the welds.(6.1) Concern with this connection led to an experimental program reported by Maddox.(6.13) Studies were also carried out in the USA because of differing opinions on the requirements for the deck-to-stiffener connection. The resistance of full and partial penetration welds was examined.(6.14)

The results of these studies are summarized in Fig. 6.35. The test data shown as crosses were reported by Maddox(6.13) and included the results of several studies. The bending stress range in the weld at its root are plotted as a function of life. As can be seen from the comparison of the test data with recent AASHTO design curves, Category C provides a reasonable lower bound to the test data. Maddox has noted that those results which provide higher fatigue strength generally result from compressive stressing at the weld root or the absence of tensile residual stresses. This is particularly noticeable with the reversal specimens reported in Ref. 6.14. It is apparent that the full stress range was not effective in these specimens. In actual bridge decks with the restraint of deck component parts, the residual tensile stresses should be high and the lower bound fatigue strength appears to model realistically what can be expected.

The trapezoidal stiffening ribs used in the orthotropic plate deck of the Rio-Niteroi bridge utilized partial penetration welds to connect the sloping sides to the deck plate. Figures 6.36(a) and 6.36(b) show etched cross-sections of the stiffening rib-deck plate weld with partial penetration. The average ratio of weld throat thickness to the sloping web plate thickness was 0.83. Hence bending stresses in the weld throat would be about $(1/0.83)^2 = 1.45$ times greater than the stress in the web plate for the same plate-bending moment. In addition, stress gradient could be expected between the weld and the bottom flange of the trapezoidal stiffener. The recorded stresses at a gage on the sloping side wall and a short distance away from the weld must be adjusted to the weld for evaluation. Since only a single gage was attached to the web surface of the trapezoidal shape, the strain gradient could not be determined experimentally. By considering the gage location and the geometry of the trapezoidal stiffener and the deck plate, the stresses at the weld were estimate to be 15% higher than those recorded at the strain gage on the stiffener web surface. Hence stresses in the weld throat were taken equal to

$$\begin{aligned}\sigma_{\text{throat}} &= 1.15 \times 1.45 \sigma_{\text{stiffener}} \\ &= 1.67 \sigma_{\text{stiffener}}\end{aligned}$$

The stress range spectrum observed near floorbeam 17 indicated that the stresses in the stiffener web were very similar as illustrated in Figs. 6.19 to 6.23. The root-mean-square stress range was about 183 kg/cm^2 . The maximum observed stress range seldom exceeded 350 kg/cm^2 . The maximum measured stress range was 420 kg/cm^2 .

Hence the maximum stress range on the weld throat would be 705 kg/cm^2 . As can be seen in Fig. 6.35 this is below the fatigue limit, and no failures should occur at any of the stiffening rib-to-deck plate connections due to transverse stresses. Even if heavier vehicles in the future generate occasional stress ranges exceeding the fatigue limit of the connection, the low value of root-mean-square range suggests that no damage should accumulate throughout the life of the structure.

6.7 Conclusions and Recommendations

The studies of the stresses in the orthotropic steel deck of the Rio-Niteroi Bridge under test trucks of known weight and under random truck traffic have shown that the structure will provide satisfactory service throughout its life. However, one detail, the splice of the trapezoidal stiffening rib, was found to have the potential for fatigue crack growth.

Following are specific conclusions that were developed from this study:

- (1) The trapezoidal stiffening ribs were observed to provide good lateral and longitudinal distribution of the concentrated wheel loads.
- (2) The stress range spectrums observed at various welded connections exhibited the same basic characteristics of other highway bridge structures in the world. The stress range spectrums were all observed to be highly skewed.
- (3) Very little dynamic effect was observed at any location due to traffic on the smooth bridge deck. The strains

developed in the steel deck were essentially the same under static and moving traffic.

- (4) Irregularities in the bridge deck surface should be promptly repaired. Pilot tests showed that sudden discontinuities in the surface, such as pot holes or sharp bumps, caused very high local stress amplifications in the steel deck. The stress range was more than doubled by running a loaded truck across a 25mm plank.
- (5) The distribution of truck and bus traffic using the bridge resulted in a frequency distribution which appeared to have the same characteristics of truck traffic in the U.S. The frequency of heavier trucks did not appear to be as great at present. It is likely that this will increase as more support arteries leading to the bridge are completed.
- (6) Considering the lateral position of random traffic crossing the bridge, the frequency of loaded vehicles, and the fact that many axle loads are small, it appears that only one stress cycle needs to be considered per vehicle passage. The probability density function of the stress range for a given location is governed by the variability in lateral position and the magnitude of the wheel loads.
- (7) Splices in the trapezoidal stiffening rib are subjected to substantial numbers of stress cycles that exceed the fatigue limit. At the current rate of cyclic load and load frequency distribution it is probable that visible fatigue damage will occur in about 30-40 years. Since the frequency of heavier

loads is likely to increase such cumulative damage may well occur at an earlier date.

- (8) The measurements of transverse stresses in the trapezoidal stiffeners indicated that there was little likelihood of fatigue damage to the partial penetration stiffener-to-deck plate welded connection. Very few of the random stress cycles exceed the fatigue limit.
- (9) Measurements at the trapezoidal stiffener-floorbeam connections also indicated that there was little probability of cumulative damage from fatigue since a non-load carrying connection was provided.

As a result of these findings it is recommended that the following action be taken:

- (1) The splices in the trapezoidal stiffening ribs should be inspected at about 5 year intervals up to 1990. Thereafter, a yearly inspection should be made.
- (2) Steps should be taken to establish the frequency distribution of the axle loads crossing the bridge structure at regular intervals of at least 5 years.
- (3) The splice plates near floorbeam 17 should provide a good indicator of the behavior and performance of the orthotropic deck. Formation of a fatigue crack will not significantly alter the structures behavior. It can be readily repaired if and when it occurs.

- (4) A more extensive experimental study is suggested of the transverse bending stresses in the trapezoidal stiffening ribs. It is desirable to define the stress gradients in the rib so that the stress in the stiffener-deck plate weld can be better defined.

6.7 Chapter 6 - Tables and Figures

Table 6.1 Deck Gages Near Floorbeam 17

Gage	Static Stress (kg/cm ²)	Stress Range (kg/cm ²)					
		1	2	3	4	5	6
1							
2							
3							
4	7						
5	49						
6	323						
7	-633						
8	-134						
9	0						
10	-21						
11	218						
12	155						
13	148						
14	-77						
15	-155	-169	-408	352	534	211	548
16	-91		-91	183			232

Gage	Static Stress (kg/cm ²)	Stress Range (kg/cm ²)					
		1	2	3	4	5	6
17	-183		295	387	380		387
18	-42		204	225	422		373
19	-197						
20	-309						
21	-84						
22	-70						
23	120						
24	-91						
25	134	-675				-647	
26	-345	-569				-640	
27	-288						
28	-387						
29	63						
30	232						
31							
32	-155						

Table 6.2 Deck Gages Near Floorbeam 42

Gage	Static Stress (kg/cm ²)	Stress Range (kg/cm ²)				
		1	2	3	4	5
34						
35						
36						
37	-63	281		394		
38	-323		190			
39	91					
40	84					
41	63					
42	98	295		366		4.2
43	49	134		345		
44	162					
45	204					
46	-98					
47	84					
48	14					
49						
50						

Gage	Static Stress (kg/cm ²)	Stress Range (kg/cm ²)				
		1	2	3	4	5
51						
52						
53	-267					
54	-176					
55	0					
56	63	323	211	373	183	232
57	7	-323	-225	-218	-204	-345
58						
59	-309					
60	-70					
61	288					
62						
63	-42					
64	80					
65	63					
66	35					
67	21					

Table 6.3 Test Truck - Maximum Static Stress Range (kg/cm²)

GAGE AXLE RUN	5		7		8		9		10		15		16		17	
	F	R	F	R	F	R	F	R	F	R	F	R	F	R	F	R
1	513	302	195	195	176	176	141	70	238	102	0	84	0	0	32	130
2	392	241	162	130	117	146	316	70	170	136	42	84	0	0	32	97
3	211	150	32	195	30	88	70	281	34	315	127	295	56	169	65	195
4	181	181	97	97	0	30	70	35	34	0	380	295	225	112	389	454
5	241	211	32	32	30	30	70	105	34	34	380	169	141	112	454	422
6	422	271	195	195	176	205	205	105	211	68	136	380	28	84	97	454
7	452	331	141	281	234	205	176	176	170	136	77	192	0	56	65	162
8	181	120	176	176	117	293	176	176	170	306	39	77	0	28	32	65
9	150	91	105	246	58	146	176	387	238	374	77	77	28	56	65	65
10	30	60	70	141	30	58	0	141	0	102	230	345	169	169	97	227
11	30	30	35	70	0	30	35	35	34	34	461	461	281	253	454	552
12	0	0	35	35	0	0	0	0	0	0	77	230	28	169	65	195
13	0	0	35	0	0	0	0	0	0	0	39	77	0	28	0	65

Table 6.3 Test Truck - Maximum Static Stress Range (kg/cm²)(Cont.)

GAGE AXLE RUN	18		19		20		21		25		27		32		33	
	F	R	F	R	F	R	F	R	F	R	F	R	F	R	F	R
1	35	70	302	120	243	243	264	330	27	53	0	0	0	0	122	243
2	35	70	241	331	108	541	231	363	0	27	0	31	0	0	122	243
3	70	176	91	361	0	108	33	165	0	27	31	62	0	39	284	446
4	281	492	60	60	56	56	0	0	0	79	62	93	39	78	325	892
5	281	176	60	30	111	139	66	99	53	105	31	155	39	78	122	690
6	211	352	60	91	222	278	99	165	79	185	62	186	39	156	81	365
7	35	316	181	271	361	194	231	264	132	343	155	341	117	234	41	325
8	35	141	91	271	83	333	132	297	105	292	93	404	195	195	81	365
9	35	70	91	211	83	194	99	198	27	238	186	310	117	234	122	406
10	35	211	60	120	56	111	66	132	27	27	124	310	78	117	365	771
11	387	281	60	60	27	56	33	33	53	79	248	310	39	39	284	730
12	105	387	0	30	0	27	33	33	105	211	124	341	78	117	41	122
13	0	70	0	0	0	0	0	0	185	369	124	372	195	234	141	41

Table 6.4 Test Truck - Maximum Dynamic Stresses Range (kg/cm²)

GAGE	5		19		20		21		25		27		32	
AXLE RUN	F	R	F	R	F	R	F	R	F	R	F	R	F	R
1	519	357	141	246	331	120	218	218	0	0	0	0	0	0
2	389	292	141	211	181	422	146	328	0	0	34	34	0	42
3	195	130	35	105	0	60	0	72	0	30	34	68	0	42
4	487	325	141	281	392	422	182	328	120	302	136	306	127	295
5	32	65	35	105	30	120	37	109	30	30	102	238	84	84
6	32	32	0	35	0	30	0	0	60	120	102	306	42	42
7	0	0	0	0	0	0	0	0	150	211	136	340	84	169

Table 6.5 Root-Mean-Square Stress Range

Gage	S_{rRMS} (kg/cm ²)
5	172
7	134
8	134
9	127
10	141
15	197
16	127
17	197
18	176
19	190
20	141
21	162
22	183
25	162
27	176
32	134
33	222

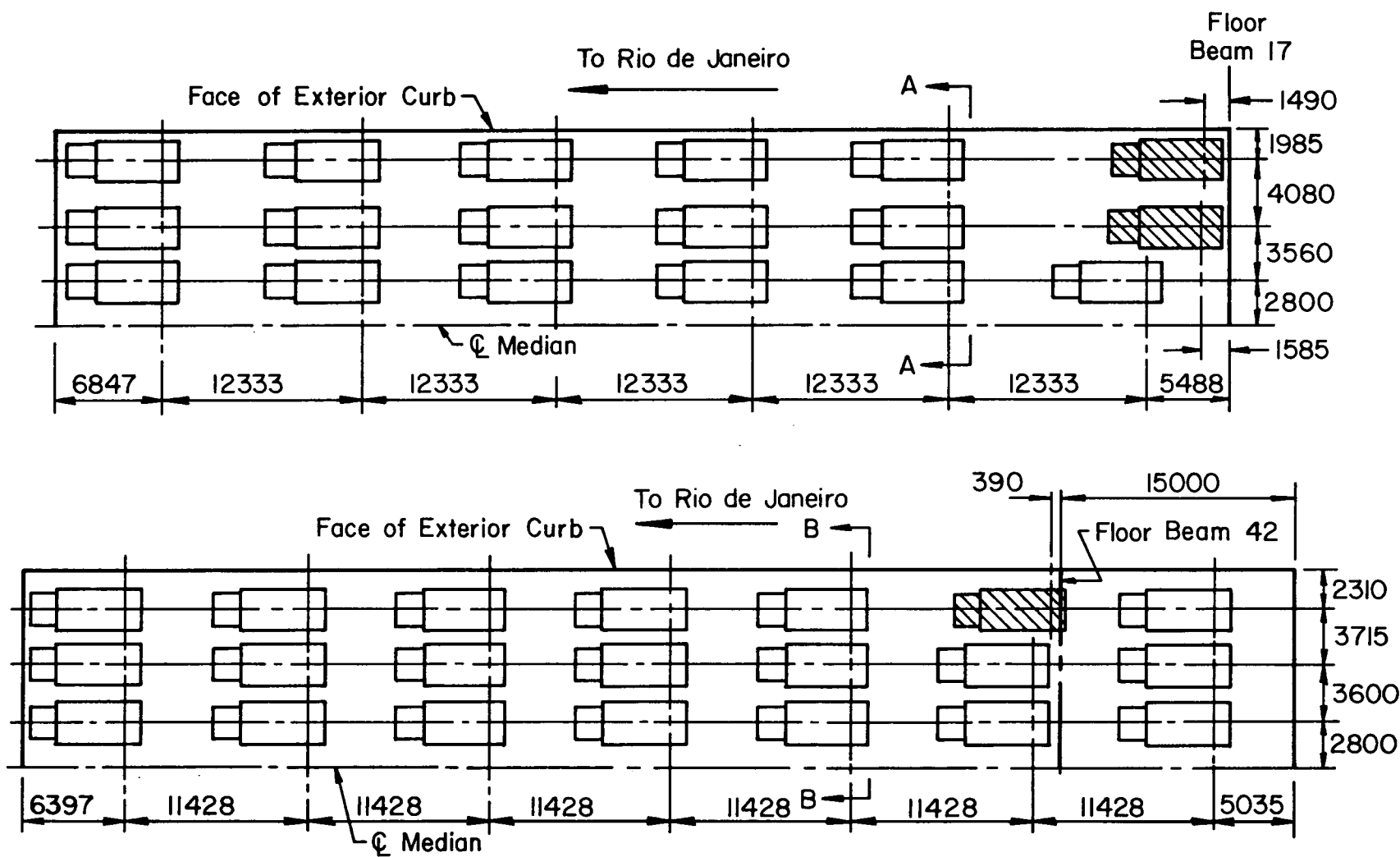


Fig. 6.1 Static Truck Position Near Floorbeams 17 and 42

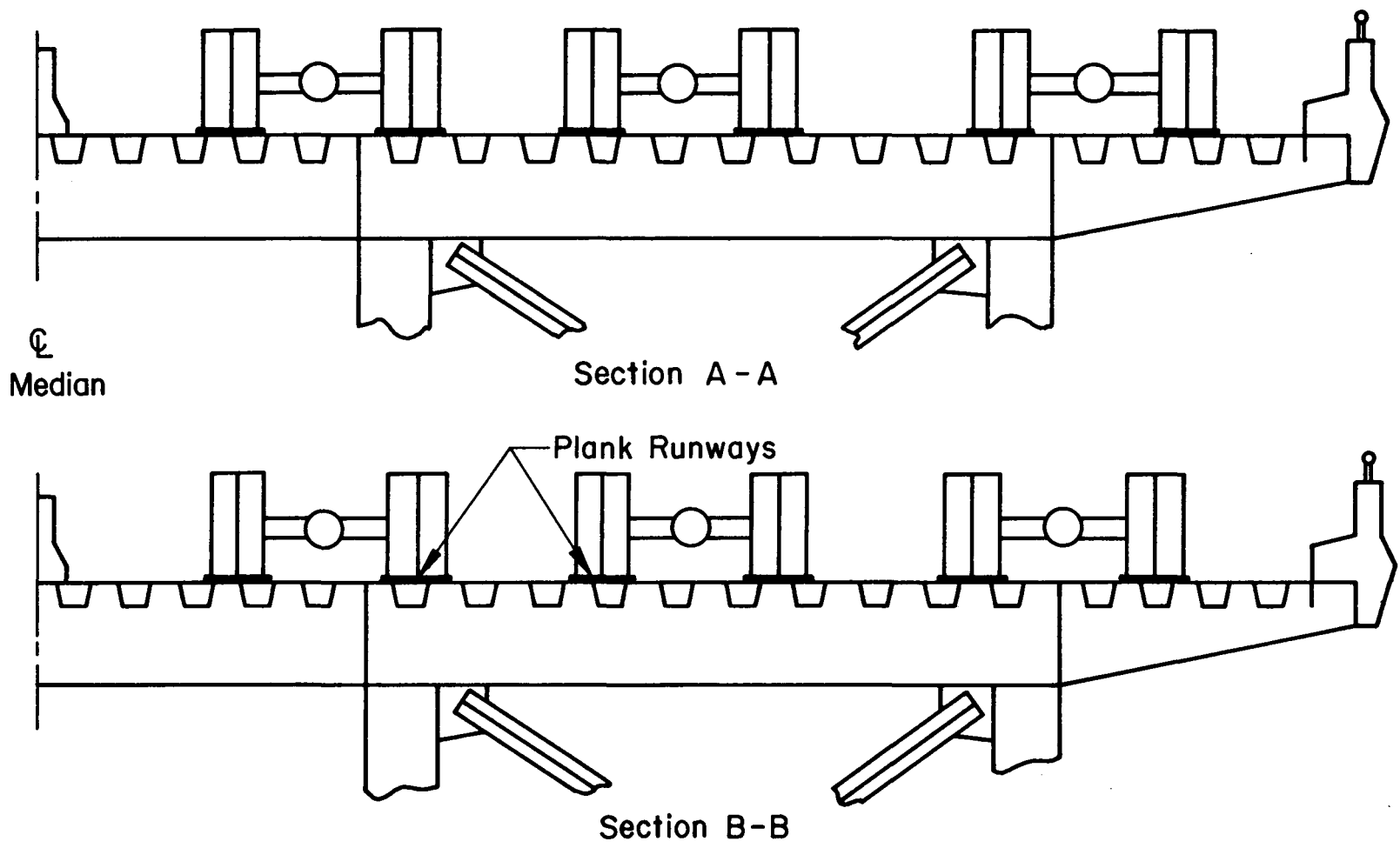
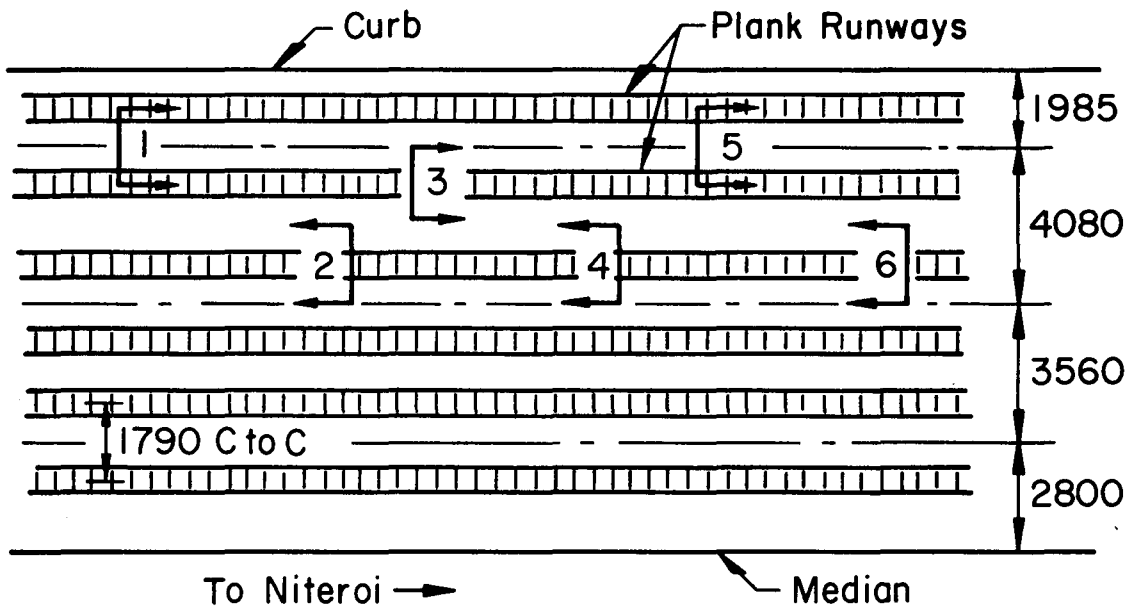
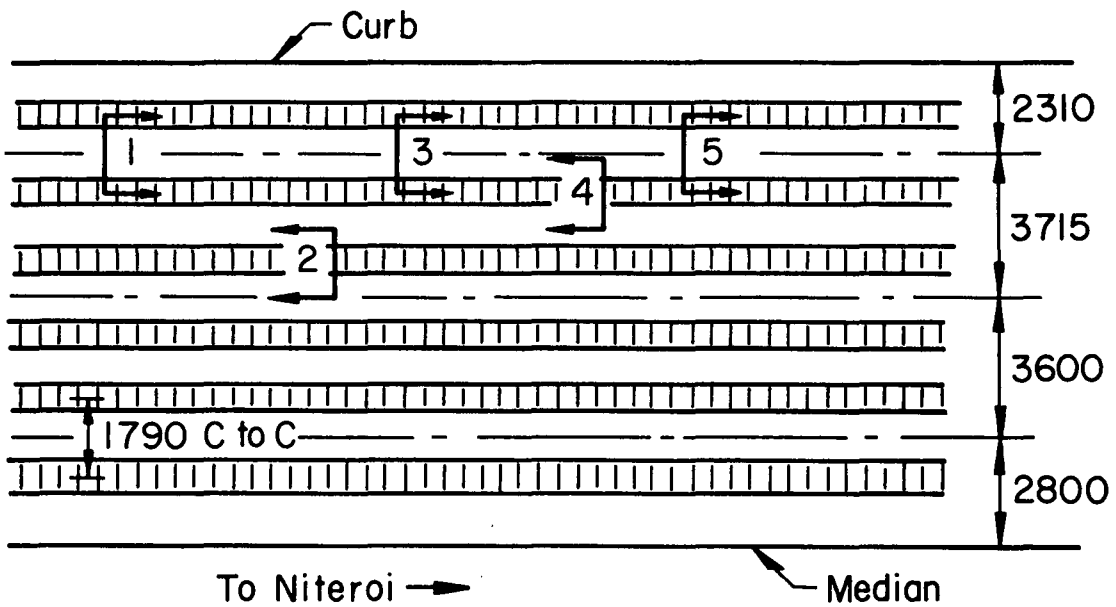


Fig. 6.2 Positions of Rear Wheels Relative to Trapezoidal Stiffening Elements - Floorbeams 17 and 42



(a) Truck Runs - FBI7



(b) Truck Runs - FB 42

Fig. 6.3 Locations of Passes Made by Truck No. 14



Fig. 6.4 Photograph of Euclid Truck

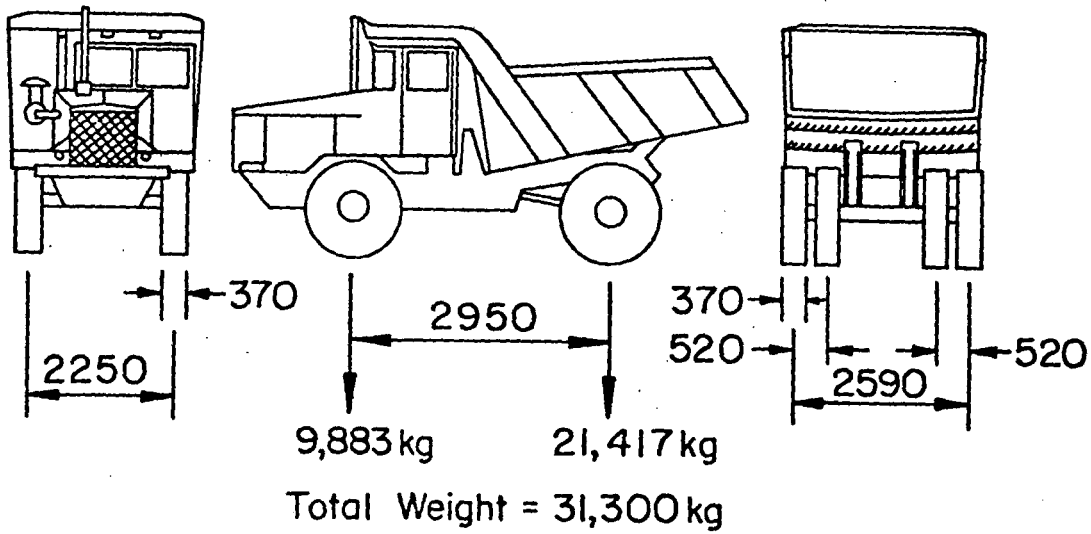


Fig. 6.5 Euclid Truck Dimensions

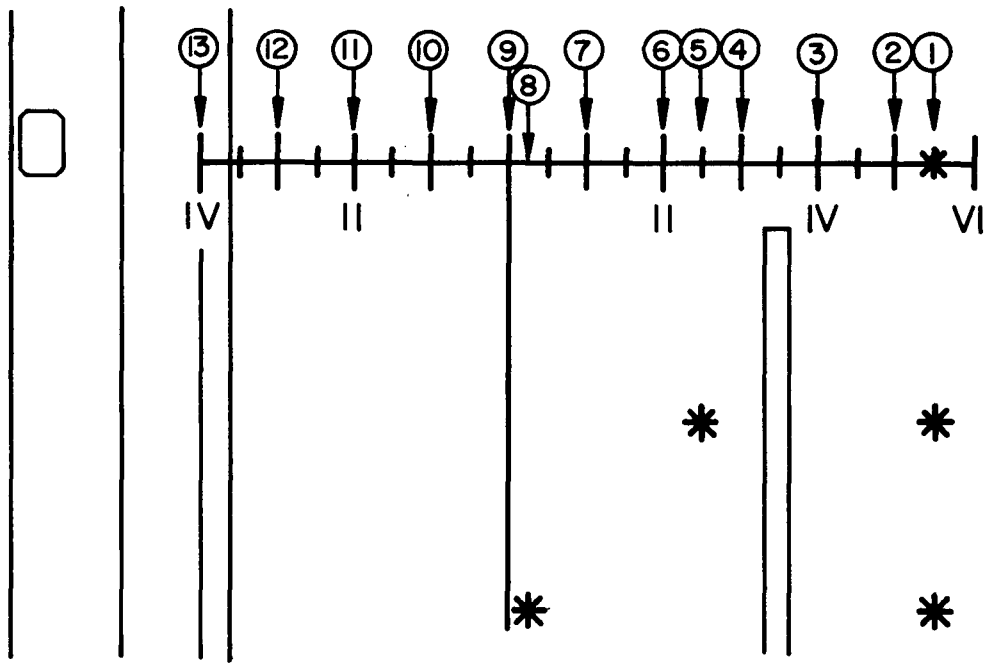


Fig. 6.6 Thirteen Crawl Positions

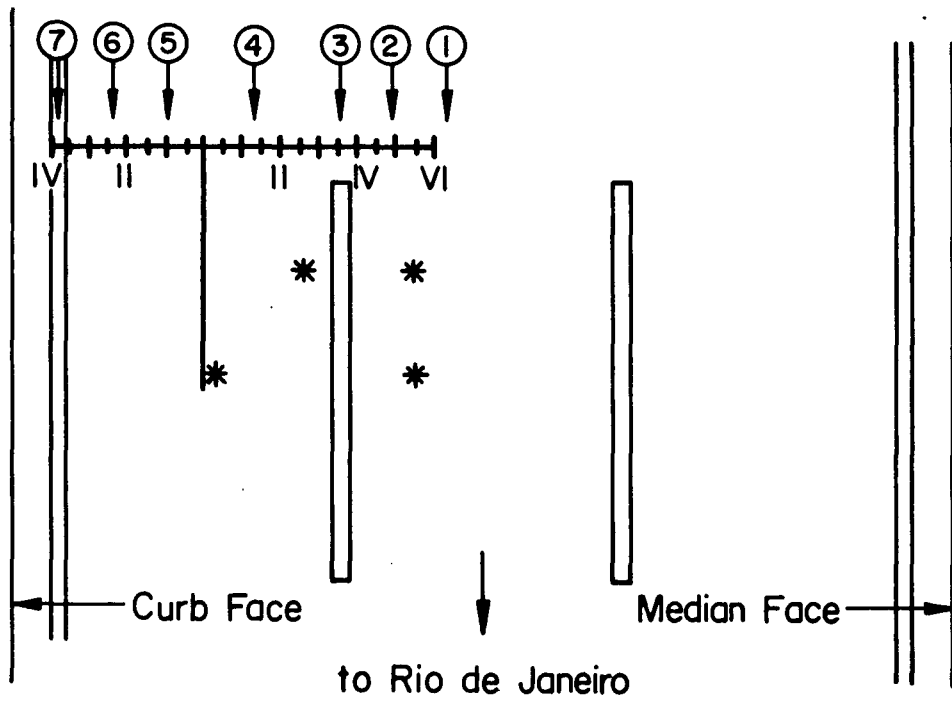


Fig. 6.7 Seven Speed Run Positions

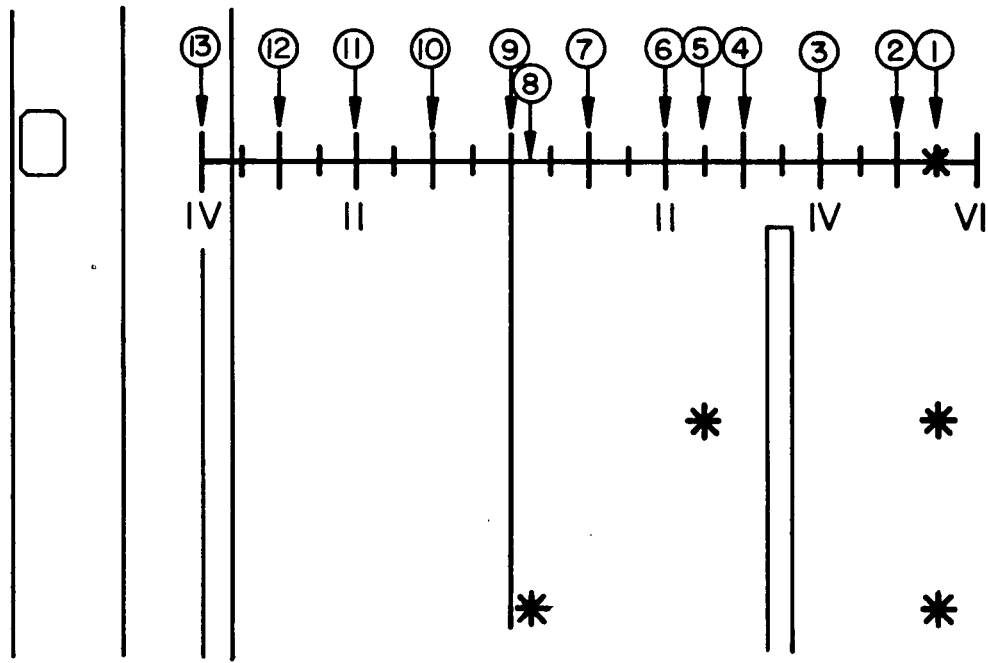


Fig. 6.6 Thirteen Crawl Positions

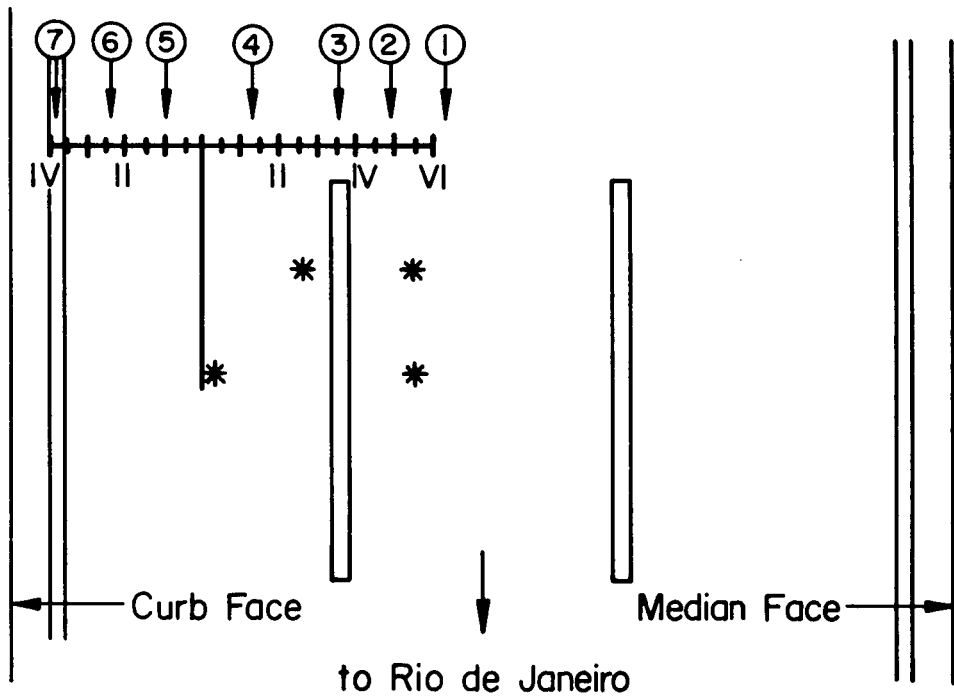


Fig. 6.7 Seven Speed Run Positions

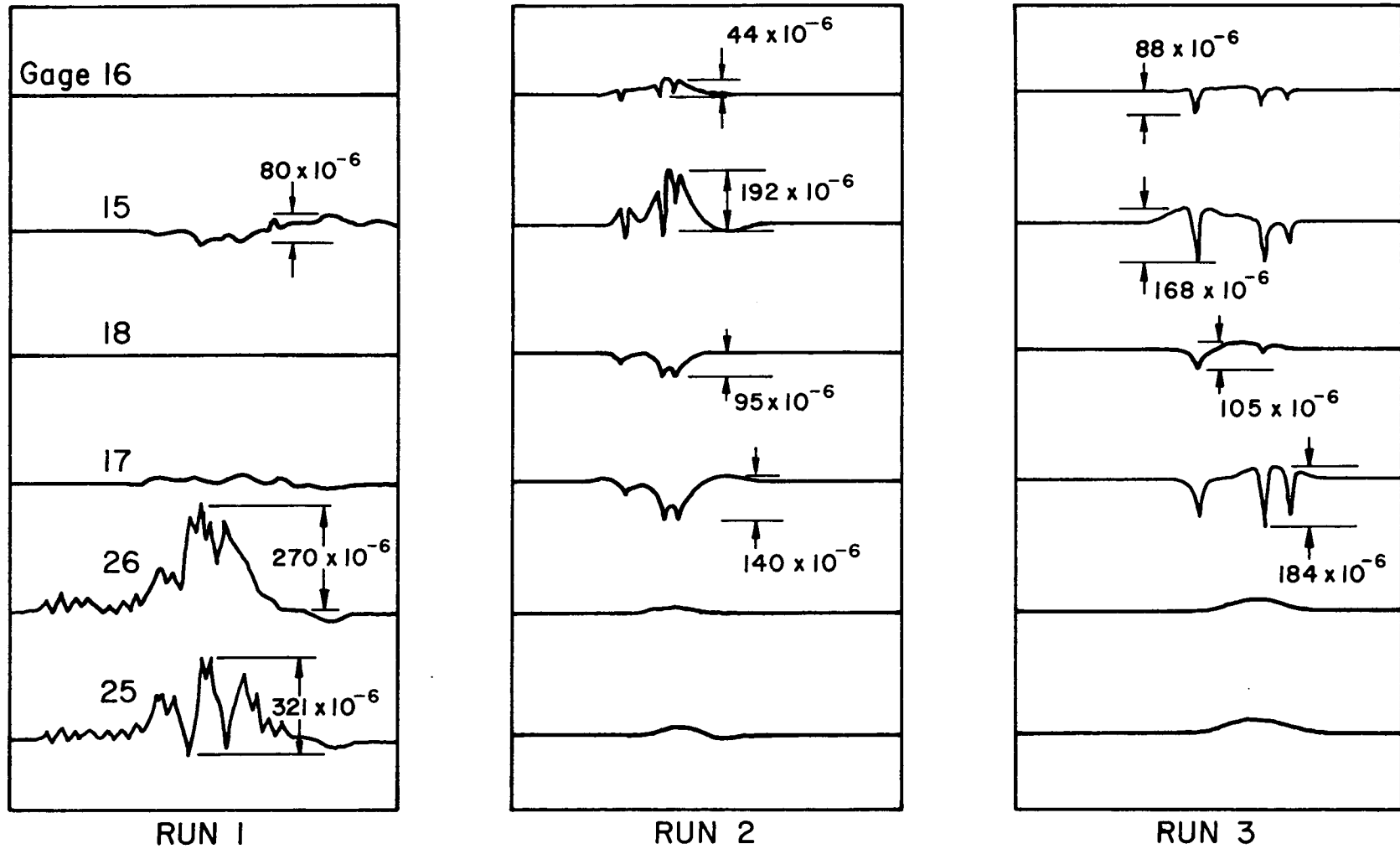
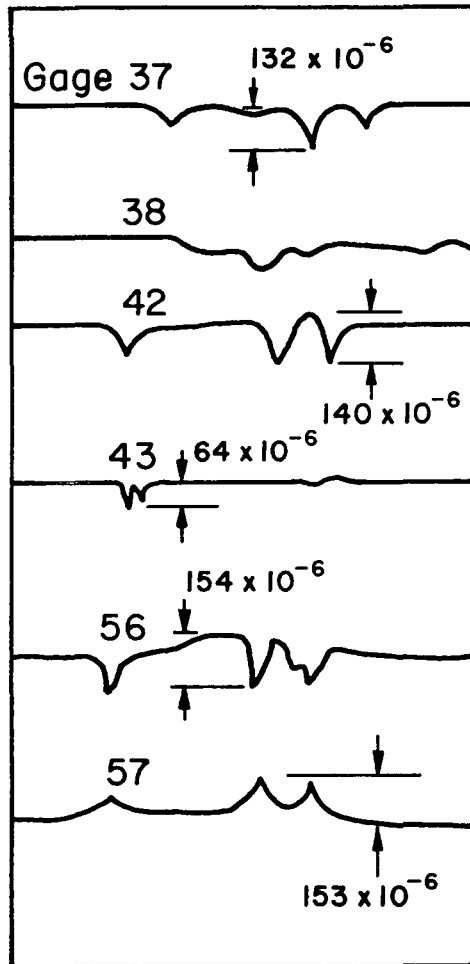
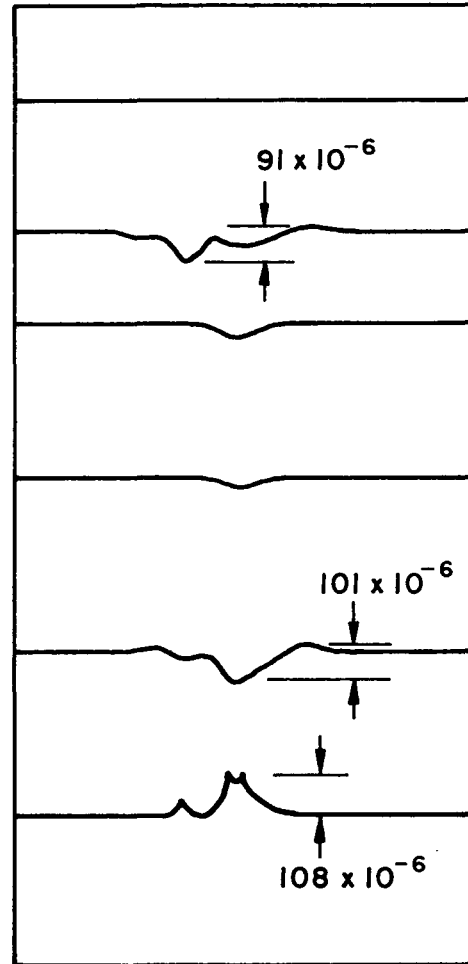


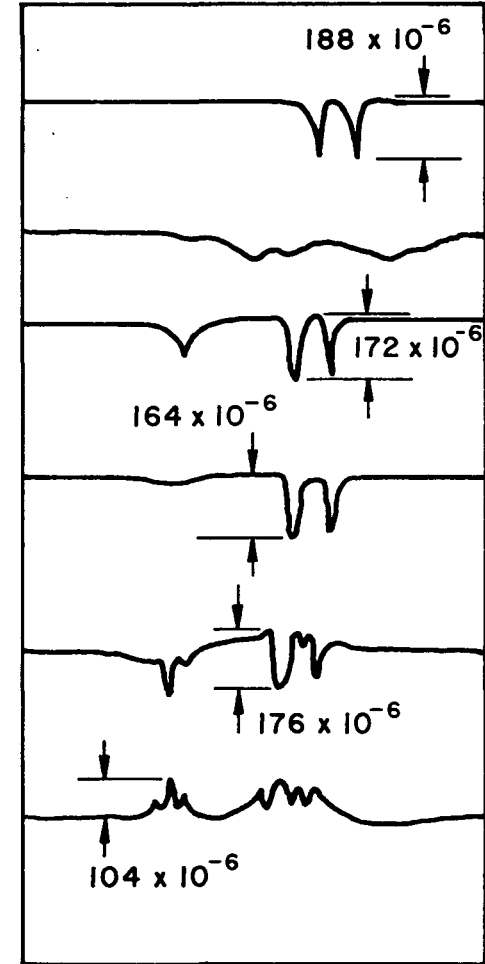
Fig. 6.8 Strain Variations for Six Strain Gages Near Floorbeam 17 - February 1974



RUN 1



RUN 2



RUN 4

Fig. 6.9 Strain Variations for Six Strain Gages Near Floorbeam 42 - February 1974

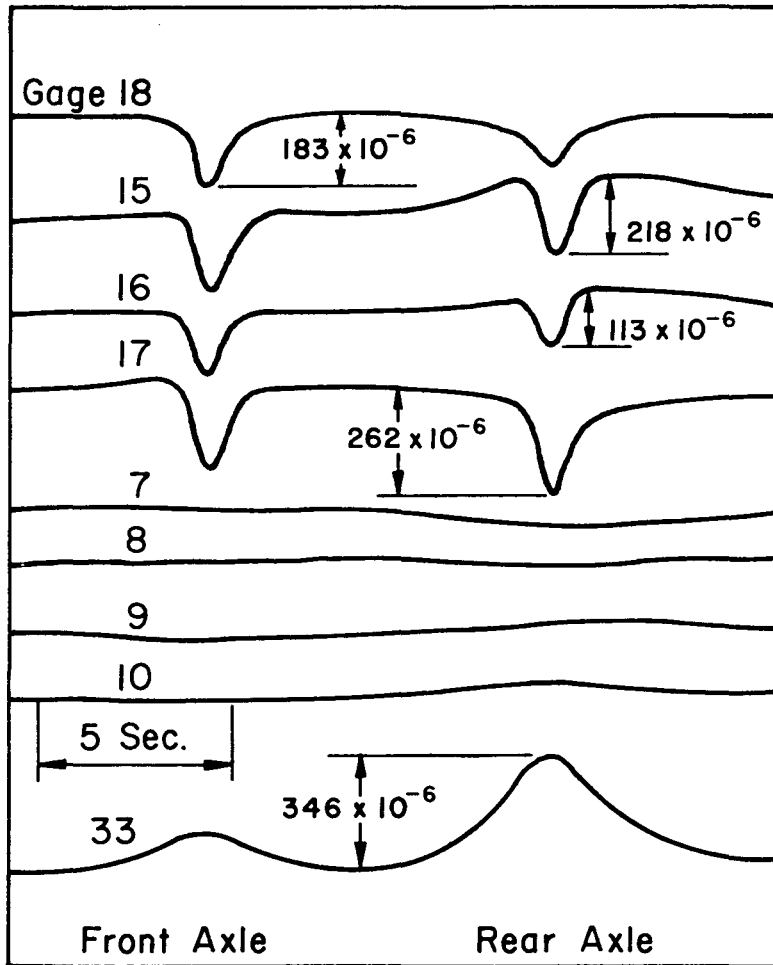


Fig. 6.10 Strain Variations for Nine Strain Gages near Floorbeam 17 - Crawl Run of Euclid Truck - June 1974

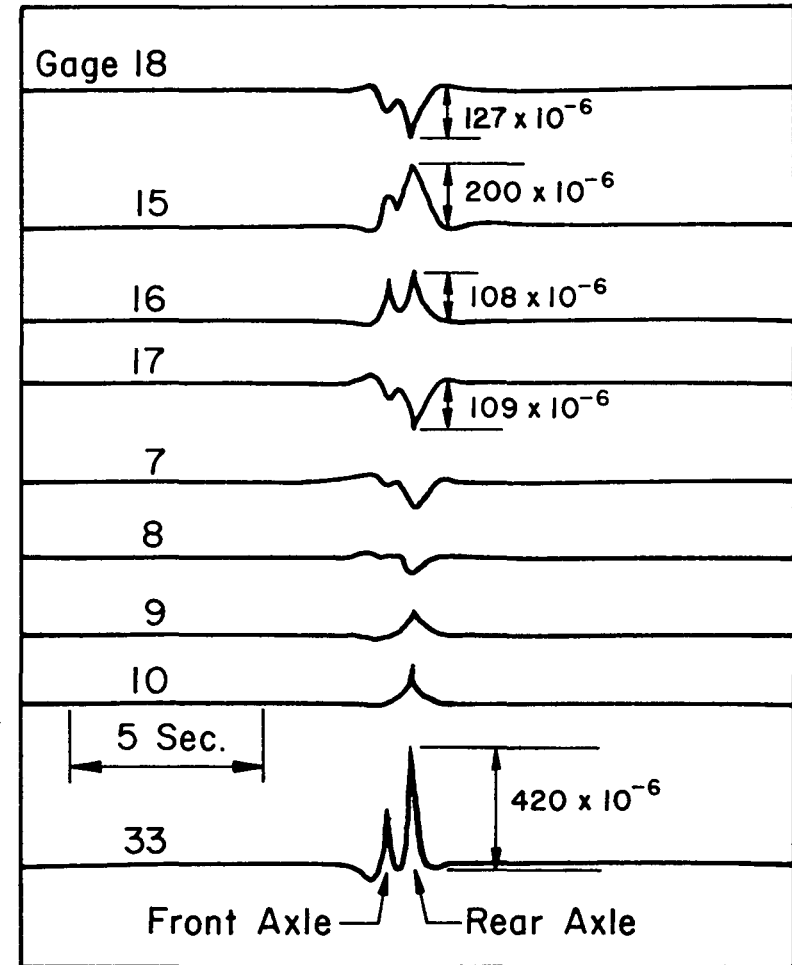


Fig. 6.11 Strain Variations for Nine Strain Gages near Floorbeam 17 - Speed Run of Euclid Truck - June 1974

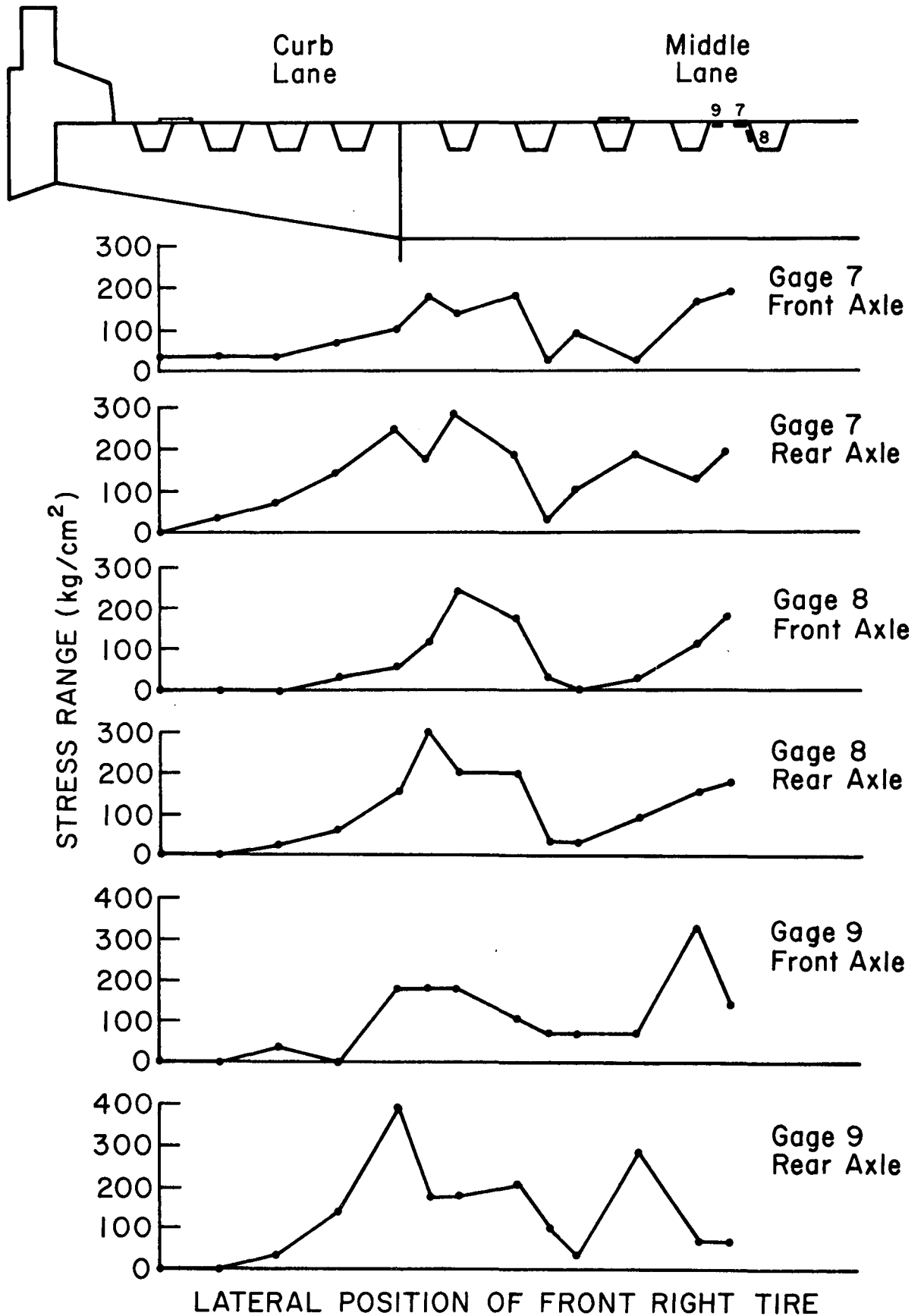


Fig. 6.12 Stress Range Variations - Crawl Runs - Euclid Test Truck

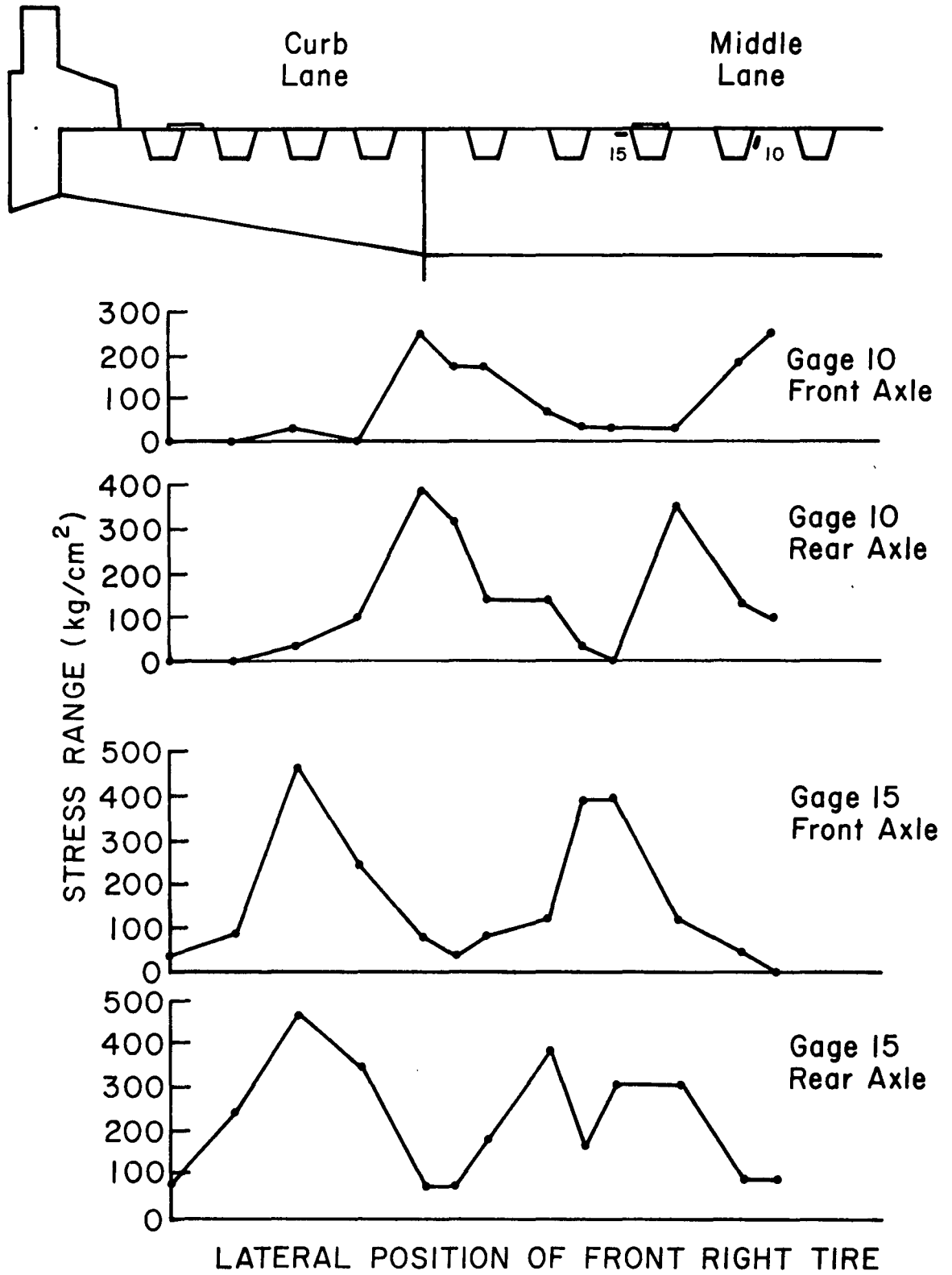


Fig. 6.13 Stress Range Variations - Crawl Runs - Euclid Test Truck

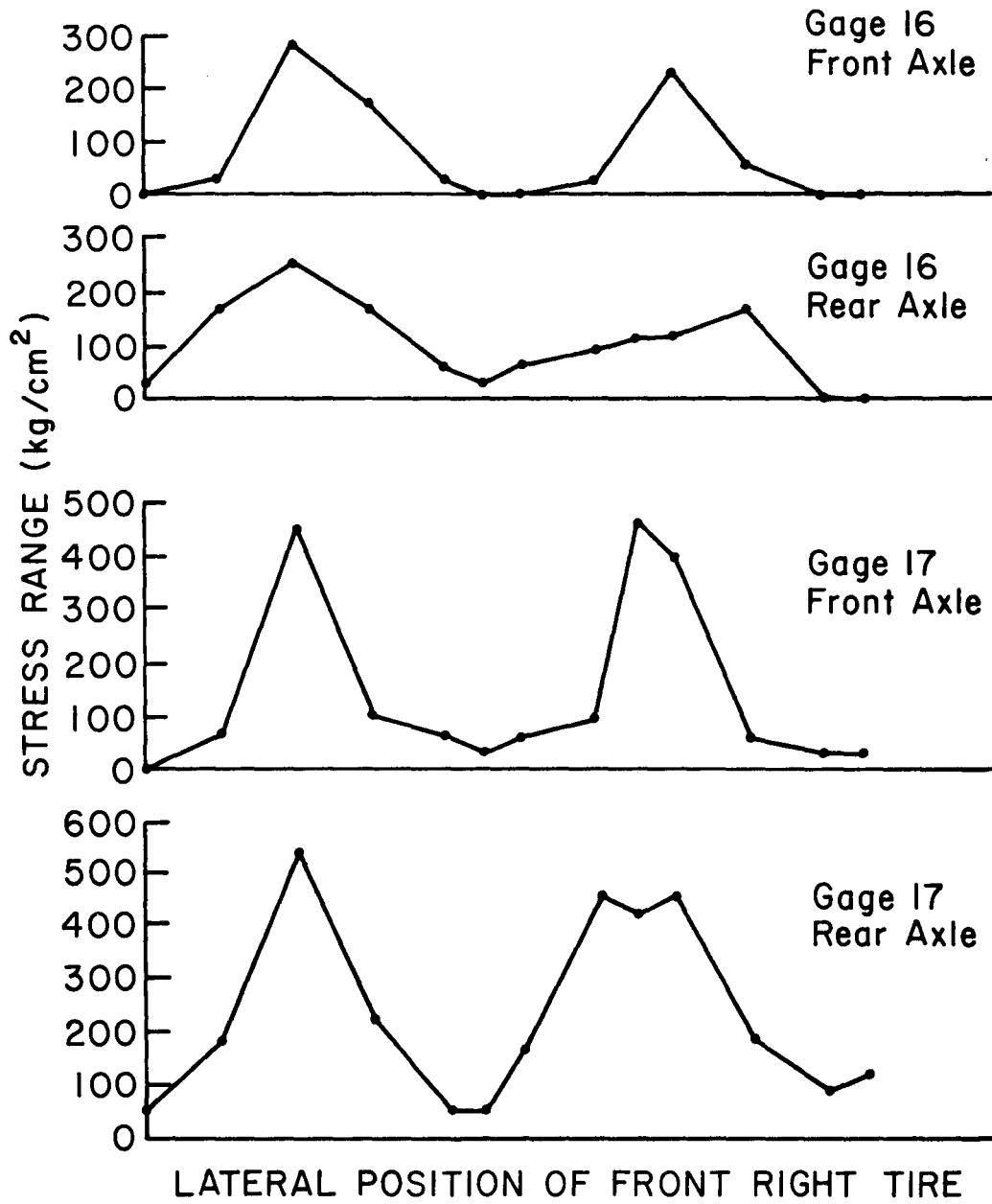
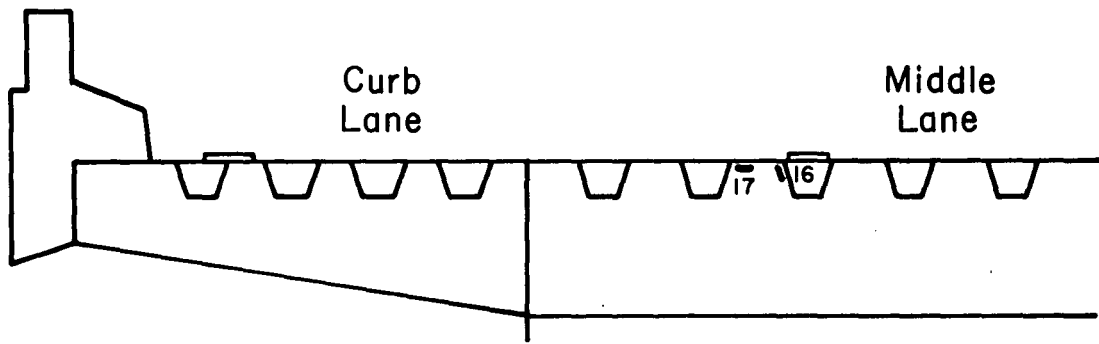


Fig. 6.14 Stress Range Variations - Crawl Runs - Euclid Test Truck

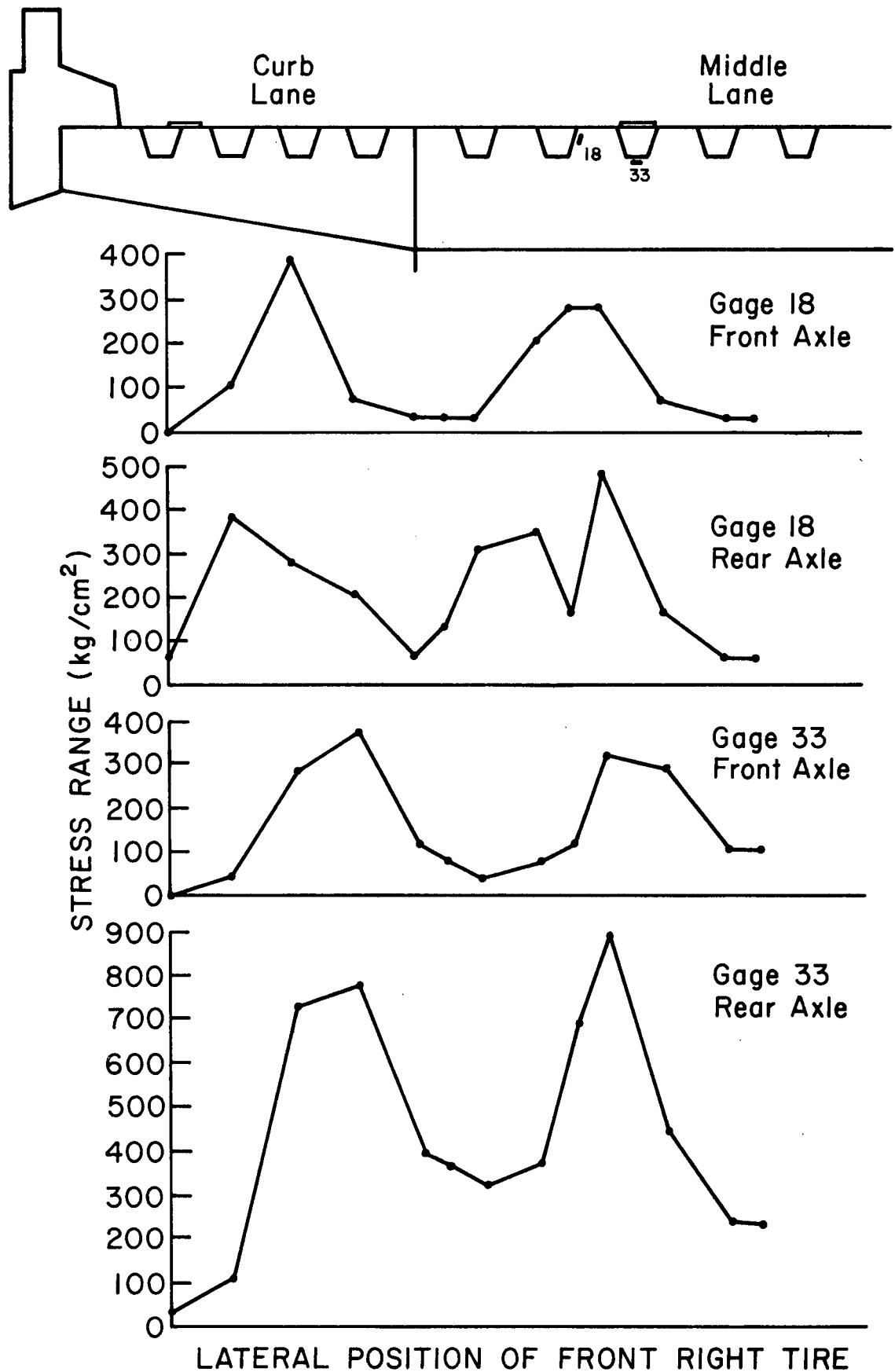


Fig. 6.15 Stress Range Variations - Crawl Runs - Euclid Test Truck

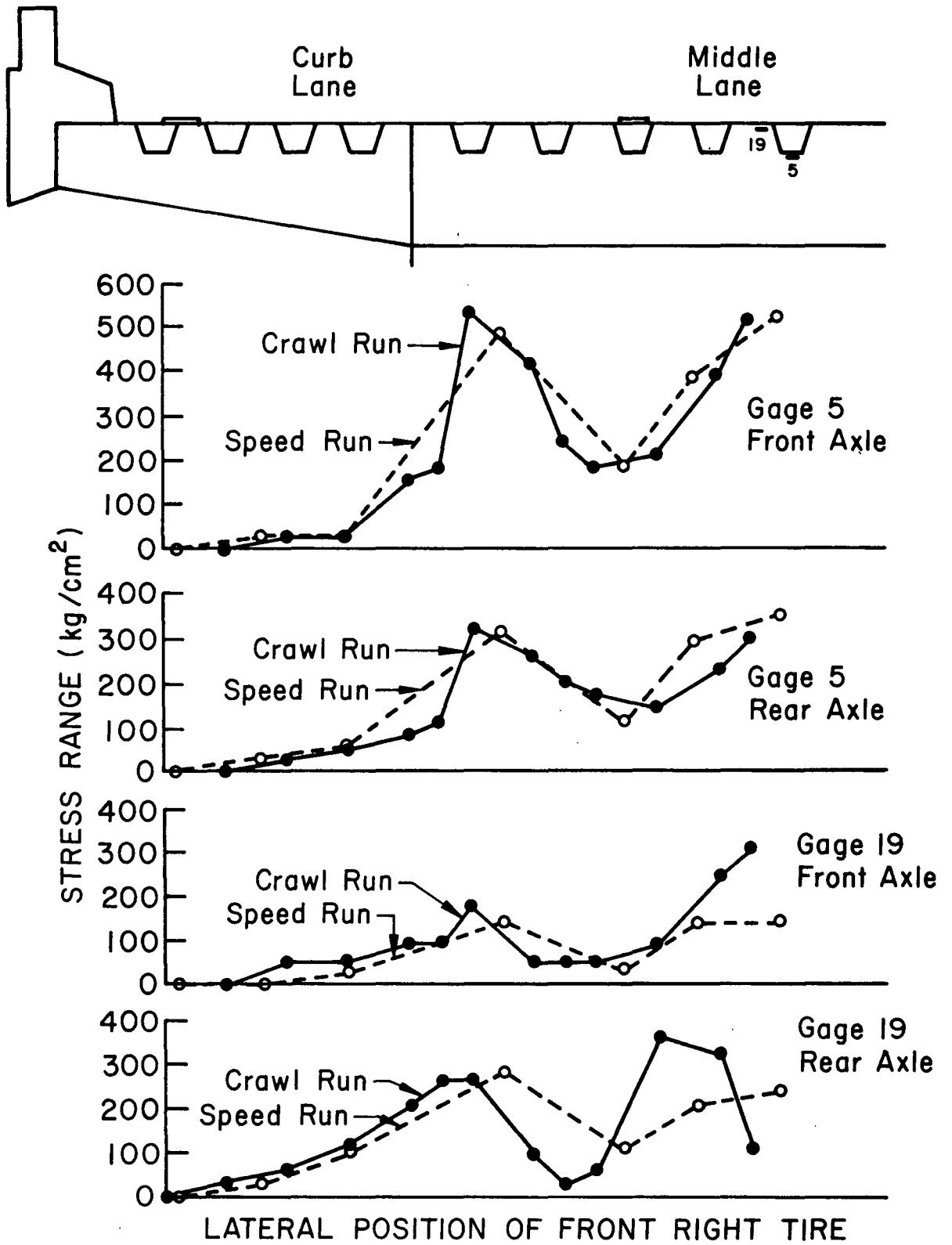


Fig. 6.16 Stress Range Variations - Crawl and Speed Runs - Euclid Test Truck

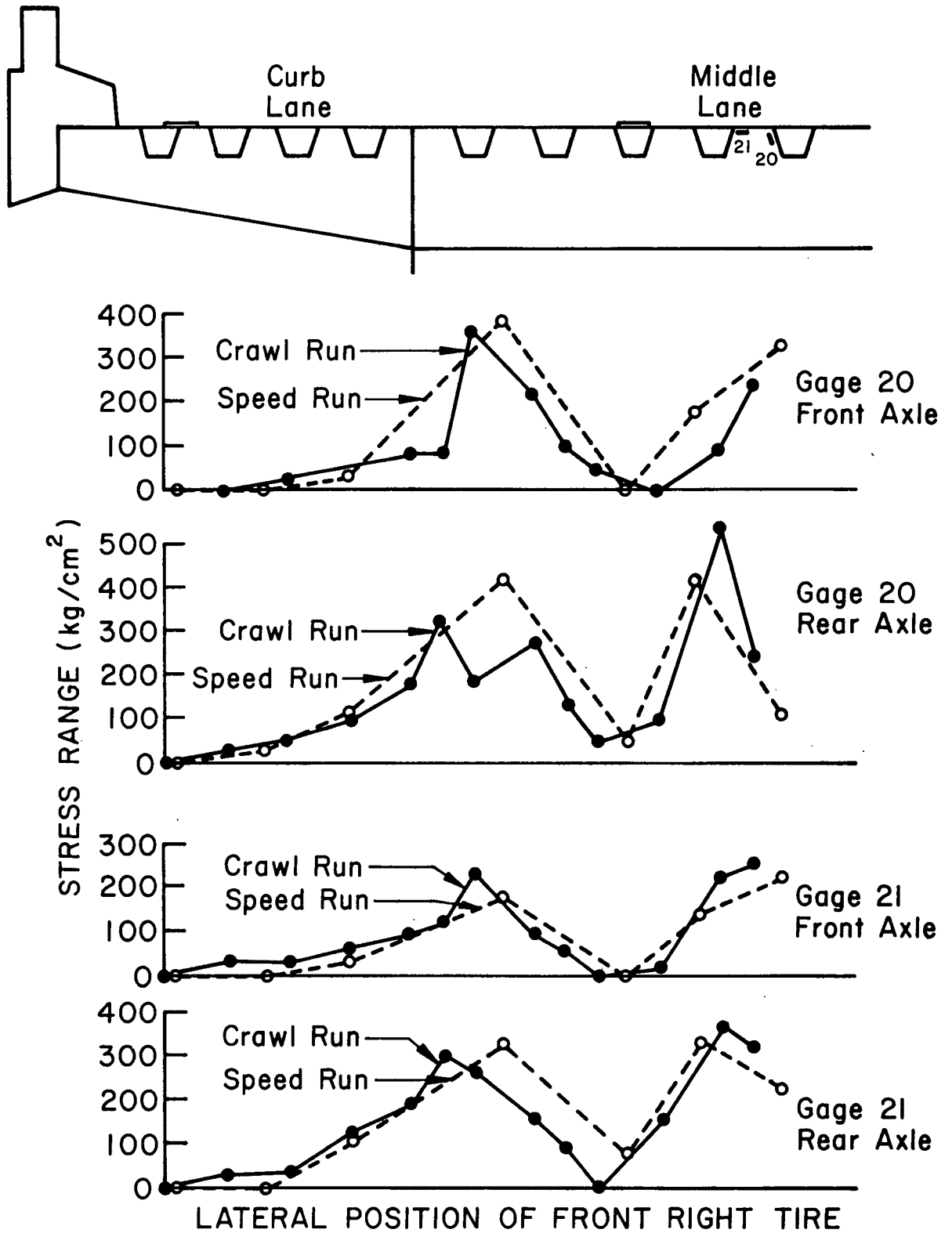


Fig. 6.17 Stress Range Variations - Crawl and Speed Runs - Euclid Test Truck

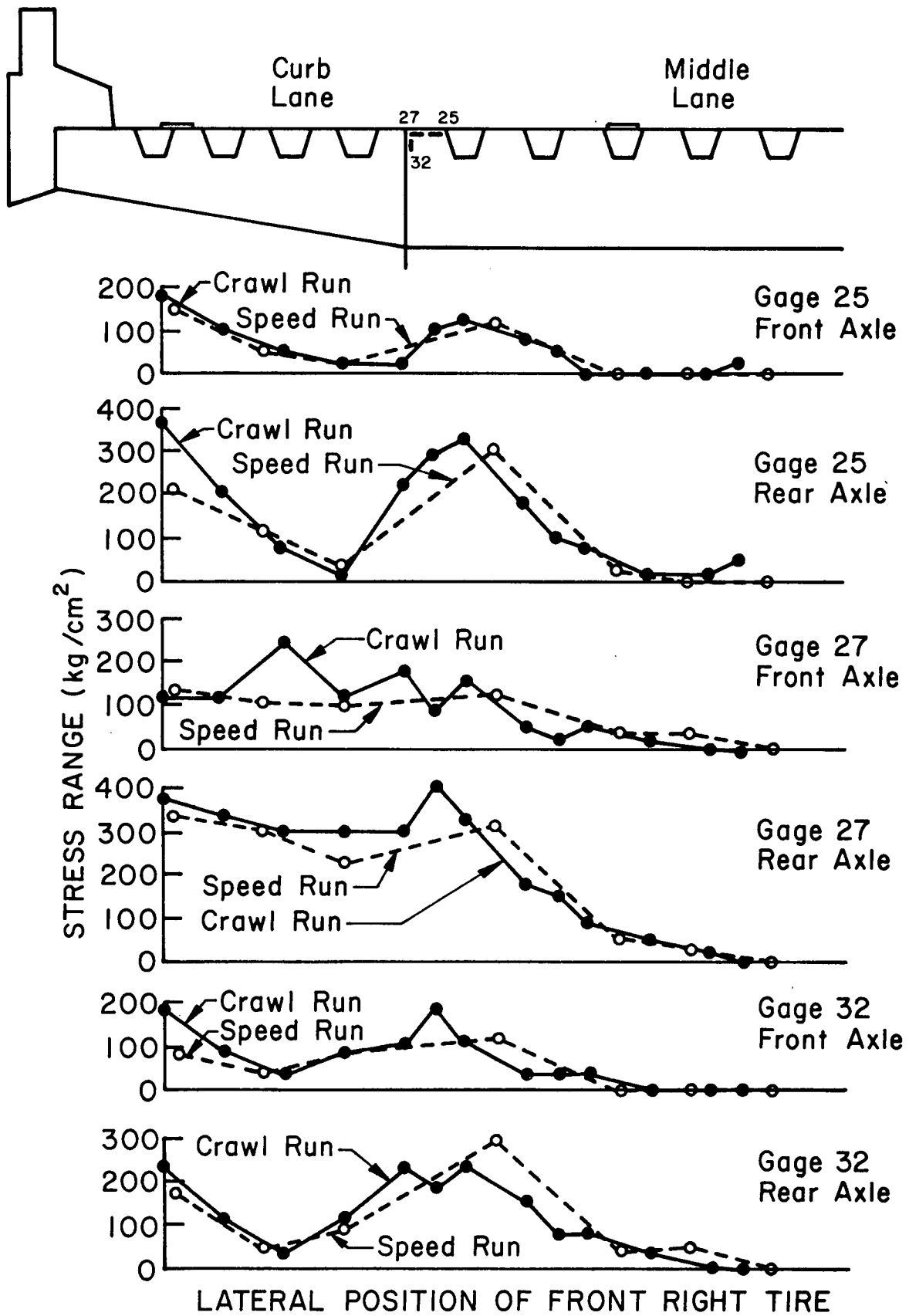


Fig. 6.18 Stress Range Variations - Crawl and Speed Runs - Euclid Test Truck

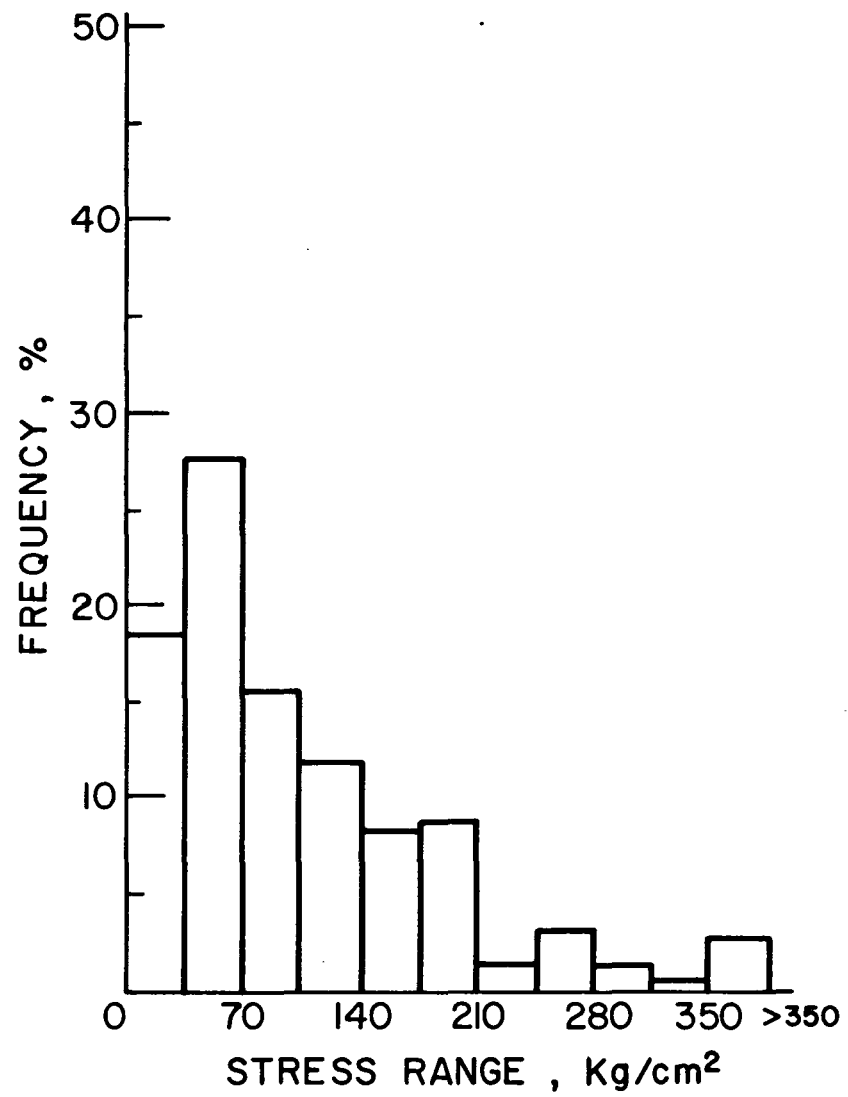


Fig. 6.19 Stress Range Histogram for Gage 5

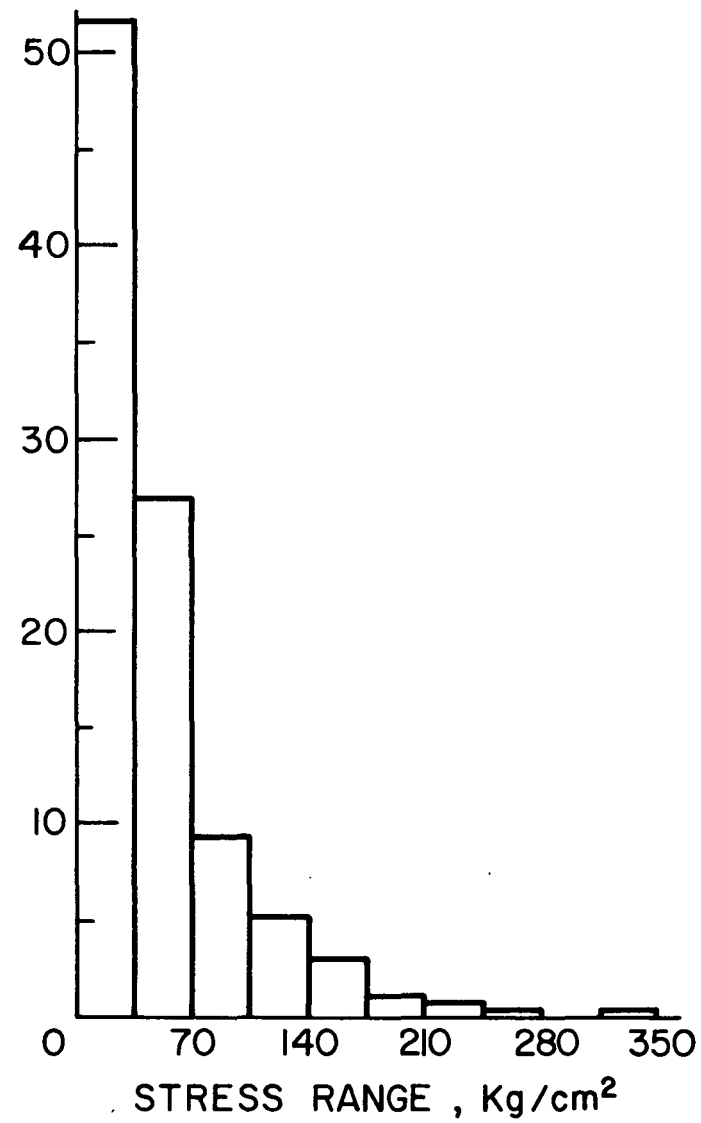


Fig. 6.20 Stress Range Histogram for Gage 7

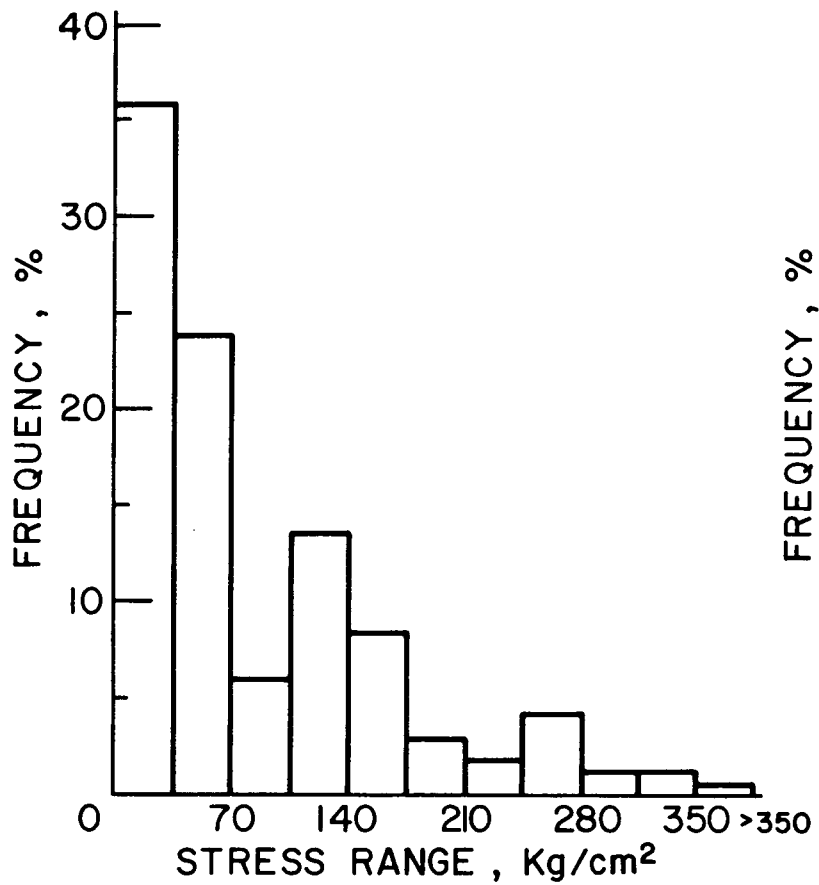


Fig. 6.21 Stress Range Histogram for Gage 22

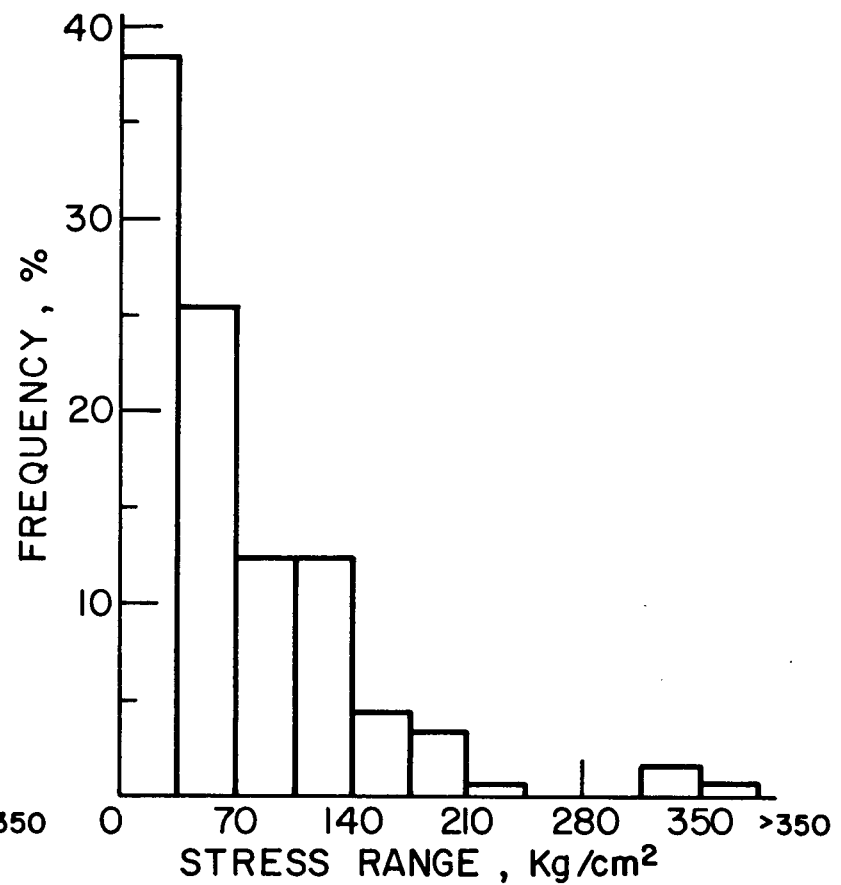


Fig. 6.22 Stress Range Histogram for Gage 25

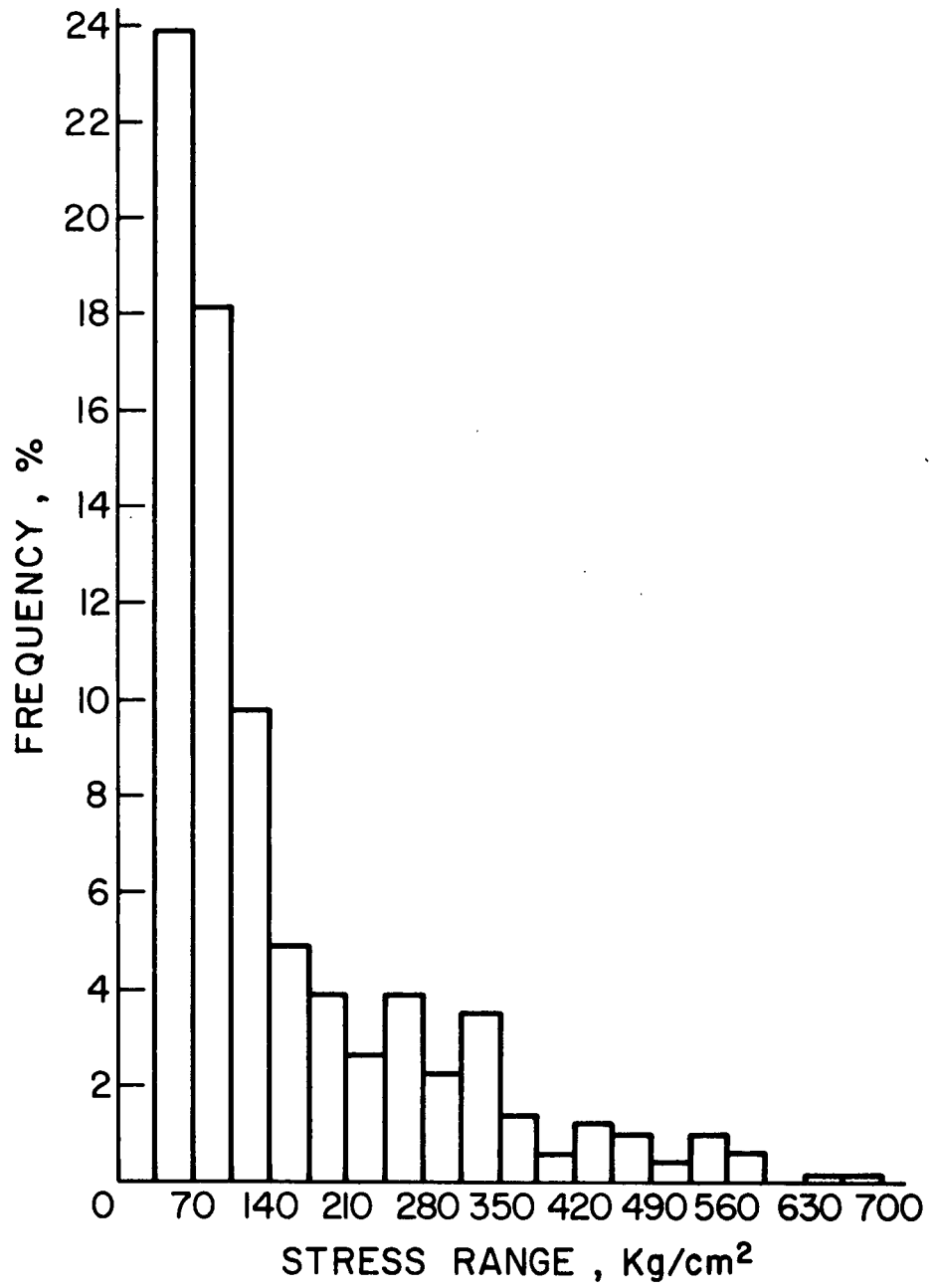


Fig. 6.23 Stress Range Histogram for Gage 33

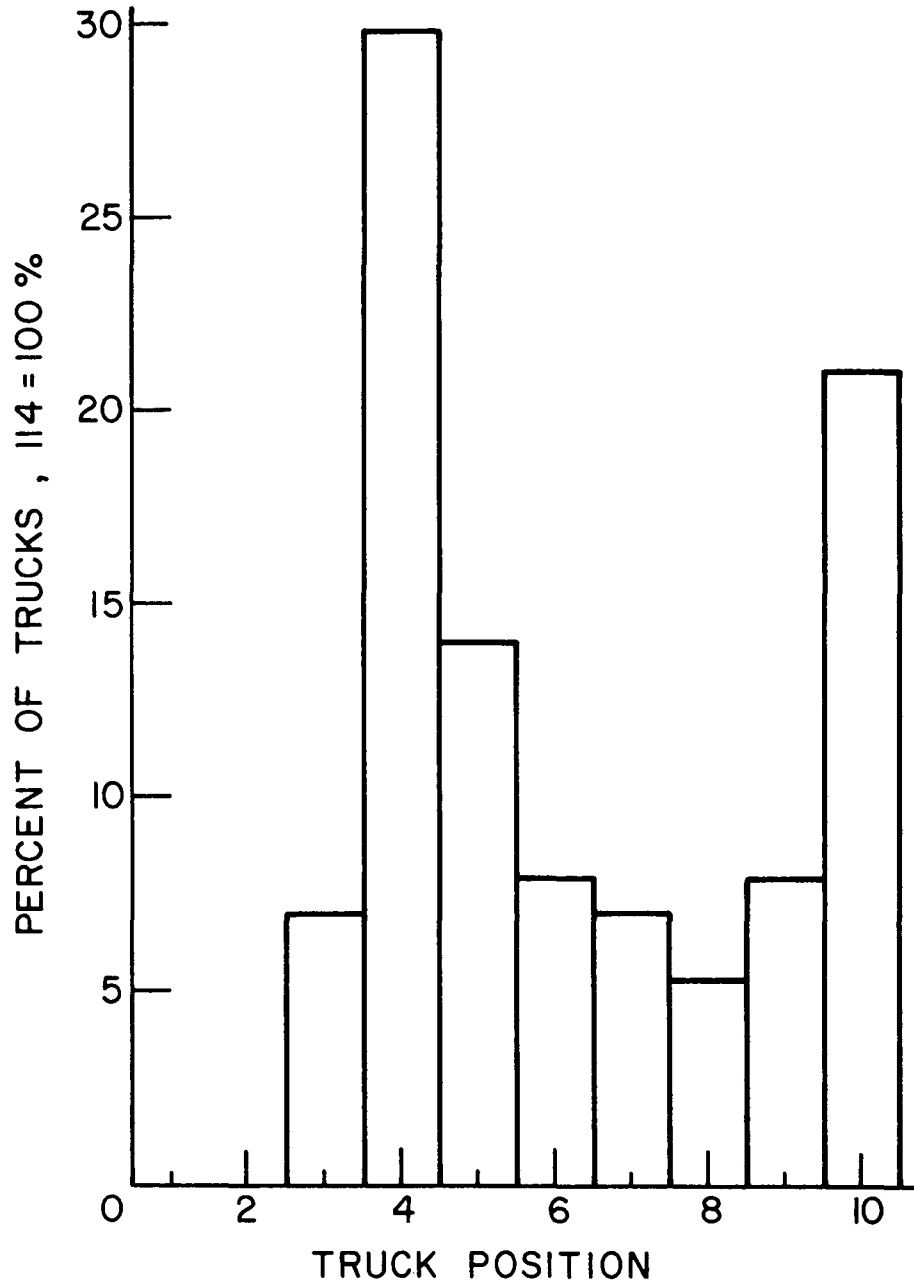


Fig. 6.24 Lateral Vehicle Position Histogram at Floorbeam 17

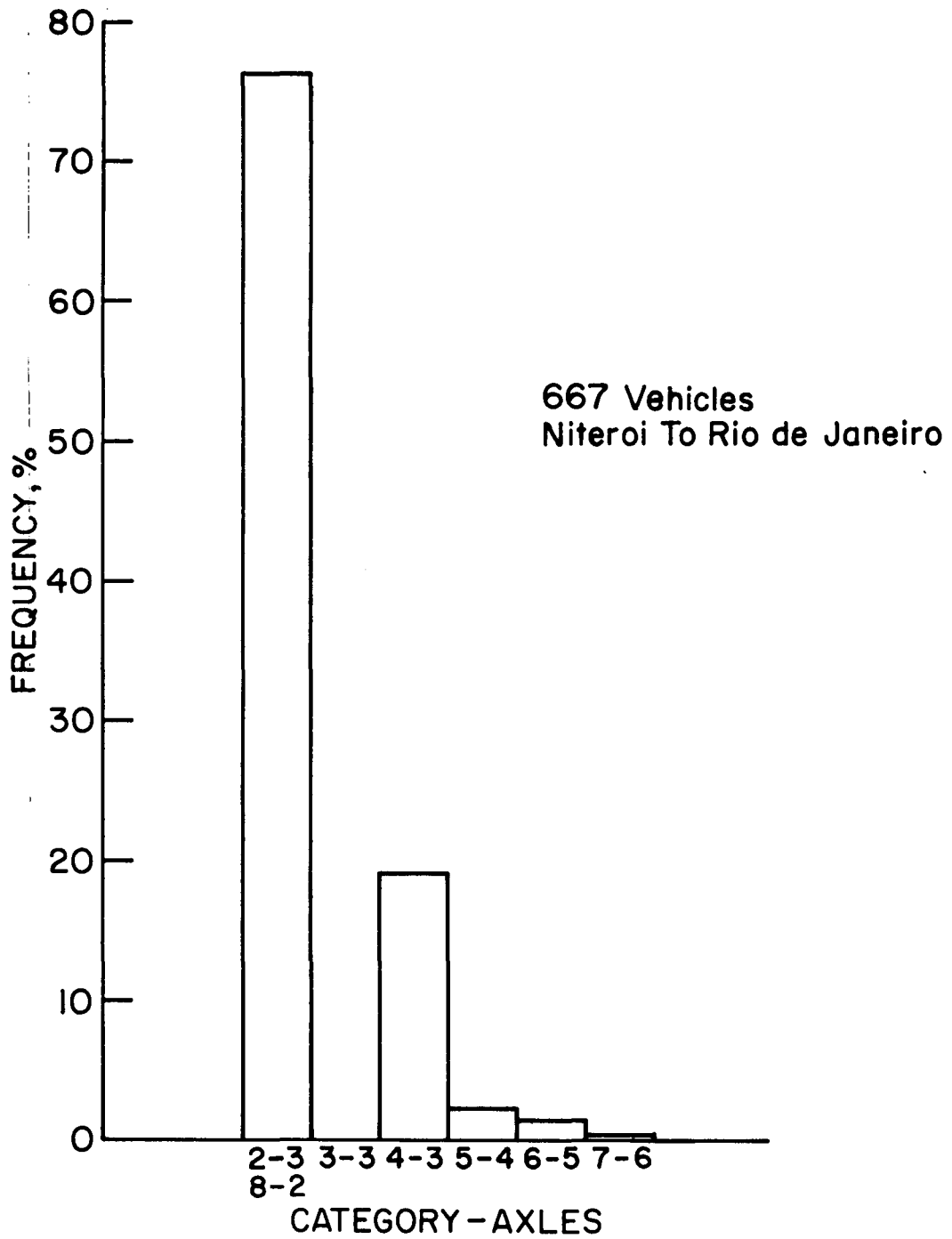


Fig. 6.25 Frequency Distribution of DNER Vehicle Classification Traffic (Table 2.5) During May - June 1974 - Niteroi to Rio de Janeiro

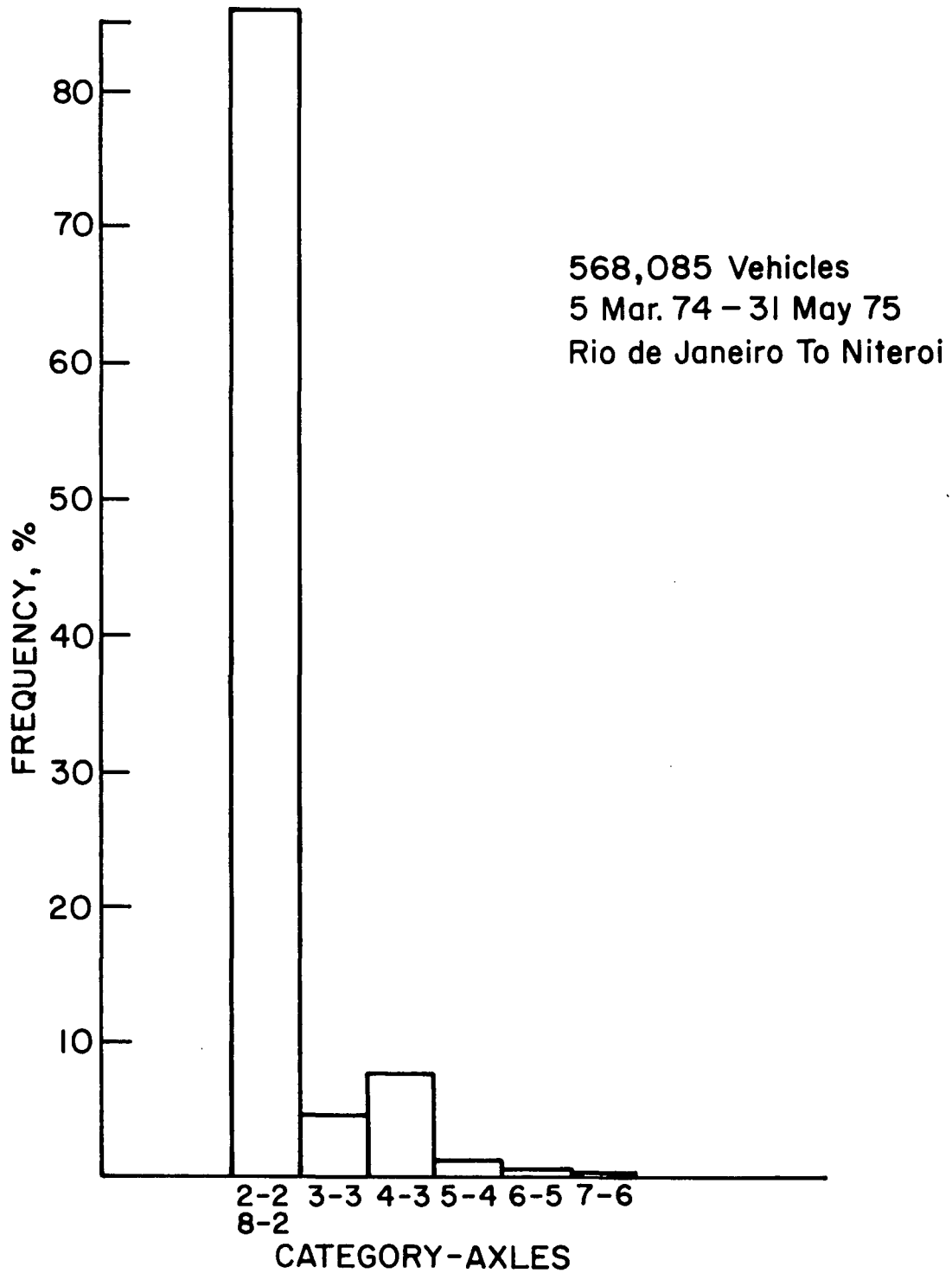


Fig. 6.26 Frequency Distribution of DNER Vehicle Classification Traffic (Table 2.5) During 15 Month Interval - Rio de Janeiro to Niteroi

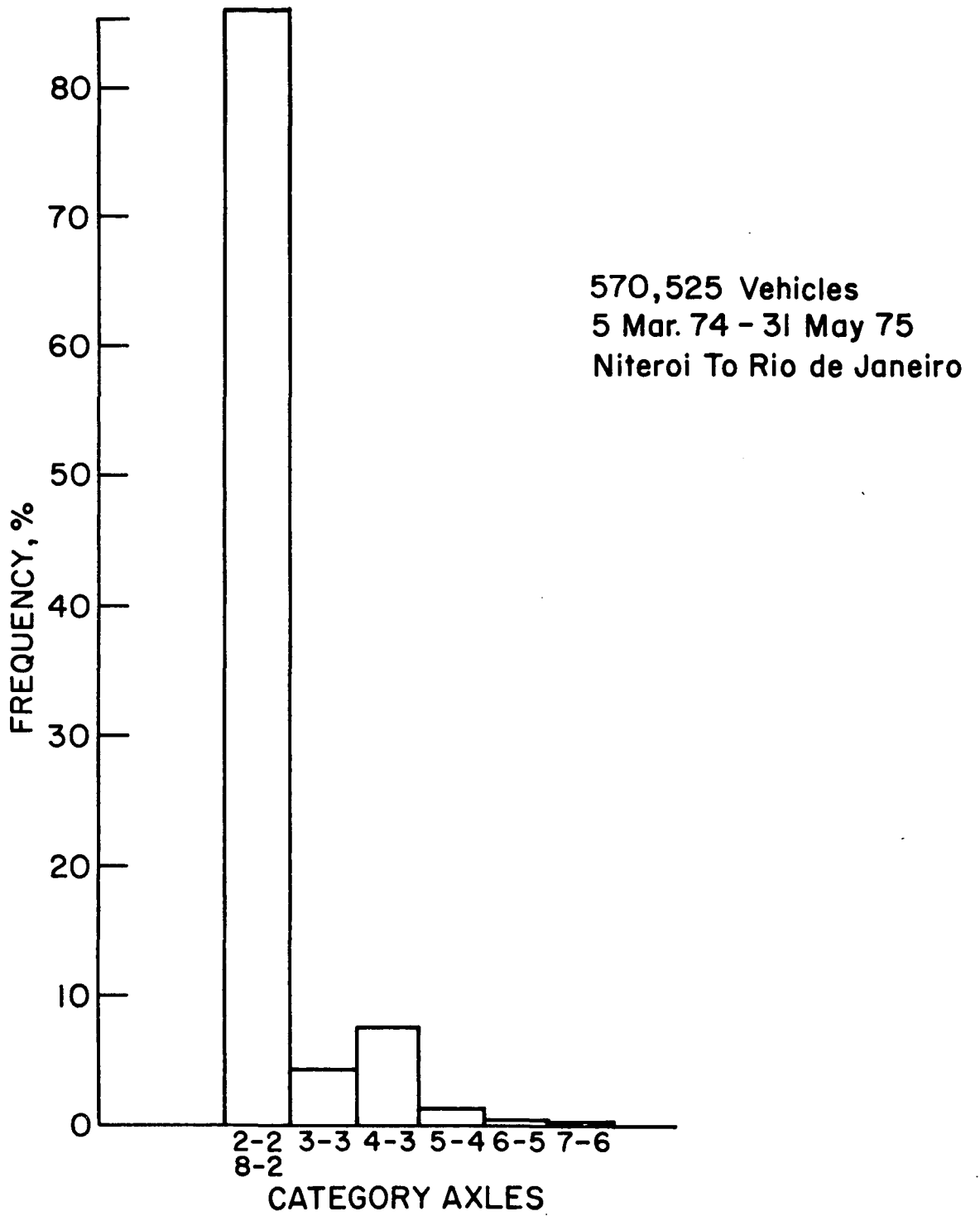
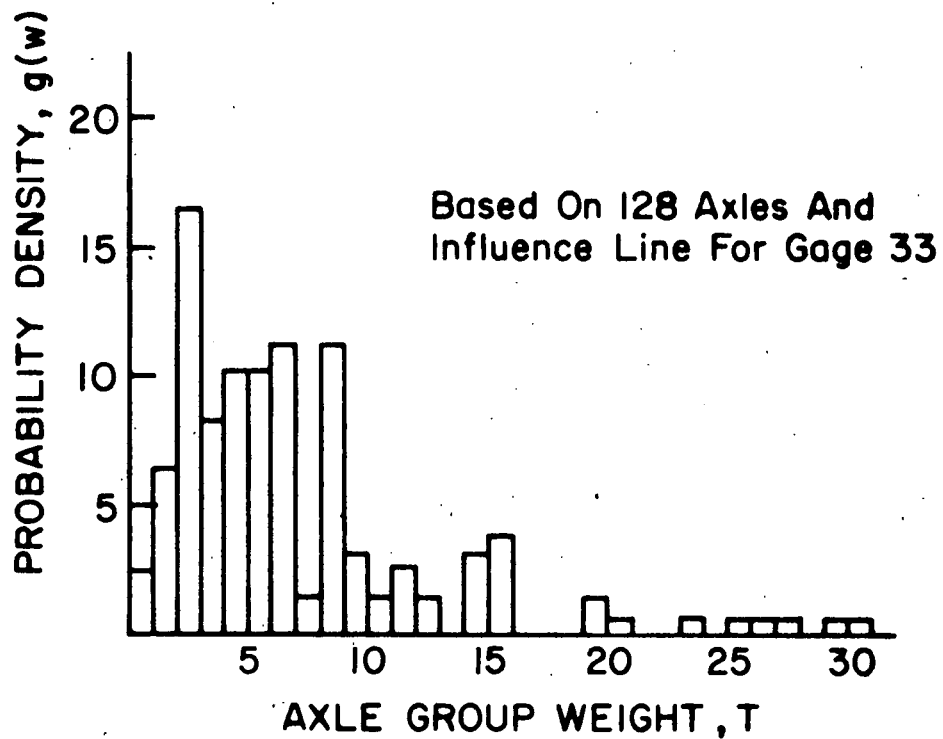
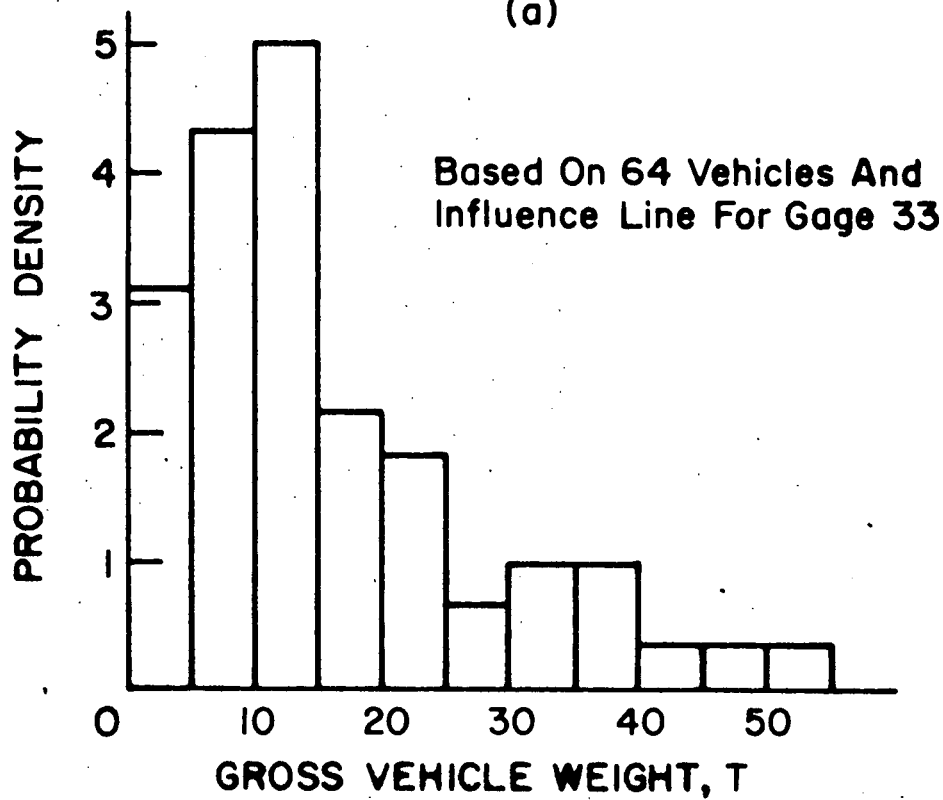


Fig. 6.27 Frequency Distribution of DNER Vehicle Classification Traffic (Table 2.5) During 15 Month Interval - Niteroi to Rio de Janeiro



(a)



(b)

Fig. 6.28 Axle Weight and Gross Vehicle Weight
Probability Density

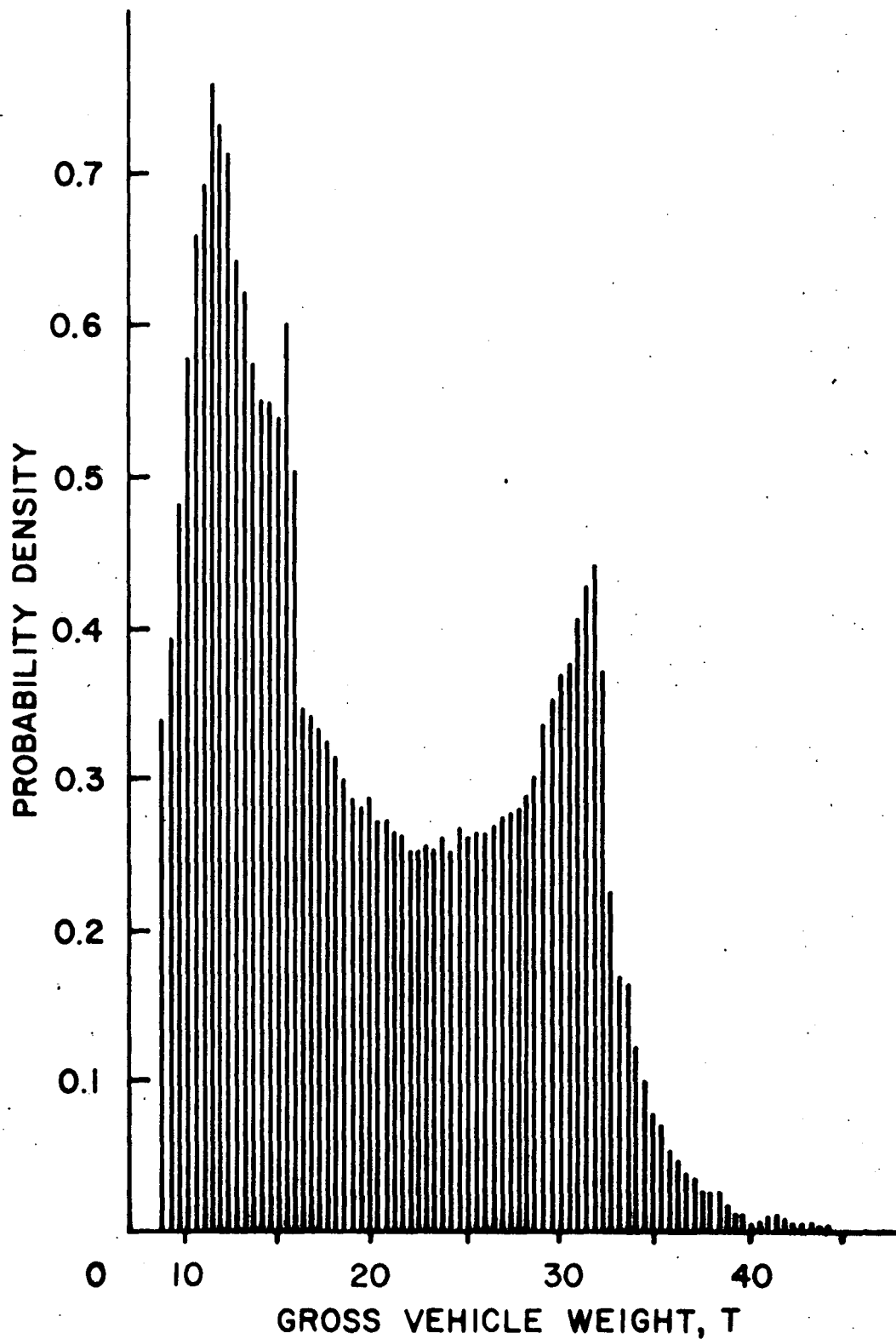


Fig. 6.29 Gross Vehicle Weight Probability Density of Total Traffic (1970 Loadometer Survey, FHWA, Nationwide)

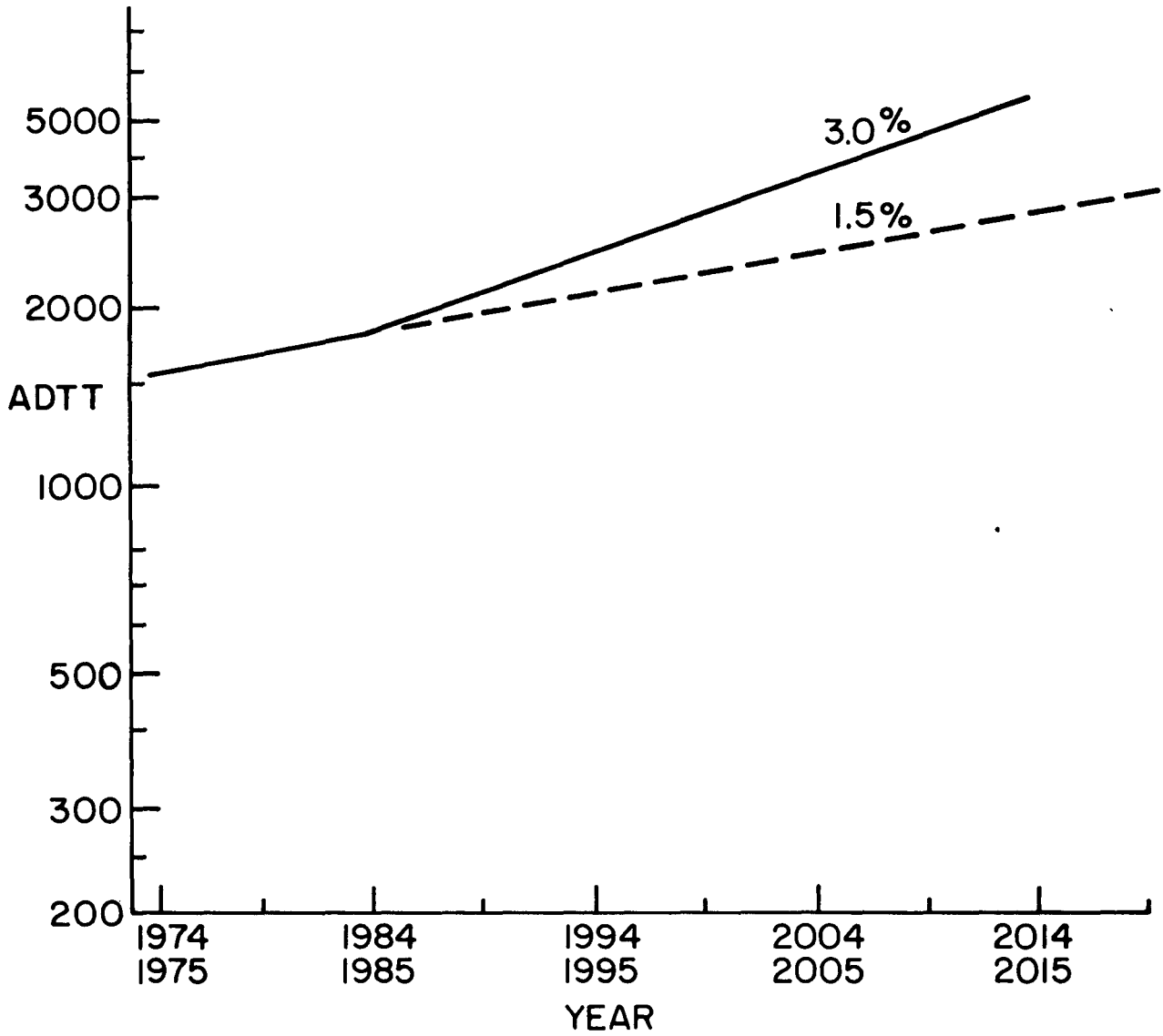


Fig. 6.30 Projected Estimates of Average Daily Truck Traffic

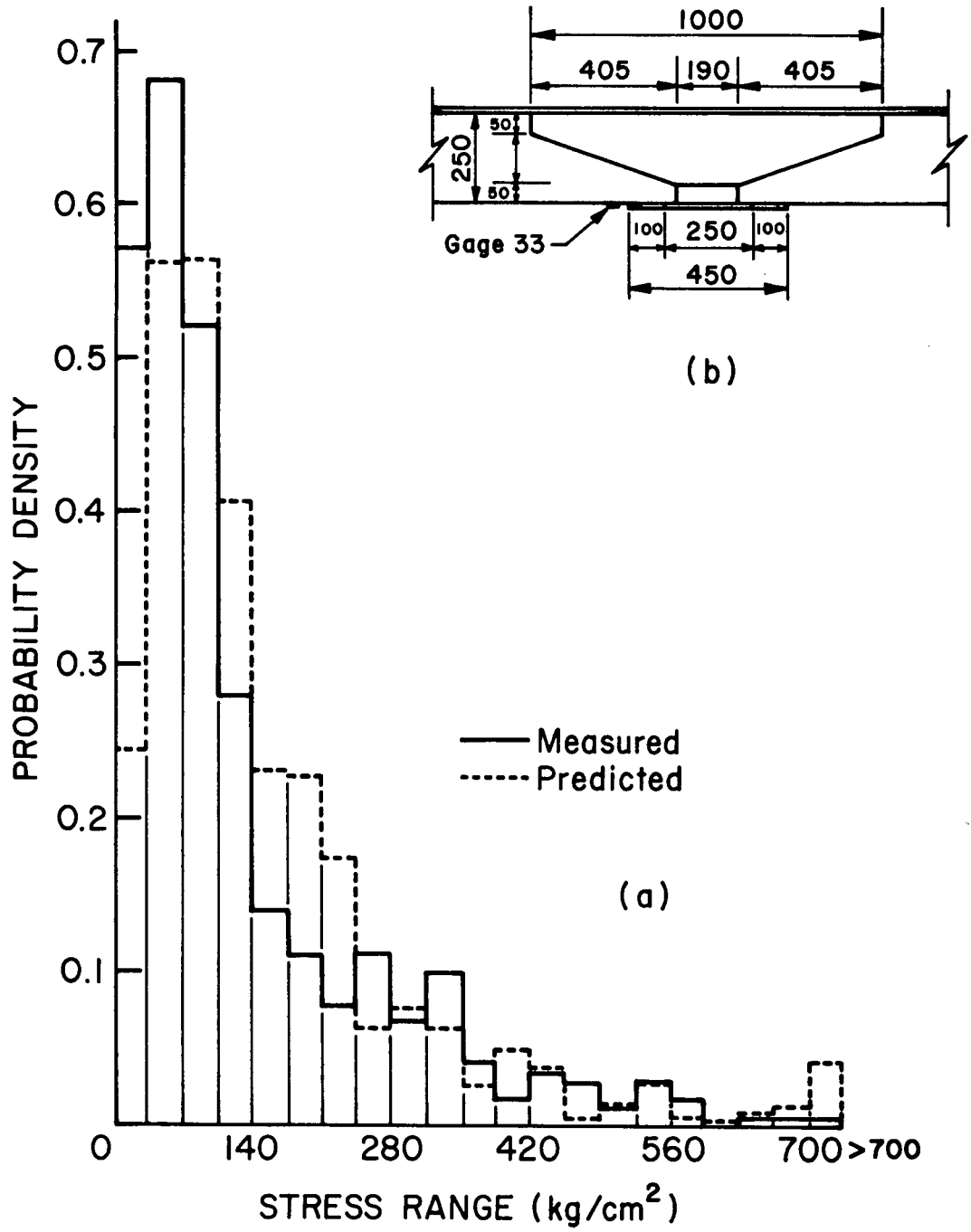


Fig. 6.31 Stress Range Histogram for Gage 33

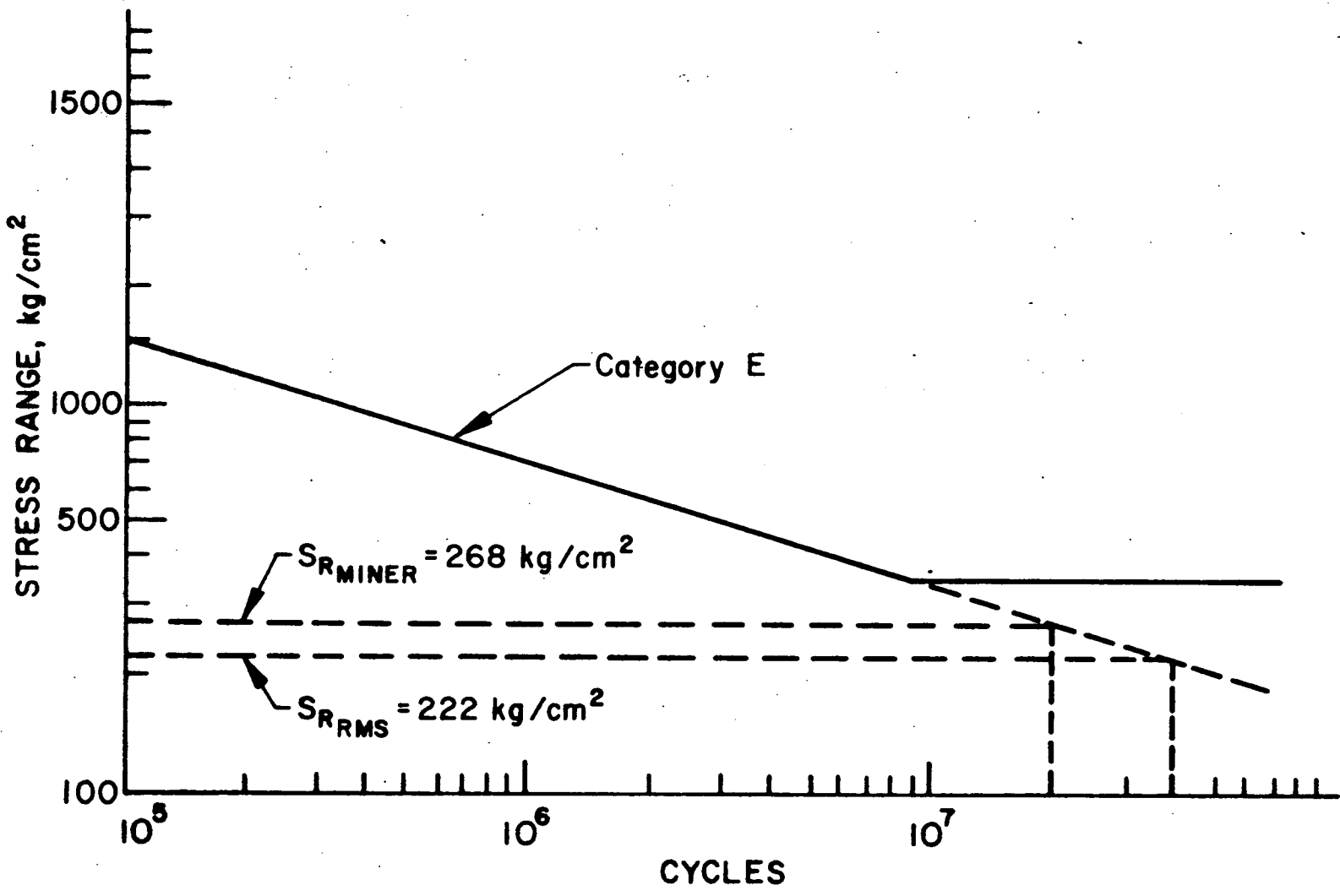


Fig. 6.32 Fatigue Strength Estimate, Splice of the Trapezoidal Stiffener at Gage 33

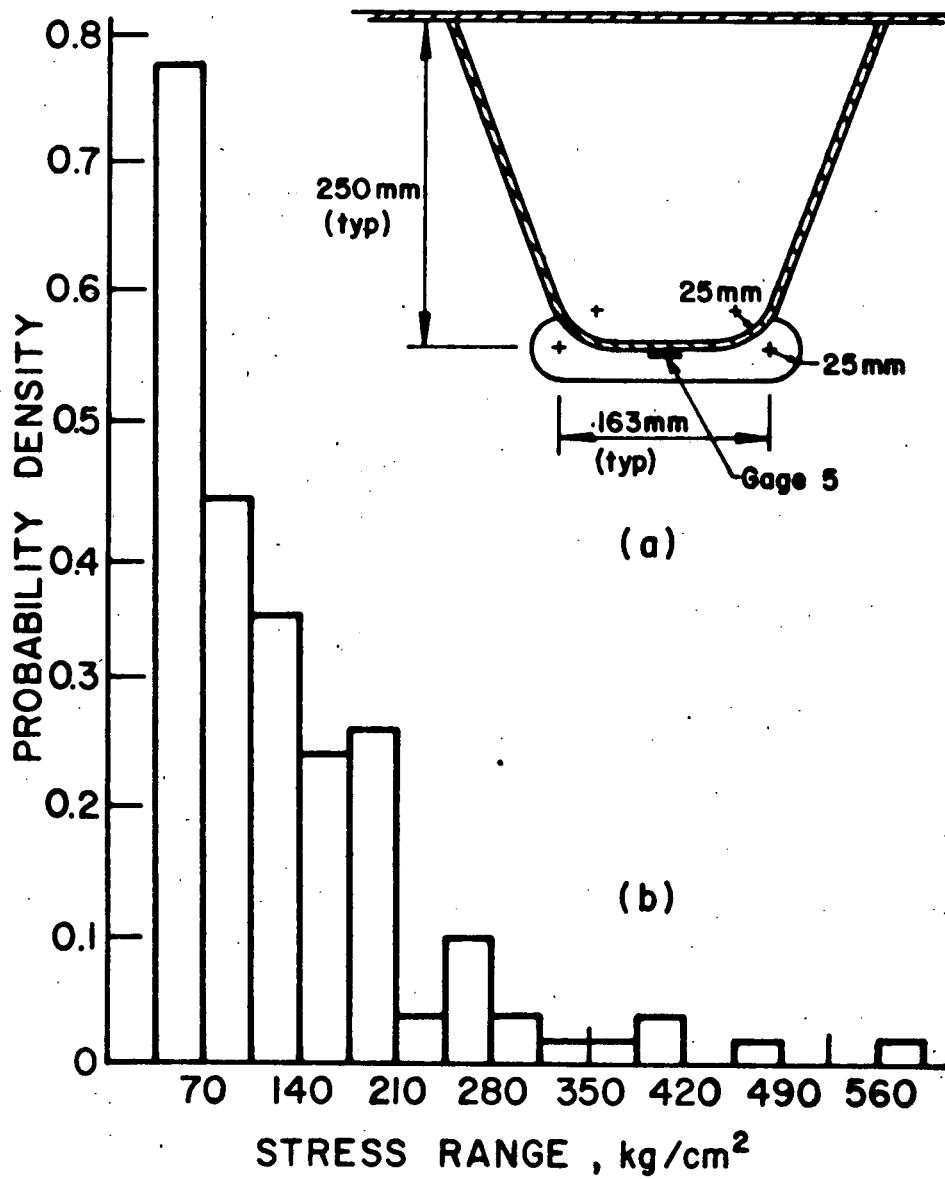


Fig. 6.33 Stress Range Histogram for Gage 5

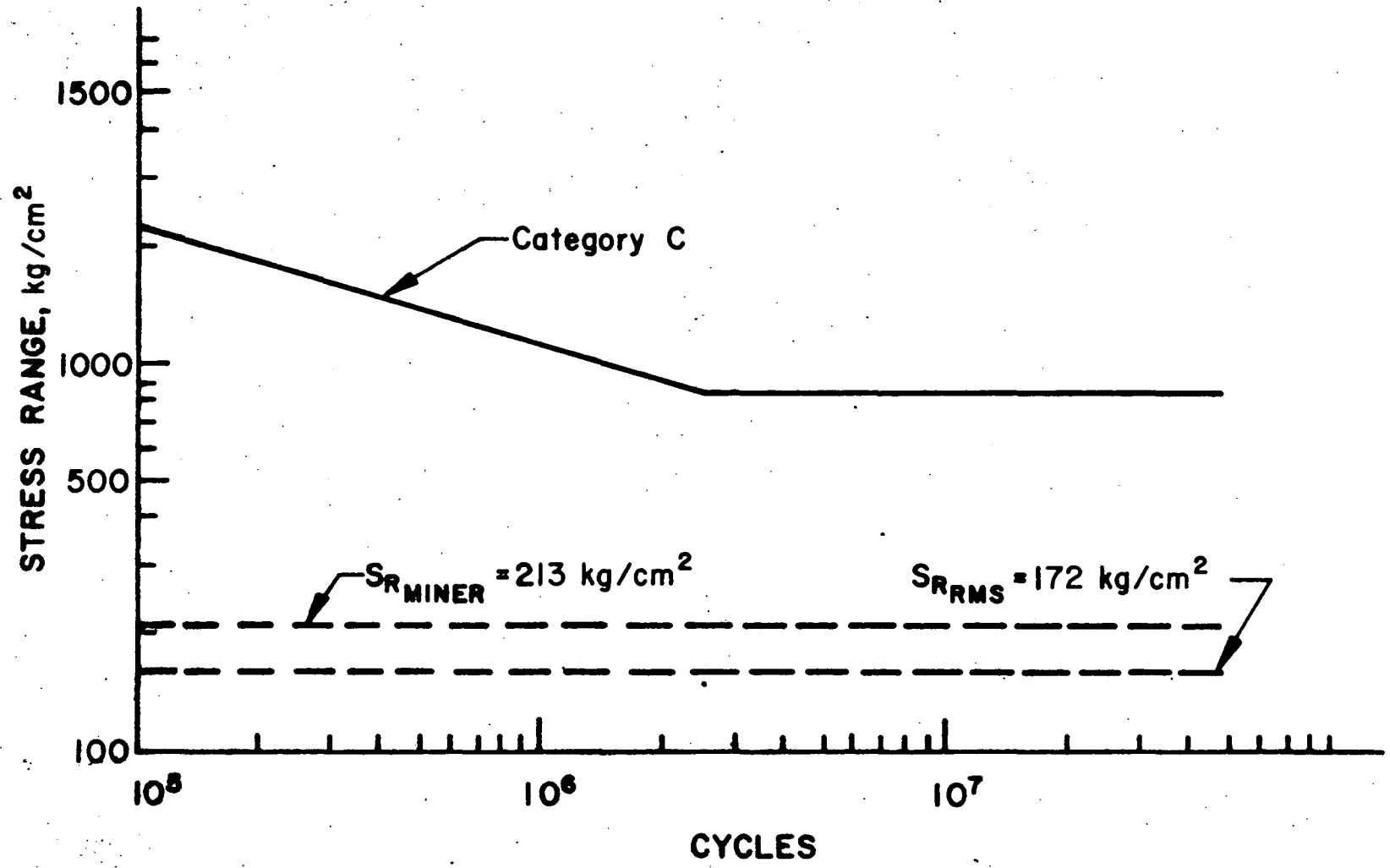


Fig. 6.34 Fatigue Strength Estimate, Deck Stiffener to Floorbeam Connection at Gage 5

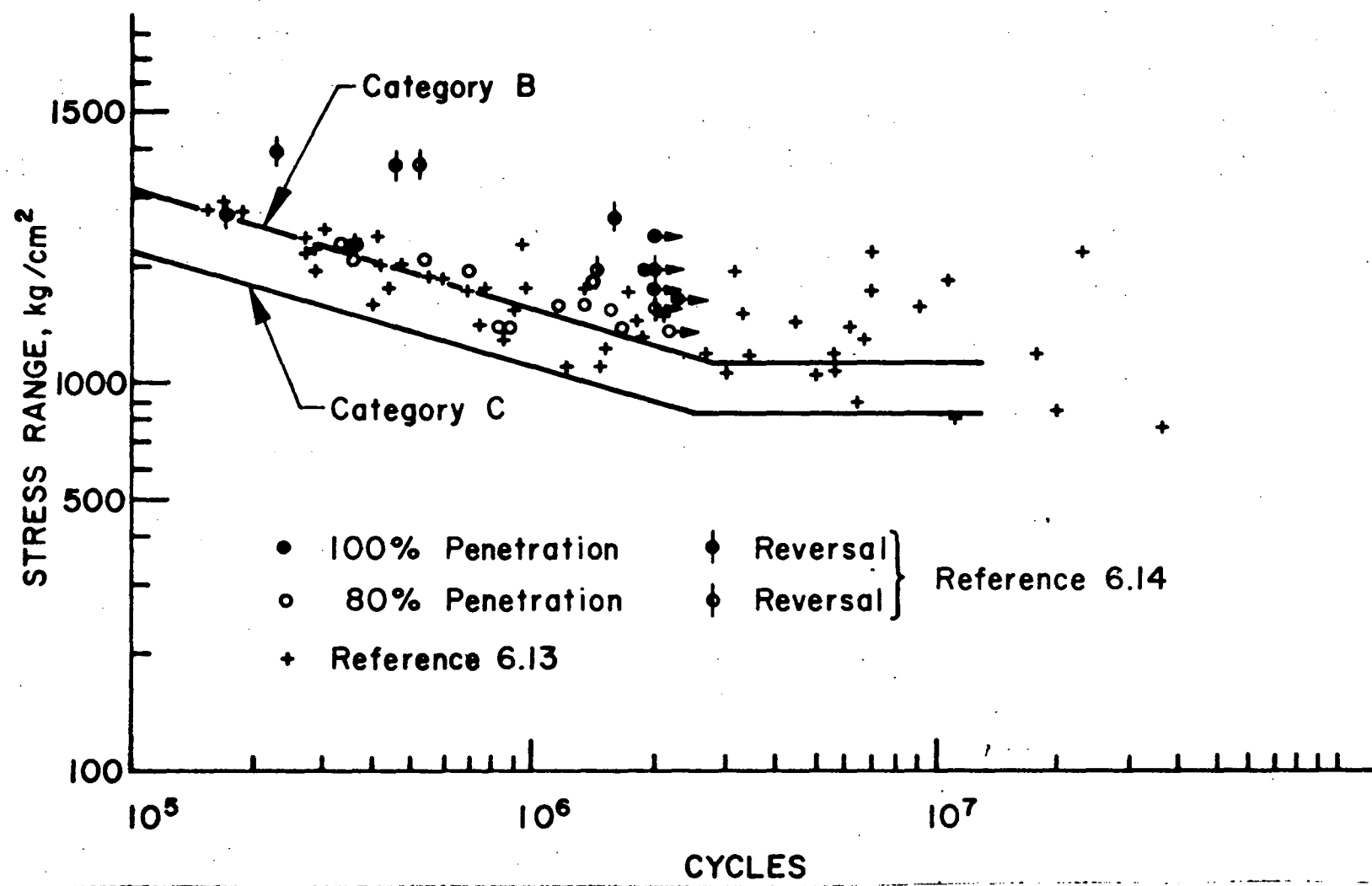


Fig. 6.35 Fatigue Strength Estimate, Deck Stiffener to Deck Plate Connection at Gage 22

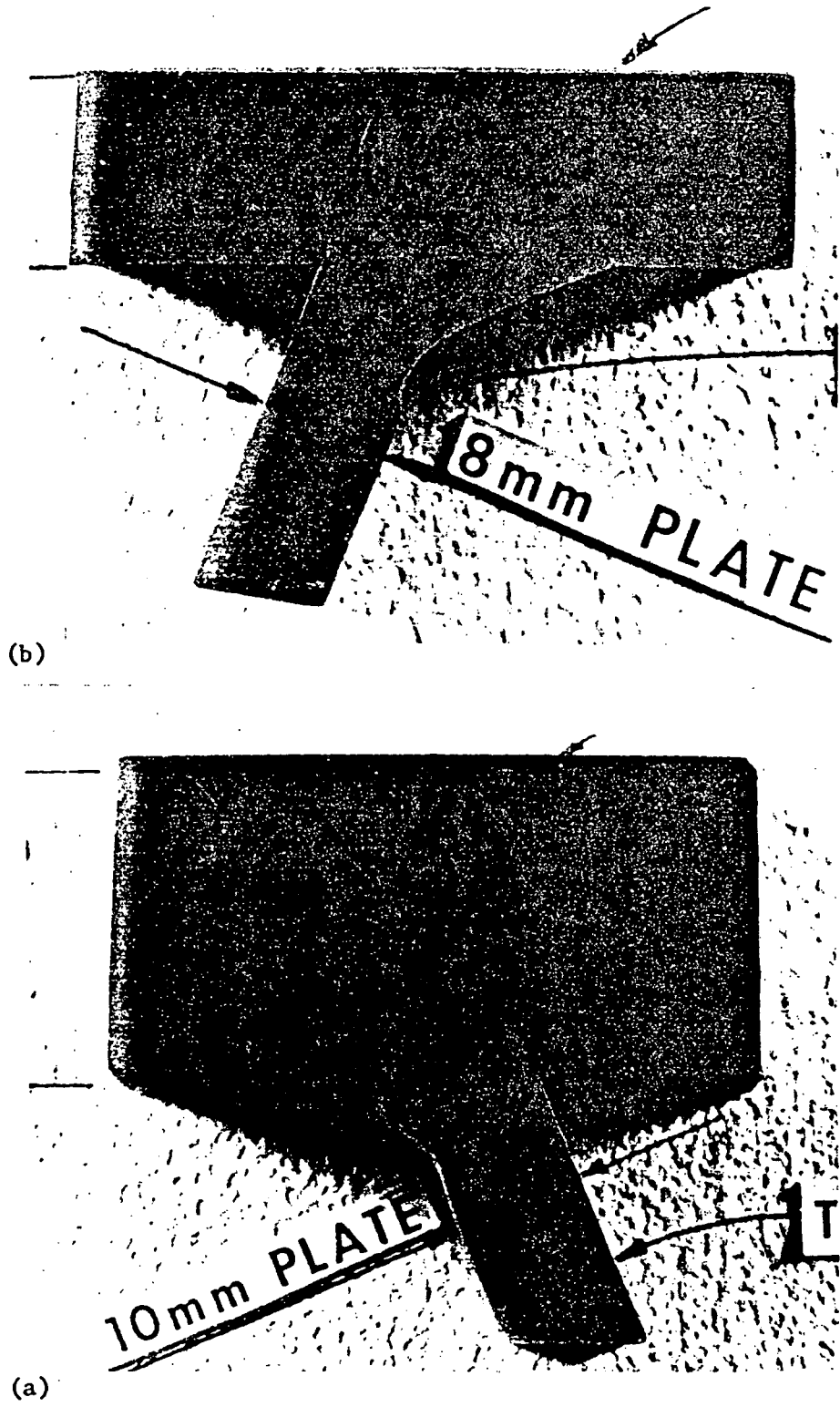


Fig. 6.36 Enlarged Cross Sections of Stiffener Web Plate to Deck Connection

7. SUMMARY AND RECOMMENDATIONS

(A. Ostapenko and J. W. Fisher)

This chapter provides a brief summary of the work performed and the principal findings. Recommendations based on these findings are presented in two parts; the first part covers the recommendations directly applicable to the President Costa e Silva Bridge and the second part gives recommendations applicable to box and plate girder bridges in general. Recommendations are also made for the future use of the instrumentation which was installed in the bridge.

7.1 Summary

The field investigation of the President Costa e Silva Bridge was conducted during the period August 1973 till August 1975. More than 400 electrical-resistance strain and temperature gages, 8 scratch gages and 40 mechanical gage locations were used on the bridge. Five cross sections of the Rio side span were instrumented for static and temperature readings and two locations of the bridge deck for dynamic readings. The investigation consisted of the following subject areas: 1) bridge behavior during construction, 2) stresses in the completed bridge under test loads; 3) temperature distribution and its effect; 4) variation of bridge forces with time--force history; 5) stresses in the orthotropic deck under traffic. The major findings in these subject areas are summarized here. A detailed discussion is given in the summaries and conclusions of the pertinent chapters in the report.

7.1.1 Bridge Behavior During Construction (Art. 3.2 and 3.3)

The principal purpose of the readings taken during construction was to confirm that the stresses in the bridge did not exceed the design stresses and to observe the development of any unforeseen conditions.

Extensive strain readings from the three measuring systems showed that the stresses throughout the bridge were very close to the design stresses and very little redistribution of stresses due to shear lag or other effects took place. The minor deviations observed could be attributed to either the accuracy of readings or to the fact that the actual dimensions of the bridge components (such as thickness and depth) apparently were in some instances slightly greater than the design values. There was a detectable shift of the centroidal axis and the stresses in the bottom flange (which are the highest in the cross section) were lower than the originally computed design levels.

An analysis of the transverse strains caused by construction loads led to the recognition of the importance of the stresses which develop due to Poisson's ratio effect of the primary normal stresses of the girder. The stress changes in transverse stiffening frames were measured up to 600 kg/cm^2 . A method of analysis was developed and the effective width of the plate participating as part of the cross section of the transverse members was determined to be a specific fraction of the member length (0.30L for floor beams and 0.19L for stiffeners). Although the transverse bending stresses due to Poisson's ratio effect were found to be at acceptable levels in the President Costa e Silva Bridge, they may be more critical for the design of

other bridges.

7.1.2 Bridge Behavior Under Test Loads (Art. 3.4)

Twenty-one 17½-ton trucks were placed in four positions on the completed bridge to evaluate the live load response. This study confirmed the accuracy of the analytical methods used in design to compute the stresses due to live load.

The moment from the test trucks placed over one box within the span was found to be distributed to both in proportion of 54% to the loaded box and 46% to the unloaded box. This verified the values of 55 and 45% which were computed theoretically and used in the design analysis. When the test trucks were placed close to the piers or on the 30-meter cantilever beyond the end pier, the load and moment distribution between the two boxes was observed to be about equal leading to a safer actual condition.

7.1.3 Temperature Studies (Chapter 4)

Three sets of readings (in February 1974, June 1974 and January 1975) were made on the bridge to evaluate the temperature distribution and its variation with time and the corresponding thermal stresses.

The greatest daily temperature change was found to occur between approximately 06:00 and 15:00 hours. The maximum temperature change was measured in the top flange. The temperature change dropped by up to 15°C within 0.20-0.30 m below the flange and remained essentially constant over the remainder of the cross section.

A computer program, developed for the thermo-elastic analysis of the President Costa e Silva Bridge, was used to calculate the thermal stresses which resulted from the observed temperature changes. The measured and calculated stresses confirmed that the most significant contribution was due to the statical indeterminance of the bridge girder.

The thermal stresses did not exceed 200 kg/cm^2 and thus posed no safety problem for the President Costa e Silva Bridge. However, they may be more significant in other bridge structures.

7.1.4 Force History--Variation of Bridge Forces With Time (Art. 3.5)

Variation of the forces and stresses in the bridge from day to day was studied by means of the scratch gages and from one period to another several months apart, by means of the mechanical gage.

Excellent scratch gage records were obtained for the construction stages--they complemented the measurements made with other types of gages.

After construction of the bridge, the scratch gages recorded the stress changes produced by the diurnal temperature fluctuation. An exact analysis of these stresses was impossible because of the unpredictable amplification of the scratched zig-zags. This was caused by an inadvertent temperature differential between the scratch gage and the structure surface to which the gage was attached. No significant record was made by the traffic loads as the maximum level of truck traffic during the period of the study was about one-third of the design level.

The scratch gage studies on the completed bridge indicated that scratch gages could provide a continuous monitoring of the bridge for abnormal loads and could be used to pinpoint the exact date of such an occurrence.

Gradual changes of bridge forces over extended periods of time could not be reliably detected with the scratch gages. Mechanical gage readings are more suitable for this purpose as long as the same reference bar is used. Four sets of readings were made with the mechanical gage on the completed bridge during the period of study. These readings also confirmed the gross seasonal deformation changes with temperature. No other significant occurrences were recorded.

7.1.5 Orthotropic Deck Stresses Under Traffic (Art. 2.4 and Chapter 6)

The stresses in the orthotropic deck which resulted from live loads were examined for two conditions: one under controlled truck loads and the other under regular traffic. The stresses were measured at two representative deck splices. They were found to be most significant at the thinnest deck plate.

Statistical analysis of the measured stresses and an examination of the available traffic records and judicious traffic projections for the future show that there is no danger of fatigue cracks developing in the bridge at most welded details. Only the orthotropic deck stiffener splices were predicted to be susceptible to fatigue damage in about fifteen years.

7.2 Recommendations Pertinent to the President Costa e Silva Bridge

The following recommendations are based on the results of the field measurements and studies of the President Costa e Silva Bridge.

7.2.1 Inspection of Orthotropic Deck Components for Fatigue Cracks (Art. 6.6)

Since fatigue cracks may develop in the orthotropic deck stiffener splices, it is recommended that the splices in the trapezoid stiffening ribs at FB17 be inspected at about five-year intervals up to 1990. Thereafter, a yearly inspection should be made. The splice detail at FB17 will thus serve as an indicator of the fatigue behavior of the orthotropic deck at other locations.

The formation of a fatigue crack will not significantly alter the structural behavior. The crack can be readily repaired if and when it occurs and should not become a significant maintenance problem.

7.2.2 Monitoring of Bridge Stresses with Scratch and Mechanical Gages (Art. 3.5.5 and 4.7.2)

A continuous day-to-day monitoring of gross bending stresses in the bridge is recommended by means of scratch gages. These gages will detect overstressing and allow the pinpointing of the date(s) of such overstressing.

Four scratch gages should suffice, one at FB87 (middle of center span), two at FB42 top and bottom, and one at FB17 bottom. The scratch gage targets need only be changed about every three years unless some event is suspected of inducing unusually high stresses. After examination the target can be reinserted back into the gage.

Periodic mechanical gage readings are recommended for detecting gradual changes in bridge forces such as would be caused by pier settlements or other unforeseen phenomena. The readings should be taken over the full cross sections (top and bottom flanges) in the north and south boxes.

7.3 Recommendations for the Use of Instrumentation Installed in the Bridge

The instrumentation installed in the bridge should be in working condition for a number of years. In addition to the work recommended in Art. 7.2, measurements can be made to clarify some uncertainties in these studies and/or to carry out new investigations.

7.3.1 Mechanical Gage System (Art. 4.7.2)

Mechanical gage readings can be used to clarify the discrepancy between the thermal stresses recorded by the scratch gages and the computed stresses. The readings should be taken at FB42 and FB27 (or FB17) on the same warm day one to two hours apart from 6:00 to 18:00 hours. Concurrent measurement of the temperature in the steel plate of the structure* should then be combined with the scratch gage traces for this day in analyzing the results.

In order to improve the accuracy, some or all of the target holes can be reamed (with drill bits) or redrilled. For continuity of the force history, a reading should be taken just prior to the reaming or drilling and right after it.

*Readings on the temperature compensating bars (where they are still intact) can be also utilized. In order to minimize the effect of temperature differential between the bar and the structure, the bar should be covered with some heat insulating material so that the temperature of the bar is the same as of the structure. Readings on the bar should be taken immediately upon uncovering it and the readings on the structure itself next.

7.3.2 Scratch Gages

The accuracy of the diurnal thermal stresses recorded by the scratch gages can be improved by placing a thermal insulation over the gages. For example, a hollowed-out piece of styrofoam placed over the scratch gage and its extension strap and tightly taped to the surface of the structure around it, should serve this purpose.

7.3.3 Orthotropic Deck Gages

The strain gages installed at the splice in the orthotropic deck near FB17 can be utilized for obtaining additional information on the stresses caused by truck traffic. This becomes especially important if the volume of traffic increases in the future beyond the projections used in the analysis reported here.

7.3.4 Additional Temperature Studies

It is recommended that the electrical temperature and strain gages in the bridge be utilized in conducting additional studies on thermal stresses.

The readings taken with the data acquisition unit (B&F) should be accompanied by extensive measurements of the air temperature with a thermometer inside and outside the boxes at different levels in the cross section. The switching panels can be modified to limit the readings only to the gages at FB27, 42 and 57. With fewer handles switched, the time for taking readings will be reduced and the accuracy increased.

Besides being of use for the bridge, the measured data can be utilized as raw material for theses work at the Fundação University, thus contributing to the development of engineering skills

of Brazilian engineers.

7.4 Recommendations for Design of other Steel Bridges

The recommendations below are based on the findings of this study and are made for the design of steel plate and box girders in general.

7.4.1 Method of Analysis

The method of analysis used in the design of the President Costa e Silva Bridge was found to be accurate and is thus recommended for design of other similar bridges.

7.4.2 Temperature Distribution (Art. 4.7.2)

The daily temperature change pattern shown in Fig. 4.22 is recommended for use in the design of plate and box girder bridges under the Rio de Janeiro and similar climatic conditions.

The pattern may be somewhat different for bridges over land and/or when the bridge direction is changed. For example, for bridges in the north-south direction, one side of the bridge may be exposed to the sun while the other is not and this will result in variation of the temperature field across the width.

Bridges which are over land probably will not be cooled as much from below and thus the temperature differential between the top deck and the remainder of the cross section may not be as great.

7.4.3 Thermo-Elastic Analysis of Steel Bridges (Art. 4.7.2)

The method and the computer program developed for thermo-elastic analysis of the President Costa e Silva Bridge can be adjusted

for other girder structures. The analysis is for continuous statically indeterminate bridges in which the thermal stresses due to the indeterminacy may be of significant magnitude.

7.4.4 Scratch Gages (Art. 4.7.2)

Scratch gages are recommended as reliable means for monitoring unforeseen stress changes in important bridge structures. The gages should be thermally insulated from the surrounding air in order to minimize the temperature differential between the gage and the structure surface to which it is attached.

7.4.5 Stresses Due to Poisson's Ratio Effect (Chap. 5)

Design of transverse members, such as floor beams and transverse vertical and bottom stiffeners, should include consideration of the stresses developing from Poisson's ratio effect. This is particularly important for the floor beams since they are also subjected to direct wheel loads. The following effective plate width is recommended for computing these stresses:

$be/L = 0.30$ for members continuous over several supporting members, such as a floor beam over several girders or cantilevering out.

$be/L = 0.20$ for members ending at other members, such as transverse stiffeners ending at the top and bottom flanges.

Depending on the relative dimensions of the cross section of the transverse member the stresses will be in the following approximate ranges:

(0 to 0.3) σ_x : in the plate

-(0.1 to 0.3) σ_x : in the web of stiffener at the junction to the plate

$-(0 \text{ to } 0.3) \sigma_x$: in the flange of the stiffener

Where σ_x is the normal longitudinal stress due to the bending movement and axial force acting on the girder cross section.

8. ACKNOWLEDGEMENTS

This study was conducted by a Lehigh University research team consisting of the following: Professors J. W. Fisher (Project Director), A. Ostapenko, J. H. Daniels, B. T. Yen, R. G. Slutter, Research Assistants J. E. O'Brien and D. H. DePaoli, and Instrumentation Associate H. T. Sutherland. All are on the staff of Fritz Engineering Laboratory, Department of Civil Engineering, Lehigh University (Dr. L. S. Beedle is Director of the laboratory and Dr. D. A. VanHorn is Chairman of the department). In addition, Mr. M. E. Bhatti, a full-time graduate student contributed to the project cost-free with his M. S. Thesis on the thermo-elastic analysis and with the development of the computer program (supervised by Prof. A. Ostapenko).

The project was sponsored by S. A. Empresa de Engenharia e Construção de Obras Especiais - ECEX (formerly called S. A. Empresa de Construção e Exploração da Ponte Presidente Costa e Silva) with Col. J. C. Guedes and Prof. F. Valle, the consecutive Presidents. The authors especially recognize the support given this project by Director of the Technical Division of ECEX, initially, the late Eng. J. P. Ferreira and, at end, Eng. J. B. S. Corrêa. Administrative Director I. M. da Silva was responsible for financial arrangements. The researchers are thankful not only for the financial support, but also for the help and equipment generously provided during the field work.

Gratitude is due to the ECEX staff who directly contributed in the field work -- Eng. C. J.A. Hess and the members of SEOBES headed by Eng. P.S. da Costa, with Mr. L. G. Chehab and others, who were particularly helpful during the January 1975 field trip.

Grateful acknowledgment is due to Messrs. G. F. Fox and H. J. Graham of Howard Needles Tammen & Bergendoff International, Inc. (HNTB) who were instrumental in initiating this project.

The researchers also extend their thanks to the resident staff of HNTB in Rio de Janeiro for their unfailing assistance in making arrangements on site, the installation of the instrumentation and in taking the readings. Particularly helpful was Mr. E. P. Rausa, the staff director. Members of the staff involved were: Messrs. M. D. Miller, S. Rosputko, R. W. Werner, R. Alhadeff, L. C. S. Ribeiro, R. D. V. Baptista, and several others.

Grateful recognition is given to those of the Fritz Engineering Laboratory Staff who contributed to the success of the project: Mr. H. T. Sutherland who tirelessly installed all the electrical gages in the bridge, several student helpers, particularly Mr. D. P. Erb who assisted during the concluding revisions of this report, Messrs. R. N. Sopko and J. M. Gera and their staffs who attended to the photographic and drafting work, and the staff of the Word Processing Center of the Laboratory who patiently typed, retyped and retyped this report.

9. REFERENCES

9.1 References for Chapter 1 - Introduction

- 1.1 Empresa de Engenharia e Construção de Obras Especiais (ECEX)
PONTE PRESIDENTE COSTA E SILVA, (Bridge Inauguration Issue),
ECEX, Rio de Janeiro, March 1974.
- 1.2 Ruiz, R.
A TRAVESSIA RIO-NITEROI (Crossing Rio-Niteroi),
Jornal dos Transportes, Vol. 4, No. 31, Publication of
Ministry of Transportation, Rio de Janeiro, 8 March 1974.
- 1.3 Cottrill, A.
RIO-NITEROI BRIDGE - FIRST MAJOR LIFT GIVES HEAD START
TO TIGHT COMPLETION PROGRAMME, New Civil Engineer,
Institution of Civil Engineers, London, 9 August 1973.
- 1.4 Lally, A.
Steel Box Girder Bridges, AISC Engineering Journal,
Vol. 10, No. 4, AISC, New York, 4th Quarter 1973.
- 1.5 Fisher, J. W.
Proposal for Research Project FIELD STUDY ON THE PRESIDENT
COSTA E SILVA BRIDGE, Submitted to ECEX, Fritz Engineering
Laboratory Report No. 397.1, Lehigh University, July 1973.
- 1.6 Ostapenko, A., Fisher, J. W.
FIELD STUDY ON THE PRESIDENT COSTA E SILVA BRIDGE --
PROGRESS REPORT No. 1 (Period from 19 July 1973 to
31 March 1974), Fritz Engineering Laboratory Report
No. 397.2, Lehigh University, April 1974.
- 1.7 Ostapenko, A., Yen, B. T., Daniels, J. H., and Fisher, J. W.
FIELD STUDY ON THE PRESIDENT COSTA E SILVA BRIDGE --
PROGRESS REPORT No. 2 (Period from 1 April 1974 to
30 September 1974), Fritz Engineering Laboratory Report
No. 397.4, Lehigh University, October 1974.
- 1.8 Ostapenko, A., Daniels, J. H. and Fisher, J. W.
FIELD STUDY ON THE PRESIDENT COSTA E SILVA BRIDGE --
PROGRESS REPORT No. 3 (Period from 1 October 1974 to
31 March 1975), Fritz Engineering Laboratory Report
No. 397.5, Lehigh University, April 1975.

REFERENCES (Cont.)9.2 References for Chapter 2 - Instrumentation Systems

- 2.1 Prewitt Associates
SCRATCH STRAIN GAGE (SSG) INSTALLATION MANUAL, Prewitt
Associates, Lexington, Ky., 1972.

9.3 References for Chapter 3 - Static Stresses and Force History

- 3.1 Departamento Nacional de Estradas de Rodagem
NORMAS BRASILEIRAS - NBC CARGAS MOVEIS EM PONTES
RODOVIARIAS, 1960.
- 3.2 Kuzmanovic, B. O.
SOME DESIGN PROBLEMS OF LARGE BOX GIRDER BRIDGES,
Journal of Structural Division, ASCE, Vol. 98, No. ST9,
Proc. Paper 9193, September 1972, pp. 2059-2077.

9.4 References for Chapter 4 - Temperature Studies

- 4.1 Reynolds, J.C. and Emanuel, J.H.
THERMAL STRESSES AND MOVEMENTS IN BRIDGES, Journal of the Structural Division, ASCE, Vol. 100, ST1, Proc. Paper 10275, January 1974, pp. 63-78.
- 4.2 Mortlock, J.D.
THE INSTRUMENTATION OF BRIDGES FOR THE MEASUREMENT OF TEMPERATURE AND MOVEMENTS, TRRL Report LR641, Transport and Road Research Laboratory, Crowthorne, Berks., 1974.
- 4.3 Emerson, Mary
THE CALCULATION OF THE DISTRIBUTION OF TEMPERATURE IN BRIDGES, TRRL Report LR561, Transport and Road Research Laboratory, Crowthorne, Berks., 1973.
- 4.4 Leger, Ph.
INFLUENCE OF TEMPERATURE GRADIENTS ON THE BEARING REACTIONS OF A STRUCTURE, Preprints of the Colloquium on Bridge Loading, IABSE, Cambridge, England, April 1975.
- 4.5 Johns, D. J.
THERMAL STRESS ANALYSIS, 1st Edition, Pergamon Press, Oxford/New York, 1965.
- 4.6 Hunt, B., and Cooke, N.
THERMAL CALCULATIONS FOR BRIDGE DESIGN, Journal of Structural Division, ASCE, Vol. 101, No. ST9, Proc. Paper 11545, September 1975, pp. 1763-1781.
- 4.7 Radolli, M., and Green, R.
THERMAL STRESSES IN CONCRETE BRIDGE SUPERSTRUCTURES UNDER SUMMER CONDITIONS, Transportation Research Record 547 (Concrete and Steel Bridges), Washington, 1975, pp. 23-36.
- 4.8 Norris, C. H. and Wilbur, J.B.
ELEMENTARY STRUCTURAL ANALYSIS, 2nd Edition, McGraw-Hill Book Company, Inc., New York, 1960.
- 4.9 Hall, A.S. and Woodhead, R.W.
FRAME ANALYSIS, Second Edition, John Wiley and Sons, Inc., New York, 1967.
- 4.10 Bhatti, M.E.
THERMO-ELASTIC STRUCTURAL ANALYSIS OF A THREE-SPAN BOX GIRDER BRIDGE, Report on Special Problems in Civil Engineering, (C.E. 481, Supervisor A. Ostapenko), Department of Civil Engineering, Lehigh University, May 1975.

9.5 References for Chapter 5 - Effective Plate Width and Transverse Stresses Due to Poisson's Ratio Effect

- 5.1 Meek, J. C.
MATRIX STRUCTURAL ANALYSIS, McGraw-Hill, New York, 1971.

9.6 References for Chapter 6 - Stress History - Orthotropic Deck
Stresses Under Traffic

- 6.1 Nunn, D.E. and Morris, S.A.H.
TRIALS OF EXPERIMENTAL ORTHOTROPIC BRIDGE DECK PANELS
UNDER TRAFFIC LOADING, Department of the Environment,
TRRL Report LR627, Crowthorne, 1974.
- 6.2 Fisher, J.W. and Viest, I.M.
FATIGUE LIFE OF BRIDGE SUBJECTED TO CONTROLLED TRUCK
TRAFFIC Preliminary Publication, 7th Congress, IABSE,
1964.
- 6.3 Cudney, G.R.
THE EFFECTS OF LOADING ON BRIDGE LIFE, Highway Research
Record No. 253, Highway Research Board, 1968.
- 6.4 Galambos, C.F. and Heins, C.P.
LOADING HISTORY OF HIGHWAY BRIDGES, COMPARISON OF STRESS
RANGE HISTOGRAMS, Highway Research Board, 1971.
- 6.5 Moses, F.
TRUCK LOADING MODEL FOR BRIDGE FATIGUE, Proceedings,
Specialty Conference on Metal Bridges, ASCE, Nov. 1974.
- 6.6 Fisher, J.W.
GUIDE TO 1974 AASHTO FATIGUE SPECIFICATIONS AISC, 1974.
- 6.7 Fisher, J.W., Yen, B.T. and Daniels, J.H.
FATIGUE DAMAGE IN THE LEHIGH CANAL BRIDGE FROM DISPLACEMENT
INDUCED SECONDARY STRESSES, Fritz Engineering Laboratory
Report No. 386.5, 1975.
- 6.8 Fisher, J.W., Albrecht, P.A. Yen, B.T., Klingerman, D.J.
McNamee, B.M.
FATIGUE STRENGTH OF STEEL BEAMS WITH TRANSVERSE
STIFFENERS AND ATTACHMENTS, NCHRP Report 147, Highway
Research Board, 1974.
- 6.9 Fisher, J.W., Frank, K.H., Hirt, M.A. and McNamee, B.M.
EFFECT OF WELDMENTS ON THE FATIGUE STRENGTH OF STEEL
BEAMS NCHRP Report 102, Highway Research Board, 1970.

- 6.10 Schilling, C.G., Klippstein, K.H., Barsom, J.M. and Blake, G.T.
FATIGUE OF WELDED STEEL BRIDGE MEMBERS UNDER VARIABLE-AMPLITUDE LOADINGS, Research Results Digest, No. 60, April 1974, TRB.
- 6.11 Miner, M.A.
CUMULATIVE DAMAGE IN FATIGUE, Journal of Applied Mechanics, Vol. 12, Sept. 1945.
- 6.12 Nunn, D.E.
AN INVESTIGATION INTO THE FATIGUE OF WELDS IN AN EXPERIMENTAL ORTHOTROPIC BRIDGE DECK PANEL, Department of the Environment, TRRL Report LR 629, Crowthorne, 1974.
- 6.13 Maddox, S.J.
THE BEHAVIOR OF TRAPEZOIDAL STIFFENER TO DECK PLATE WELDS IN ORTHOTROPIC BRIDGE DECKS, Department of the Environment, TRRL Report SR 96, UC, Crowthorne, 1974.
- 6.14 Seim, C. and Ferwerda, R.
FATIGUE STUDY OF ORTHOTROPIC BRIDGE DECK WELDS, Report M & R No. 666473, California Dept. of Public Works, Div. of Highways and Div. of Bay Toll Crossings, 1972.

APPENDIX A -- SYSTEM OF ELECTRICAL STRAIN
AND TEMPERATURE GAGES

(A. Ostapenko and J. E. O'Brien)

A general description of the electrical gage instrumentation is presented in Articles 2.1, 2.2 and 2.4. A more detailed description for the purpose of trouble shooting and modification is given in this appendix.

Location of the instrumented cross sections is shown in Fig. 2.1 and a summary of all electrical gages installed in the bridge is given in Table A.1. The gages are subdivided into the linear (longitudinal or transverse), three-gage rosettes, and temperature gages. The number of each type is given for each cross section separated between the north and south boxes. At the bottom of the table are shown the single-gage equivalents for each section and box. These are obtained by counting the three gages of each rosette individually and adding the other gages in a cross section or box.

The gages installed on the orthotropic deck at FB17 and FB42 for dynamic readings are shown in parenthesis. Their exact location is described in Art. 2.4, and the details of other gages are given in Articles A.1, A.2, and A.3.

A.1 Location of Gages in Cross Sections

Figures A.1 through A.6 show the location of the gages in the cross sections. The linear gages running parallel to the roadway

(longitudinal gages) are indicated by dots (•); those running perpendicular to the roadway (transverse gages) are indicated by dashes (-). Temperature gages (located only at FB27 and FB57) are indicated by triangles (▲). Rosettes, indicated by crosses (+), are located at the position where the cross intersects the outline of the cross section. One figure is used per section except for the section at FB27, the transverse gages are shown separately from the other gages in Figs. A.2 and A.3.

The system for identifying and labeling gages is based on using each six-lead cable for two gages. Thus each cable was given a number (shown inside an ellipse in Figs. A.1 to A.6) and the two three-lead parts of each cable were designated by A and B; part A having black, yellow, and red leads and part B having blue, green and white leads. The arrowed lines going from one gage to another through one or more ellipses became the method of identifying gages. If it is not indicated, it is understood that A precedes B for each cable number. If the arrows go from a one-component gage to another one-component gage, then only one cable is used; the first gage (indicated by the arrows) is the A part and the second is the B part. Since rosettes have three gage components, the following order is used: the longitudinal component (parallel to the roadway) first, the diagonal component second, and the transverse component (perpendicular to the roadway) third. Thus, for example, in Fig. A.2 the arrows go from a single longitudinal gage through ellipses 43 and 44 to a rosette, two cables (Nos. 43 and 44) are needed (4 components). The A part of the first cable (No. 43) serves

the longitudinal part of the rosette, and the A and B parts of the No. 44 cable serve the diagonal and transverse components of the rosette, respectively. This basic rule is used in all Figures A.1 to A.6 unless otherwise indicated in the ellipse.

The group of numbers for the gages at FB17 and FB27 is independent from the numbers used for the gages at FB42, FB51 and FB57. However, this duplication should not cause any confusion since each group is connected to a separate switching panel -- one at FB27 and the other at FB51.

A.2 Wiring and Switching System, Correlation Table

A.2.1 Wiring System in Bridge

The general layout of the wiring system is shown in Fig. 2.4c. The cables from the gages in the instrumented sections go to the connection panels inside the north box at FB27 and 51 as symbolically indicated in Fig. 2.4c by the rectangles with dashes. Here, connection is made by soldering together the terminals of the connection panel with the terminals on the movable "handles" (bastões). These handles are indicated as brushes with projecting terminals. The cables from the handles (brushes) go through a hole in the north web of the north box at FB51 and are connected to the plug terminals in the junction box installed in the curb. For taking readings, the sockets of the cables from the data acquisition unit on a truck are plugged into the terminals in the junction box. This connection is indicated in Fig. 2.4c with a small plug to the left of the truck.

Different numbering systems are used for the cables leading from the handles to the junction box than for the cables from the gages to the switching panels. The long cables from the handles at FB27 to the junction box consist of two portions with different sets of numbers. The splice is indicated with a solid dot on the cable line between FB42 and FB51 in Fig. 2.4c.

A.2.2 Switching Stations -- Connection Panels

The gages were read in four groups of 90 gages. The change from group to group was performed at the switching stations by unsoldering the handles on the connection panels from one group of gages and soldering them to the next group. The arrangement of the gage terminals on the connection panels is shown in Figs. A.7 and A.8 for FB27 and FB51, respectively. The basic arrangement of the panels is the same except for the number of handles used -- four at FB27 (40 gages) and five at FB51 (50 gages).

For example, in Fig. A.8, the panel is subdivided into two parts: Part 1 for Handles (bast.) Nos. 1 and 2 and Part 2 for Handles No. 3,4 and 5. In each part there are four groups of columns of gages (cabos) for switching each set of handles (bast.). This arrangement was found to be convenient for having two or three solderers work simultaneously in order to reduce the time needed for each switching operation. Figure A.8a shows a switching operation in progress.

A.2.3 Correlation Table of B & F, Cable and Gage Nos.

In order to facilitate identification of recorded data, trouble shooting and/or modification of the system, the numbering (labeling) sets of the gages, cables, connectors, and the channels of the data acquisition unit (B & F) are correlated in Fig. A.9. The tabulation in the figure follows the path from a channel of the data acquisition unit (B & F) to the corresponding gage in a particular group.

Column 1 - B & F channel numbers from 00 to 99. The first 14 channels (Nos. 00 to 13) were modified for reading temperature gages. SHD means "shielding" of the cable which is grounded to the chassis of B & F. The listing is subdivided into sets according to the plug numbers given in Column 2. Channel Nos. 90 to 99 are connected only to Plug No. 5 but not to the gages.

Columns 2 and 3 - Plug No. and the pin Nos. are given for each channel (three pins are needed per channel). The plugs are housed in the junction box at FB51. Each plug has a corresponding socket with the cables permanently connected to the channels inside the B & F unit. The arrangement of the plugs in the junction box and of the pins in each plug are described in Art. A.3.

Column 4 - The No. of the cable going from the junction box through the web at FB51 to a handle at a switching station. However, the cables leading to the station at FB27 (channel Nos. 08 to 47) are first spliced near FB51 to long extension cables whose numbers are shown in Col. 5.

Column 5 - Extension cables from FB51 to the handles at FB27.

Column 6 - Handle No. for the switching station at FB27. The first figure is the sequential number for all nine handles of the stations at FB27 and FB51 (1 to 9). The second figure in parenthesis is the local handle number at FB27 ((1) to (4)) which is used in Fig. A.7.

Column 7 - Handle number for the switching station at FB51.

Column 8 - Position of each gage channel on the handle, ten channels (five cables, 30 wires) per handle. The number runs from the tip to the holding end, that is, from top to bottom of the columns in the connection panels (Figs. A.7 and A.8).

Columns 9 to 12 - Each column gives the gages read in a particular group when the five handles are correspondingly soldered on the connection panels.

Plugs 6 and 7 in the junction box serve one cable each. One cable (No. 6) is for the telephone and the other (No. 7) for power. The power cable has outlets at the switching stations at FB27 and FB51 to be used for lighting and for electric soldering guns. The power can be either tapped in the bridge or from an outside generator.

A.3 Junction Box in Curb at FB51

The junction box at FB51 is a steel plate box embedded in the concrete curb and covered with a steel plate measuring 27 by 38 cm. The cover plate has a rubber seal and is fastened with six flash counter-sunk screws. Inside is an aluminum alloy plate on which the plugs for connecting the B & F unit and the telephone are mounted.

Arrangement of the plugs is shown in Fig. A.10. Plug Nos. 1 to 5 are for the B & F channels, Plug No. 6 for the telephone and the rectangle labeled No. 7 is the hold through which goes a power cable with a regular outlet at the end. A circle with a center dot in plug outline indicates a screw and a double circle a sleeve which are used for joining or separating the plug and the socket. Letters SHD indicate location of the pins in a plug where the shielding is connected.

Figures A.11 to A.16 give the following: arrangement of the pins on the plugs, the pin numbering system on the plugs, and Nos. of the cables connected to the pins. The arrangement of the pinholes in the corresponding sockets is shown in Figs. A.17 to A.21. The following symbols are used in Figs. A.11 to A.21:

- Large numbers designate the cables going through the web into the junction box, e.g., 4.
- Small encircled numbers designate the B & F channels, e.g., (98).
- The pins in the plugs and pinholes in the sockets are denoted with solid dots and their arrangement and labeling are shown exactly as they appear in reality.

A.4 Appendix A - Tables and Figures

Table A.1 Summary of Electric - Resistance Gages
Installed in Rio Side Span

Floor Beam	17			27		42			51			57		Total	
	Deck	Box		Box		Deck	Box		Truss	Box		Box			
		No.	So.	No.	So.		No.	So.		No.	So.	No.	So.		
1	2	3	4	5	6	7	8	9	10	11	12	13	14	15	
Linear Gages	Long.	(3)	6	3	6	4	(5)	8	4	-	5	-	8	8	52
	Trans.	(18)	-	-	22	6	(20)	24	20	10	-	-	-	-	82
Rosettes		(4)	12	5	8	4	(3)	-	-		8	2	12	6	57
Temperature		-	-	-	14	10	-	-	-		-	-	18	10	52
Single Gage Equivalents*															
Static Readings			42	18	66	32		32	24	10	29	6	62	36	357
Dynamic Readings		(33)					(34)								(67)
Total of Single Gage Equivalents														424	

* A rosette has three single gages
() Deck gages were for dynamic readings

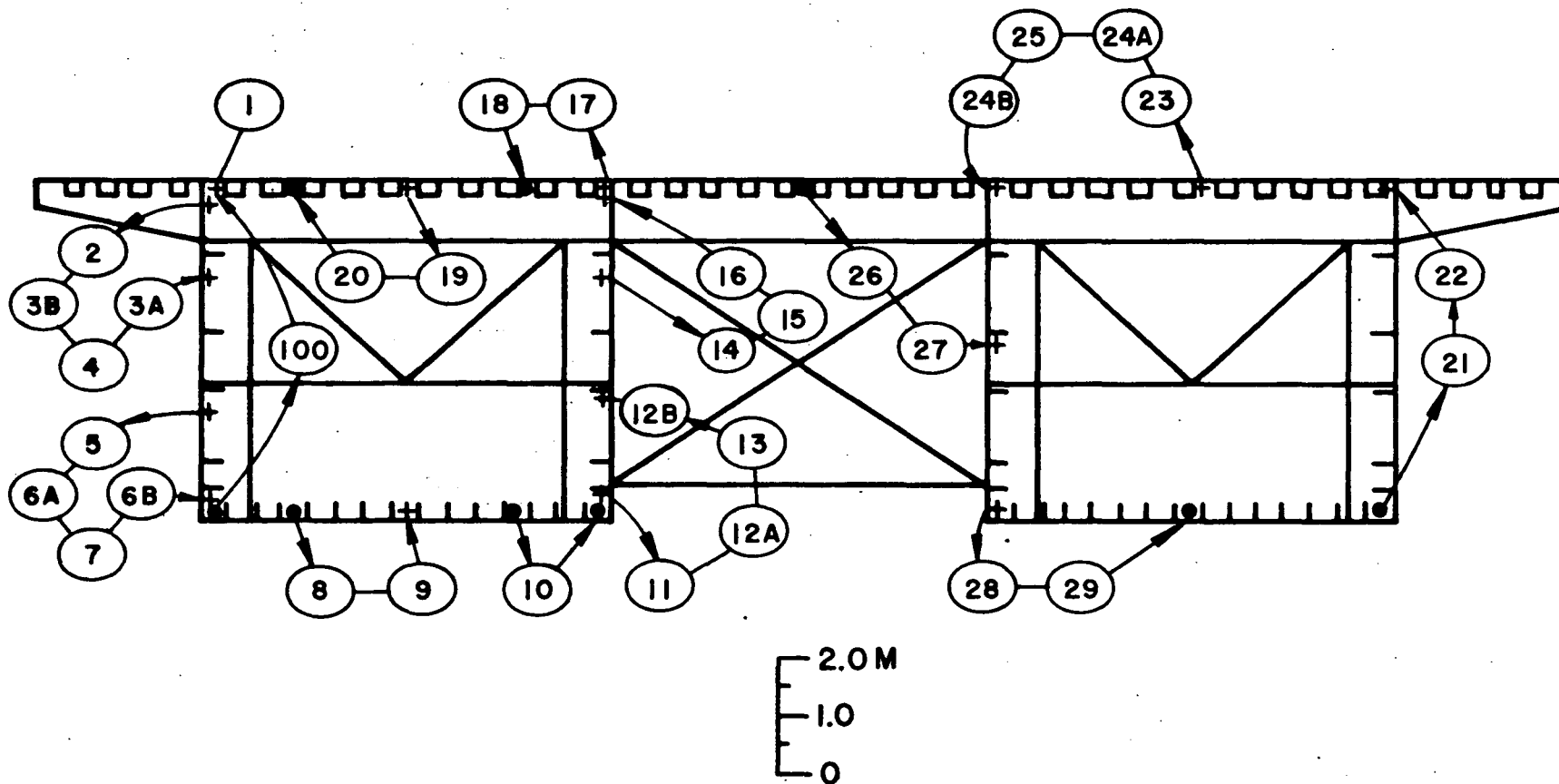


Fig. A.1 Location of Electrical Gages in Section at FB17

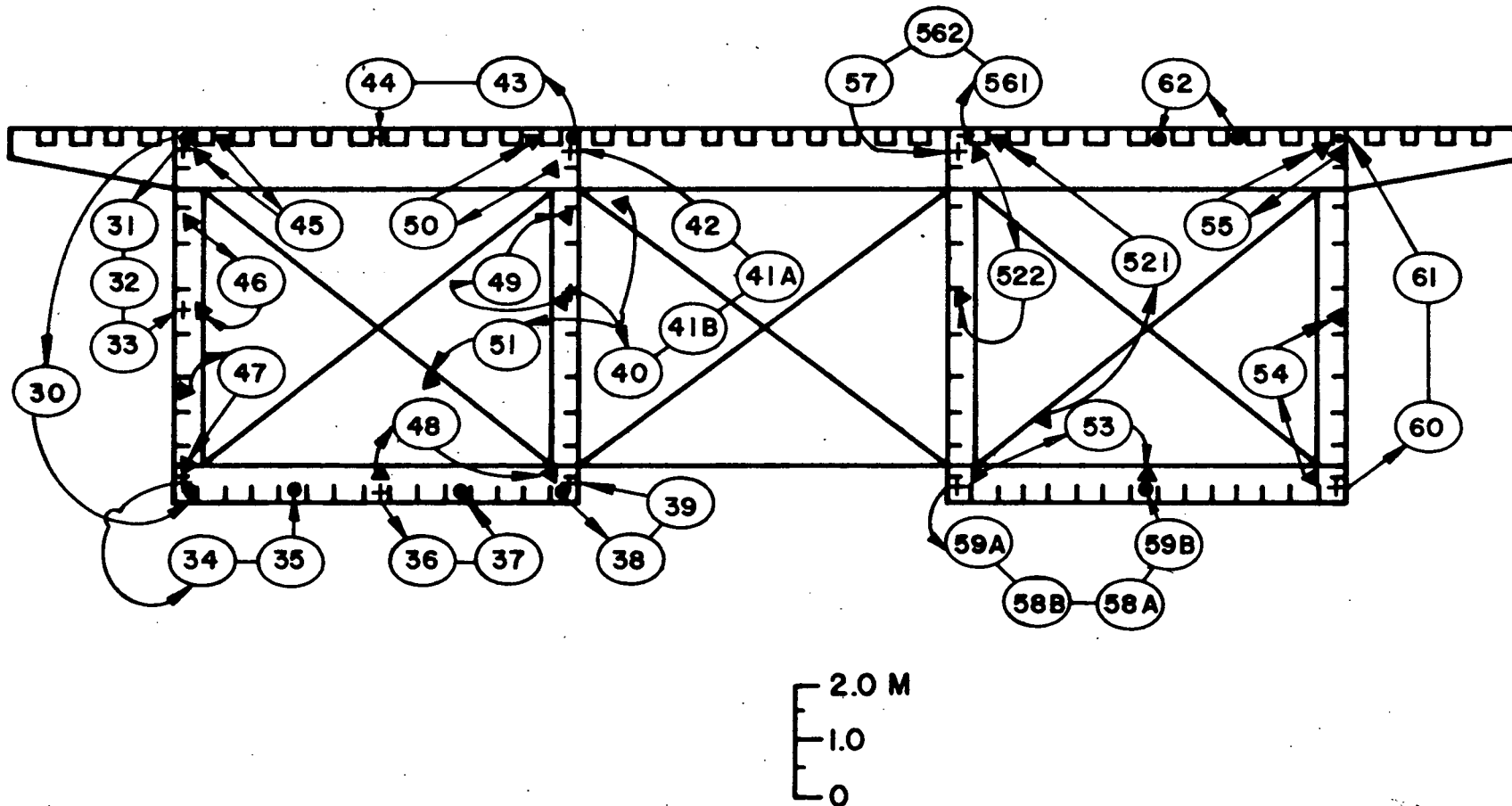


Fig. A.2 Location of Electrical Gages (except for transverse) in Section at FB27

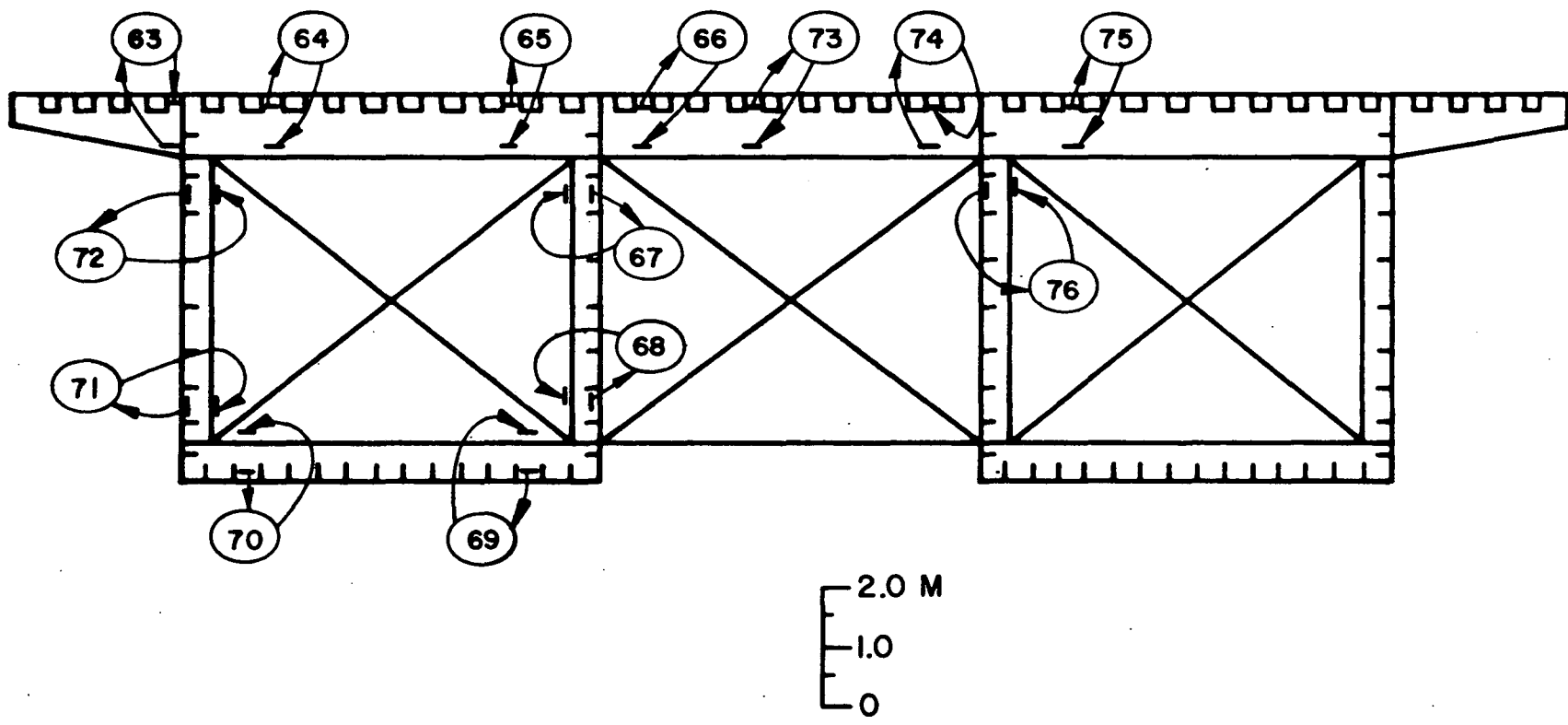


Fig. A.3 Location of Transverse Electrical Gages in Section at FB27

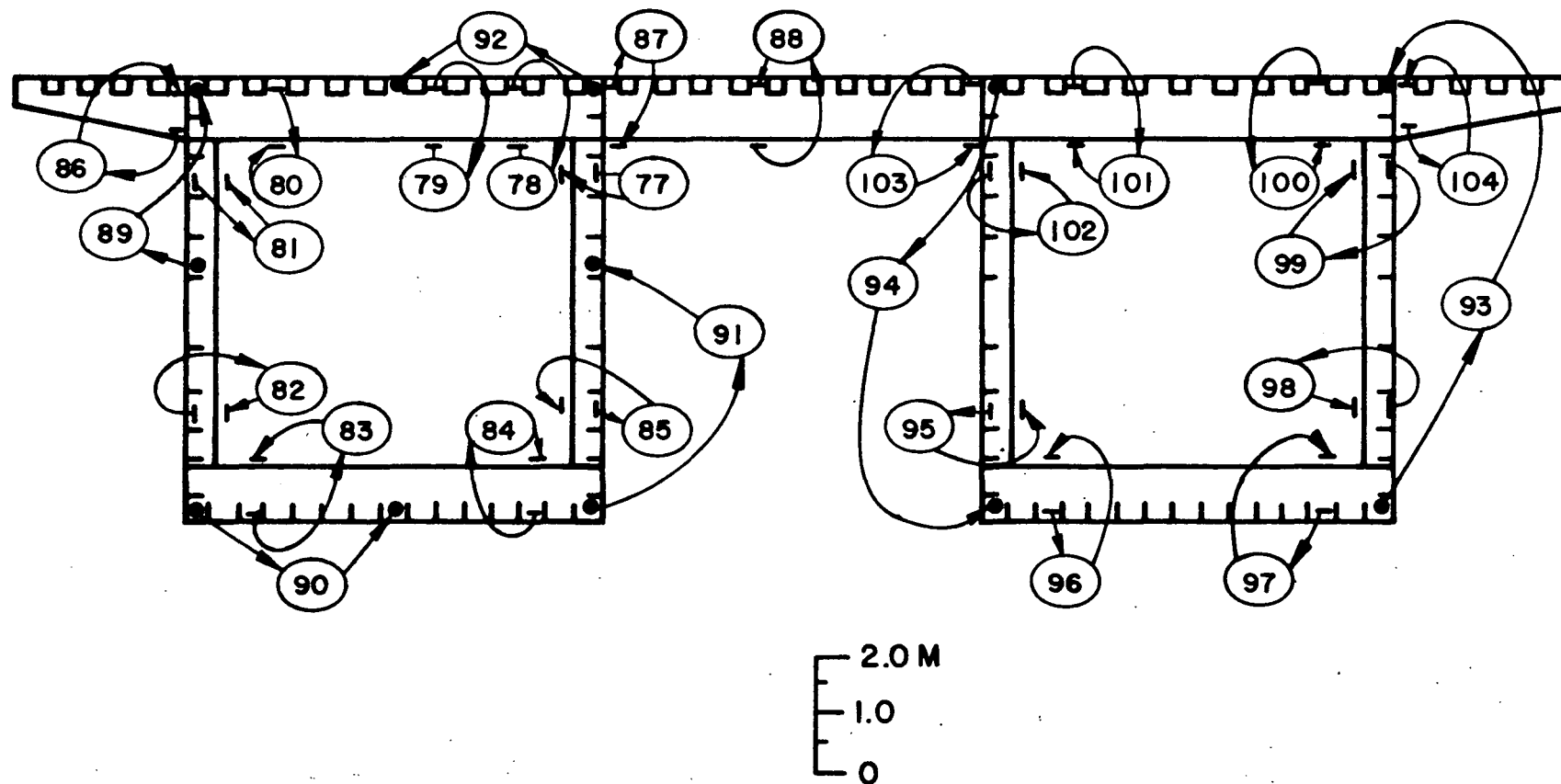


Fig. A.4 Location of Electrical Gages in Section at FB42

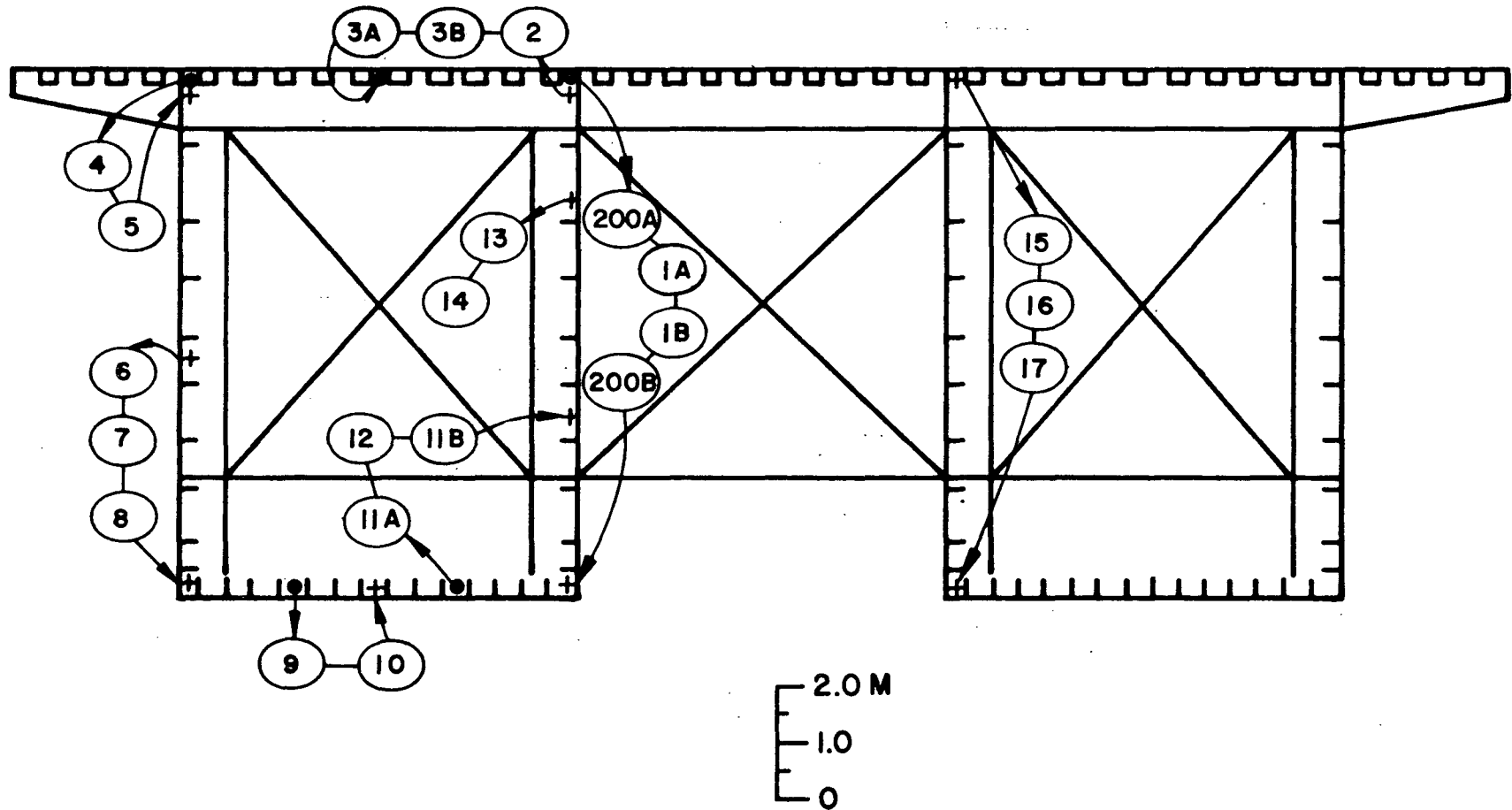


Fig. A.5 Location of Electrical Gages in Section at FB51

Disposição dos Cabos no Quadro das Ligações -- FB27N
 (Cable Arrangement on the Connection Panel -- FB27N)

FB27

Grupo	Parte 1								Parte 2							
	1		2		3		4		1		2		3		4	
	1	2	1	2	1	2	1	2	3	4	3	4	3	4	3	4
Cabos	100A	1A	5A	38A	8A	13A	23A	28A	32A	43A	64A	36A	18A	33A	74A	562A
	100B	1B	5B	38B	8B	13B	23B	28B	32B	43B	64B	36B	18B	33B	74B	562B
	21A	2A	6A	39A	9A	14A	24A	29A	59A	44A	70A	37A	19A	62A	75A	57A
	21B	2B	6B	39B	9B	14B	24B	29B	59B	44B	70B	37B	19B	62B	75B	57B
	30B	3A	7A	40A	10A	15A	25A	71A	34A	45A	65A	48A	20A	521B		51A
	30A	3B	7B	40B	10B	15B	25B	71B	34B	45B	65B	48B	20B	522A		51B
	60A	4A	68A	41A	11A	16A	26A	72A	35A	46A	66A	49A	22A	54A	76A	521A
	61B	4B	68B	41B	11B	16B	26B	72B	35B	50A	66B	49B	22B	54B	76B	53A
	31A	60B	69A	42A	12A	17A	27A	73A	561A	50B	67A	46B	58A	55A	63A	53B
	61A	31B	69B	42B	12B	17B	27B	73B	561B	47B	67B	47A	58B	55B	63B	522B
Col.	1	2	3	4	5	6	7	8	9	10	11	12	13	14	15	16

Fig. A.7 Arrangement of Cables on Connection Panel at FB27

Disposição dos Cabos no Quadro das Ligações -- FB51N
(Cable Arrangement on the Connection Panel)

FB 51

Grupo	Parte 1								Parte 2											
	1		2		3		4		1			2			3			4		
	Bast.	1	2	1	2	1	2	1	2	3	4	5	3	4	5	3	4	5	3	4
Cabos	91A	25B	77A	82A	87A	95A	7A	12A	22A	21A	28A	29A	4A	36A	100A	141A	24A	62A	61A	66A
	91B	18A	77B	82B	87B	95B	7B	12B	22B	21B	28B	29B	4B	36B	100B	141B	24B	62B	61B	66B
	93A	18B	78A	83A	88A	96A	8A	13A	17A	22A	44A	35A	30A	41A	101A	142A		57A	56A	49A
	93B	25A	78B	83B	88B	96B	8B	13B	17B	22B	44B	35B	30B	41B	101B	142B		57B	56B	49B
	200B	15B	79A	84A	90A	97A	9A	14A	6A	23A	45A	31A	39A	45B	102A	143A		64A	63A	50A
	200A	16A	79B	84B	90B	97B	9B	14B	6B	23B	42A	31B	39B	46A	102B	143B		65B	63B	50B
	92B	1A	80A	85A	89A	98A	10A	54A	19A	26A	42B	32A	37A	47A	103A	34A	40A	59A	58A	51A
	92B	1B	80B	85B	89B	98B	10B	54B	19B	26B	46B	32B	37B	47B	103B	34B	40B	59B	64B	51B
	16B	2A	81A	86A	94A	99A	11A	55A	20A	27A	43A	33A	38A	48A	104A	5A	53A	60A	65A	52A
	15A	2B	81B	86B	94B	99B	11B	55B	20B	27B	43B	33B	38B	48B	104B	5B	53B	60B	58B	52B
Col.	1	2	3	4	5	6	7	8	9	10	11	12	13	14	15	16	17	18	19	20

397.6

Fig. A.8 Arrangement of Cables on Connection Panel at FB57

B&F No.	Plug No.	Pin No.	Cable No.		Handle No.		Gage No. at Handle	Gage No. by Groups			
			Thru web FB51	FB27 to FB51	at FB27	at FB51		1	2	3	4
1	2	3	4	5	6	7	8	9	10	11	12
00	1	66,65,64	41A			5	3	44A	41A		49A
01		63,62,61	B				4	B	B		B
02		60,59,58	42A				5	45A	45B		50A
03		57,56,55	B				6	42A	46A		B
04		54,53,52	43A				7	B	47A	40A	51A
05		51,50,49	B				8	46B	B	B	B
06		48,47,46	45A				9	43A	48A	53A	52A
07		45,44,43	B				10	B	B	B	B
08		42,41,40	46A	211A	9(4)		5	45A	48A	521B	51A
09		39,38,37	B	B			6	B	B	522A	B
10		36,35,34	47A	212A			7	46A	49A	54A	521A
11		33,32,31	B	B			8	50A	B	B	53A
12		30,29,28	48A	215A			9	B	46B	55A	B
13		27,26,25	B	B			10	47B	47A	B	522B
14		24,23,22	35A	220A	6(1)		1	100A	5A	8A	23A
15		21,20,19	B	B			2	B	B	B	B
16		18,17,16	36A	216A			3	21A	6A	9A	24A
17		15,14,13	B	B			4	B	B	B	B
18		12,11,10	37A	217A			5	30B	7A	10A	25A
19	9, 8, 7	B	B			6	30A	B	B	B	
SHD		1 to 6									
20	2	4,12,18	38A	218A			7	60A	68A	11A	26A
21		25,31,37	B	B			8	61B	B	B	B
22		43,49,55	39A	221A			9	31A	69A	12A	27A
23		62,70,76	B	B			10	61A	B	B	B
24		1, 8,15	90A	219A	7(2)		1	1A	38A	13A	28A
25		22,28,34	B	B			2	B	B	B	B
26		40,46,52	18A	201A			3	2A	39A	14A	29A
27		58,65,73	B	B			4	B	B	B	B
28		5,13,20	25A	204A			5	3A	40A	15A	71A
29		26,32,38	B	B			6	B	B	B	B
30		44,50,56	77A	207A			7	4A	41A	16A	72A
31		63,71,77	B	B			8	B	B	B	B
32		2,10,16	78A	208A			9	60B	42A	17A	73A
33		23,29,35	B	B			10	31B	B	B	B

Fig. A.9 Correlation of B&F, Plug, Cable and Gage Nos.

B&F No.	Plug No.	Pin No.	Cable No.		Handle No.		Gage No. at Handle	Gage No. by Groups			
			Thru web FB51	FB27 to FB51	at FB27	at FB51		1	2	3	4
1	2	3	4	5	6	7	8	9	10	11	12
34		41,47,53	79A	200A	8(3)		1	32A	64A	18A	74A
35		59,66,74	B	B			2	B	B	B	B
36		7,14,21	80A	202A			3	59A	70A	19A	75A
37		27,33,39	B	B			4	B	B	B	B
38		45,51,57	81A	203A			5	34A	65A	20A	
39		64,72,78	B	B			6	B	B	B	
40		3,11,17	82A	205A			7	35A	66A	22A	76A
41		24,30,36	B	B			8	B	B	B	B
42		42,48,54	83A	206A			9	561A	67A	58A	63A
43		60,67,75	B	B			10	B	B	B	B
SHD		79,80,82									
44	3	4,12,18	89A	209A	9(4)		1	43A	36A	33A	562A
45		25,31,37	B	B			2	B	B	B	B
46		43,39,55	85A	210A			3	44A	37A	62A	57A
47		62,70,76	B	B			4	B	B	B	B
48		1, 8,15	86A			1	1	91A	77A	87A	7A
49		22,28,34	B				2	91B	B	B	B
50		40,46,52	87A				3	93A	78A	88A	8A
51		58,65,73	B				4	93B	B	B	B
52		5,13,20	88A				5	200B	79A	90A	9A
53		26,32,38	B				6	200A	B	90B	B
54		44,50,56	84A				7	92A	80A	89A	10A
55		63,71,77	B				8	92B	B	89B	B
56		2,10,16	91A				9	16B	81A	94A	11A
57		23,29,35	B				10	15A	B	B	B
58		41,47,53	92A			2	1	25B	82A	95A	12A
59		59,66,74	B				2	18A	B	B	B
60		7,14,21	19A				3	18B	83A	96A	13A
61		27,33,39	B				4	25A	B	B	B
62		45,51,57	20A				5	15B	84A	97A	14A
63		64,72,78	B				6	16A	B	B	B
64		3,11,17	21A				7	1A	85A	98A	54A
65		24,30,36	B				8	1B	B	B	B
66		42,48,54	22A				9	2A	86A	99A	55A
67		60,67,75	B				10	2B	B	B	B
SHD		79,80,82									

Fig. A.9 (Cont. 1) Correlation of B&F, Plug, Cable and Gage Nos.

B&F No.	Plug No.	Pin No.	Cable No.		Handle No.		Gage No. at Handle	Gage No. by Groups				
			Thru web FB51	FB27 to FB51	at FB27	at FB51		1	2	3	4	
1	2	3	4	5	6	7	8	9	10	11	12	
68	4	4,12,18	23A			3	1	22A	29A	100A	62A	
69		25,31,37	B				2	22B	B	B	B	
70		43,49,55	24A				3	17A	35A	101A	57A	
71		62,70,76	B				4	B	B	B	B	
72		1, 8,15	26A				5	6A	31A	102A	64A	
73		22,28,34	B				6	B	B	B	65A	
74		40,46,52	27A				7	19A	32A	103A	59A	
75		58,65,73	B				8	B	B	B	B	
76		5,13,20	28A				9	20A	33A	104A	60A	
77		26,32,38	B				10	B	B	B	B	
78		44,50,56	29A				4	1	21A	4A	141A	61A
79		63,71,77	B				2	2	21B	4B	B	B
80		2,10,16	30A				3	3	3A	30A	142A	56A
81		23,29,35	B				4	4	3B	B	B	B
82		41,47,53	31A				5	5	23A	39A	143A	63A
83		59,66,74	B				6	6	B	39B	B	B
84		7,14,21	32A				7	7	26A	37A	34A	58A
85	27,33,39	B				8	8	B	B	34B	64B	
86	45,51,57	33A				9	9	27A	38A	5A	65A	
87	64,72,78	B				10	10	B	B	B	58B	
88	3,11,17	34A				5	1	28A	36A	24A	66A	
89	24,30,36	B				2	2	28B	36B	B	B	
SHD		79,80,82										
90	5	C, H, M	1A									
91		S, W,AA	B									
92		A, E, K	4A									
93		P, U, Y	B									
94		D, J, N	11A									
95		T, X, BB	B									
96		B, F, L	12A									
97		R, V, Z	B									
98		EE, KK, CC	?A									
99		HH, MM, FF	B									
SHD		DD, JJ, NN										
SHD	6	1, 2, 3 5, 6, 7 4, 8	14A B	214A B				Telephone				
	7		13A B	213A B				Power				

Fig. A.9 (Cont. 2) Correlation of B&F, Plug, Cable and Gage Nos.

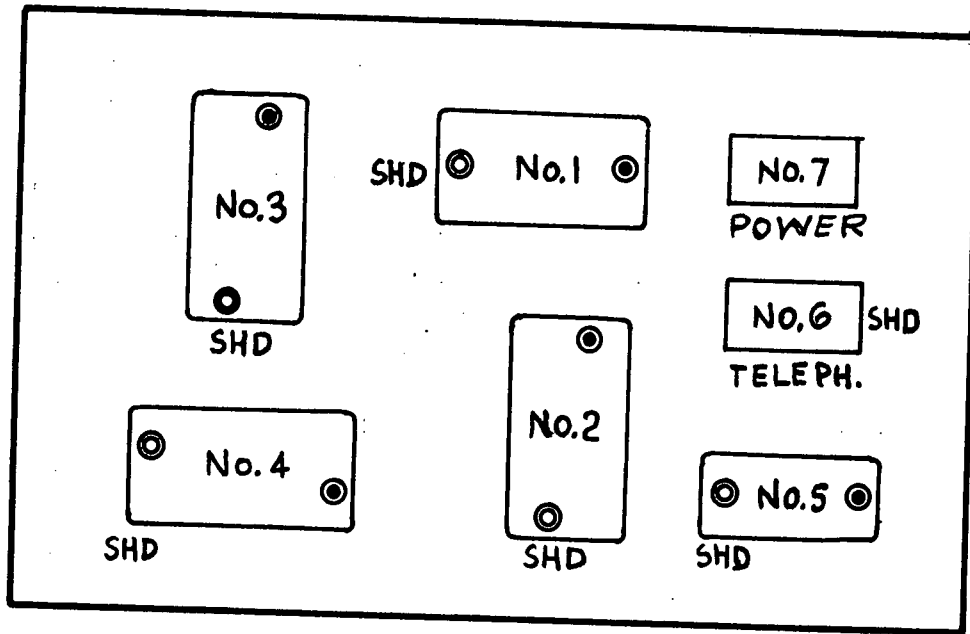


Fig. A.10 Arrangement of Plugs in Junction Box at FB51

SHIELDING					
06	05	04	03	02	01
012	011	010 37	09	08	07
018	017	016 36	015	014	013
024	023	022 35	021	020	019
030	029	028 48	027	026	025
036	035	034 47	033	032	031
042	041	040 46	039	038	037
048	047	046 45	045	044	043
054	053	052 43	051	050	049
060	059	058 42	057	056	055
066 bk	065 y	064 r	063 bu	062 g	061 w
black	yellow	red	blue	green	white

Fig. A.11 Arrangement of Pins and Cables on Plug No. 1

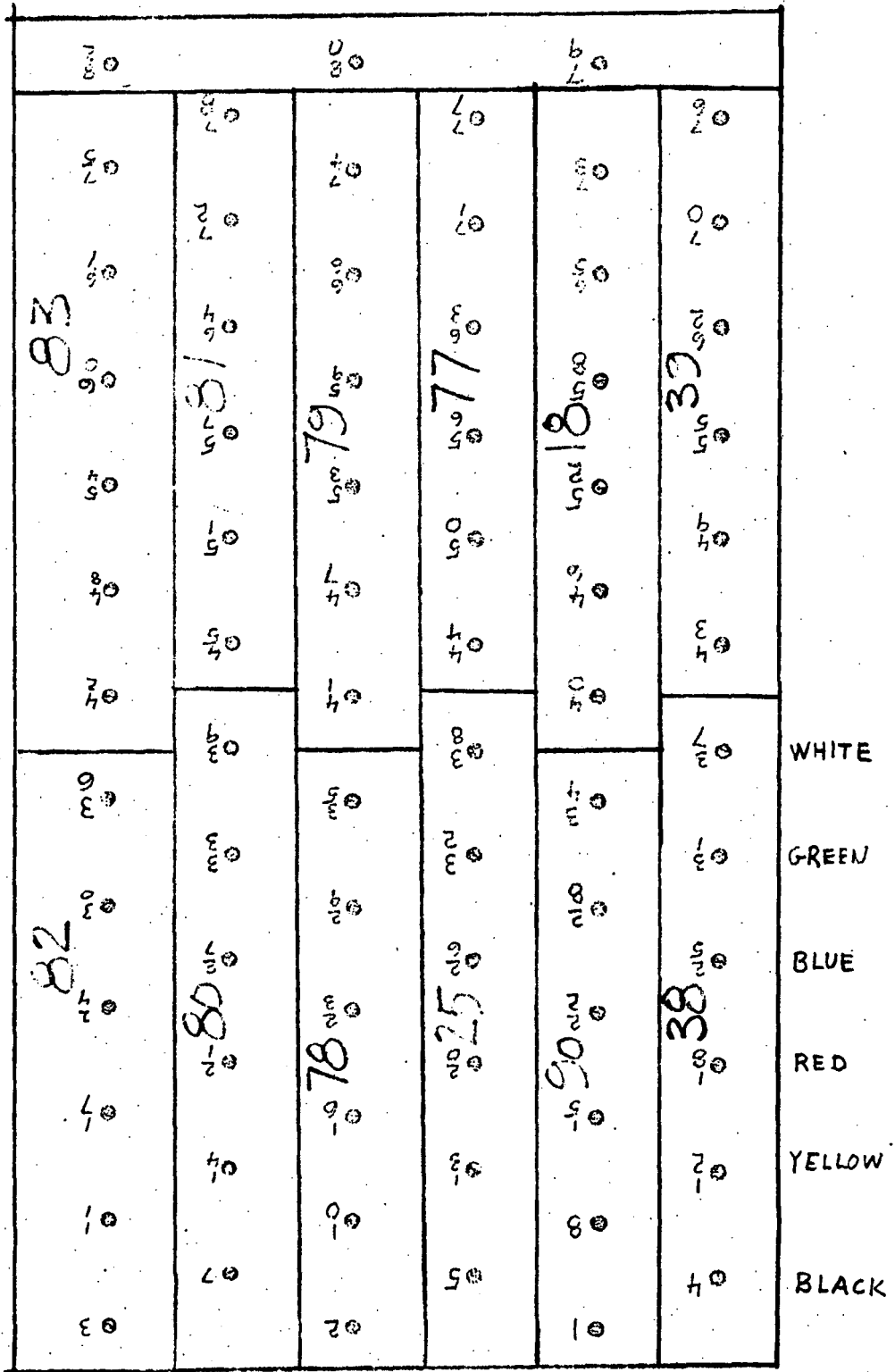
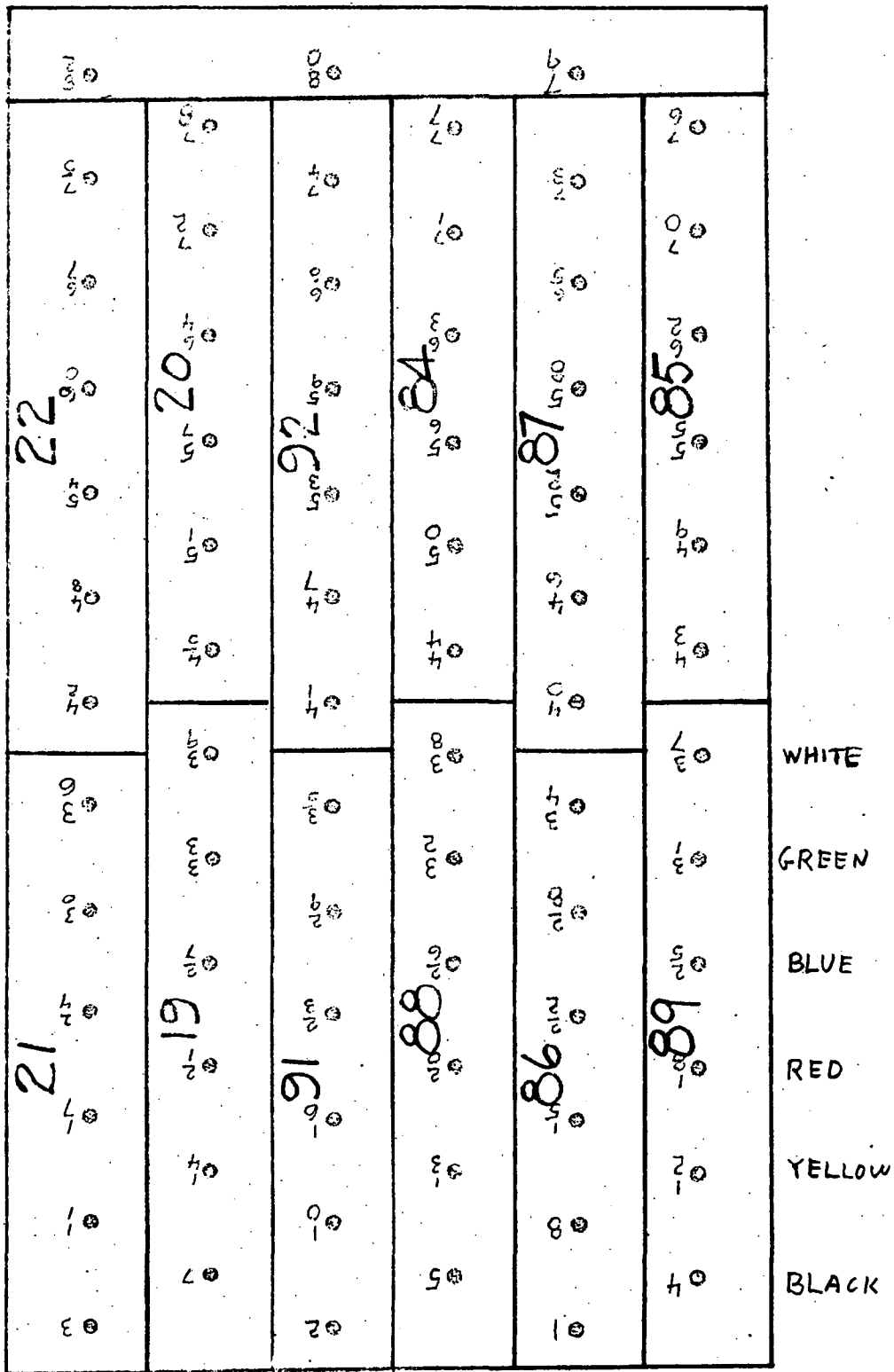


Fig. A.12 Arrangement of Pins and Cables on Plug No. 2



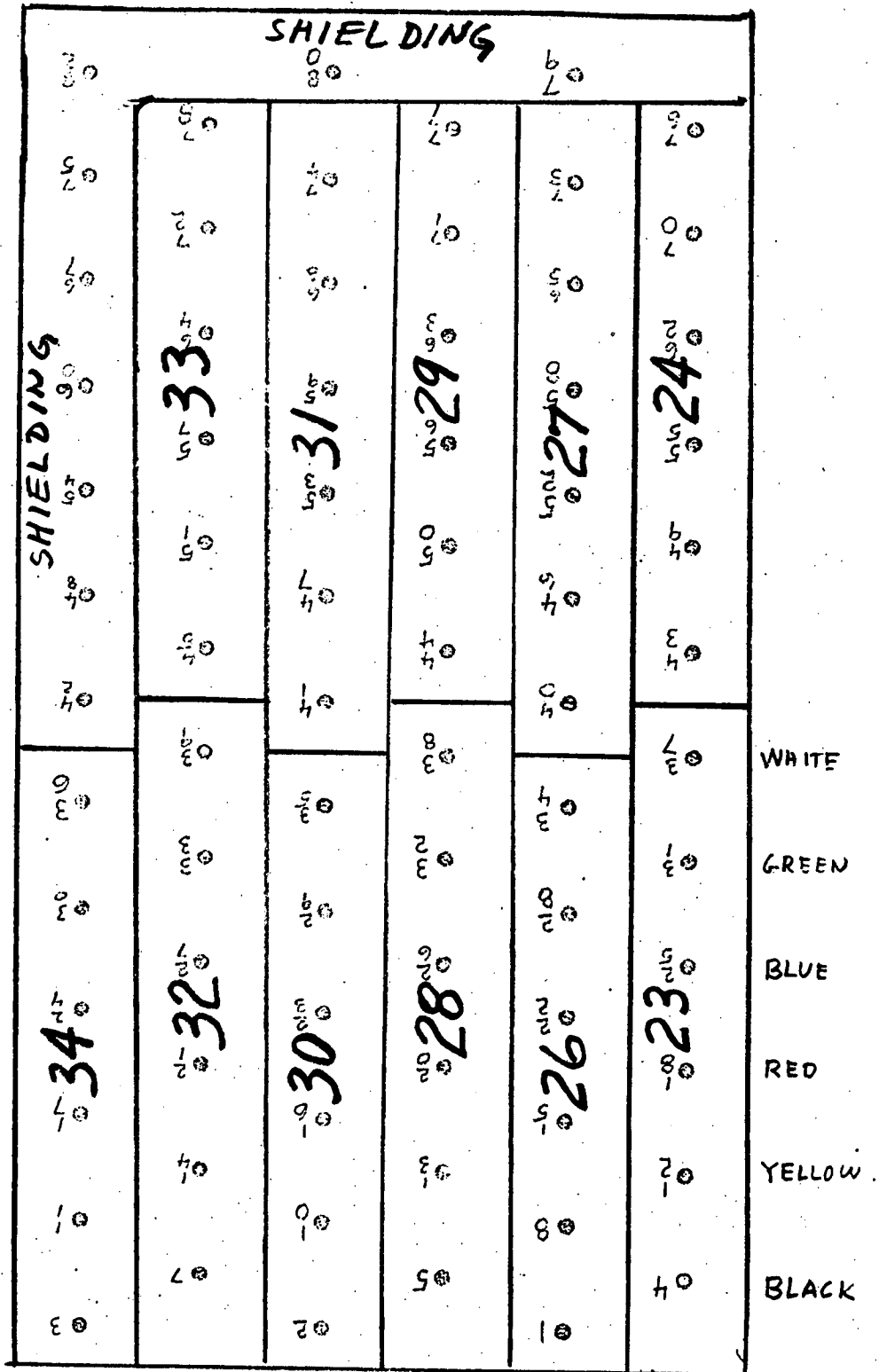


Fig. A.14 Arrangement of Pins and Cables on Plug No. 4

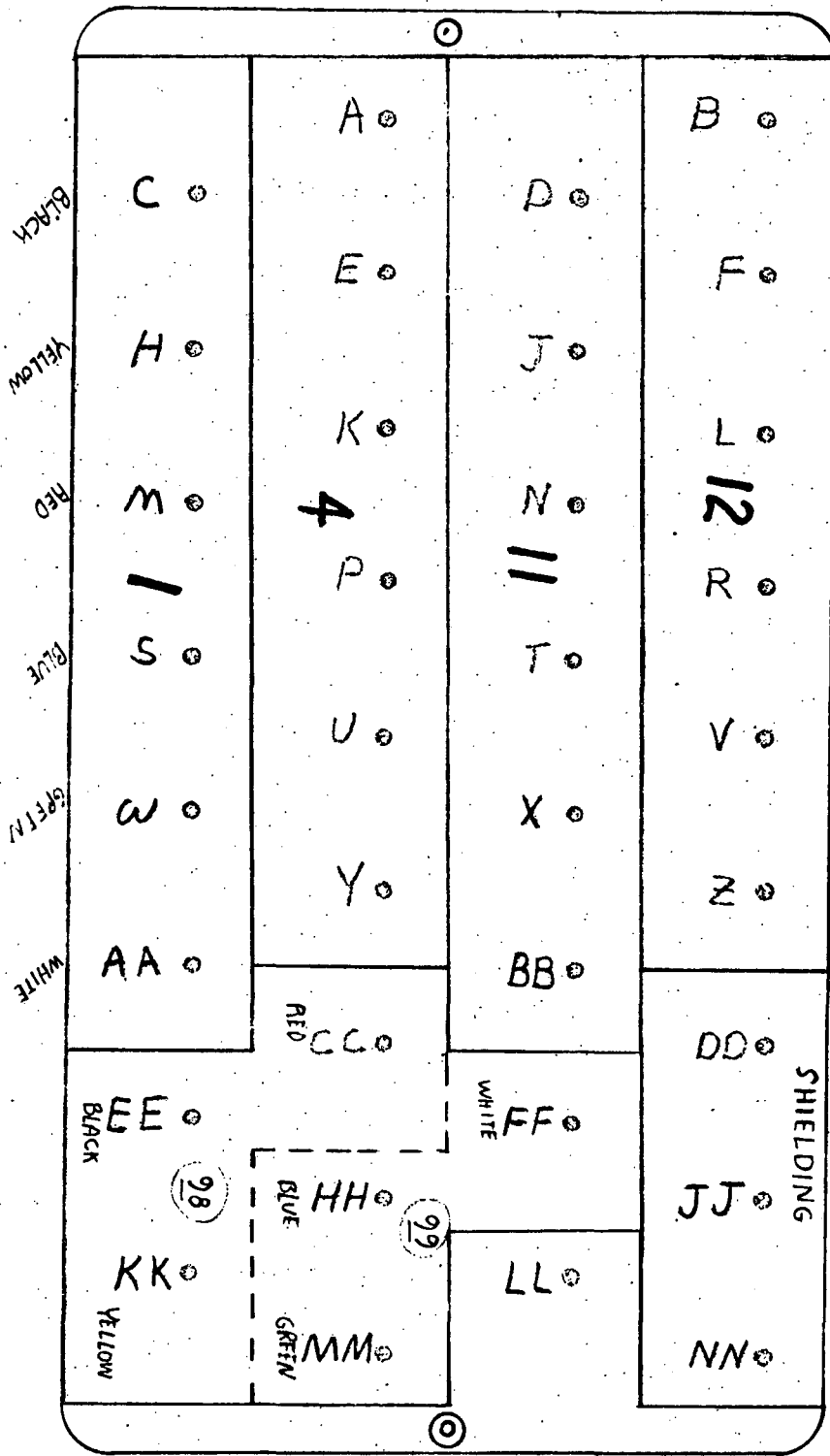


Fig. A.15 Arrangement of Pins and Cables on Plug No. 5

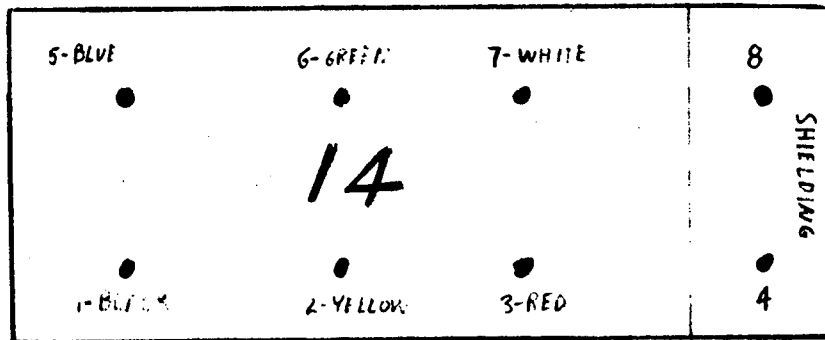


Fig. A.16 Arrangement of Pins on Plug No. 6 Used for Telephone Cable

SHIELDING					
1	2	3	4	5	6
7	8	9	37	10	12
13	14	15	36	16	18
19	20	21	35	22	24
25	26	27	48	28	30
31	32	33	47	34	36
37	38	39	46	40	42
43	44	45	45	46	48
49	50	51	43	52	54
55	56	57	42	58	60
61	62	63	41	64	66
w	g	bu	r	y	bk

white green blue red yellow black

Fig. A.17 Arrangement of Pinholes and Cables on Socket No. 1

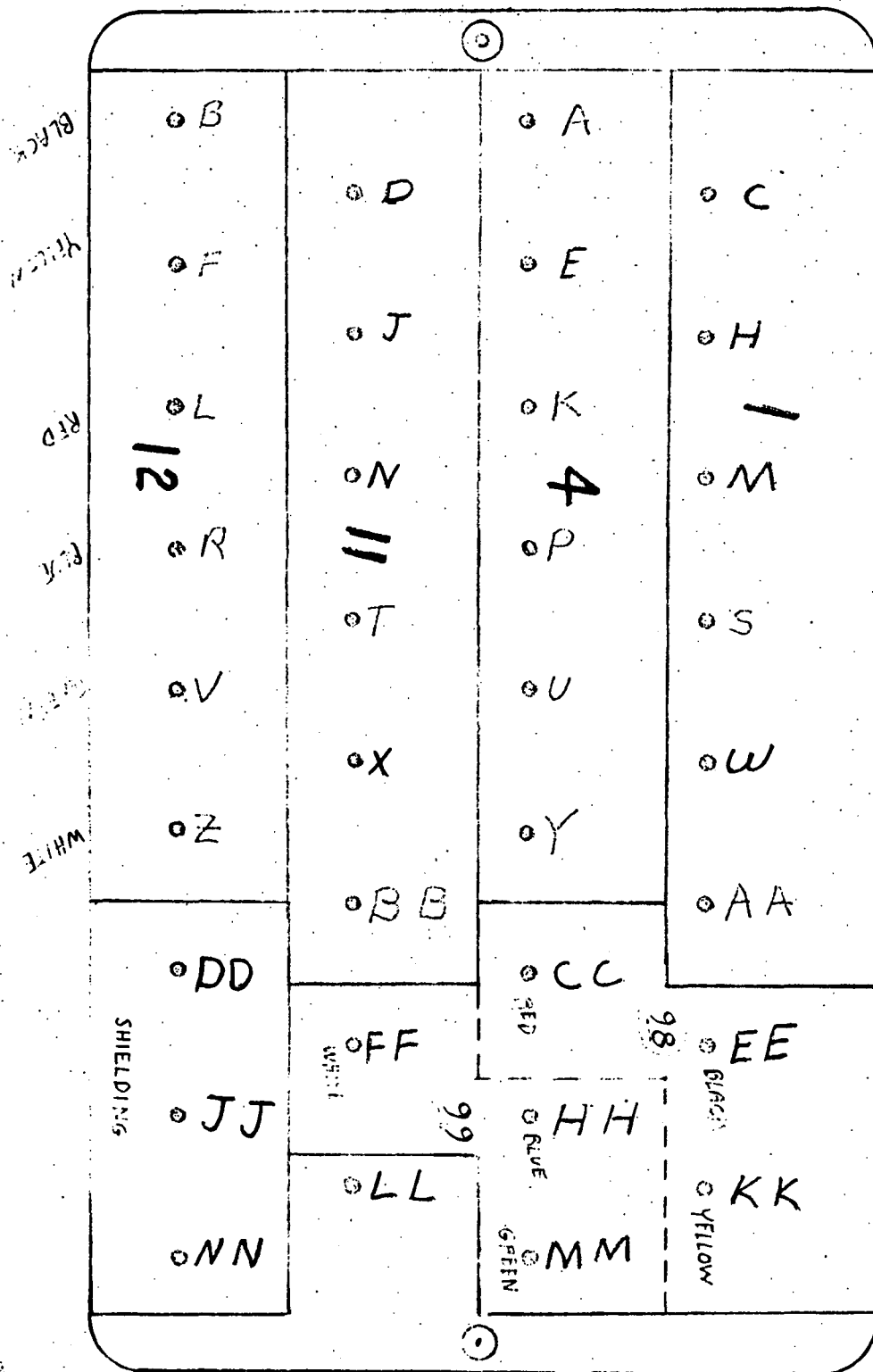


Fig. A.21 Arrangement of Pinholes and Cables on Socket No. 5 (98 and 99 designate B&F channels)

APPENDIX BCOMPUTER PROGRAM FOR THERMO-ELASTIC
ANALYSIS OF THE PRESIDENT COSTA E SILVA BRIDGE

(M. E. Bhatti and A. Ostapenko)

B.1 Introduction

A thermal stress analysis of the steel portion of the President Costa e Silva Bridge was performed by a numerical solution using finite numerical summation; the bridge girder was divided into 35 small prismatic segments and each section into 171 elements. The computer program, THERMO, developed for the analysis is described in this appendix. Explained are the structure and background of the program, as well as the instructions and limitations of its use for any set of thermal field data. The program is attached for reference, and the symbols and variables used are explained. A sample input and output are enclosed to illustrate and facilitate application.

B.2 The Structure of Program and Identification

1. Program Title: THERMO.

2. Brief Description: This program establishes the thermal field for the steel structure of the President Costa e Silva Bridge and performs a thermo-elastic analysis. (With minor adjustment, primarily the insertion of new sectional properties, the program can perform thermo-elastic analysis on other similar bridge girders, see Art. B.4, Limitations.) The program consists of two main parts:

(1) Part 1 establishes the temperature field for the whole structure from the temperature distribution plots made from field data measurements at cross sections FB27 and FB57.

(2) Part 2 analyzes the structure to find the changes in strain and stress due to the temperature changes.

Part 2 is subdivided under the following headings:

- a) Calculation of Sectional Properties for each segment.
- b) Calculation of Fictitious Bending Moments due to Unsymmetrical Non-linear Temperature Distribution in Cross Sections.
- c) Calculation of Support Reactions due to Thermal Effects.
- d) Calculation of Changes in Stresses and Strains due to a Change in Temperature.
- e) Printing of the Stress and Strain Changes.

3. Language: Fortran IV.

4. Machine: CDC 6400 (any other machine accepting Fortran IV and with a central memory capacity of 75k can be used).

5. Time and Cost per Run: Approximately 150 cp seconds; \$35.00

B.3 Purpose and Method

1. Theoretical Background: The theory and process of solving the problem are described in detail in Chapter 4 of this report.

2. Assumptions: The theoretical assumptions are the same as mentioned earlier in connection with analysis of the structure.

B.4 Restrictions and Limitations

1. General Restrictions: None

2. Limitation of Usage: The limitations of using this program pertain to the geometry and the location of temperature input.

- (1) The scheme of subdivision of the bridge into segments and of the cross sections into elements should be the same as in the President Costa e Silva Bridge. The designation of each section and their location and relative size should also remain the same. This is necessary because the variables are defined as having particular dimensions. However, by modifying the array dimensions and sectional properties, the program can be used for other similar structures.
- (2) The location of the elements with specified temperature should be the same as in the sections at FB27 and FB57. A thermal distribution, for the whole structure is automatically developed from the data at these locations. To use field data at some other locations along the girder, it would be necessary to revise the first part of the program entitled "DEVELOPING THERMAL FIELD."

(3) Non-Standard Hardware and Tapes: None

(4) Maximum Array Sizes: Following is the list of arrays with maximum dimensions given in parentheses.

A(35)	FT(35)	MTY(35)	T(171)
Al(35)	H(171)	MTZ(35)	T27(55)
AO(35)	IBYY(35)	MYY(35)	T57(55)
AC(35)	IBZZ(35)	MZZ(35)	TB(35)
B(171)	K(35)	NOO(35)	TD(35)
BC(35)	KC(35)	NOI(35)	TR(35)
BRB(35)	KK(35)	Nll(35)	X(35)
BRT(35)	KTY(35)	P(35)	Y(171)
CC(35)	KTZ(35)	PL(171)	YBT(35)
D(35)	M1(35)	SECN(35)	YN(171)
DELA(171)	M4(35)	STST(171)	Z(171)
DR(35)	M5(35)	STSR(171)	ZBL(35)
DW(35)	M6(35)	STS(171)	ZN(171)
ELE(171)	M7(35)	STN(171)	

B.5 Non-Standard Machine Operations Instructions

1. Special Operating Instructions: None
2. Restart Instructions: None
3. Error Corrections: None

B.6 Data Preparation and Input

The data is input in two stages, firstly the temperature values at floor beams FB27 and FB57, T27 and T57, and secondly, the geometrical values which give the dimensions and locations of all the segments and elements. This information is then recorded as DATA on a permanent file called MARY which is used whenever the job is

executed by an ATTACH statement (explained later under B.7, Instructions for Job Execution). For reference, a printout of this program is attached as it appears on the permanent file. All DATA exists in the same order as it is input, DATA 5 through DATA 10 is T27, DATA 11 through DATA 16 is T57 and DATA 17 through DATA 6071 gives the geometrical values of elements at each segment. DATA 17 through DATA 6071 are constant for this bridge structure, but DATA 5 through DATA 16, T27 and T57 values, are different for each set of field data of temperature. Originally, 55 values of T27 and 55 values of T57 as DATA 5 through DATA 16 are dummy values and are deleted each time a new set of field thermal data is input by using statement *D.DATA.5,DATA.16. After this, new data cards, 6 for T27 and 6 for T57, respectively are input. They are the only cards to be punched each time. These twelve cards will automatically replace the dummy values with a new identification instead of DATA. The overall arrangement of cards and the program for job execution are explained in Art. B.7.

B.6.1 Card Input Form: Temperature

<u>Card</u>	<u>Format</u>	<u>Variable Name</u>	<u>Comments</u>
1	10F8.2	T27	A total of 55 temperature change values at FB27 are entered, 10 values per card, only 5 values on the last (6th) card.
2	10F8.2	T27	
3	10F8.2	T27	
4	10F8.2	T27	
5	10F8.2	T27	
6	5F8.2	T27	

7	10F8.2	T57] A total of 55 temperature change values at FB57 are entered, 10 values per card, only 5 values on the last (12th) card.
8	10F8.2	T57	
9	10F8.2	T57	
10	10F8.2	T57	
11	10F8.2	T57	
12	5F8.2	T57	

B.6.2 Card Input Form: Geometry

<u>Card</u>	<u>Format</u>	<u>Variable Name</u>	<u>Comments</u>
1	I10	N	Number of sections where thermal field is developed.
2	I10	NN	Number of sections where stress and strains are computed
3	I20	M	Number of elements per section
4 thru 9	10F8.2	T27	55 dummy temperature values at FB27 (can all be blank cards).
10 thru 15	10F8.2	T57	55 dummy temperature values at FB57 (can all be blank cards).
One group of (2 + M) cards for each of the (N) sections. [One card for each element of the section.]	I5, 3F10.4	SECN, X, TD, TB,	These two cards give the number of the section, its location, and basic dimensions.
	6F10.2	BRT, BRB, DR, DW, TW, TR	
	I5, 4F10.4	ELE, B, H, Y, Z	These M cards give the element number and basic geometric data for each of the M elements.

B.7 Instructions for Job Execution

The program THERMO and the data were put on magnetic tape identified as P5144 in the Fritz Engineering Laboratory Library. The first step is to catalog the program and data as the two permanent files designated THERMO and MARY, respectively. This setup is taken to eliminate repetitious reading of the magnetic tape for the execution of each new set of thermal data. The cards to be read in are the following:

<u>CARD</u>	<u>STATEMENT</u>
1	Job Card - - - - -
2	LABEL (AAA, VSN=P5144, L=5144)
3	REWIND (AAA)
4	COPYBF (AAA,X1)
5	COPYBF (AAA, X2)
6	UPDATE (P=X1, N=THERMO, A, D)
7	UPDATE (P=X2, N=MARY, A, D)
8	CATALOG (THERMO, THERMO, ID=MB, XR=THERMO, PR=100, PW=THERMO)
9	CATALOG (MARY, MARY, ID=MB, XR=MARY, PR=100, PW=MARY)
10	UNLOAD (AAA)
11	6/7/8/9

Reading in of the magnetic tape and of the above set of cards will catalog the program and data as permanent files for 100 days (PR = number of days in cards 8 and 9); the printout will be with the record number allocations. For example, MARY file consists of a record designated as DATA2 through DATA6071.

The second step is the actual execution of the job. Here, the permanent files, THERMO and MARY, developed above, are called, and the dummy values of T27 and T57 as DATA 5 through DATA 16 are replaced by the new set of T27 and T57 values punched on twelve cards as explained above in B.6.1. The overall arrangement of the cards for job execution for a set of temperature changes is as follows:

<u>CARD</u>	<u>STATEMENT</u>
1	Job Card - - - - -
2	PAGES (500)
3	ATTACH (B, THERMO, ID=MB, PW=THERMO)
4	ATTACH (A, MARY, ID=MB, PW=MARY)
5	UPDATE (P=B, F, D=BHATTI)
6	RFL (75000)
7	FTN (I=BHATTI, R=3)
8	UPDATE (P=A, F, D)
9	REWIND (COMPILE)
10	LDSET (PRESET=NGINF, MAP=B)
11	LGO (COMPILE)
12	7/8/9
13	*ID/MASON
14	7/8/9
15	*ID/MAGY
16	*D/ DATA.5, DATA.16
17	- - - - -
thru	- - - - -
28	- - - - -
29	6/7/8/9

] Twelve cards of temperature changes are prepared in B.6.1

B.8 Output Form Description

The output consists first of the sectional properties, such as depth D, moments of inertia IYY and IZZ, area A, location of centroidal axes, i.e., distances YBT and ZBL, and the sectional torsional constant K; the sections being at the midpoint of the segments with mean values of the properties. The section itself is identified by the section number and its location is defined by the distance from the side pier. Beneath each set of sectional properties are printed in tabular form the element number, its location as Y and Z, temperature change T, stress STS and strain STN. All lengths are in centimeters and forces in kilograms. The temperature changes T are in degrees of Celsius (centigrade). A sample output is attached for reference.

B.9 Symbol List and Definitions

A list of variable names and of their definitions is given below for convenience of modifying or trouble shooting the program.

<u>Symbol</u>	<u>Definition</u>
A	Total area of a section (at mid-point of segment).
A1	Area circumscribed by center line of three sides of rib and deck plate; used in calculation of torsional constant K.
AA	A constant of parabola equation: $y^2 = 4ax$.
AC	A constant used in calculation of torsional constant $= A_{oi} + 10(A_i) \left(\frac{\eta_{01}}{\eta_{11}} \right)_i$. See Art. 4.2.3.
ALPH	Coefficient of thermal expansion.

<u>Symbol</u>	<u>Definition</u>
A0	Area circumscribed by the center line of main cell when using one box for calculation of torsional constant.
B	Breadth of element (dimension parallel to Z - axis)
B1,B2,B3	Constants used in solution of simultaneous equations to find R_{1E} , R_{2E} , R_{3E} .
BC	A constant used in calculations of the torsional constant $= \eta_{00_i} - 10 (A1_i) \left(\frac{\eta_{01}}{\eta_{11}} \right)_i$
BRB	Mean breadth of rib at bottom.
BRT	Mean breadth of rib at top.
CC	A constant used in calculation of torsional constant $= 10 (A_1^2)_i (\eta_{11})_i$
D	Depth of box.
D1	Distance from top of deck to the center of pin at bearing shoe at side piers.
D2	Distance from top of deck to the center of pin at the bearing shoe at central pier.
DELA	Cross-sectional area of element.
DR	Depth of rib (center to center of plates).
DW	Depth of web.
E	Modulus of elasticity.
ELE(I)	I-th element.
F11V	Means ' f_{11} ' the vertical deflection (the relative deflection of point 1 in x-y plane due to unit redundant).
F12V	Means ' f_{12} ' the horizontal deflection (relative deflection of point 1 due to unit redundant applied at point 2; in x-y plane).

<u>Symbol</u>	<u>Definition</u>
F13V	Means ' f_{13} ' the horizontal deflection (relative deflection of point 1 due to unit redundant applied at point 3; in x-y plane).
F21V	Means ' f_{21} ' the vertical deflection in x-y plane.
F22V	Means ' f_{22} ' the vertical deflection in x-y plane.
F23V	Means ' f_{23} ' the vertical deflection at point 2 due to horizontal unit redundant applied at point 3; in x-y plane.
F31V	Means ' f_{31} ' the horizontal deflection at point 3 due to unit redundant applied at point 1 in vertical direction (all being in x-y plane).
F32V	Means ' f_{32} ' the horizontal deflection at point 3 due to unit redundant applied at point 1 in vertical direction (all being in x-y plane).
F33V	Means ' f_{33} ' the horizontal deflection at point 3 due to unit redundant load applied horizontally at point 3; (all being in x-y plane).
FT	The imaginary force at the section; it is in equilibrium with internal restraint stresses in a unit long segment.
G	Modulus of rigidity.
H	Height of element (y-axis).
IBYY	Moment of inertia about $\bar{y}-\bar{y}$ axis; i.e. I_{yy} .
IBZZ	Moment of inertia about $\bar{z}-\bar{z}$ axis, i.e. I_{zz} .
IBYZ	Product of inertia; I_{yz} .
IQ	$= (I_{yy} \cdot I_{zz} - I_{yz}^2)$
K	Torsional constant.
KC	A constant used in calculation of torsional constant.
KK	-same-
KP	-same-
KTY	$= (I_{yz} M_{zzt} - I_{zz} M_{yyt})$

<u>Symbol</u>	<u>Definition</u>
KTZ	$= (I_{yz} M_{yy_t} - I_{yy} M_{zz_t})$
M1	Moment due to R1E. (In x-y plane).
M2	Moment due to vertical reaction at 3rd pier (= -R1E) (x-y plane).
M3	Moment due to horizontal lateral reaction at 3rd pier (x-z plane).
M4	Moment due to vertical reaction at 2nd pier from left, (in x-y plane).
M5	Moment due to horizontal longitudinal reaction at 2nd pier (in x-y plane).
M6	Moment due to horizontal lateral reaction at first pier, (in x-z plane).
M7	Moment due to horizontal lateral reaction at 2nd pier, (in x-z plane).
MEU	Poisson's ratio (= 0.25).
MZZ	Net moment about $\bar{z} - \bar{z}$ axis due to support reactions.
MYY	Net moment about $\bar{y} - \bar{y}$ axis due to support reactions.
MTY	= KTY/IQ
MTZ	= KTZ/IQ
NOO	$= \eta_{00} = \int_0 \frac{ds}{t}$; contour integral along the circumference of base cell, i.e., of A_0 area; refer to torsional constant calculations.
NO1	$= \eta_{01} = \int_{0,1} \frac{ds}{t}$; integration along the center line of the wall separating the base cell and one sub-cell.
N11	$= \eta_{11} = \int_{1,1} \frac{ds}{t}$; contour integral along the circum- ference of the sub-cell.
p	= R3E; the force applied caused by reaction of support restraint against horizontal movement.
P1	= (α TEdA); for a differential element.
R1E	Vertical reaction at pier No. 1 from left hand side; being opposite at pier No. 2.

<u>Symbol</u>	<u>Definition</u>
R2E	Vertical reaction at pier No. 4 from left hand side; being opposite at pier No. 3.
R3E	Horizontal longitudinal reaction in x-y plane at pier No. 3, and being opposite at pier No. 2.
R1P	Horizontal lateral reaction in x-z plane at piers No. 1 and 4; these are opposite to the reactions at piers No. 2 and No. 3.
SECN	Section Number.
SET	$= 1/k_x$.
SETT	$= 1/k_z$.
SK11	$= (F_t) (\bar{Y}_t - YT)$.
SK111	$= (F_t) (\bar{Z}_l - ZT)$.
STIFF	Bending stiffness of the pier parallel to z-axis $= k_z = 8 (k_x)$.
STIFFF	Bending stiffness of the pier parallel to x-axis $= k_x = 62.00 \text{ T/cm} = (62) (908) \text{ kg/cm}$.
STN	Net or total strain $(= \epsilon_t + \epsilon_R)$.
STNR	Strain due to support reaction forces $(= \epsilon_R)$.
STNT	Strain due to thermal load on free body or determinate structure $(= \epsilon_t)$.
STS	Net or total stress $(= \sigma_t + \sigma_R)$.
STSR	Stress due to support reaction forces $(= \sigma_R)$.
T	Temperature change at an element in °C.
TB	Thickness of bottom plate of the girder.
TD	Thickness of deck plate of the girder.
TK	An arbitrary constant name for temperature change at a certain location.
TR	Thickness of the rib plate.

<u>Symbol</u>	<u>Definition</u>
TTX	Temperature change values at an imaginary line 55.65 cm above bottom of the web plate.
TW	Thickness of the web plate.
T27	Temperature change values at location of FB27.
T57	Temperature change values at location of FB57.
TT27	Same as TTX; at the location of FB27. At the four web walls the values are designated as TT271, TT272, TT273 and TT274.
TT57	Same as TTX; at the location of FB57. At the four web walls the values are designated as TT571, TT572, TT573 and TT574.
TAR271	Temperature change value as calculated at bottom corner No. 1 at location of FB27.
TAR272	Temperature change value as calculated at bottom corner No. 2 at location of FB27.
TAR273	Temperature change value as calculated at bottom corner No. 3 at location of FB27.
TAR274	Temperature change value as calculated at bottom corner No. 4 at location of FB27.
TAR571	Temperature change value as calculated at bottom corner No. 1 at location of FB57.
TAR572	Temperature change value as calculated at bottom corner No. 2 at location of FB57.
TAR573	Temperature change value as calculated at bottom corner No. 3 at location of FB57.
TAR574	Temperature change value as calculated at bottom corner No. 4 at location of FB57.
U10V	Vertical deflection (parallel to y-axis) of girder at location No. 1 due to thermal loading.
U20V	Vertical deflection (parallel to y-axis) of girder at location No. 2 due to thermal loading.

<u>Symbol</u>	<u>Definition</u>
U30V	Horizontal deflection (parallel to x-axis) of girder at location No. 3 due to thermal loading.
U10H	Horizontal deflection (parallel to z-axis) of girder at location No. 1 due to thermal loading.
U20H	Horizontal deflection (parallel to z-axis) of girder at location No. 2 due to thermal loading.
X	Designates the distance along x-axis from the origin.
XX	The distance along x-axis, going left from the pier located at FB57; used for the computations of YPX and YEX in the parabola.
Y	Designates the distance along y-axis from the origin.
YBT	Distance of $\bar{Z}-\bar{Z}$ from z-axis ($= \bar{Y}_t$).
YEX	A variable used to establish web depth along the parabolic edge.
YK	An arbitrary location from z-axis where the value of TK is computed.
YN	$= (\bar{Y}_t - Y)$.
YNT	$= (\bar{Y}_t - YT)$.
YPX	A variable dimension, used along parabolic edge to find the depth.
YT	Distance of thermal centroid from z-axis.
YYX	Distance of the location from z-axis, where the TTX is computed.
Z	Distance from the origin parallel to z-axis.
ZBL	Distance of $\bar{Y}-\bar{Y}$ from the y-axis ($= \bar{Z}_\ell$).
ZN	$= (\bar{Z}_\ell - Z)$.
ZNT	$= (\bar{Z}_\ell - ZT)$.
ZT	Distance of thermal centroid from y-axis.

B.10 Listing of Computer Program

PROGRAM THERMO(INPUT,TAPE8=INPUT,OUTPUT,STORE1,TAPE1=STORE1,
 2STORE2,TAPE2=STORE2,STORE3,TAPE3=STORE3,STORE4,TAPE4=STORE4,
 3STORE5,TAPE5=STORE5,STORE6,TAPE6=STORE6,STORE7,TAPE7=STORE7,
 4STOR11,TAPE11=STOR11,STOR12,TAPE12=STOR12)

DIMENSION DELA(171),T(171),STST(171),STSR(171),STS(171),STN(171)
 DIMENSION ELE(171),B(171),H(171),Y(171),Z(171),P1(171)
 DIMENSION M6(35),IBZZ(35),TD(35),TB(35),P(35),X(35),YN(171)
 DIMENSION SECN(35),A(35),D(35),MTZ(35),YBT(35),MTY(35),T27(55)
 DIMENSION FT(35),M1(35),M4(35),M5(35),MZZ(35)
 DIMENSION ZBL(35),IBYY(35),M7(35),ZN(171),MY(35),T57(55)
 DIMENSION IBYZ(35),IQ(35),KTZ(35),KTY(35),STNT(171),STNR(171)
 DIMENSION BRT(35),BRB(35),DR(35),DW(35),TW(35),TR(35)
 DIMENSION K(35),KK(35),KC(35),N00(35),N01(35),N11(35)
 DIMENSION A1(35),A0(35),AC(35),BC(35),CC(35)
 DIMENSION YT(35),ZT(35),YNT(35),ZNT(35)
 DIMENSION M2(35),M3(35)

INTEGER ELE,SECN
 REAL IBZZ,IBYY,MZZ,MY,MTY,MTZ,M1,KP,M4,M5,M6,M7
 REAL K,KK,KC,N00,N01,N11,MEU
 REAL IBYZ,IQ,KTZ,KTY
 REAL M2,M3

ALPH=.0000117
 E=2100000.
 MEU=0.3
 G=E/(2.*(1+MEU))
 STIFFF=62.
 STIFF=496.
 O1=575.5
 O2=1311.4

200 READ 200,N
 FORMAT (I10)
 250 READ 250,NN
 FORMAT (I10)
 500 READ 500,M
 FORMAT (I20)
 601 READ 601,T27
 FORMAT (10F8.2)
 602 READ 602,T57
 FORMAT (10F8.2)

*
 *
 * DEVELOPING THERMAL FIELD IN STRUCTURE *
 *
 *

TAR271=T27(11)-(T27(11)-T27(10))*225./150.
 TAR272=T27(13)+(T27(14)-T27(13))*187.6/119.5
 TAR273=T27(34)-(T27(34)-T27(33))*225./150.
 TAR274=T27(36)+(T27(37)-T27(36))*187.6/119.5
 TAR571=T57(11)-(T57(11)-T57(10))*225./150.
 TAR572=T57(13)+(T57(14)-T57(13))*187.6/119.5
 TAR573=T57(34)-(T57(34)-T57(33))*225./150.
 TAR574=T57(36)+(T57(37)-T57(36))*187.6/119.5
 DO 900 I=1,N
 READ 300,SECN(I),X(I),TD(I),TB(I)
 READ 301,BRT(I),BRB(I),DR(I),DW(I),TW(I),TR(I)

```

300 FORMAT (I5,3F10.4)
301 FORMAT (6F10.2)
DO 700 J=1,M
READ 600,ELE(J),B(J),H(J),Y(J),Z(J)
600 FORMAT (I5,4F10.4)
GO TO 805
137 IF(J-28)31,31,32
805 IF(J-5)31,31,32
31 IF(X(I)-5000.)33,33,34
33 T(J)=T27(J)
GO TO 290
34 IF(X(I)-20000.)35,35,36
35 T(J)=T27(J)+(T57(J)-T27(J))/15000.*(X(I)-5000.)
GO TO 290
36 IF(X(I)-35000.)37,37,38
37 T(J)=T57(J)-(T57(J)-T27(J))/15000.*(X(I)-20000.)
GO TO 290
38 IF(X(I)-50000.)39,39,40
39 T(J)=T27(J)+(T57(J)-T27(J))/15000.*(X(I)-35000.)
GO TO 290
40 IF(X(I)-65000.)41,41,42
41 T(J)=T57(J)-(T57(J)-T27(J))/15000.*(X(I)-50000.)
GO TO 290
42 IF(X(I)-70000.)943,943,32
943 T(J)=T27(J)
GO TO 290
32 IF(J.GT.5.AND.J.LT.24)GO TO 29
IF(J.GT.28.AND.J.LT.47)GO TO 28
29 IF(J-9)43,43,44
28 IF(J-32)43,43,44
43 IF(X(I)-5000.)45,45,46
45 IF(J.GT.5.AND.J.LT.24)GO TO 27
IF(J.GT.28.AND.J.LT.47)GO TO 26
27 TT27=T27(6)-(T27(6)-TAR271)/90.5*55.65
GO TO 25
26 TT27=T27(29)-(T27(29)-TAR273)/90.5*55.65
25 YEX=(631.-561.3)/5000.*X(I)
YY27=(561.3+YEX+TD(I))-55.65
IF(Y(J).NE.0.0)GO TO 47
IF(Y(J).EQ.0.0)GO TO 48
47 IF(J.GT.5.AND.J.LT.24)GO TO 24
IF(J.GT.28.AND.J.LT.47)GO TO 23
24 T(J)=T(5)+(TT27-T(5))/(YY27-Y(4))*(Y(J)-Y(5))
GO TO 290
23 T(J)=T(28)+(TT27-T(28))/(YY27-Y(28))*(Y(J)-Y(28))
GO TO 290
48 T(J)=0.
GO TO 290
46 IF(X(I)-20000.)49,49,50
49 IF(J.GT.5.AND.J.LT.24)GO TO 22
IF(J.GT.28.AND.J.LT.47)GO TO 21
22 TT27=T27(6)-(T27(6)-TAR271)/90.5*55.65
TT57=T57(9)-(T57(9)-TAR571)/123.7*55.65
GO TO 806
21 TT27=T27(29)-(T27(29)-TAR273)/90.5*55.65
TT57=T57(32)-(T57(32)-TAR573)/123.7*55.65
806 ITX=(TT57-TT27)/15000.*(X(I)-5000.)+TT27
IF(X(I)-14000.)51,51,52
51 YEX=(742.4-561.3)/14000.*(X(I)-5000.)
YYX=(631.+TD(I)+YEX)-55.65
GO TO 951
52 XX=(X(I)-25000.)
AA=(550.*550.)/(4.*5940.)
YPX=SQRT(-4.*AA*XX)
YEX=(550.-YPX)
YYX=(742.4+TD(I)+YEX)-55.65
951 IF(Y(J).NE.0.0)GO TO 53
IF(Y(J).EQ.0.0)GO TO 54
53 IF(J.GT.5.AND.J.LT.24)GO TO 19
IF(J.GT.28.AND.J.LT.47)GO TO 18
19 T(J)=T(5)+(ITX-T(5))/(YYX-Y(5))*(Y(J)-Y(5))
GO TO 290
18 T(J)=T(28)+(ITX-T(28))/(YYX-Y(28))*(Y(J)-Y(28))
GO TO 290
54 T(J)=0.
GO TO 290
50 IF(X(I)-35000.)55,55,56

```

PROGRAM

THERMO

TRACE

CDC 6600 FTN V3.0-P380 OPT=0

```

5   55   IF(J.GT.5.AND.J.LT.24)GO TO 17
      IF(J.GT.28.AND.J.LT.47)GO TO 16
      17   TT27=T27(6)+(T27(6)-TAR271)/46.2*55.65
          TT57=T57(9)-(T57(9)-TAR571)/123.7*55.65
          GO TO 15
0   16   TT27=T27(29)+(T27(29)-TAR273)/46.2*55.65
          TT57=T57(32)-(T57(32)-TAR573)/123.7*55.65
      15   TTX=TT57-(TT57-TT27)/15000.*(X(I)-20000.)
          IF(X(I)-26000.)57,57,58
      57   XX=(X(I)-20000.)
          AA=(550.*550.)/(4.*5940.)
          YPX=SQRT(4.*AA*XX)
          YEX=(1292.4-YPX)
          YYX=(YEX+TD(I))-55.65
          GO TO 952
0   58   YYX=(742.4+TD(I))-55.65
      952  IF(Y(J).NE.0.0)GO TO 59
          IF(Y(J).EQ.0.0)GO TO 60
      59   IF(J.GT.5.AND.J.LT.24)GO TO 14
          IF(J.GT.28.AND.J.LT.47)GO TO 13
5   14   T(J)=T(5)+(TTX-T(5))/(YYX-Y(5))*(Y(J)-Y(5))
          GO TO 290
      13   T(J)=T(28)+(TTX-T(28))/(YYX-Y(28))*(Y(J)-Y(28))
          GO TO 290
0   60   T(J)=0.
          GO TO 290
      56   IF(X(I)-50000.)61,61,62
      61   IF(J.GT.5.AND.J.LT.24)GO TO 701
          IF(J.GT.28.AND.J.LT.47)GO TO 702
5   701  TT27=T27(6)+(T27(6)-TAR271)/46.2*55.65
          TT57=T57(9)-(T57(9)-TAR571)/123.7*55.65
          GO TO 703
0   702  TT27=T27(29)+(T27(29)-TAR273)/46.2*55.65
          TT57=T57(32)-(T57(32)-TAR573)/123.7*55.65
      703  TTX=TT27+(TT57-TT27)/15000.*(X(I)-35000.)
          IF(X(I)-44000.)63,63,64
0   63   YYX=(742.4+TD(I))-55.65
          GO TO 953
      64   XX=(X(I)-50000.)
          AA=(550.*550.)/(4.*5940.)
          YPX=SQRT(-4.*AA*XX)
          YEX=(550.-YPX)
          YYX=(742.4+TD(I)+YEX)-55.65
0   953  IF(Y(J).NE.0.0)GO TO 804
          IF(Y(J).EQ.0.0)GO TO 66
      804  IF(J.GT.5.AND.J.LT.24)GO TO 704
          IF(J.GT.28.AND.J.LT.47)GO TO 705
5   704  T(J)=T(5)+(TTX-T(5))/(YYX-Y(5))*(Y(J)-Y(5))
          GO TO 290
      705  T(J)=T(28)+(TTX-T(28))/(YYX-Y(28))*(Y(J)-Y(28))
          GO TO 290
0   66   T(J)=0.
          GO TO 290
      62   IF(X(I)-65000.)67,67,68
      67   IF(J.GT.5.AND.J.LT.24)GO TO 706
          IF(J.GT.28.AND.J.LT.47)GO TO 707
0   706  TT27=T27(6)-(T27(6)-TAR271)/90.5*55.65
          TT57=T57(9)-(T57(9)-TAR571)/123.7*55.65
          GO TO 708
5   707  TT27=T27(29)-(T27(29)-TAR273)/90.5*55.65
          TT57=T57(32)-(T57(32)-TAR573)/123.7*55.65
      708  TTX=TT57-(TT57-TT27)/15000.*(X(I)-50000.)
          IF(X(I)-56000.)69,69,70
0   69   XX=(X(I)-50000.)
          AA=(550.*550.)/(4.*5940.)
          YPX=SQRT(4.*AA*XX)
          YEX=(1292.4-YPX)
          YYX=(YEX+TD(I))-55.65
          GO TO 954
5   70   YEX=742.4-(742.4-561.3)/14000.*(X(I)-56000.)
          YYX=(YEX+TD(I))-55.65
0   954  IF(Y(J).NE.0.0)GO TO 71
          IF(Y(J).EQ.0.0)GO TO 72
      71   IF(J.GT.5.AND.J.LT.24)GO TO 709
          IF(J.GT.28.AND.J.LT.47)GO TO 710
0   709  T(J)=T(5)+(TTX-T(5))/(YYX-Y(5))*(Y(J)-Y(5))
          GO TO 290

```

```

710 T(J)=T(28)+(TTX-T(28))/(YYX-Y(28))*(Y(J)-Y(28))
GO TO 290
72 T(J)=0.
GO TO 290
68 IF(X(I)-70000.)173,73,74
73 IF(J.GT.5.AND.J.LT.24)GO TO 711
GO TO 712
711 TT27=T27(6)-(T27(6)-TAR271)/90.5*55.65
GO TO 713
712 TT27=T27(29)-(T27(29)-TAR273)/90.5*55.65
713 YEX=(631.-561.3)/5000.*(X(I)-65000.)
YYX=(561.3+YEX+TD(I))-55.65
IF(Y(J).NE.0.0)GO TO 74
IF(Y(J).EQ.0.0)GO TO 75
74 IF(J.GT.5.AND.J.LT.24)GO TO 714
IF(J.GT.28.AND.J.LT.47)GO TO 715
714 T(J)=T(5)+(TTX-T(5))/(YYX-Y(5))*(Y(J)-Y(5))
GO TO 290
715 T(J)=T(28)+(TTX-T(28))/(YYX-Y(28))*(Y(J)-Y(28))
GO TO 290
75 T(J)=0.
GO TO 290
44 IF(J.GT.9.AND.J.LT.24)GO TO 716
IF(J.GT.32.AND.J.LT.47)GO TO 717
716 IF(J-14)77,77,78
717 IF(J-37)77,77,78
77 IF(X(I)-5000.)79,79,80
79 T(J)=T27(J)
GO TO 290
80 IF(X(I)-20000.)81,81,82
81 T(J)=T27(J)+(T57(J)-T27(J))/15000.*(X(I)-5000.)
GO TO 290
82 IF(X(I)-35000.)83,83,84
83 T(J)=T57(J)-(T57(J)-T27(J))/15000.*(X(I)-20000.)
GO TO 290
84 IF(X(I)-50000.)86,86,87
86 T(J)=T27(J)+(T57(J)-T27(J))/15000.*(X(I)-35000.)
GO TO 290
87 IF(X(I)-65000.)88,88,89
88 T(J)=T57(J)-(T57(J)-T27(J))/15000.*(X(I)-50000.)
GO TO 290
89 IF(X(I)-70000.)90,90,78
90 T(J)=T27(J)
GO TO 290
78 IF(J.GT.14.AND.J.LT.24)GO TO 718
IF(J.GT.37.AND.J.LT.47)GO TO 719
718 IF(J-18)91,91,92
719 IF(J-41)91,91,92
91 IF(X(I)-5000.)93,93,94
93 IF(J.GT.14.AND.J.LT.24)GO TO 720
IF(J.GT.37.AND.J.LT.47)GO TO 721
720 TT27=T27(19)-(T27(19)-TAR272)/90.5*55.65
GO TO 722
721 TT27=T27(42)-(T27(42)-TAR274)/90.5*55.65
722 YEX=(631.-561.3)/5000.*X(I)
YY27=(561.3+YEX+TD(I))-55.65
IF(Y(J).EQ.0.0)GO TO 95
IF(Y(J).NE.0.0)GO TO 96
95 T(J)=0.
GO TO 290
96 IF(J.GT.14.AND.J.LT.24)GO TO 723
IF(J.GT.37.AND.J.LT.47)GO TO 724
723 TK=T27(19)
YK=350.+TD(I)
T(J)=TK+(TT27-TK)/(YY27-YK)*(Y(J)-YK)
GO TO 290
724 TK=T27(42)
YK=350.+TD(I)
T(J)=TK+(TT27-TK)/(YY27-YK)*(Y(J)-YK)
GO TO 290
94 IF(X(I)-20000.)97,97,98
97 IF(J.GT.14.AND.J.LT.24)GO TO 725
IF(J.GT.37.AND.J.LT.47)GO TO 726
725 TT27=T27(19)-(T27(19)-TAR272)/90.5*55.65
TT57=T57(15)-(T57(15)-TAR572)/123.7*55.65
GO TO 727
726 TT27=T27(42)-(T27(42)-TAR274)/90.5*55.65

```

PROGRAM

THERMO

TRACE

CDC 6600 FTN V3.0-P330 OPT=0

```

0 727 TT57=I57(38)-(T57(38)-TAR574)/123.7*55.65
    TTX=(TT57-TT27)/15000.*(X(I)-5000.)+TT27
    IF(X(I)-14000.)99,99,802
5 99 YEX=(742.4-561.3)/14000.*(X(I)-5000.)
    YYX=(631.+TD(I)+YEX)-55.65
    GO TO 955
802 XX=(X(I)-20000.)
    AA=(550.*550.)/(4.*5940.)
    YPX=SQRT(-4.*AA*XX)
    YEX=(550.-YPX)
    YYX=(742.4+TD(I)+YEX)-55.65
0 955 IF(Y(J).EQ.0.0)GO TO 101
    IF(Y(J).NE.0.0)GO TO 102
101 T(J)=0.
    GO TO 290
102 IF(J.GT.14.AND.J.LT.24)GO TO 728
    IF(J.GT.37.AND.J.LT.47)GO TO 729
728 TK=(T57(19)-T27(19))/15000.*(X(I)-5000.)+T27(19)
    YK=350.+TD(I)
    T(J)=TK+(TTX-TK)/(YYX-YK)*(Y(J)-YK)
    GO TO 290
729 TK=(T57(42)-T27(42))/15000.*(X(I)-5000.)+T27(42)
    YK=350.+TD(I)
    T(J)=TK+(TTX-TK)/(YYX-YK)*(Y(J)-YK)
    GO TO 290
5 98 IF(X(I)-35000.)103,103,104
103 IF(J.GT.14.AND.J.LT.24)GO TO 730
    IF(J.GT.37.AND.J.LT.47)GO TO 731
730 TT27=T27(19)+(T27(19)-TAR272)/46.2*55.65
    TT57=T57(15)-(T57(15)-TAR572)/123.7*55.65
    GO TO 732
731 TT27=T27(42)+(T27(42)-TAR274)/46.2*55.65
    TT57=T57(38)-(T57(38)-TAR574)/123.7*55.65
732 TTX=TT57-(TT57-TT27)/15000.*(X(I)-20000.)
    IF(X(I)-26000.)105,105,106
5 105 XX=(X(I)-20000.)
    AA=(550.*550.)/(4.*5940.)
    YPX=SQRT(4.*AA*XX)
    YEX=(1292.4-YPX)
    YYX=(YEX+TD(I))-55.65
    GO TO 956
106 YYX=(742.4+TD(I))-55.65
956 IF(Y(J).EQ.0.0)GO TO 107
    IF(Y(J).NE.0.0)GO TO 108
107 T(J)=0.
    GO TO 290
108 IF(J.GT.14.AND.J.LT.37)GO TO 733
    IF(J.GT.37.AND.J.LT.47)GO TO 734
733 TK=T57(19)-(T57(19)-T27(19))/15000.*(X(I)-20000.)
    YK=350.+TD(I)
    T(J)=TK+(TTX-TK)/(YYX-YK)*(Y(J)-YK)
    GO TO 290
734 TK=T57(42)-(T57(42)-T27(42))/15000.*(X(I)-20000.)
    YK=350.+TD(I)
    T(J)=TK+(TTX-TK)/(YYX-YK)*(Y(J)-YK)
    GO TO 290
5 104 IF(X(I)-50000.)109,109,110
109 IF(J.GT.14.AND.J.LT.24)GO TO 735
    IF(J.GT.37.AND.J.LT.47)GO TO 736
735 TT27=T27(19)+(T27(19)-TAR272)/46.2*55.65
    TT57=T57(15)-(T57(15)-TAR572)/123.7*55.65
    GO TO 737
736 TT27=T27(42)+(T27(42)-TAR274)/46.2*55.65
    TT57=T57(38)-(T57(38)-TAR574)/123.7*55.65
737 TTX=(TT57-TT27)/15000.*(X(I)-35000.)+TT27
    IF(X(I)-44000.)111,111,112
5 111 YYX=(742.4+TD(I))-55.65
    GO TO 957
112 XX=(X(I)-50000.)
    AA=(550.*550.)/(4.*5940.)
    YPX=SQRT(-4.*AA*XX)
    YEX=(550.-YPX)
    YYX=(742.4+TD(I)+YEX)-55.65
0 957 IF(Y(J).EQ.0.0)GO TO 113
    IF(Y(J).NE.0.0)GO TO 114
113 T(J)=0.
    GO TO 290

```

PROGRAM

THERMO TRACE

```

114 IF(J.GT.14.AND.J.LT.24)GO TO 738
    IF(J.GT.37.AND.J.LT.47)GO TO 739
738 TK=T27(19)+(T57(19)-T27(19))/15000.*(X(I)-35000.)
    YK=350.+TD(I)
    T(J)=TK+(TTX-TK)/(YYX-YK)*(Y(J)-YK)
    GO TO 290
739 TK=T27(42)+(T57(42)-T27(42))/15000.*(X(I)-35000.)
    T(J)=TK+(TTX-TK)/(YYX-YK)*(Y(J)-YK)
    GO TO 290
110 IF(X(I)-65000.)115,115,116
115 IF(J.GT.14.AND.J.LT.24)GO TO 740
    IF(J.GT.37.AND.J.LT.47)GO TO 741
740 TT27=T27(19)-(T27(19)-TAR272)/90.5*55.65
    TT57=T57(15)-(T57(15)-TAR572)/90.5*55.65
    GO TO 742
741 TT27=T27(42)-(T27(42)-TAR274)/90.5*55.65
    TT57=T57(38)-(T57(38)-TAR574)/123.7*55.65
742 TTX=TT57-(TT57-TT27)/15000.*(X(I)-50000.)
    IF(X(I)-56000.)117,117,118
117 XX=(X(I)-50000.)
    AA=(550.*550.)/(4.*5940.)
    YPX=SQRT(4.*AA*XX)
    YEX=(1292.4-YPX)
    YYX=(YEX+TD(I))-55.65
    GO TO 958
118 YEX=742.4-(742.4-561.3)/14000.*(X(I)-56000.)
    YYX=(YEX+TD(I))-55.65
958 IF(Y(J).EQ.0.0)GO TO 119
    IF(Y(J).NE.0.0)GO TO 120
119 T(J)=0.
    GO TO 290
120 IF(J.GT.14.AND.J.LT.24)GO TO 743
    IF(J.GT.37.AND.J.LT.47)GO TO 744
743 TK=T57(19)-(T57(19)-T27(19))/15000.*(X(I)-50000.)
    YK=350.+TD(I)
    T(J)=TK+(TTX-TK)/(YYX-YK)*(Y(J)-YK)
    GO TO 290
744 TK=T57(42)-(T57(42)-T27(42))/15000.*(X(I)-50000.)
    YK=350.+TD(I)
    T(J)=TK+(TTX-TK)/(YYX-YK)*(Y(J)-YK)
    GO TO 290
116 IF(X(I)-70000.)121,121,92
121 IF(J.GT.14.AND.J.LT.24)GO TO 745
    IF(J.GT.37.AND.J.LT.47)GO TO 746
745 TT27=T27(19)-(T27(19)-TAR272)/90.5*55.65
    GO TO 747
746 TT27=T27(42)-(T27(42)-TAR274)/90.5*55.65
747 YEX=631.-(631.-561.3)/5000.*(X(I)-65000.)
    YY27=(YEX+TD(I))-55.65
    IF(Y(J).EQ.0.0)GO TO 122
    IF(Y(J).NE.0.0)GO TO 123
122 T(J)=0.
    GO TO 290
123 IF(J.GT.14.AND.J.LT.24)GO TO 748
    IF(J.GT.37.AND.J.LT.47)GO TO 749
748 TK=T27(19)
    YK=350.+TD(I)
    T(J)=TK+(TT27-TK)/(YY27-YK)*(Y(J)-YK)
    GO TO 290
749 TK=T27(42)
    YK=350.+TD(I)
    T(J)=TK+(TT27-TK)/(YY27-YK)*(Y(J)-YK)
    GO TO 290
92 IF(J.GT.18.AND.J.LT.42)GO TO 801
    IF(J.GT.41.AND.J.LT.172)GO TO 751
801 IF(J-23)124,124,137
751 IF(J-46)124,124,125
124 IF(X(I)-50000.)126,126,127
126 T(J)=T27(J)
    GO TO 290
127 IF(X(I)-20000.)128,128,129
128 T(J)=T27(J)+(T57(J)-T27(J))/15000.*(X(I)-50000.)
    GO TO 290
129 IF(X(I)-35000.)130,130,131
130 T(J)=T57(J)-(T57(J)-T27(J))/15000.*(X(I)-20000.)
    GO TO 290
131 IF(X(I)-50000.)132,132,133

```

```

132 T(J)=T27(J)+(T57(J)-T27(J))/15000.*(X(I)-35000.)
GO TO 290
133 IF(X(I)-65000.)134,134,135
134 T(J)=T57(J)-(T57(J)-T27(J))/15000.*(X(I)-50000.)
GO TO 290
135 IF(X(I)-70000.)136,136,125
136 T(J)=T27(J)
GO TO 290
125 IF(J-55)139,139,146
139 IF(X(I)-50000.)141,141,142
141 T(J)=T27(J)
GO TO 290
142 IF(X(I)-20000.)143,143,144
143 T(J)=T27(J)+(T57(J)-T27(J))/15000.*(X(I)-5000.)
GO TO 290
144 IF(X(I)-35000.)145,145,146
145 T(J)=T57(J)-(T57(J)-T27(J))/15000.*(X(I)-20000.)
GO TO 290
146 IF(X(I)-50000.)147,147,148
147 T(J)=T27(J)+(T57(J)-T27(J))/15000.*(X(I)-35000.)
GO TO 290
148 IF(X(I)-65000.)149,149,150
149 T(J)=T57(J)-(T57(J)-T27(J))/15000.*(X(I)-50000.)
GO TO 290
150 IF(X(I)-70000.)151,151,140
151 T(J)=T27(J)
140 IF(J-66)152,152,153
152 IF(H(J).EQ.0.0) GO TO 154
GO TO 155
154 T(J)=0
GO TO 290
155 IF(Y(J)-Y(3))160,160,161
160 T(J)=T(2)+(T(3)-T(2))/(Y(2)-Y(1))*(Y(J)-Y(1))
GO TO 290
161 IF(Y(J)-Y(4))162,162,163
162 T(J)=T(3)+(T(4)-T(3))/(Y(3)-Y(2))*(Y(J)-Y(3))
GO TO 290
163 IF(Y(J)-Y(5))164,164,165
164 T(J)=T(4)+(T(5)-T(4))/(Y(5)-Y(4))*(Y(J)-Y(4))
GO TO 290
165 IF(Y(J)-Y(6))166,166,167
166 T(J)=T(5)+(T(6)-T(5))/(Y(6)-Y(5))*(Y(J)-Y(5))
GO TO 290
167 IF(Y(J)-Y(7))168,168,169
168 T(J)=T(6)+(T(7)-T(6))/(Y(7)-Y(6))*(Y(J)-Y(6))
GO TO 290
169 IF(Y(J)-Y(8))170,170,153
170 T(J)=T(7)+(T(8)-T(7))/(Y(8)-Y(7))*(Y(J)-Y(7))
GO TO 290
153 IF(J-77)173,173,993
173 IF(H(J).EQ.0.0) GO TO 174
GO TO 175
174 T(J)=0
GO TO 290
175 IF(Y(J)-Y(21))180,180,181
180 T(J)=T(22)+(T(21)-T(22))/(Y(21)-Y(22))*(Y(J)-Y(22))
GO TO 290
181 IF(Y(J)-Y(20))182,182,183
182 T(J)=T(21)+(T(20)-T(21))/(Y(20)-Y(21))*(Y(J)-Y(21))
GO TO 290
183 IF(Y(J)-Y(19))184,184,185
184 T(J)=T(20)+(T(19)-T(20))/(Y(19)-Y(20))*(Y(J)-Y(20))
GO TO 290
185 IF(Y(J)-Y(18))186,186,187
186 T(J)=T(19)+(T(18)-T(19))/(Y(18)-Y(19))*(Y(J)-Y(19))
GO TO 290
187 IF(Y(J)-Y(17))188,188,189
188 T(J)=T(18)+(T(17)-T(18))/(Y(17)-Y(18))*(Y(J)-Y(18))
GO TO 290
189 IF(Y(J)-Y(16))190,190,191
190 T(J)=T(17)+(T(16)-T(17))/(Y(16)-Y(17))*(Y(J)-Y(17))
GO TO 290
191 IF(Y(J)-Y(15))192,192,993
192 T(J)=T(16)+(T(15)-T(16))/(Y(15)-Y(16))*(Y(J)-Y(16))
GO TO 290
993 IF(J-88)193,193,194
193 IF(H(J).EQ.0.0) GO TO 195

```

PROGRAM

THERMO TRACE

```

GO TO 196
195 T(J)=0
GO TO 290
196 IF(Y(J)-Y(26))201,201,202
201 T(J)=T(25)+(T(25)-T(25))/(Y(26)-Y(25))*(Y(J)-Y(25))
GO TO 290
202 IF(Y(J)-Y(27))203,203,204
203 T(J)=T(26)+(T(27)-T(26))/(Y(27)-Y(26))*(Y(J)-Y(26))
GO TO 290
204 IF(Y(J)-Y(28))205,205,206
205 T(J)=T(27)+(T(28)-T(27))/(Y(28)-Y(27))*(Y(J)-Y(27))
GO TO 290
206 IF(Y(J)-Y(29))207,207,208
207 T(J)=T(28)+(T(29)-T(28))/(Y(29)-Y(28))*(Y(J)-Y(28))
GO TO 290
208 IF(Y(J)-Y(29))209,209,210
209 T(J)=T(29)+(T(30)-T(29))/(Y(30)-Y(29))*(Y(J)-Y(29))
GO TO 290
210 IF(Y(J)-Y(31))211,211,212
211 T(J)=T(30)+(T(31)-T(30))/(Y(31)-Y(30))*(Y(J)-Y(30))
212 IF(Y(J)-Y(32))213,213,194
213 T(J)=T(31)+(T(32)-T(31))/(Y(32)-Y(31))*(Y(J)-Y(31))
GO TO 290
194 IF(J-99)214,214,215
214 IF(H(J).EQ.0.0)GO TO 216
GO TO 217
216 T(J)=0.
GO TO 290
217 IF(Y(J)-Y(44))222,222,223
222 T(J)=T(45)+(T(44)-T(45))/(Y(44)-Y(45))*(Y(J)-Y(45))
GO TO 290
223 IF(Y(J)-Y(43))224,224,225
224 T(J)=T(44)+(T(43)-T(44))/(Y(43)-Y(44))*(Y(J)-Y(44))
GO TO 290
225 IF(Y(J)-Y(42))226,226,227
226 T(J)=T(43)+(T(42)-T(43))/(Y(42)-Y(43))*(Y(J)-Y(43))
GO TO 290
227 IF(Y(J)-Y(41))228,228,229
228 T(J)=T(42)+(T(41)-T(42))/(Y(41)-Y(42))*(Y(J)-Y(42))
GO TO 290
229 IF(Y(J)-Y(40))230,230,231
230 T(J)=T(41)+(T(40)-T(41))/(Y(40)-Y(41))*(Y(J)-Y(41))
GO TO 290
231 IF(Y(J)-Y(39))232,232,233
232 T(J)=T(40)+(T(39)-T(40))/(Y(39)-Y(40))*(Y(J)-Y(40))
GO TO 290
233 IF(Y(J)-Y(38))234,234,215
234 T(J)=T(39)+(T(38)-T(39))/(Y(38)-Y(39))*(Y(J)-Y(39))
GO TO 290
215 IF(J-113)235,235,236
235 IF(Z(10)-Z(J))237,237,238
237 T(J)=T(10)-(T(11)-T(10))/(Z(11)-Z(10))*(Z(10)-Z(J))
GO TO 290
238 IF(Z(11)-Z(J))239,239,240
239 T(J)=T(10)+(T(11)-T(10))/(Z(11)-Z(10))*(Z(J)-Z(10))
GO TO 290
240 IF(Z(12)-Z(J))241,241,242
241 T(J)=T(11)+(T(12)-T(11))/(Z(12)-Z(11))*(Z(J)-Z(11))
GO TO 290
242 IF(Z(13)-Z(J))243,243,244
243 T(J)=T(12)+(T(13)-T(12))/(Z(13)-Z(12))*(Z(J)-Z(12))
GO TO 290
244 IF(Z(14)-Z(J))245,245,246
245 T(J)=T(13)+(T(14)-T(13))/(Z(14)-Z(13))*(Z(J)-Z(13))
GO TO 290
246 IF((-978.)-Z(J))247,247,236
247 T(J)=T(14)+(T(14)-T(13))/(Z(14)-Z(13))*(Z(J)-Z(14))
GO TO 290
236 IF(J-127)248,248,249
248 IF(Z(33)-Z(J))994,994,251
994 T(J)=T(33)-(T(34)-T(33))/(Z(34)-Z(33))*(Z(J)-Z(33))
GO TO 290
251 IF(Z(34)-Z(J))252,252,253
252 T(J)=T(33)+(T(34)-T(33))/(Z(34)-Z(33))*(Z(J)-Z(33))
GO TO 290
253 IF(Z(35)-Z(J))254,254,255
254 T(J)=T(34)+(T(35)-T(34))/(Z(35)-Z(34))*(Z(J)-Z(34))

```


PROGRAM

THERMO

TRACE

```

GO TO 290
255 IF (Z(36)-Z(J)) 256,256,257
256 T(J)=T(35)+(T(36)-T(35))/(Z(36)-Z(35))*(Z(J)-Z(35))
GO TO 290
257 IF (Z(37)-Z(J)) 258,258,259
258 T(J)=T(36)+(T(37)-T(36))/(Z(37)-Z(36))*(Z(J)-Z(36))
GO TO 290
259 IF ((-2298.)-Z(J)) 260,260,249
260 T(J)=T(37)+(T(37)-T(36))/(Z(37)-Z(36))*(Z(J)-Z(37))
GO TO 290
249 IF (J-165) 261,261,262
261 IF (Z(47)-Z(J)) 263,263,264
263 T(J)=T(47)-(T(48)-T(47))/(Z(48)-Z(47))*(Z(47)-Z(J))
GO TO 290
264 IF (Z(48)-Z(J)) 265,265,266
265 T(J)=T(47)+(T(48)-T(47))/(Z(48)-Z(47))*(Z(J)-Z(47))
GO TO 290
266 IF (Z(49)-Z(J)) 267,267,268
267 T(J)=T(48)+(T(49)-T(48))/(Z(49)-Z(48))*(Z(J)-Z(48))
GO TO 290
268 IF (Z(50)-Z(J)) 269,269,270
269 T(J)=T(49)+(T(50)-T(49))/(Z(50)-Z(49))*(Z(J)-Z(49))
GO TO 290
270 IF (Z(51)-Z(J)) 271,271,272
271 T(J)=T(50)+(T(51)-T(50))/(Z(51)-Z(50))*(Z(J)-Z(50))
GO TO 290
272 IF (Z(52)-Z(J)) 273,273,274
273 T(J)=T(51)+(T(52)-T(51))/(Z(52)-Z(51))*(Z(J)-Z(51))
GO TO 290
274 IF (Z(53)-Z(J)) 275,275,276
275 T(J)=T(52)+(T(53)-T(52))/(Z(53)-Z(52))*(Z(J)-Z(52))
GO TO 290
276 IF (Z(54)-Z(J)) 277,277,278
277 T(J)=T(53)+(T(54)-T(53))/(Z(54)-Z(53))*(Z(J)-Z(53))
GO TO 290
278 IF (Z(55)-Z(J)) 279,279,280
279 T(J)=T(54)+(T(55)-T(54))/(Z(55)-Z(54))*(Z(J)-Z(54))
GO TO 290
280 IF ((-2518.)-Z(J)) 281,281,262
281 T(J)=T(55)+(T(55)-T(54))/(Z(55)-Z(54))*(Z(J)-Z(55))
GO TO 290
262 IF (J-168) 282,282,283
282 IF ((-1.3)-Z(J)) 284,284,285
284 T(J)=T(47)-(T(48)-T(47))/(Z(48)-Z(47))*(Z(47)-Z(J))
GO TO 290
285 IF ((-8.)-Z(J)) 286,286,287
286 T(J)=T(166)
GO TO 290
287 IF ((-41.7)-Z(J)) 288,288,283
288 T(J)=T(166)
GO TO 290
283 IF (J-171) 289,289,290
289 IF (2589.7+Z(J)) 291,291,292
291 T(J)=T(55)+(T(55)-T(54))/(Z(55)-Z(54))*(Z(J)-Z(55))
GO TO 290
292 IF (2582.+Z(J)) 293,293,294
293 T(J)=T(169)
GO TO 290
294 T(J)=T(169)
290 WRITE(11)ELE(J),B(J),H(J),Y(J),Z(J),T(J)
700 CONTINUE
WRITE(12)SECN(I),X(I),TD(I),TB(I),BRT(I),BRB(I),DR(I),
30W(I),TW(I),TR(I)
900 CONTINUE

```

```

* *****
*          CALCULATING SECTIONAL PROPERTIES          *
*          *
* *****

```

```

REWIND11
REWIND12

```

```

GO 100 I=1,N
READ(12)SECN(I),X(I),TD(I),TB(I),BRT(I),BRB(I),DR(I),

```

```

200(I),TW(I),TR(I)
SWD=0.
SA=0.
SAY=0.
SAYY=0.
SIOZ=0.
SAZZ=0.
SIOY=0.
SP1=0.
SP11=0.
SP111=0.
DO 400 J=1,M
READ(1)ELE(J),B(J),H(J),Y(J),Z(J),T(J)
IF (J-9)2,2,5
2 SWD=SWD+H(J)
5 DELA(J)=B(J)*H(J)
SA=SA+DELA(J)
SAY=SAY+DELA(J)*Y(J)
SAYY=SAYY+DELA(J)*Y(J)*Y(J)
SIOZ=SIOZ+((1./12.)*B(J)*(H(J)**3))
SAZZ=SAZZ+DELA(J)*Z(J)*Z(J)
SIOY=SIOY+((1./12.)*H(J)*(B(J)**3))
P1(J)=T(J)*DELA(J)*ALPH*E
SP1=SP1+P1(J)
SP11=SP11+P1(J)*Y(J)
SP111=SP111+P1(J)*Z(J)
400 WRITE(1)ELE(J),Y(J),Z(J),T(J),DELA(J),P1(J)
CONTINUE
A(I)=SA
D(I)=SWD+TB(I)+TD(I)
YBT(I)=SAY/SA
ZBL(I)=-1295.
IBZZ(I)=SAYY-(YBT(I)**2*A(I))+SIOZ
IBYY(I)=SAZZ-(ZBL(I)**2*A(I))+SIOY
IBYZ(I)=0.
YT(I)=SP11/SP1
ZT(I)=SP111/SP1
FT(I)=SP1
YNT(I)=(YT(I)-YBT(I))
ZNT(I)=(ZT(I)-ZBL(I))
N11(I)=69./TR(I)+BRT(I)/TD(I)
NO1(I)=69./BRB(I)
N00(I)=(686.-TW(I))/TB(I)+2.*(DW(I)+1./2.*TB(I)+1./2.*TD(I))/TW(I)
2*(686.-TW(I)-10.*BRT(I))/TD(I)
A1(I)=(BRB(I)+BRT(I))/2.*DR(I)
A0(I)=(686.-TW(I))*(DW(I)+TD(I)+TB(I))-10.*A1(I)
AC(I)=A0(I)+10.*A1(I)*NO1(I)/N11(I)
BC(I)=NOJ(I)-10.*(NO1(I)**2)/N11(I)
CC(I)=10.*(A1(I)**2)/N11(I)
KC(I)=4.*(AC(I)**2+BC(I)*CC(I))/BC(I)
KK(I)=4.*(A1(I)**2)/(69./TR(I)+BRT(I)/TD(I))
K(I)=2.*KC(I)+18.*KK(I)
WRITE(2)SECN(I),X(I),A(I),D(I),YBT(I),ZBL(I),IBZZ(I),IBYY(I)
2,IBYZ(I),K(I),YNT(I),ZNT(I),FT(I)
100 CONTINUE

```

```

*
* *****
*
*          CALCULATING      FITICIOUS      BENDING
*          MOMENTS      DUE      TO      UNSYMMETRICAL
*          TEMPERATURE      DISTRIBUTION      IN      THE
*          SECTION      OF      BRIDGE      STRUCTURE
*
* *****

```

```

REWIND1
REWIND2
DO 650 I=1,N
READ(2) SECN(I),X(I),A(I),D(I),YBT(I),ZBL(I),IBZZ(I),IBYY(I)
2,IBYZ(I),K(I),YNT(I),ZNT(I),FT(I)
DO 640 J=1,M
READ(1)ELE(J),Y(J),Z(J),T(J),DELA(J),P1(J)
YN(J)=YBT(I)-Y(J)
ZN(J)=ZBL(I)-Z(J)

```

```

640 WRITE(3)ELE(J),Y(J),Z(J),T(J),YN(J),ZN(J)
CONTINUE
SK11=FT(I)*YNT(I)
SK111=FT(I)*ZNT(I)
IQ(I)=IBYY(I)*IBZZ(I)-(IBYZ(I)**2)
KTZ(I)=(SK111*IBYZ(I))-(SK11*IBYY(I))
KTY(I)=(SK11*IBYZ(I))-(SK111*IBZZ(I))
MTZ(I)=KTZ(I)/IQ(I)
MTY(I)=KTY(I)/IQ(I)
WRITE(4)SECN(I),X(I),A(I),D(I),YBT(I),ZBL(I),IBZZ(I),IBYY(I),
3MTZ(I),MTY(I),FT(I),K(I),IBYZ(I)
650 CONTINUE

```

```

*
*
*          CALCULATING      SUPPORT      REACTIONS
*          DUE      TO      THERMAL      STIMULAI
*
*

```

```

REWIND4
SU101V=0.
SU102V=0.
SF111V=0.
SF112V=0.
SF122V=0.
SF132V=0.
SU302V=0.
SF232V=0.
SF332V=0.
SU101H=0.
SU102H=0.
SF111H=0.
SF112H=0.
SF122H=0.
SF111T=0.
SF112T=0.
SF113T=0.
SF122T=0.
SF123T=0.
DO 750 I=1,N
READ(4)SECN(I),X(I),A(I),D(I),YBT(I),ZBL(I),IBZZ(I),IBYY(I),
2MTZ(I),MTY(I),FT(I),K(I),IBYZ(I)
IF (I-10)3,3,6
3 SU101V=SU101V+(MTZ(I))*(-X(I))*2000./E
SF111V=SF111V+(X(I)**2*2000./(E*IBZZ(I)))
SU101H=SU101H+(MTY(I))*(-X(I))*2000./E
SF111H=SF111H+(X(I)**2*2000./(E*IBYY(I)))
SF111T=SF111T+(D1-YBT(I))*2/(G*K(I))*2000.
6 IF (I-25)7,7,8
7 SU102V=SU102V+(MTZ(I))*(2./3.*X(I)-100000./3.)*2000./E
SU302V=SU302V+(MTZ(I))*(D2-YBT(I))*2000./E
SF112V=SF112V+(2./3.*X(I)-100000./3.)*2*2000./(E*IBZZ(I))
SF122V=SF122V+2./3.*(20000.-X(I))*(2./3.*X(I)-100000./3.)*
22000./(E*IBZZ(I))
SF132V=SF132V+(YBT(I)-D2)*(100000./3.-2./3.*X(I))*
22000./(E*IBZZ(I))
SF232V=SF232V+(YBT(I)-D2)*2./3.*(X(I)-20000.)*2000./(E*IBZZ(I))
SF332V=SF332V+(YBT(I)-D2)*2*2000./(E*IBZZ(I))
SU102H=SU102H+(MTY(I))*(2./3.*X(I)-100000./3.)*2000./E
SF112H=SF112H+(2./3.*X(I)-100000./3.)*2*2000./(E*IBYY(I))
SF122H=SF122H+2./3.*(20000.-X(I))*(2./3.*X(I)-100000./3.)*
22000./(E*IBYY(I))
SF112T=SF112T+((D1-YBT(I))-5./3.*(D2-YBT(I)))*2/(G*K(I))*2000.
SF122T=SF122T+(2./3.*(D2-YBT(I)))*((D1-YBT(I))-5./3.
2*(D2-YBT(I)))/(G*K(I))*2000.
8 SF113T=SF113T+((D1-YBT(I))-(D2-YBT(I)))*2*2000./(G*K(I))
SF123T=SF123T+(YBT(I)-D2)*((D1-YBT(I))-(D2-YBT(I)))*2000./(G*K(I))
WRITE(5)SECN(I),X(I),A(I),D(I),YBT(I),ZBL(I),IBZZ(I),IBYY(I),
2MTZ(I),MTY(I),FT(I),K(I),IBYZ(I)
750 CONTINUE

```

SET=1./(908.00*STIFF)

PROGRAM

IHERMO

TRACE

CDC 6600 FTN V3.0-P390 OPT=0

```

5      M4(I)=-R1E*(X(I)-20000.)
      M5(I)=-R3E*(D2-YBT(I))
      M6(I)=R1P*X(I)
      M7(I)=-R1P*(X(I)-20000.)
      M2(I)=-R2E*(X(I)-50000.)
      M3(I)=-R1P*(X(I)-50000.)

20     IF (X(I)-20000.)20,20,30
      P(I)=0.
      MZZ(I)=M1(I)
      MYI(I)=M6(I)
      GO TO 65
30     IF(X(I)-50000.)9005,9005,9006
9005   P(I)=R3E
      MZZ(I)=M1(I)+M4(I)+M5(I)
      MYI(I)=M6(I)+M7(I)
      GO TO 65
9006   P(I)=0
      MZZ(I)=M1(I)+M2(I)+M4(I)
      MYI(I)=M6(I)+M3(I)+M7(I)
      GO TO 65

```

```

*
* *****
*
*          CALCULATING      CHANGE      IN      STRESSES
*          AND      STRAINS      DUE      TO      CHANGE
*          IN      THE      TEMPERATURE
*
* *****

```

```

65     DO 799 J=1,M
      READ(3)ELE(J),Y(J),Z(J),T(J),YN(J),ZN(J)
      STST(J)=(FT(I)/A(I))+(MTZ(I)*YN(J))+(MTY(I)*ZN(J))-(ALPH*E*T(J))
      STSR(J)=- (MZZ(I)*YN(J)/IBZZ(I))-(MYI(I)*ZN(J)/IBYI(I))+(P(I)/A(I))
      STS(J)=STST(J)+STSR(J)
      STN(J)=(STST(J)+ALPH*E*T(J)+STSR(J))/E
      WRITE(6)ELE(J),Y(J),Z(J),T(J),STS(J),STN(J)
799    CONTINUE
      WRITE(7)SECN(I),X(I),A(I),D(I),YBT(I),ZBL(I),IBZZ(I),IBYI(I)
3,IBYZ(I),K(I)
800    CONTINUE

```

```

*
* *****
*
*          PRINTING      THE      CHANGE      IN      STR-
*          -ESS      AND      THE      STRAIN      DUE      TO
*          CHANGE      IN      TEMPERATURE
*
* *****

```

```

REWIND6
REWIND7
DO 10 I=1,NN
READ(7) SECN(I),X(I),A(I),D(I),YBT(I),ZBL(I),IBZZ(I),IBYI(I)
3,IBYZ(I),K(I)
PRINT 1000,SECN(I),X(I)
1000  FORMAT(///,30X,*SECTION NO.=*,I2,5X,*AT*5X,*X=*,F10.4)
PRINT 1200,A(I)
PRINT 1300,D(I)
PRINT 1400,YBT(I)
PRINT 1500,ZBL(I)
PRINT 1600,IBZZ(I)
PRINT 1700,IBYI(I)
PRINT 1800,IBYZ(I)
PRINT 2222,FT(I)
2222  FORMAT(39X,*FT=*,F14.2)
PRINT 1900,K(I)
PRINT 7001,MTZ(I),MTY(I),YT(I),ZT(I)
7001  FORMAT(38X,*MTZ=*,G14.5/38X,*MTY=*,G14.5,/,39X,*YT=*,G14.5,/,39X,
2*ZT=*,G14.5)
1200  FORMAT(/,40X,*A=*,F10.2)

```

PROGRAM

THERMO TRACE

CDC 6600 FTN V3.0-P380 OPT=0 03

```
1300 FORMAT (40X,*D=*,F7.2)
1400 FORMAT (38X,*YBT=*,F6.2)
1500 FORMAT (38X,*ZBL=*,F8.2)
1600 FORMAT (37X,*IBZZ=*,F14.2)
1700 FORMAT (37X,*IBYY=*,F14.2)
1800 FORMAT (37X,*IBYZ=*,F14.2)
1900 FORMAT (40X,*K=*,F14.2)
      PRINT 2000
2000 FORMAT (//5X,*ELEMENT NO.*,2X,*Y*,10X,*Z*,5X,*TEMP(T)*,4X,*STRESS*
2,7X,*STRAIN*,//)
      DO 11 J=1,M
      READ(6)ELE(J),Y(J),Z(J),T(J),STS(J),STN(J)
      PRINT 3000,ELE(J),Y(J),Z(J),T(J),STS(J),STN(J)
3000 FORMAT (I12,F10.2,F11.2,F10.3,F11.2,F14.8)
      11 CONTINUE
      10 CONTINUE
      END
```

B.11 Sample Input -- Temperature Data for January 1975

An example of input of the temperature data is given below using the data of January 1975.

17.5	17.	13.	9.	9.	9.	0.	0.	0.	7.5
6.5	5.5	5.5	6.	0.	0.	0.	6.	6.	6.
8.	14.	14.5	14.5	14.	8.	6.	6.	6.	0.
0.	0.	6.	5.5	5.5	6.5	7.5	0.	0.	0.
9.	9.	9.	13.	17.	17.5	16.5	16.5	15.	14.5
14.	14.5	15.	16.5	16.5					
17.5	17.	13.	9.	9.	9.	9.	9.	9.	7.5
6.5	5.5	5.5	6.	6.	6.	6.	6.	6.	6.
8.	14.	14.5	14.5	14.	8.	6.	6.	6.	6.
6.	6.	6.	5.5	5.5	6.5	7.5	9.	9.	9.
9.	9.	9.	13.	17.	17.5	16.5	16.5	15.	14.5
14.	14.5	15.	16.5	16.5					

B.12 Selected Sample Output for Temperature Data of January 1975

The sample input of Art. B.11 resulted in the printout of data for each element of the cross section at each of the 35 stations.

The printout is arranged in six columns giving for each element:

(1) Element No., (2) and (3) y and z coordinates of the centroid of element, (4) Temperature, (5) Thermal stress, (6) Total strain. Only the output for the following three sections was selected for a comparison with future trial runs:

- 1) Section 3 (x = 5000.0 cm, at FB27) -- all 171 elements.
- 2) Section 7 (x = 13000.0 cm, near FB42) -- elements 1 to 72.
- 3) Section 10 (x = 19000.0 cm, near FB57) -- elements 1 to 72.

Sample Output for Temperature Data of January 1975

SECTION NO. = 3 AT X = 5000.0000

A = 15670.00
 C = 633.80
 YBT = 297.13
 ZBL = -1295.00
 IBZZ = 1075016146.62
 IBYY = 8028265858.61
 IBYZ = .00
 FT = 3828600.46
 K = 1157586423.50
 MTZ = .32512
 MTY = -.29346E-02
 YT = 205.84
 ZT = -1288.8

ELEMENT NO.	Y	Z	TEMP (T)	STRESS	STRAIN
1	6.00	-293.20	17.500	-123.08	.00014614
2	16.00	-293.20	17.000	-112.88	.00014515
3	66.00	-293.20	13.000	-25.03	.00014018
4	201.00	-293.20	9.000	45.10	.00012677
5	351.00	-293.20	9.000	13.81	.00011188
6	541.50	-293.20	8.688	-18.25	.00009296
7	.00	.00	.000	308.69	.00014699
8	.00	.00	.000	308.69	.00014699
9	.00	.00	.000	308.69	.00014699
10	632.90	-368.20	7.500	-8.26	.00008382
11	632.90	-518.20	6.500	16.03	.00008368
12	632.90	-668.20	5.500	40.33	.00008355
13	632.90	-793.20	5.500	40.09	.00008344
14	632.90	-912.70	6.000	27.59	.00008334
15	.00	.00	.000	308.69	.00014699
16	.00	.00	.000	308.69	.00014699
17	.00	.00	.000	308.69	.00014699
18	541.50	-976.80	5.148	42.89	.00009236
19	351.00	-976.80	6.000	86.26	.00011128
20	201.00	-976.80	6.000	117.54	.00012617
21	66.00	-976.80	8.000	96.56	.00013958
22	16.00	-976.80	14.000	-40.44	.00014454
23	6.00	-976.80	14.500	-50.64	.00014554
24	6.00	-1613.20	14.500	-51.81	.00014498
25	16.00	-1613.20	14.000	-41.61	.00014398
26	66.00	-1613.20	8.000	95.38	.00013902

27	201.00	-1613.20	6.000	116.37	.00012561
28	351.00	-1613.20	6.000	85.08	.00011072
29	541.50	-1613.20	6.130	42.15	.00009180
30	.00	.00	.000	308.69	.00014699
31	.00	.00	.000	308.69	.00014699
32	.00	.00	.000	308.69	.00014699
33	632.90	-1688.20	6.000	26.16	.00008266
34	632.90	-1838.20	5.500	38.16	.00008252
35	632.90	-1988.20	5.500	37.89	.00008239
36	632.90	-2113.20	6.500	13.09	.00008228
37	632.90	-2232.70	7.500	-11.71	.00008218
38	.00	.00	.000	308.69	.00014699
39	.00	.00	.000	308.69	.00014699
40	.00	.00	.000	308.69	.00014699
41	541.50	-2296.80	8.517	-17.74	.00009120
42	351.00	-2296.80	9.000	10.11	.00011011
43	201.00	-2296.80	9.000	41.39	.00012501
44	66.00	-2296.80	13.000	-28.73	.00013842
45	16.00	-2296.80	17.000	-116.59	.00014338
46	6.00	-2296.80	17.500	-126.78	.00014438
47	.50	-150.00	16.500	-97.10	.00014681
48	.50	-450.00	16.500	-97.66	.00014655
49	.50	-750.00	15.000	-61.35	.00014628
50	.50	-1050.00	14.500	-49.62	.00014602
51	.50	-1350.00	14.000	-37.89	.00014576
52	.50	-1650.00	14.500	-50.73	.00014549
53	.50	-1950.00	15.000	-63.57	.00014523
54	.50	-2250.00	16.500	-100.98	.00014496
55	.50	-2495.00	16.500	-101.43	.00014475
56	61.00	-299.00	-5.000	418.26	.00014067
57	126.00	-299.00	8.200	80.38	.00013422
58	191.00	-299.00	3.000	194.59	.00012776
59	261.00	-299.00	9.000	32.57	.00012081
60	342.00	-299.00	9.000	15.68	.00011277
61	417.00	-299.00	8.892	2.63	.00010532
62	482.00	-299.00	8.785	-8.24	.00009886
63	537.00	-299.00	8.695	-17.50	.00009340
64	587.00	-299.00	7.961	-9.90	.00008844
65	.00	.00	.000	308.69	.00014699
66	.00	.00	.000	308.69	.00014699
67	61.00	-974.00	8.600	82.86	.00014008
68	126.00	-974.00	7.111	105.89	.00013362
69	191.00	-974.00	6.148	115.99	.00012717
70	261.00	-974.00	6.000	105.03	.00012022
71	342.00	-974.00	6.000	88.14	.00011217
72	417.00	-974.00	6.051	71.24	.00010472
73	482.00	-974.00	6.102	56.44	.00009827
74	537.00	-974.00	6.145	43.92	.00009281

75	587.00	-974.00	6.256	30.75	.00008784
76	-.00	-.00	.000	308.69	.00014699
-0	-.00	-.00	.000	308.69	.00014699
78	61.00	-1298.00	8.600	82.26	.00013979
79	126.00	-1298.00	7.111	105.29	.00013334
80	191.00	-1298.00	6.148	115.39	.00012688
81	261.00	-1298.00	6.000	104.44	.00011993
82	342.00	-1298.00	6.000	87.54	.00011189
83	417.00	-1298.00	6.045	70.80	.00010444
84	482.00	-1298.00	6.089	56.15	.00009798
85	537.00	-1298.00	6.127	43.76	.00009252
86	587.00	-1298.00	4.699	68.41	.00008756
87	-.00	-.00	.000	308.69	.00014699
88	-.00	-.00	.000	308.69	.00014699
89	61.00	-1976.00	13.400	-36.93	.00013920
90	126.00	-1976.00	11.222	3.03	.00013274
91	191.00	-1976.00	9.296	36.79	.00012629
92	261.00	-1976.00	9.000	29.47	.00011933
93	342.00	-1976.00	9.000.	12.58	.00011129
94	417.00	-1976.00	8.832	1.06	.00010384
95	482.00	-1976.00	8.668	-8.45	.00009739
96	537.00	-1976.00	8.528	-16.49	.00009193
97	587.00	-1976.00	5.500	47.48	.00008696
98	-.00	-.00	.000	308.69	.00014699
99	-.00	-.00	.000	308.69	.00014699
100	619.50	-338.70	7.697	-10.24	.00008517
101	619.50	-384.20	7.393	-2.87	.00008513
102	619.50	-429.70	7.090	4.49	.00008509
103	619.50	-457.20	6.907	8.95	.00008507
104	619.50	-520.70	6.483	19.23	.00008501
105	619.50	-566.20	6.180	26.60	.00008497
106	619.50	-611.70	5.877	33.97	.00008493
107	619.50	-657.20	5.573	41.34	.00008489
108	619.50	-702.70	5.500	43.06	.00008485
109	619.50	-748.20	5.500	42.97	.00008481
110	619.50	-793.70	5.502	42.84	.00008477
111	619.50	-839.20	5.692	38.07	.00008473
112	619.50	-884.70	5.883	33.31	.00008469
113	619.50	-930.20	6.073	28.55	.00008465
114	619.50	-1660.00	5.906	31.31	.00008401
115	619.50	-1705.50	5.942	30.34	.00008397
116	619.50	-1751.00	5.791	33.98	.00008393
117	619.50	-1796.50	5.639	37.62	.00008389
118	619.50	-1842.00	5.500	40.95	.00008385
119	619.50	-1887.50	5.500	40.87	.00008381
120	619.50	-1933.00	5.500	40.78	.00008377
121	619.50	-1978.50	5.500	40.70	.00008373
122	619.50	-2024.00	5.786	33.58	.00008369

123	619.50	-2069.50	6.150	24.55	.00008365
124	619.50	-2115.00	6.515	15.51	.00008361
125	619.50	-2160.50	6.896	6.07	.00008357
126	619.50	-2206.00	7.277	-3.37	.00008353
127	619.50	-2251.50	7.657	-12.81	.00008349
128	16.00	-81.60	16.500	-100.21	.00014533
129	16.00	-138.30	16.500	-100.31	.00014528
130	16.00	-195.00	16.500	-100.42	.00014523
131	16.00	-251.70	16.500	-100.52	.00014518
132	16.00	-340.80	16.500	-100.69	.00014510
133	16.00	-406.20	16.500	-100.81	.00014505
134	16.00	-471.60	16.392	-98.27	.00014499
135	16.00	-537.00	16.065	-90.36	.00014493
136	16.00	-602.40	15.738	-82.45	.00014487
137	16.00	-667.80	15.411	-74.53	.00014482
138	16.00	-733.20	15.084	-66.62	.00014476
139	16.00	-798.60	14.919	-62.69	.00014470
140	16.00	-864.00	14.810	-60.13	.00014464
141	16.00	-929.40	14.701	-57.57	.00014459
142	16.00	-1022.40	14.546	-53.94	.00014450
143	16.00	-1083.40	14.444	-51.55	.00014445
144	16.00	-1143.60	14.344	-49.20	.00014440
145	16.00	-1204.20	14.243	-46.83	.00014434
146	16.00	-1264.80	14.142	-44.46	.00014429
147	16.00	-1325.40	14.041	-42.09	.00014424
148	16.00	-1386.00	14.060	-42.67	.00014418
149	16.00	-1446.60	14.161	-45.26	.00014413
150	16.00	-1507.20	14.262	-47.85	.00014408
151	16.00	-1567.80	14.363	-50.45	.00014402
152	16.00	-1660.80	14.518	-54.43	.00014394
153	16.00	-1726.20	14.627	-57.23	.00014389
154	16.00	-1791.60	14.736	-60.03	.00014383
155	16.00	-1857.00	14.845	-62.82	.00014377
156	16.00	-1922.40	14.954	-65.62	.00014371
157	16.00	-1987.80	15.189	-71.52	.00014366
158	16.00	-2053.20	15.516	-79.67	.00014360
159	16.00	-2118.60	15.843	-87.83	.00014354
160	16.00	-2184.60	16.173	-96.06	.00014348
161	16.00	-2249.40	16.497	-104.14	.00014342
162	16.00	-2338.40	16.500	-104.38	.00014335
163	16.00	-2395.10	16.500	-104.48	.00014330
164	16.00	-2451.80	16.500	-104.59	.00014325
165	16.00	-2517.50	16.500	-104.71	.00014319
166	16.50	-1.30	16.500	-100.16	.00014535
167	32.60	-8.00	16.500	-103.53	.00014375
168	13.50	-41.70	16.500	-99.61	.00014562
169	16.50	-2589.70	16.500	-104.95	.00014308
170	32.60	-2582.00	16.500	-108.29	.00014148
171	13.50	-2548.30	16.500	-104.24	.00014341

SECTION NO.= 7 AT X=13000.0000

A= 19113.60
 D= 738.10
 YBT=315.66
 ZBL=-1295.00
 IBZZ= 1781863029.40
 IBYY= 9852930638.80
 IBYZ= .00
 FT= 4860199.62
 K= 1691632782.80
 MTZ= .28532
 MTY= -.26259E-02
 YT= 211.06
 ZT= -1289.7

ELEMENT NO.	Y	Z	TEMP (T)	STRESS	STRAIN
1	6.00	-293.20	17.500	-143.64	.00013635
2	16.00	-293.20	17.000	-132.38	.00013586
3	66.00	-293.20	13.000	-39.23	.00013342
4	201.00	-293.20	9.000	45.22	.00012683
5	351.00	-293.20	9.000	29.85	.00011952
6	551.00	-293.20	6.680	17.22	.00010976
7	693.30	-293.20	8.453	8.23	.00010281
8	.00	.00	.000	287.04	.00013669
9	.00	.00	.000	287.04	.00013669
10	737.10	-368.20	7.500	27.12	.00010067
11	737.10	-518.20	6.500	51.64	.00010064
12	737.10	-668.20	5.500	76.16	.00010062
13	737.10	-793.20	5.500	76.12	.00010060
14	737.10	-912.70	6.000	63.80	.00010058
15	.00	.00	.000	287.04	.00013669
16	.00	.00	.000	287.04	.00013669
17	693.30	-976.80	6.156	64.43	.00010271
18	551.00	-976.80	6.091	80.61	.00010965
19	351.00	-976.80	6.000	103.34	.00011941
20	201.00	-976.80	6.000	118.71	.00012673
21	66.00	-976.80	8.000	83.40	.00013332
22	16.00	-976.80	14.000	-58.89	.00013576
23	6.00	-976.80	14.500	-70.15	.00013624
24	6.00	-1613.20	14.500	-70.36	.00013615

25	16.00	-1613.20	14.000	-59.10	.00013566
26	66.00	-1613.20	8.000	83.20	.00013322
27	201.00	-1613.20	6.000	118.51	.00012663
28	351.00	-1613.20	6.000	103.14	.00011931
29	551.00	-1613.20	6.080	80.68	.00010955
30	693.30	-1613.20	6.137	64.70	.00010261
31	.00	.00	.000	287.04	.00013669
32	.00	.00	.000	287.04	.00013669
33	737.10	-1688.20	6.000	63.55	.00010046
34	737.10	-1838.20	5.500	75.79	.00010044
35	737.10	-1988.20	5.500	75.74	.00010042
36	737.10	-2113.20	6.500	51.13	.00010040
37	737.10	-2232.70	7.500	26.52	.00010038
38	.00	.00	.000	287.04	.00013669
39	.00	.00	.000	287.04	.00013669
40	693.30	-2295.80	8.491	6.64	.00010251
41	551.00	-2296.80	8.703	16.01	.00010945
42	351.00	-2296.80	9.000	29.20	.00011921
43	201.00	-2296.80	9.000	44.57	.00012653
44	66.00	-2296.80	13.000	-39.87	.00013311
45	16.00	-2296.80	17.000	-133.03	.00013555
46	6.00	-2296.80	17.500	-144.29	.00013604
47	.50	-150.00	16.500	-118.46	.00013664
48	.50	-450.00	16.500	-118.56	.00013659
49	.50	-750.00	15.000	-81.80	.00013655
50	.50	-1050.00	14.500	-69.61	.00013650
51	.50	-1350.00	14.000	-57.43	.00013645
52	.50	-1650.00	14.500	-69.81	.00013641
53	.50	-1950.00	15.000	-82.19	.00013636
54	.50	-2250.00	16.500	-119.14	.00013632
55	.50	-2495.00	16.500	-119.22	.00013628
56	61.60	-299.00	-5.240	409.38	.00013364
57	126.60	-299.00	8.152	73.68	.00013046
58	191.60	-299.00	2.952	194.78	.00012729
59	261.60	-299.00	9.000	39.01	.00012388
60	326.00	-299.00	9.000	32.41	.00012073
61	446.10	-299.00	8.848	23.84	.00011487
62	521.10	-299.00	8.728	19.11	.00011121
63	586.10	-299.00	8.624	15.00	.00010804
64	641.10	-299.00	8.536	11.53	.00010536
65	691.10	-299.00	8.456	8.37	.00010292
66	-.00	-.00	.000	287.04	.00013669
67	61.00	-974.00	8.600	69.17	.00013356
68	126.60	-974.00	7.102	99.25	.00013036
69	191.60	-974.00	6.139	116.25	.00012719
70	261.60	-974.00	6.000	112.50	.00012377
71	326.00	-974.00	6.000	105.90	.00012063
72	446.10	-974.00	6.043	92.53	.00011477

SECTION NO.=10 AT X=19000.0000

A= 36605.64
 D=1154.50
 YBT=585.15
 ZBL=-1295.00
 IBZZ= 8150770869.54
 IBYY=19056653512.28
 IBYZ= .00
 FT= 8399178.71
 K= 5253629777.50
 MTZ= .16417
 MTY= -.24774E-02
 YT= 425.83
 ZT= -1289.4

ELEMENT	NO.	Y	Z	TEMP(T)	STRESS	STRAIN
1	6.00	-293.20	17.500	-138.54	.00013878	
2	16.00	-293.20	17.000	-127.31	.00013827	
3	66.00	-293.20	13.000	-34.32	.00013576	
4	201.00	-293.20	9.000	49.68	.00012896	
5	351.00	-293.20	9.000	33.82	.00012141	
6	551.00	-293.20	8.861	16.09	.00011133	
7	751.00	-293.00	8.722	-1.64	.00010126	
8	951.00	-293.00	8.583	-19.37	.00009119	
9	1099.80	-293.20	8.479	-32.57	.00008370	
10	1152.25	-368.20	7.500	-14.11	.00008103	
11	1152.25	-518.20	6.500	10.35	.00008098	
12	1152.25	-668.20	5.500	34.81	.00008092	
13	1152.25	-793.20	5.500	34.71	.00008088	
14	1152.25	-912.70	6.000	22.34	.00008084	
15	1099.80	-976.80	6.148	24.19	.00008346	
16	951.00	-976.80	6.119	40.66	.00009095	
17	751.00	-976.80	6.079	62.78	.00010102	
18	551.00	-976.80	6.039	84.91	.00011109	
19	351.00	-976.80	6.000	107.03	.00012117	
20	201.00	-976.80	6.000	122.89	.00012872	
21	66.00	-976.80	8.000	88.03	.00013552	
22	16.00	-976.80	14.000	-54.11	.00013803	
23	6.00	-976.80	14.500	-65.33	.00013854	
24	5.00	-1613.20	14.500	-65.80	.00013832	

25	16.00	-1613.20	14.000	-54.58	.00013781
26	66.00	-1613.20	8.000	87.56	.00013529
27	201.00	-1613.20	6.000	122.42	.00012850
28	351.00	-1613.20	6.000	106.56	.00012094
29	551.00	-1613.20	6.035	84.55	.00011087
30	751.00	-1613.20	6.070	62.55	.00010080
31	951.00	-1613.20	6.104	40.54	.00009073
32	1099.80	-1613.20	6.130	24.17	.00008323
33	1152.25	-1688.20	6.000	21.77	.00008057
34	1152.25	-1838.20	5.500	33.94	.00008051
35	1152.25	-1988.20	5.500	33.83	.00008046
36	1152.25	-2113.20	6.500	9.17	.00008042
37	1152.25	-2232.70	7.500	-15.49	.00008038
38	1099.80	-2296.80	8.515	-34.94	.00008299
39	951.00	-2296.80	8.612	-21.57	.00009049
40	751.00	-2296.80	8.742	-3.61	.00010056
41	551.00	-2296.80	8.871	14.36	.00011063
42	351.00	-2296.80	9.000	32.34	.00012070
43	201.00	-2296.80	9.000	48.21	.00012826
44	66.00	-2296.80	13.000	-35.80	.00013505
45	16.00	-2296.80	17.000	-128.79	.00013757
46	6.00	-2296.80	17.500	-140.02	.00013808
47	.50	-150.00	16.500	-113.28	.00013911
48	.50	-450.00	16.500	-113.50	.00013900
49	.50	-750.00	15.000	-76.87	.00013890
50	.50	-1050.00	14.500	-64.81	.00013879
51	.50	-1350.00	14.000	-52.74	.00013868
52	.50	-1650.00	14.500	-65.25	.00013858
53	.50	-1950.00	15.000	-77.76	.00013847
54	.50	-2250.00	16.500	-114.83	.00013837
55	.50	-2495.00	16.500	-115.01	.00013828
56	127.50	-299.00	8.080	80.06	.00013266
57	262.50	-299.00	9.000	43.18	.00012586
58	426.10	-299.00	8.948	27.16	.00011762
59	555.70	-299.00	8.858	15.67	.00011110
60	678.70	-299.00	8.772	4.76	.00010490
61	792.10	-299.00	8.693	-5.29	.00009919
62	878.50	-299.00	8.633	-12.95	.00009484
63	942.60	-299.00	8.588	-18.63	.00009161
64	1000.30	-299.00	6.129	35.70	.00008871
65	1055.20	-299.00	6.140	29.63	.00008594
66	1109.30	-299.00	7.961	-20.85	.00008322
67	127.50	-974.00	7.089	103.91	.00013242
68	262.50	-974.00	6.000	116.39	.00012562
69	426.10	-974.00	6.015	98.72	.00011738
70	555.70	-974.00	6.040	84.39	.00011086
71	678.70	-974.00	6.065	70.78	.00010466
72	792.10	-974.00	6.087	58.24	.00009895

APPENDIX C - COMPUTER PROGRAM FOR ANALYSIS
OF POISSON'S RATIO EFFECT

(A. Ostapenko and J. E. O'Brien)

C.1 Introduction

A computer program is presented here which was developed for the computation of the effective plate widths of floor beams and transverse stiffeners in resisting Poisson's ratio effect, that is, the effect of primary bending stresses. The program is based on the method of analysis described in Art. 5.2 and it uses an error minimization process to calculate the effective width values and the corresponding stresses.

In the following are given the fundamental matrices of the force method of analysis and their form as used in this program. Then follows the actual listing of the program and the formats and samples of the input and output. The program language is FORTRAN IV with some special library subroutines available in the CDC 6400 computer at Lehigh University.

C.2 Fundamental Matrices for Force Method of Analysis

As described in Section 5.2, the basic equation of the member bar forces is:

$$S = (B_0)R + (B_1)X \quad (5.1)$$

But since $R = 0$:

$$S = (B_1)X \quad (5.2)$$

where:

$$X = -[(B_1)^T \cdot F \cdot B_1]^{-1} \cdot (B_1)^T \cdot V \quad (5.3)$$

In order to solve these equations, the B_1 , F , and V matrices must be formulated. The B_1 and F matrices are formulated routinely and are listed in Figs. C-1 and C-2, respectively. All notation is defined in Chapter 5 and dimensions are shown in Fig. 5.8.

The remaining V matrix is formulated below.

By definition, the V matrix is a list of the deflections at the end of the released cantilever elements resulting from the applied loads (in this case, Poisson's effect). These deflections are the rotation (θ), the transverse displacement (v), and the elongation (e). The only effects on the released elements (primary structure) are the curvatures, ϕ , and axial strains, ϵ , described in Section 5.2. Since shear deformations are negligible,

the deflections can be calculated from the following equations:

$$\theta = \int_0^L \phi \, dx \quad (C-1)$$

$$v = \int_0^L \phi \, x \, dx \quad (C-2)$$

$$e = \int_0^L \varepsilon \, dx \quad (C-3)$$

As in Section 5.2, L is the length of the member along the x -axis with the origin at the released end of the member (the cantilevers of Fig. 5.9).

The V matrix then takes the form of a column matrix:

$$V = \left\{ \begin{array}{cccc} \theta_1 & v_1 & e_1 & \\ \theta_2 & v_2 & e_2 & \\ \theta_3 & v_3 & e_3 & \\ \theta_4 & v_4 & e_4 & \\ \theta_5 & v_5 & e_5 & e_6 \end{array} \right\} \quad (C-4)$$

where the subscripts are the member numbers. The final form of the V matrix is given in Fig. C-3 after making the needed calculations. The notation of the V matrix is defined in Section 5.2 and the dimensions D , W , and H are shown in Fig. 5.8.

With all the needed matrices formulated, the redundants X can be solved with Eq. 5.3 and the strains and stresses computed as described in Section 5.2.2.

1	-W	0	0	0
0	0	+1	1	$+\cos(\tan^{-1} \frac{D}{W})$
0	-1	0	0	$-\sin(\tan^{-1} \frac{D}{W})$
1	0	0	0	0
0	+1	0	0	0
0	0	+1	0	0
1	0	-D	0	0
0	0	-1	0	0
0	+1	0	0	0
1	-W	-D	0	$-W\sin(\tan^{-1} \frac{D}{W})$
0	-1	0	0	$-\sin(\tan^{-1} \frac{D}{W})$
0	0	-1	0	$-\cos(\tan^{-1} \frac{D}{W})$
0	0	0	-D	0
0	0	0	0	0
0	0	0	+1	0
0	0	0	0	1

Figure C-1: Matrix B_1 , Bar Forces Due to Unit Redundant Forces Applied on the Primary Structure

$\frac{D}{E(I_v)}$	$\frac{-D^2}{2E(I_v)}$	0	0	0	0	0	0	0	0	0	0	0	0	0	0
$\frac{-D^2}{2E(I_v)}$	$\frac{D^3}{3E(I_v)}$	0	0	0	0	0	0	0	0	0	0	0	0	0	0
0	0	$\frac{D}{E(A_v)}$	0	0	0	0	0	0	0	0	0	0	0	0	0
0	0	0	$\frac{W}{E(I_b)}$	$\frac{-W^2}{2E(I_b)}$	0	0	0	0	0	0	0	0	0	0	0
0	0	0	$\frac{-W^2}{2E(I_b)}$	$\frac{W^3}{3E(I_b)}$	0	0	0	0	0	0	0	0	0	0	0
0	0	0	0	0	$\frac{W}{E(A_b)}$	0	0	0	0	0	0	0	0	0	0
0	0	0	0	0	0	$\frac{D}{E(I_v)}$	$\frac{-D^2}{2E(I_v)}$	0	0	0	0	0	0	0	0
0	0	0	0	0	0	$\frac{-D^2}{2E(I_v)}$	$\frac{D^3}{3E(I_v)}$	0	0	0	0	0	0	0	0
0	0	0	0	0	0	0	0	$\frac{D}{E(A_v)}$	0	0	0	0	0	0	0
0	0	0	0	0	0	0	0	0	$\frac{W}{E(I_t)}$	$\frac{-W^2}{2E(I_t)}$	0	0	0	0	0
0	0	0	0	0	0	0	0	0	$\frac{-W^2}{2E(I_t)}$	$\frac{W^3}{3E(I_t)}$	0	0	0	0	0
0	0	0	0	0	0	0	0	0	0	0	$\frac{W}{E(A_t)}$	0	0	0	0
0	0	0	0	0	0	0	0	0	0	0	0	$\frac{H}{E(I_t)}$	$\frac{-H^2}{2E(I_t)}$	0	0
0	0	0	0	0	0	0	0	0	0	0	0	$\frac{-H^2}{2E(I_t)}$	$\frac{H^3}{3E(I_t)}$	0	0
0	0	0	0	0	0	0	0	0	0	0	0	0	0	$\frac{H}{E(A_t)}$	0
0	0	0	0	0	0	0	0	0	0	0	0	0	0	0	$\frac{\sqrt{D^2+W^2}}{E(A_d)^*}$

*A_d = Area of Member 5

Figure C-2: Matrix F, Total Structure Flexibility Matrix

$$\mathbf{V} = \begin{bmatrix}
 \frac{1}{2}(\phi_{vt} + \phi_{vb})D \\
 -(\frac{1}{6}\phi_{vb} + \frac{1}{3}\phi_{vt})D^2 \\
 \frac{1}{2}(\epsilon_{vt} + \epsilon_{vb})D \\
 \phi_b \cdot W \\
 -\frac{1}{2}(\phi_b)W^2 \\
 \epsilon_b \cdot W \\
 \frac{1}{2}(\phi_{vb} + \phi_{vt})D \\
 -(\frac{1}{6}\phi_{vt} + \frac{1}{3}\phi_{vb})D^2 \\
 \frac{1}{2}(\epsilon_{vb} + \epsilon_{vt})D \\
 \phi_t \cdot W \\
 -\frac{1}{2}(\phi_t)W^2 \\
 \epsilon_t \cdot W \\
 -\phi_t \cdot H \\
 -\frac{1}{2}(\phi_t)H^2 \\
 \epsilon_t \cdot H \\
 0
 \end{bmatrix}$$

Figure C-3: Matrix V, Deflections at the Ends of the Released Members from Poisson's Effect

C.3 Computer Program

C.3.1 General Procedure and Subroutines

The general computational procedure employed in the program is shown by the flow chart in Fig. 5.7 and described in Art. 5.2. Basically the program consists of the main program XELA which calls a number of subroutines to perform particular tasks. The names and functions of these subroutines are listed below.

PROGRAM XELA - This is the main program which reads the input data, prints it for checking purposes, performs the minimization process, and prints the output.

<u>Subroutines</u>	<u>Description</u>
REDUN	This subroutine constructs the B1 matrix for the force method of analysis.
MATRIX	It constructs the F and V matrices.
ALPHA	It calculates the section properties of all members of the transverse frame and performs the force method of analysis.
BETA	It calculates the error for the minimization process.
POINTS	It calculates the stresses and strains for the current set of effective widths.

In addition to the above, the following six subroutines are called from the library of the Lehigh University computer. Their function is described here so that they can be replaced by equivalent subroutines if the program is used elsewhere.

<u>L.U. Subroutines</u>	<u>Description</u>
MINV(A,N,DET,NEXCH)	This subroutine performs inversion of matrix A.
MULT (A,B,C,L,M,N)	It postmultiplies matrix A by Matrix B to create Matrix C; $C = AB$.
OUTG (A,I,J, TITLE, TITEL)	It prints out Matrix A.
SCMUL (A,M,N,X)	It multiplies Matrix A by constant x, $A = xA$.
TMULT (A,B,C,L, M,N)	It postmultiplies the transverse of Matrix A by Matrix B to create Matrix C: $C = A^T B$.
XATBAC (A,B,C,L, M,X)	It postmultiplies the transpose of Matrix B by Matrix B, then postmultiplies the result by Matrix A to create Matrix C; $C = A^T B A$.

C.3.2 Symbol List and Definitions

Names of variables and their definitions are given for the convenience of modifying or trouble shooting the program. They are listed in groups of the input, output, and other symbols used in the program.

Definition of Input Symbols

<u>Symbol</u>	<u>Definition</u>
BBFT, BBFV, BBFB	width of the flange of the top, vertical, and bottom stiffeners, respectively
BE	matrix of effective widths of the top, vertical and bottom stiffeners inputted as assumed numbers and outputted as calculated values
DB	first increment used in the minimization process
DIS	matrix of the distances from the end of the corresponding member to the points on it where the strain readings were taken
DWT, DWV, DWB	depth of the web of the top, vertical, and bottom stiffeners, respectively
E	modulus of elasticity
EM	matrix of measured strain readings used to determine effective widths
H	half the distance between box girders
M	number of strain readings used in the program
MEM	matrix of member numbers designating the member number for each strain reading
N	number of effective widths used in the program to be solved for
NF	number of member forces
NLC	number of load cases
NX	number of redundants
POS	position in the cross section of the member where the strain reading was taken (ITOP or IBOT)

SIGMAT, SIGMAD	normal stresses in the top and bottom flanges of the box girder, respectively
TBFT, TBFV, TBFB	thickness of the flange of the top, vertical, and bottom stiffeners, respectively
TTFT, TTFV, TTFB	thickness of the plate stiffened by the top, vertical, and bottom stiffeners, respectively
TWT, TWV, TWB	thickness of the web of the top, vertical, and bottom stiffeners, respectively
W	width of the box girder

Definition of Output Symbols

<u>Symbol</u>	<u>Definition</u>
B1	matrix of bar forces due to unit redundant forces applied on the primary structure
EC	matrix of calculated strains
ERROB	matrix of the error associated with the incrementation of effective widths and the value which must be minimized to find the best value of effective widths
ES	matrix of calculated stresses at points of measured strains
EX	matrix of calculated stresses at points of interface between the stiffeners and the girder plates
F	total flexibility matrix
S	matrix of member end forces
V	matrix of deflections at the end of each member created by Poisson's effect on the released member
X	matrix of the values of redundants

Definition of Other Symbols Used in Program

<u>Symbol</u>	<u>Definition</u>
AD	area of the diagonal bracing
AET,AEV,AEB	area of the top, bottom, and vertical members
CBT,CBV,CBB	distance from the centroidal axis to the bottom fiber of the top, vertical, and bottom members
CTT,CTV,CTB	distance from the centroidal axis to the top fiber of the top, vertical and bottom members
ERR	temporary storage variable used in minimizing error
ERROR	temporary storage matrix for calculation of minimum error
I,J,K	counters
IB,IT,IV	moments of inertia of the bottom, top and vertical members of the frame
MT,MVT,MVB,MB	curvature in the primary structure (top member, vertical member at the top, vertical member at the bottom, and bottom member, respectively)
NEXCH,BF,BFT, XS,BV	temporary storage matrices for the matrix operations
NT,NVT,NVB,NB	axial strain in the primary structure due to Poisson's effect
YBARB,YBARTV, YBARTB	CTT,CTV,CTB
YBARBT,YVARBV, YBARBB	CBT,CBV,CBB

C.3.3 Listing of Computer Program

The printout of the main program XELA and the subroutines
is reproduced below.

```

PROGRAM XELA(INPUT,OUTPUT,TAPE1=OUTPUT)
REAL IB,IT,IV,MB,MT,MVB,MVT,NB,NT,NVT,NVB
REAL BE(3),EC(20),EM(20),ERROR(3),ERROB(3),EP(20),BFT(3,3),ES(30)
REAL F(16,16),S(16,1),V(16,1),B1(16,3),DIS(20),XS(16),BV(3,1)
REAL X(3,1),EX(20)
INTEGER NEM(20),POS(20),NEXCH(20)
COMMON/BLA/TTFT,DWT,TWT,BBFT,TBFT,TTFV,DWV,TWV,BBFV,TBFV,TTFB,DWB,
$TWB,BBFB,TBFB,W,D,E,SIGMAT,SIGMAB,H
COMMON/BLD/AET,AEV,AEB,IT,IV,IB,CTT,CTV,CTB,CBT,CBV,CBB
COMMON/BLE/NT,MT,NVT,MVT,NVB,MVB,NB,MB
READ 1,W,D,H,E
PRINT2,W,D,H,E
READ 1,TTFT,DWT,TWT,BBFT,TBFT
PRINT2,TTFT,DWT,TWT,BBFT,TBFT
READ 1,TTFV,DWV,TWV,BBFV,TBFV
PRINT2,TTFV,DWV,TWV,BBFV,TBFV
READ 1,TTFB,DWB,TWB,BBFB,TBFB
PRINT2,TTFB,DWB,TWB,BBFB,TBFB
READ 1,SIGMAT,SIGMAB
PRINT2,SIGMAT,SIGMAB
1 FORMAT(8F10.0)
2 FORMAT(/,1X,8F12.4,/)
READ 60,BE,DB,N,M
PRINT 3,BE,DB,N,M
3 FORMAT(/,1X,4F12.4,2I5)
C N IS THE NUMBER OF EFFECTIVE WIDTHS
C M IS THE NUMBER OF STRAIN READING POINTS
60 FORMAT(4F10.0,2I5)
READ 59,NF,NX,NLC
PRINT 4,NF,NX,NLC
59 FORMAT(3I3)
4 FORMAT(/,1X,3I3,/)
DO 58 I=1,M
READ 57,MEM(I),DIS(I),POS(I),EM(I)
PRINT 5,MEM(I),DIS(I),POS(I),EM(I)
57 FORMAT(I1,F9.0,A4,F10.0)
5 FORMAT(/,1X,I1,F12.4,A4,F12.9,/)
58 CONTINUE
C IF POS=ITOP THEN TOP OF FLOOR BEAM,IBOT IS BOTTOM
CALL REDUN(NF,NX,B1)
DO 61 K=1,9
CALL ALPHA(BE,NX,NF,NLC,M,N,BFT,BV,B1,XS,X,S,F,V,EP,NEXCH,EC,
1DIS,MEM,POS,ES,EX)
CALL BETA(EC,EM,M,ERR)
ERROR(1)=ERR
62 CONTINUE
DO 63 I=1,N
BE(I)=BE(I)+DB

```

```

CALL ALPHA(BE,NX,NF,NLC,M,N,BFT,BV,B1,XS,X,S,F,V,EP,NEXCH,EC,
1DIS,MEM,POS,ES,EX)
CALL BETA(EC,EM,M,ERR)
ERROR(2)=ERR
IF(ERROR(2).GT.ERROR(1))GOTO 64
ERROB(I)=ERROR(2)
GOTO 69
64 CONTINUE
BE(I)=BE(I)-2.*DB
CALL ALPHA(BE,NX,NF,NLC,M,N,BFT,BV,B1,XS,X,S,F,V,EP,NEXCH,EC,
1DIS,MEM,POS,ES,EX)
CALL BETA(EC,EM,M,ERR)
ERROR(3)=ERR
IF(ERROR(3).GT.ERROR(1))GOTO 65
ERROB(I)=ERROR(3)
GOTO 69
65 CONTINUE
BE(I)=BE(I)+DB
ERROB(I)=ERROR(1)
69 CONTINUE
ERROR(1)=ERROB(I)
63 CONTINUE
PRINT 70,BE,ERROB
70 FORMAT(///,1X,3F10.0,3G15.8)
DO 66 J=2,N
IF(ERROB(J-1).EQ.ERROB(J)) GOTO 66
GOTO 67
66 CONTINUE
GOTO 68
67 ERROR(1)=ERROB(N)
GOTO 62
68 DB=DB/2.
61 CONTINUE
PRINT 8
CALL OUTG(V,NF,NLC,1HV,TIT)
CALL OUTG(F,NF,NF,1HF,TIT)
CALL OUTG(B1,NF,NX,2HB1,TIT)
CALL OUTG(X,NX,NLC,1HX,TIT)
CALL OUTG(S,NF,NLC,1HS,TIT)
PRINT 71
71 FORMAT(///,15X,*ACTUAL STRESSES AT POINTS OF MEASUREMENT*,//)
PRINT 72
72 FORMAT(2X,*MEMBER*,5X,*POSITION*5X,*DISTANCE*,10X,*STRAIN*,10X,
$*STRAIN*,10X,*STRESS*/62X,*MEASURED*,7X,*CALCULATED*)
DO 75 I=1,M
PRINT 73,MEM(I),POS(I),DIS(I),EM(I),EC(I),ES(I),EX(I)
73 FORMAT(//,5X,I1,9X,A4,7X,F8.0,8X,F10.8,6X,F10.8,4X,G15.7,4X,G15.7)
75 CONTINUE
PRINT 8
8 FORMAT(///)
STOP
END

```

```
SUBROUTINE REDUN(NF,NX,B1)
REAL B1(NF,NX)
COMMON/BLA/TTFT,DWT,TWT,BBFT,TBFT,TTFV,DWV,TWV,BBFV,TBFV,TTFB,DWB,
$TWB,BBFB,TBFB,M,D,E,SIGMAT,SIGMAB,M
DO 1 I=1,NF
DO 2 J=1,NX
B1(I,J)=0.0
2 CONTINUE
1 CONTINUE
B1(1,1)=1.
B1(4,1)=1.
B1(7,1)=1.
B1(10,1)=1.
B1(1,2)=-W
B1(3,2)=-1.
B1(5,2)=1.
B1(9,2)=1.
B1(10,2)=-W
B1(11,2)=-1.
B1(2,3)=+1.
B1(6,3)=+1.
B1(7,3)=-D
B1(8,3)=-1.
B1(10,3)=-D
B1(12,3)=-1.
IF(NX.EQ.3) GOTO 3
B1(2,4)=1.
B1(13,4)=-D
B1(15,4)=1.
B1(2,5)=COS(ATAN(D/W))
B1(3,5)=-SIN(ATAN(D/W))
B1(10,5)=-W*SIN(ATAN(D/W))
B1(11,5)=-SIN(ATAN(D/W))
B1(12,5)=-COS(ATAN(D/W))
B1(16,5)=1.
3 CONTINUE
RETURN
END
```

```
MT=-NT*(CTT-TTFT/2.)
NVT=EAT*TTFV*BEV
MVT=-NVT*(CTV-TTFV/2.)
NVB=EAB*TTFV*BEV
MVB=-NVB*(CTV-TTFV/2.)
NB=EAB*TTFB*BEB
MB=-NB*(CTB-TTFB/2.)
V(1,1)=.5*(MVB+MVT)*D/(E*IV)
V(2,1)=(-1./6.*MVB-1./3.*MVT)*D**2/(E*IV)
V(3,1)=.5*(NVB+NVT)*D/(E*AEV)
V(4,1)=MB*W/(E*IB)
V(5,1)=-.5*MB*W**2/(E*IB)
V(6,1)=NB*W/(E*AEB)
V(7,1)=V(1,1)
V(8,1)=(-1./6.*MVT-1./3.*MVB)*D**2/(E*IV)
V(9,1)=V(3,1)
V(10,1)=MT*W/(E*IT)
V(11,1)=-1./2.*MT*W**2/(E*IT)
V(12,1)=NT*W/(E*AET)
V(13,1)=-MT*H/(E*IT)
V(14,1)=1./2.*MT*H**2/(E*IT)
V(15,1)=NT*H/(E*AET)
V(16,1)=0.0
RETURN
END
```

```

SUBROUTINE MATRIX(BET, BEV, BEB, NF, NLC, NX, F, V)
REAL IT, IV, IB, NT, MT, NVT, MVT, NVB, MVB, NB, MB
REAL F(NF, NF), V(NF, NLC)
COMMON/BLA/TTFT, DMT, TMT, BBFT, TBFT, TTFV, DMV, TMV, BBFV, TBFV, TTFB, DMG,
$TWB, BBFB, TBFB, W, D, E, SIGMAT, SIGMAB, H
COMMON/BLD/AET, AEV, AEB, IT, IV, IB, CTT, CTV, CTB, CBT, CBV, CBB
COMMON/BLE/NT, MT, NVT, MVT, NVB, MVB, NB, MB
DO 1 I=1, NF
DO 2 J=1, NF
F(I, J)=0.0
2 CONTINUE
1 CONTINUE
IF(NX.EQ.3) GOTO 3
AD=10.**100
GOTO 4
3 CONTINUE
AD=0.001
4 CONTINUE
F(1,1)=D/(E*IV)
F(7,7)=F(1,1)
F(1,2)=-D**2/(2.*E*IV)
F(7,8)=F(1,2)
F(2,1)=F(1,2)
F(8,7)=F(1,2)
F(2,2)=D**3/(3.*E*IV)
F(8,8)=F(2,2)
F(3,3)=D/(AEV*E)
F(9,9)=F(3,3)
F(4,4)=W/(E*IB)
F(4,5)=-W**2/(2.*E*IB)
F(5,4)=F(4,5)
F(5,5)=W**3/(3.*E*IB)
F(6,6)=W/(AEB*E)
F(10,10)=W/(E*IT)
F(10,11)=-W**2/(2.*E*IT)
F(11,10)=F(10,11)
F(11,11)=W**3/(3.*E*IT)
F(12,12)=W/(AET*E)
F(13,13)=W/(E*IT)
F(13,14)=-W**2/(2.*E*IT)
F(14,13)=F(13,14)
F(14,14)=W**3/(3.*E*IT)
F(15,15)=W/(AET*E)
F(16,16)=SQRT(D**2+W**2)/(AD*E)
EAT=(-.3)*SIGMAT
EAB=(-.3)*SIGMAB
NF=(EAT)*TTFT*BET

```

```

SUBROUTINE ALPHA(BE,NX,NF,NLC,M,N,BFT,BV,B1,XS,X,S,F,V,EP,NEXCH,EC
1,DIS,MEM,POS,ES,EX)
  REAL BFT(NX,NX),BV(NX,NLC),B1(NF,NX),XS(NF),X(NX,NLC),
+S(NF,NLC),BE(N),F(NF,NF),V(NF,NLC),EP(M),EG(M),DIS(M),ES(M)
  REAL IB,IT,IV,MB,MT,MVB,MVT,NB,NT,NWT,NVB,EX(M)
  INTEGER NEXCH(NX),MEM(M),POS(M)
  COMMON/BLA/TTFT,DWT,TNT,BBFT,TBFT,TTFV,DWV,TWV,BBFV,TBFV,TTFB,DWB,
$TWB,BBFB,TBFB,W,D,E,SIGMAT,SIGMAB,H
  COMMON/BLD/AET,AEV,AEB,IT,IV,IB,CTT,CTV,CTB,CBT,CBV,CBB
  COMMON/BLE/NT,MT,NWT,MVT,NVB,MVB,NB,MB
  BET=BE(1)
  BEV=BE(2)
  BEB=BE(3)
  AET=BBFT*TBFT+DWT*TNT+BET*TTFT
  AEV=BBFV*TBFV+DWV*TWV+BEV*TTFV
  AEB=BBFB*TBFB+DWB*TWB+BEB*TTFB
  YBARTT=(BET*TTFT*(TTFT/2.)+DWT*TNT*(TTFT+DWT/2.)+TBFT*BBFT*(TTFT+
$DWT+TBFT/2.))/AET
  YBARTV=(BEV*TTFV*(TTFV/2.)+DWV*TWV*(TTFV+DWV/2.)+TBFV*BBFV*(TTFV+
$DWV+TBFV/2.))/AEV
  YBARTB=(BEB*TTFB*(TTFB/2.)+DWB*TWB*(TTFB+DWB/2.)+TBFB*BBFB*(TTFB+
$DWB+TBFB/2.))/AEB
  YBARBT=TTFT+DWT+TBFT-YBARTT
  YBARBV=TTFV+DWV+TBFV-YBARTV
  YBARBB=TTFB+DWB+TBFB-YBARTB
  CTT=YBARTT
  CBT=YBARBT
  CTV=YBARTV
  CBV=YBARBV
  CTB=YBARTB
  CBB=YBARBB
  IT=1./12.*BET*TTFT**3+BET*TTFT*(YBARTT-TTFT/2.)**2+
$ 1./12.*TNT*DWT**3+TNT*DWT*(CTT-TTFT-DWT/2.)**2+
$ 1./12.*BBFT*TBFT**3+TBFT*BBFT*(CTT-TTFT-DWT-TBFT/2.)**2
  IV=1./12.*BEV*TTFV**3+BEV*TTFV*(CTV-TTFV/2.)**2+
$ 1./12.*TWV*DWV**3+TWV*DWV*(CTV-TTFV-DWV/2.)**2+
$ 1./12.*BBFV*TBFV**3+TBFV*BBFV*(CTV-TTFV-DWV-TBFV/2.)**2
  IB=1./12.*BEB*TTFB**3+BEB*TTFB*(CTB-TTFB/2.)**2+
$ 1./12.*TWB*DWB**3+TWB*DWB*(CTB-TTFB-DWB/2.)**2+
$ 1./12.*BBFB*TBFB**3+TBFB*BBFB*(CTB-TTFB-DWB-TBFB/2.)**2
  C=-1.8
  CALL MATRIX(BET,BEV,BEB,NF,NLC,NX,F,V)
  CALL XATBAC(B1,F,BFT,NF,NX,XS)
  CALL MINV(BFT,NX,DET,NEXCH)
  CALL TMULT(B1,V,BV,NF,NX,NLC)
  CALL MULT(BFT,BV,X,NX,NX,NLC)
  CALL SCHUL(X,NX,NLC,C)
  CALL MULT(B1,X,S,NF,NX,NLC)
  CALL POINTS(NX,NF,NLC,M,N,S,DIS,EC,EP,MEM,POS,ES,EX,BET,BEV,BEB)
  RETURN
  END

```



```
SUBROUTINE BETA(EC,EM,M,ERR)
REAL EC(M),EM(M)
ERR=0.0
DO 1 I=1,M
ERR=ERR+ABS(EC(I)-EM(I))
1 CONTINUE
RETURN
END
```

```

SUBROUTINE POINTS(NX,NF,NLC,M,N,S,DIS,EC,EP,MEM,POS,ES,EX,BET,BEV,
$BEB)
  REAL S(NF,NLC),DIS(M),EC(M),EP(M),ES(M),EX(M)
  REAL NT,MT,NVT,MVT,NVB,MVB,NB,MB,IT,IB,IV
  INTEGER MEM(M),POS(M)
  COMMON/BLA/TTFT,DWT,TWT,BBFT,TBFT,TTFV,DWV,TWV,BBFV,TBFV,TTFB,DWB,
$TWB,BBFB,TBFB,H,D,E,SIGMAT,SIGMAB,H
  COMMON/BLD/AET,AEV,AEB,IT,IV,IB,CTT,CTV,CTB,CBT,CBV,CBB
  COMMON/BLE/NT,MT,NVT,MVT,NVB,MVB,NB,MB
  IBOT=4HIBOT
  ITOP=4HITOP
  DO 12 I=1,M
  EX(I)=0
12 CONTINUE
  DO 1 I=1,M
  IF(MEM(I).GT.1) GOTO 2
  IF(POS(I).EQ.IBOT) GOTO 3
  EC(I)=(S(2)*DIS(I)-S(1))*(CTV-TTFV)/(E*IV)+S(3)/(AEV*E)
  EP(I)=(NVB-(NVB-NVT)*DIS(I)/D)/(E*AEV)-(MVB-(MVB-MVT)*DIS(I)/D)*(C
1TV-TTFV)/(E*IV)
  EX(I)=- (NVB-(NVB-NVT)*DIS(I)/D)*(1./((BEV*TTFV)-1./AEV)+S(3)/AEV-
1(MVB-(MVB-MVT)*DIS(I)/D)*CTV/IV+(S(2)*DIS(I)-S(1))*CTV/IV
  ES(I)=(NVB-(NVB-NVT)*DIS(I)/D+S(3))/AEV-
1(MVB-(MVB-MVT)*DIS(I)/D-(S(2)*DIS(I)-S(1)))*(CTV-TTFV)/IV
  GOTO 1
3 CONTINUE
  EC(I)=S(3)/(AEV*E)-(S(2)*DIS(I)-S(1))*CBV/(E*IV)
  EP(I)=(NVB-(NVB-NVT)*DIS(I)/D)/(E*AEV)+(MVB-(MVB-MVT)*DIS(I)/D)*CB
+V/(E*IV)
  ES(I)=(NVB-(NVB-NVT)*DIS(I)/D+S(3))/AEV+
1(MVB-(MVB-MVT)*DIS(I)/D-(S(2)*DIS(I)-S(1)))*(CBV)/IV
  GOTO 1
2 CONTINUE
  IF(MEM(I).GT.2)GOTO 4
  IF(POS(I).EQ.IBOT) GOT05
  EC(I)=S(6)/(AEB*E)+(S(5)*DIS(I)-S(4))*(CTB-TTFB)/(E*IB)
  EP(I)=NB/(AEB*E)-MB*(CTB-TTFB)/(E*IB)
  EX(I)=-NB/(BEB*TTFB)+(NB+S(6))/AEB-(MB-(S(5)*DIS(I)-S(4)))*CTB/IB
  ES(I)=(NB+S(6))/AEB-(MB-(S(5)*DIS(I)-S(4)))*(CTB-TTFB)/IB
  GOT01
5 CONTINUE
  EC(I)=S(6)/(AEB*E)-(S(5)*DIS(I)-S(4))*CBB/(E*IB)

```

```

EP(I)=NB/(AEB*E)+NB*CBB/(E*IB)
ES(I)=(NB+S(6))/AEB+(NB-(S(5)*DIS(I)-S(4)))*(CBB)/IB
GOTO 1
4 CONTINUE
IF(MEM(I).GT.3)GOTO 6
IF(POS(I).EQ.IBOT)GOTO 7
EC(I)=S(9)/(E*AEV)+(S(8)*DIS(I)-S(7))*(CTV-TTFV)/(E*IV)
EP(I)=(NVT-(NVT-NVB)*DIS(I)/D)/(E*AEV)-(MVT-(MVT-MVB)*DIS(I)/D)*(C
1TV-TTFV)/(E*IV)
EX(I)=- (NVT-(NVT-NVB)*DIS(I)/D)*(1./(BEV*TTFV)-1./AEV)+S(9)/AEV-
1(MVT-(MVT-MVB)*DIS(I)/D)*CTV/IV+(S(8)*DIS(I)-S(7))*CTV/IV
ES(I)=(NVT-(NVT-NVB)*DIS(I)/D+S(9))/AEV-
1(MVT-(MVT-MVB)*DIS(I)/D-(S(8)*DIS(I)-S(7)))*(CTV-TTFV)/IV
GOTO 1
7 CONTINUE
EC(I)=S(9)/(E*AEV)-(S(8)*DIS(I)-S(7))*CBV/(E*IV)
EP(I)=(NVT-(NVT-NVB)*DIS(I)/D)/(E*AEV)+(MVT-(MVT-MVB)*DIS(I)/D)*CB
+V/(E*IV)
ES(I)=(NVT-(NVT-NVB)*DIS(I)/D+S(9))/AEV+
1(MVT-(MVT-MVB)*DIS(I)/D-(S(8)*DIS(I)-S(7)))*(CBV)/IV
GOTO 1
6 CONTINUE
IF(MEM(I).GT.4)GOTO 8
IF(POS(I).EQ.IBOT)GOTO 9
EC(I)=S(12)/(E*AET)+(S(11)*DIS(I)-S(10))*(CTT-TTFT)/(E*IT)
EP(I)=NT/(E*AET)-MT*(CTT-TTFT)/(E*IT)
EX(I)=-NT/(BET*TTFT)+(NT+S(12))/AET-(MT-(S(11)*DIS(I)-S(10)))*CTT/
1IT
ES(I)=(NT+S(12))/AET-(MT-(S(11)*DIS(I)-S(10)))*(CTT-TTFT)/IT
GOTO 1
9 CONTINUE
EC(I)=S(12)/(E*AET)-(S(11)*DIS(I)-S(10))*CBT/(E*IT)
EP(I)=NT/(E*AET)+MT*CBT/(E*IT)
ES(I)=(NT+S(12))/AET+(MT-(S(11)*DIS(I)-S(10)))*(CBT)/IT
GOTO 1
8 CONTINUE
IF(POS(I).EQ.IBOT)GOTO 10
EC(I)=S(15)/(E*AET)+(S(13)-S(14)*DIS(I))*(CTT-TTFT)/(E*IT)
EP(I)=NT/(E*AET)-MT*(CTT-TTFT)/(E*IT)
EX(I)=-NT/(BET*TTFT)+(NT+S(15))/AET-(MT-S(14)*DIS(I)+S(13))*CTT/IT
ES(I)=(NT+S(15))/AET-(MT-(S(14)*DIS(I)-S(13)))*(CTT-TTFT)/IT
GOTO 1
10 CONTINUE
EC(I)=S(15)/(E*AET)-(S(13)-S(14)*DIS(I))*CBT/(E*IT)
EP(I)=NT/(E*AET)+MT*CBT/(E*IT)
ES(I)=(NT+S(15))/AET+(MT-(S(14)*DIS(I)-S(13)))*(CBT)/IT
1 CONTINUE
DO 11 I=1,M
EC(I)=EC(I)+EP(I)
11 CONTINUE
RETURN
END

```

C.3.4 Input Format and Sample

The input for this program consists of seven cards giving the geometric data, the primary longitudinal bending stresses in the top and bottom flanges of the box cross section and the initial values and specified increments for the effective widths. The eighth and the subsequent cards give the measured values of transverse strains and their locations, one strain per card. The variables listed for each card are defined above in Art. C.3.2.

A sample input is printed out at the end.

<u>Card No.</u>	<u>Format</u>	<u>Variables</u>
1	4F10.0	W,D,H,E
2	5F10.0	TIFT,DWT,TWT,BBFT,TBFT
3	5F10.0	TIFV,DWV,TWV,BBFV,TBFV
4	5F10.0	TTFB,DWB,TWB,BBFB,TBFB
5	2F10.0	SIGMAT,SIGMAB
6	4F10.0,2I5	BE(1),BE(2),BE(3),DB,N,M
7	3I3	NF,NX,NLC
8	I1,F9.0,A4,F10.0	MEM(I),DIS(I),POS(I),EM(I)
etc. (one card for each strain reading point)		

Sample Input

6850.	7280.	0.0	21000.		
16.	1000.	10.	200.	16.	
12.	618.	12.	200.	12.	
20.	600.	10.	200.	20.	
-18.04	25.22				
1000.	1000.	1000.	256.	3	14
16	3	1			
11046.	ITOP-.000153				
11046.	IBOT-.000124				
21046.	ITOP-.000291				
21046.	IBOT-.000233				
25800.	ITOP-.000282				
25800.	IBOT-.000212				
31430.	ITOP.000095				
36242.	ITOP-.000137				
36242.	IBOT-.000178				
41397.	ITOP.000212				
41397.	IBOT.000075				
42657.	ITOP.000126				
45476.	ITOP.000217				
45476.	IBOT.000052				
42657.	IBOT.0000257				
31430.	IBOT.000184				
1000.	1000.	1000.	256.	3	16

C.3.5 Description and Sample of Output

Beside the computed values of the stresses, strains and effective widths, the computer program in its present form prints out for the purpose of checking, the original data and some intermediate computed values. The full printout consists of the following arrays:

- 1) Input data arranged as on input cards.
- 2) Array of intermediate values of effective widths and the current errors. The first three columns give the effective width of the top, vertical and bottom members, respectively, and the last three columns give the current errors. The last line contains the final minimized values.

- 3) V-matrix printed as a column.
- 4) F-matrix printed as a square array.
- 5) Bl-matrix printed as a rectangular array.
- 6) X-redundant values printed as a column matrix.
- 7) S-values printed as a column matrix.
- 8) Measured strains and computed strains and stresses are printed for each location on a member in seven columns.

Col. 1 - member number

Col. 2 - position on member section: ITOP means on the stiffener web at the interface with the plate, IBOT means on the outside surface of the stiffener flange.

Col. 3 - distance from the end of the member to the specified location.

Col. 4 - strain, measured at the specified location.

Col. 5 - strain calculated at the specified location.

Col. 6 - stress, calculated at the specified location.

Col. 7 - stress, calculated in the plate at the specified location. It is given on the line designated by ITOP.

Arrays 1, 3, 4, 5, 6 and 7, as well as all of array 2 except for the last line, are printed only for checking purposes and the program can be correspondingly modified to suppress this if so desired.

A sample printout of the last few lines of Array 2 is shown below. It is seen that the effective width values on the last two

lines agree fully and the error is stabilized.

1992.	1256.	1416.	.16046830E-03	.16046830E-03	.16046830E-03
2008.	1256.	1416.	.16039974E-03	.16039974E-03	.16039974E-03
2000.	1256.	1416.	.16033683E-03	.16033683E-03	.16033683E-03
2004.	1256.	1416.	.16030791E-03	.16030791E-03	.16030791E-03
2002.	1256.	1418.	.16030410E-03	.16030410E-03	.16030238E-03
2002.	1256.	1418.	.16030238E-03	.16030238E-03	.16030238E-03
2003.	1256.	1417.	.16028567E-03	.16028567E-03	.16025411E-03
2003.	1256.	1417.	.16025411E-03	.16025411E-03	.16025411E-03

A printout of a portion of Array 8 giving the measured and computed values for the sample input is reproduced on the next page for checking trial runs.

MEMBER POSITION	DISTANCE	STRAIN MEASURED	STRAIN CALCULATED	STRESS	
1 ITOP	1046.	-.00015300	-.00015297	-3.212428	2.508275
1 IBOT	1046.	-.00018400	-.00020147	-4.230854	.0
2 ITOP	1046.	-.00029100	-.00028194	-5.920748	1.607889
2 IBOT	1046.	-.00023300	-.00022679	-4.762492	.0
2 ITOP	5800.	-.00028200	-.00028194	-5.920748	1.607889
2 IBOT	5800.	-.00021200	-.00022679	-4.762492	.0
3 ITOP	1430.	.00009500	.00006670	1.400610	-1.489032
3 ITOP	6242.	-.00013700	-.00015334	-3.220110	2.514931
3 IBOT	6242.	-.00017800	-.00020203	-4.242583	.0
4 ITOP	1397.	.00021200	.00021200	4.451970	-.9143002